

**Theoretical Investigation on Structure and Reactivity
Properties of Molecule and Metal Clusters: A Conceptual
DFT and *Ab initio* Molecular Dynamics Approach**

Thesis submitted to the

Savitribai Phule Pune University

for the Degree of

Doctor of Philosophy
in
Chemistry

By

Susanta Das

Dr. Sourav Pal
(Research Guide)

Physical Chemistry Division
CSIR–National Chemical Laboratory
Pune 411008

March 2015

CERTIFICATE

CERTIFIED THAT the work done in the thesis entitled,

Theoretical Investigation on Structure and Reactivity Properties of
Molecule and Metal Clusters: A Conceptual DFT and *Ab initio*
Molecular Dynamics Approach

Submitted by **Susanta Das** was carried out by the candidate under my supervision in the Physical Chemistry Division, CSIR–National Chemical Laboratory, Pune 411008, India. Any material that has been obtained from other sources has been duly acknowledged in the thesis.

Date:

Place:

Dr. Sourav Pal
(Research Guide)
Physical Chemistry Division
CSIR–National Chemical Laboratory
Pune 411008, India

DECLARATION

I hereby declare that the work incorporated in the thesis entitled

**Theoretical Investigation on Structure and Reactivity Properties of
Molecule and Metal Clusters: A Conceptual DFT and *Ab initio*
Molecular Dynamics Approach**

Submitted by me to **Savitribai Phule Pune University** for the degree of Doctor of Philosophy is original and has not been submitted to this or other University or Institution for the award of Degree or Diploma. I further declare that the material obtained from other sources has been duly acknowledged in the thesis.

Date:

Place:

Susanta Das

TO MY PARENTS

Acknowledgements

It is my great pleasure to thank my research supervisor, Prof. Sourav Pal for giving me the freedom to think and to express myself. He taught me how to do research in an individualistic way. I would especially like to mention our classes, where he introduced us and made us understand basic and advanced knowledge of quantum chemistry without which this work would not have been possible. I really appreciate his way of imagining things and his good sense of humor.

I owe a special debt to my co-supervisor Dr. Sailaja Krishnamurty for introducing me to the field of *ab initio* molecular dynamics. I thank Sailaja for her sincere and continuous support throughout my PhD tenure, especially the AI-cluster study. I must acknowledge Sailaja for the enriching discussions which helped improve the quality of my work on many an occasion. I will always remember a conversation during which she said that science should be a passion and not a profession.

I thank my all lab seniors Dr. Subrata Banik, Dr. Sumantra Bhattacharya, Dr. Himadri Dey, Dr. Lalitha Ravichandan, Dr. Sapna Shedge and Dr. Depti Mishra for making my life comfortable in my initial days. I should also acknowledge my labmates Debaratidi, Mudit, Jitendra, Sayali, Achintya, Aryya, Kamalika, Sayali, Anagha, Himadri, Manzoor, Turbasu, Sudip, Depak and Kausik for giving me a nice working environment in lab.

I thank all my friends Tamos da, Chandan da, Partha da, Sajal da, Sujit da, Jayasis da, Krishanu da, Shyam da, Saikat da, Debasis da, Subha di, Sujit, Arpan, Mrinmoy, Sujit, Anup, Anjan, Kanak, Pravat, Anjan, Abhik, Jhumur, Souvik, Prithvi, Doss, Subhadip, Munmun, Soumen, Saibal, Santigopal, Atanu, Santanu, Suman, Arunava, Hridesh and Prasenjit.

I want to express my gratitude towards my university teachers Dr. Pranab Sarkar, Dr. Bidhan Chandra Bag. They are my inspiration in whatever I have done and achieved till

now.

I am very lucky to get kind and unwavering support from my my families. My parents made tremendous sacrifices to ensure that I had good education. I thank u Mom and Dad for your seamless patience, words of wisdom, and the independence that you gave. I have no words to thank my sister for her love and affection.

I am very grateful to all kinds of facility provided by CSIR–NCL. I thank the Director, CSIR–NCL for allowing me to present the work in the form of the thesis.

Susanta

Contents

Acknowledgements	ii
Abstract	xii
List of Publications	1
1 Introduction	2
1.1 Introduction and Motivation	3
1.2 General Overview	4
1.3 Metal Clusters	7
1.3.1 General Features	8
1.3.2 Homoatomic and Heteroatomic Metal Clusters	8
1.4 Catalysts and reaction energetics	10
1.5 Types of catalysts	11
1.6 Applications, Advantages and Disadvantages	12
1.7 Motivation for Theoretical Investigation	15
1.8 Enhancement of catalyst by melting: Recent studies and advances	16
1.9 Characterization: Experiment and Theory	19
1.10 General Overview of Reactivity Descriptors	23
1.11 The Concepts of Hardness and Softness Parameters: A Historical Perspective	24

1.12	Reactivity descriptors: Application to the chemical problems	28
1.13	Organization of the thesis	31
2	Theoretical Methods and Computational Aspects	52
2.1	The Schrödinger Equation	53
2.2	The Born – Oppenheimer Approximation	54
2.3	Density Functional Theory	54
2.3.1	Hohenberg–Kohn Theorems	55
2.3.2	Kohn–Sham Method	55
2.4	Classical Molecular Dynamics	57
2.5	<i>Ab Initio</i> Molecular Dynamics	58
2.5.1	Car Parrinello Molecular Dynamics	59
2.5.2	Born Oppenheimer Molecular Dynamics	60
2.5.3	Comparison of CPMD and BOMD	60
2.6	Optimization Techniques	61
2.7	Conceptual DFT	63
2.7.1	Global Reactivity Descriptors	63
2.7.2	Local Reactivity Descriptors	67
2.7.3	Atom Condensed Local Descriptors	69
2.8	Hard Soft Acid Base principle (HSAB)	71
2.8.1	Expression for ΔE_{μ}	75
2.8.2	Local HSAB Principle	76
3	Critical Study of the Charge Transfer Parameter for the Calculation of Interaction Energy Using the Local Hard–Soft Acid–Base Principle	81
3.1	Introduction	82
3.2	Theory	85
3.2.1	Derivation for Charge Transfer Parameter	85
3.2.2	Global and Local Reactivity Descriptors	87

3.2.3	Expression for the Interaction Energy (IE)	89
3.3	Methodology and Computational Details	91
3.4	Results and Discussions	92
3.5	Conclusion	97
4	Understanding the Site Selectivity in Small-Sized Neutral and Charged Al_n ($4 \leq n \leq 7$) Clusters Using Density Functional Theory Based Reactivity Descriptors: A Validation Study on Water Molecule Adsorption	109
4.1	Introduction	111
4.2	Theoretical Methods	113
4.3	Computational Details	115
4.4	Results and Discussion	116
4.4.1	Site selectivity of aluminum clusters using relative reactivity descriptors	116
4.4.2	Understanding the site selectivity in aluminum clusters using explicit water molecule adsorption: Case study on Al_4	122
4.5	Conclusion	123
5	Dinitrogen Activation by Silicon and Phosphorus Doped Aluminum Clusters	140
5.1	Introduction	141
5.2	Computational Details	144
5.3	Results and Discussions	145
5.4	Conclusions	150
6	Effect on Structure and Stability of Aluminum Cluster with the Successive Gallium Substitution	171
6.1	Introduction	172
6.2	Computational Details	175
6.3	Results and Discussion	176

6.3.1	Equilibrium geometries	176
6.3.2	Thermodynamics	177
6.4	Conclusions	180
7	Mechanism for C–I Bond Dissociation in Iodoethane, Iodoethene and Iodoben- zene for the C–C Cross Coupling Reactions over Aluminum Clusters	205
7.1	Introduction and methodology	206
7.2	Results and Discussion	209
7.3	Conclusion and Scope	212

List of Tables

3.1	Value of Charge Transfer Parameters for the Multiple Bonded Complexes. Values are in Atomic Units.	99
3.2	Values of the Chemical Potential (μ), Hardness (η), and Hyperhardness (γ) of all Monomers Calculated at the DFT, MP2, and CCSD(T) Levels. Values are in Atomic Units.	99
3.3	Condensed Local Softness (S_k^+ and S_k^-) ^a of the Reactive Atoms. Values are in Atomic Units.	100
3.4	ΔE_v , ΔE_μ , and Total Interaction Energy of all the Complexes as Described in the Text, Calculated by the Parameters ΔN_{1st} and ΔN_{2nd} using the DFT/6-311G(d,p) Method ^b	100
3.5	ΔE_v , ΔE_μ and Total Interaction Energies (ΔE_{tot}) of all Complexes as Described in the Text, Calculated by the Parameters ΔN_{1st} and ΔN_{2nd} using the MP2/6-311G(d,p) Method ^c	101
3.6	ΔE_v , ΔE_μ and Total Interaction Energy of all the Complexes as Described in the Text, Calculated by the Parameters ΔN_{1st} and ΔN_{2nd} using the CCSD(T)/6-311G(d,p) Method ^d	101
4.1	Structural, Electronic and Reactivity Parameters of Al ₄ conformations. The values given next to the conformations in column II of the table correspond to the inter-atomic distances (in Å) between various unique sites.	124

4.2	Structural, Electronic and Reactivity Parameters of Al ₄ conformations. The values given next to the conformations in column II of the table correspond to the inter-atomic distances (in Å) between various unique sites.	125
4.3	Structural, Electronic and Reactivity Parameters of Al ₄ conformations. The values given next to the conformations in column II of the table correspond to the inter-atomic distances (in Å) between various unique sites.	126
4.4	Structural, Electronic and Reactivity Parameters of Al ₅ conformations. The values given next to the conformations in column II of the table correspond to the inter-atomic distances (in Å) between various unique sites.	127
4.5	Structural, Electronic and Reactivity Parameters of Al ₅ conformations. The values given next to the conformations in column II of the table correspond to the inter-atomic distances (in Å) between various unique sites.	128
4.6	Structural, Electronic and Reactivity Parameters of Al ₆ conformations. The values given next to the conformations in column II of the table correspond to the inter-atomic distances (in Å) between various unique sites.	129
4.7	Structural, Electronic and Reactivity Parameters of Al ₆ conformations. The values given next to the conformations in column II of the table correspond to the inter-atomic distances (in Å) between various unique sites.	130
4.8	Structural, Electronic and Reactivity Parameters of Al ₇ conformations. The values given next to the conformations in column II of the table correspond to the inter-atomic distances (in Å) between various unique sites.	131

4.9	Interaction energy of water adsorption on Al_4 conformations.	132
4.10	Interaction energy of water adsorption on Al_4 conformations.	133
5.1	Ground and excited state conformations of Al_8 and their corresponding N_2 complexes.	152
5.2	Most effective site of Al_7^1Si and Al_7^1P clusters towards N_2 activation. . .	153
5.3	Other potential sites for N_2 adsorption on Al_7^1Si and Al_7^1P clusters. . . .	154
5.4	The $N\equiv N$ bond length fluctuations in $Al_8^1-N_2$, $Al_7^1Si-N_2$ and $Al_7^1P-N_2$ complexes at 300K and 450K.	155
5.5	Mulliken charge analysis of the complexes in ground, excited and doped clusters with N_2 molecule	156
5.6	Ground and excited state conformations of Al_7 and their corresponding N_2 complexes.	157
5.7	Most effective sites of Al_6^1Si and Al_6^1P clusters towards N_2 activation . .	158
5.8	Other potential sites for N_2 adsorption on Al_6^1Si and Al_6^1P clusters. . . .	159
5.9	Ground and excited state conformations of Al_6 and their corresponding N_2 complexes.	160
5.10	Most effective site of Al_5^1Si and Al_5^1P clusters towards N_2 activation. . .	161
5.11	Other potential sites for N_2 adsorption on Al_5^1Si and Al_5^1P clusters. . . .	162
5.12	Ground and excited state conformations of Al_5 and their corresponding N_2 complexes.	163
5.13	Most effective site of Al_4^1Si and Al_4^1P clusters towards N_2 activation. . .	164
5.14	Other potential sites for N_2 adsorption on Al_4^1Si and Al_4^1P clusters. . . .	165
7.1	Thermodynamic data of C–I bond dissociation of ethyl iodide, ethylene iodide and benzyl iodides on Al nanoclusters in B3PW91, BHandHLYP and M06–2X functionals	216

7.2	Thermodynamic data of C–I bond dissociation of ethyl iodide, ethylene iodide and benzyl iodides on Al nanoclusters in B3PW91, BHandHLYP and M06–2X functionals	216
7.3	Thermodynamic data of C–I bond dissociation of ethyl iodide, ethylene iodide and benzyl iodide on Al nanoclusters in B3PW91, BHandHLYP and M06–2X functionals	217

Abstract

In this thesis, we will focus on some aspects of reactivity of molecular systems and metal clusters using density functional theory based global and local reactivity descriptors, viz., chemical potential, hardness, Fukui function and local softness[1–9]. In particular, an attempt will impel to correlate the reactivity pattern of molecular systems using these descriptors in a semi–quantitative way. Essentially, we will propose a new charge transfer parameter to calculate the interaction energy of the multiple site based interactions of prototype molecules in terms of these reactivity descriptors of the individual interacting systems[10–12]. The ad hoc charge transfer parameter will be derive from Sandersons electronegativity equalization principle[13]. The local hard soft acid base principle (HSAB) principle developed by Gazquez and co–workers, is the basis of the proposed model presented in the dissertation[14, 15]. We will investigate the efficiency of the model by taking suitable examples and also discuss the advantages and limitations of the proposed model.

The development of new cost–effective catalysts is a key objective for a cleaner and sustainable chemistry[16–18]. Metal nano clusters with variable number of atoms, finely tunable by doping and phase transitions are the promising catalyst for a large class of chemical reactions[19–21]. The structure of the catalyst itself can be studied by a variety of spectroscopic and crystallographic techniques[22–24]. The surface of the solid presents a variety of sites, including defects such as steps with variable coordination for the active element. Moreover, the nature of the surface can change upon the reaction conditions, and its structure is more difficult to characterize from microscopy and spectroscopy. The determination of the active site is hence a challenge, and most probably several possible *ab initio* methods based on quantum–chemistry and thermodynamics are helpful tool to extract necessary information on them[25, 26].

Thus, the main motivation of this thesis is to use a computational approach to model the metal clusters, to understand the reactivity related to their unique structural features.

In the thesis, we will be mainly studying aluminum clusters doped with Si, P and Ga. N_2 reduction is crucial for life, and very few catalysts are currently available to carry out this process at ambient temperature and pressure[27–31]. Our combined DFT and *ab initio* Born Oppenheimer molecular dynamics (BOMD) based calculations reveal that the Si and P atom doping on Al nano clusters presents new promising catalyst towards di-nitrogen activation. To the other end, in the thesis, we will perform DFT based molecular dynamics (BOMD) to investigate the finite temperature behavior, structure and stability, of the Al cluster with the successive Ga atom doping. In the final chapter of the thesis we would like to study the energetics of C–I bond dissociation, the key step of cross-coupling reaction[32–34], of aliphatic and aromatic halides in the framework of DFT.

The organization of the thesis will be as follows:

Chapter 1

In Chapter 1, we will begin by giving a brief introduction to general definition of catalyst and general terms related to it, such as energetics, type of catalysts, their advantages and applications. Thereafter we will focus on the metal clusters describing the enhancement of their catalytic properties by melting. This will be followed by providing a brief discussion on the recent experimental and theoretical research advances. We describe the peculiar surprises of metal cluster resulting in their stability and size sensitivity. Similarly, the enhancement of reactivity of metal clusters by melting is discussed with several examples in the proceeding section. In addition at the end we will review selected metal cluster reports including Al clusters. We have also discussed in this chapter the reactivity descriptors, Hard Soft Acid Base (HSAB) principle and their application to the chemical problems. We will end the chapter by describing the motivation behind the research carried out and by presenting an outline of the thesis.

Chapter 2

In Chapter 2, we will present an outline of the theoretical framework behind the methodology used in the most part of the work presented in the thesis. We begin the discussion on the use of density functional theory (DFT) as an alternative route for performing

quantum chemical calculations. Next, a description of the concepts of molecular dynamics and *ab initio* molecular dynamics will be given and also explain and compare the ideas and algorithms behind Born–Oppenheimer molecular dynamics and Car–Parrinello molecular dynamics. Lastly, we will briefly review the earlier theoretical developments made towards the broad subject of chemical reactivity using the quantum chemical methods and describe how the empirical conceptual ideas (electronegativity, chemical potential, hardness, softness, etc.) have been theoretically quantified within the framework of DFT. The success and failure of these descriptors in predicting the reactivity of molecular systems will be discussed in detail along with other recent developments and applications that are relevant to the present objective of the thesis. We will then outline the energy–density perturbation methods within the domain of DFT and the different semi–quantitative models, including local HSAB principle, in finding a direct correlation between the density based descriptors and the molecular interaction energy.

Chapter 3

In this chapter, we calculate interaction energy of several prototype organic molecules with multiple site based weak interactions using local hard–soft acid–base (HSAB) principle. The local HSAB principle is semiquantitative in nature due to the presence of an *ad hoc* charge transfer parameter. The accuracy of HSAB principle significantly depends on the definition of this *ad hoc* parameter. For the first time, we will derive the second–order approximation of ΔN (ΔN_{second}) as an *ad hoc* parameter for charge transfer to calculate interaction energies of multiple site based interactions using local hard soft acid base principle. The second – order approximation of ΔN will be derive from Sandersons electronegativity equalization principle. To validate our approach, we will study interaction energies of several prototype molecules. The interaction energies obtain from our approach will be further compare with the interaction energies of those obtained using other charge transfer parameters (ΔN_{first} and λ) and the conventional methods. We will further discussed the advantages and limitations of the approach.

Chapter 4

In the chapter 4, we study reactivity of aluminum clusters. Aluminum clusters are technologically important due to their high catalytic activity. Our study on the small-sized aluminum clusters applies density functional theory (DFT)-based reactivity descriptors to identify potential sites for adsorption and eventual chemical reaction. Depending on symmetry, susceptibility of various type of reactive sites within a cluster toward an impending electrophilic and/or nucleophilic attack will be predict using the reactivity descriptors. In addition, the investigations devises general rules as to how the size, shape, and charge of the cluster influences the number of available sites for an electrophilic and/or nucleophilic attack. The predictions by reactivity descriptors will be validate by performing an explicit adsorption of water molecule on Al clusters. The adsorption studies reveal that the most stable water-cluster complex is obtained when the molecule is adsorbed through an oxygen atom on the site with the highest relative electrophilicity.

Chapter 5

In this present chapter, we will study di-nitrogen activation on the doped aluminum clusters. As we know, N_2 reduction is crucial for life, and very few catalysts are currently available to carry out this process at ambient temperature and pressure. In this chapter, density functional theory based calculations demonstrate doped aluminum clusters to be highly reactive toward molecular nitrogen and hence are prospective materials for its activation at low temperatures. Calculations on silicon and phosphorus doped aluminum clusters with 5–8 atoms reveal an enhanced N_2 activation with respect to their pristine ground state and high energy counterparts. This increased efficiency of N_2 activation by doped ground state Al clusters is corroborated by an increment of the $N\equiv N$ bond length, a red shift in $N\equiv N$ bond stretching frequency, and adsorption energy (E_{ad}). *Ab initio* molecular – dynamics simulations exhibit consequential efficiency of doped clusters toward dinitrogen activation at finite temperature. The ability of doped clusters toward activation of molecular nitrogen is site and shape sensitive. In short, this theoretical study highlights the critical role of doping foreign impurities for future endeavors in the design of cost-effective and efficient catalysts for N_2 activation at ambient temperatures. This

observation may spur further studies in the field of aluminum nanocatalysis by doping silicon and phosphorus atom in aluminum clusters.

Chapter 6

In the chapter 6, we will investigate structure and stability of aluminum clusters with successive substitution of gallium atom. Stability and electronic charge on a aluminum clusters are two main factors governs its catalytic property. However, little is known on the finite temperature behavior of various aluminum cluster conformations. Much less is known the effect of doping with successive increasing ratio. In this chapter, we will carry out *ab initio* density functional theory (DFT) based molecular dynamics simulations (BOMD) on pure and successive gallium doped on Al_8 clusters with an aim of understanding the thermodynamic properties of ground state conformations as a function of doping ratio. Our simulations reveal cluster properties does not follow a monotonic relation with the increasing doping percentage. 12.5%, 25% and 37.5% doping of gallium (i.e Al_7Ga_1 , Al_6Ga_2 , and Al_5Ga_3) become liquidlike at much lower temperature (200 – 250K) than its pristine Al_8 analogue (450K). On the other hand, cluster with 50% gallium doping (i.e Al_4Ga_4) remarkably stable (solidlike upto 600K) as compared to its pristine counterpart. In order to look into the factors leading to the stabilization structural and electronic properties will be analyze. Factors such as charge redistribution within the atoms and composition of molecular orbitals are seen to contribute towards stronger Al – Ga bonds in Al_4Ga_4 thereby stabilizing it considerably.

Chapter 7

In the last chapter, we would like to study energetics of the key step of cross-coupling reaction, dissociation of aliphatic and aromatic iodides using aluminium nanoclusters as catalyst. Density functional theory will be use to understand the facts. In spite of being an unconventional catalyst for radical polymerization, cross-coupling or similar type of reactions in bulk state, selected Al clusters (size 3 to 20 atoms) can show significantly low activation barrier. Further investigations exploits the activation energies are sensitive to the shape and electronic structure of catalyst rather than the size of them, making

Abstract

the Al clusters attractive in the area of nanocatalysis and nanoscience. To understand the insight into the reaction mechanism, mode of binding will be investigate with the *ab initio* Born Oppenheimer Molecular Dynamics (BOMD) simulation and the Natural Bond Orbital (NBO) analysis. In short, our theoretical study highlights the efficiency of the aluminium clusters for future endeavors in the design of cost-effective and efficient catalyst for cross-coupling reaction.

Bibliography

- [1] Fukui, K. Theory of Orientation and Stereo Selection *Springer-Verlag, Berlin* **1975**
- [2] Chermette, H. *J. Comput. Chem* **1999**, *20*, 129 – 154.
- [3] Parr, R.G.; Yang, W. *Oxford University Press, New York* **1989**
- [4] Chandra, A.K.; Geerlings, P.; Nguyen, M.T. *J. Org. Chem.* **1997**, *62*, 6417 – 6419.
- [5] Geerlings, P.; Vivas – Reyes, R.; De, P.F.; Biesemans, M.; Willem, R. *NATO Sci Ser, II* **2003**, *116*, 461 – 495.
- [6] Roy, R.K. *J. Phys. Chem. A.* **2004**, *108*, 4934 – 4939.
- [7] Chandrakumar, K.R.S.; Pal, S. *Colloids and Surfaces* **2002**, *205*, 127 – 138
- [8] Roy, R.; Chandra, A.K.; Pal, S. *J. Phys. Chem.* **1994**, *98*, 10447 – 10450
- [9] Kar, R.; Chandrakumar, K.R.S.; Pal, S. *J. Phys. Chem. A.* **2007**, *111*, 375 – 383
- [10] Pal, S.; Chandrakumar, K.R.S. *J. Am. Chem. Soc.* **2000**, *122*, 4145 – 4153
- [11] Chandrakumar, K.R.S.; Pal, S. *J. Phys. Chem. A.* **2002**, *106*, 5737 – 5744
- [12] Chandrakumar, K.R.S.; Pal, S. *J. Phys. Chem. B.* **2001**, *105*, 4541 – 4544
- [13] Bratsch, G. S. *J. Chem. Educ.* **1984**, *61*, 588
- [14] Gazquez, J. L. *J. Phys. Chem. A* **1997**, *101*, 8967 – 8969
- [15] Gazquez, J. L. *J. Phys. Chem. A* **1997**, *101*, 9464 – 9469
- [16] Rezaeifard, A.; Haddad, R.; Jafarpour, M.; Hakimi, M. *ACS Sustainable Chem. Eng.* **2014**, *2*, 942 – 950
- [17] Kumar, M.; Deka, S. *ACS Appl. Mater. Interfaces* **2014**, *6*, 16071 – 16081

- [18] Xing, M.; Kong, L - B.; Liu, M - C.; Liu, L - Y.; Kang, L.; Luo, Y - C. *J. Mater. Chem. A* **2014**, *2*, 18435 – 18443
- [19] Khanna, S. N. Jena, P. *Phys. Rev. B* **1995**, *51*, 13705 – 13716
- [20] Liddicoat, P. V.; Liao, X.-Z.; Zhao, Y.; Zhu, Y.; Murashkin, M. Y.; Lavernia, E. J.; Valiev, R. Z.; Ringer, S. P. *Nat. Commun.* **2010**, *1*, 1062 – 1062
- [21] Jarrold, M. F.; Bower, J. E. *J. Am. Chem. Soc.* **1988**, *110*, 70 – 78
- [22] Chakrabarty, R.; Bora, S. J.; Das, K. B. *Inorg. Chem.* **2007**, *46*, 9450 – 9462
- [23] Kulkarni, A.; Lobo - Lapidus, J. R.; Gates, C. B. *Chem. Commun.* **2010**, *46*, 5997 – 6015
- [24] Chen, Y.; Trzop E.; Makal, A.; Sokolow, D. J.; Coppens, P. *Inorg. Chem.* **2013**, *52*, 4750 – 4752
- [25] De, S. H.; Krishnamurty, S.; Pal, S. *J. Phys. Chem. C* **2010**, *114*, 6690 – 6703
- [26] Willis, B. G.; Jensen, K. F. *J. Phys. Chem. A* **1998**, *102*, 2613 – 2623
- [27] Deng, H.; Hoffmann, R. *Angew. Chem., Int. Ed.* **1993**, *32*, 1062 – 1065
- [28] Schrock, R. R. *Angew. Chem., Int. Ed.* **2008**, *47*, 5512 – 5522
- [29] Gambarotta, S.; Scott, J. *Angew. Chem., Int. Ed.* **2004**, *43*, 5298 – 5308
- [30] Kerpál, C.; Harding, J. D.; Lyon, T. J.; Meijer, G.; Fielicke, A. *J. Phys. Chem. C* **2013**, *117*, 12153 – 12158
- [31] Roy, D.; Navarro – Vazquez, A.; Schleyer, P. v. R. *J. Am. Chem. Soc.* **2009**, *131*, 13045 – 13053
- [32] Gagnon, A.; Duplessis, M.; Alsabeh, P.; Barabé, F. *J. Org. Chem.* **2008**, *73*, 3604 – 3607

[33] Lauterbach, T.; Livendahl, M.; Rosellón, A.; Espinet, P.; Antonio, M. A. *Org. Lett.* **2010**, *12*, 3006 – 3009

[34] Nijamudheen, A.; Datta, A. *J. Phys. Chem. C* **2013**, *117*, 21433 – 21440

List of Publications

1. Deepti Mishra , Susanta Das, Sailaja Krishnamurty and Sourav Pal, ‘Understanding the Orientation of Water Molecules Around the Phosphate and Attached Functional Groups in a Phospholipid Molecule: a DFT-Based Study’ **Molecular Simulation**, 2013, 39, 937 – 955.
2. Susanta Das, Sailaja Krishnamurty and Sourav Pal, ‘Understanding the Site Selectivity in Small-Sized Neutral and Charged Al_n ($4 \leq n \leq 7$) Clusters Using Density Functional Theory Based Reactivity Descriptors: A Validation Study on Water Molecule Adsorption’ **J. Phys. Chem. A**, 2013, 117, 8691 – 8702.
3. Susanta Das, Sapana V. Shedge and Sourav Pal, ‘Critical Study of the Charge Transfer Parameter for the Calculation of Interaction Energy Using the Local Hard-Soft Acid-Base Principle’ **J. Phys. Chem. A**, 2013, 117, 10933 – 10943. .
4. Susanta Das, Sailaja Krishnamurty and Sourav Pal, ‘Dinitrogen Activation by Silicon and Phosphorus Doped Aluminum Clusters’ **J. Phys. Chem. C**, 2014, 118, 19869 – 19878.
5. Susanta Das, Turbasu Sengupta, Achintya Kumar Dutta and Sourav Pal, ‘Electron Detachment and Subsequent Structural Changes of Water Cluster’ (Submitted to **J. Phys. Chem. B**).
6. Rupesh Gawade; Debamitra Chakravarty, Amol Kotmale, Ekta Sangtani; Pranaya Joshi, Susanta Das, P. Rajamohanan, Vedavati Puranik and Rajesh Gonnade, ‘Additive Mediated Syn-anti Conformational Tuning at Nucleation: Remarkable Role of Extended π -Stacking Interactions in Driving the Self-Assembly’ (Submitted to **Chem. Sci.**)
7. Susanta Das, Sailaja Krishnamurty and Sourav Pal, ‘Effect on Structure and Stability of Aluminum Cluster with the Successive Gallium Substitution’ (Manuscript in preparation).

CHAPTER 1

Introduction

1.1 Introduction and Motivation

Chemistry in the 20th century was characterized by tremendous growth and advances, stimulated by revolutionary theories and experimental breakthroughs. It has built our current society by providing energy, local grocery, crop protection, drug, foodstuffs, and new materials worldwide. Unfortunately, even though chemistry is the central science being an impressive array of commonly use of chemical tools, chemicals and the chemical industry still have lacking of good public image. Many people have fear due to hazardous and polluting nature of traditional chemical processes. In recent times, the accelerating costs of petrochemicals, medicine, and raw energy materials demands in emerging markets of worldwide, are forcing a change. Two important terms correlated with this change are sustainability and sustainable development. A sustainable modern society is one that meets the needs of the current generation without sacrificing the ability to meet the needs of future generations. Sustainable development can be reached using the strategic goals, the practical approaches, and the operational and monitoring tools. For example, if you use less or no solvent, and replace stoichiometric reagents with catalytic cycles, reactor space–time yields go up[1]. To achieve this objective, research into catalytic materials is developing rapidly, so as to elucidate their fundamental properties for synthesizing specifically–tailored materials for various applications. In addition, finding new methodologies such as providing environment friendly process using the existing knowledge about these important and remarkable materials is a ongoing research problem. As pressure increases on the World’s finite and dwindling supplies of hydrocarbons, obtained mainly from crude oil developments, the use of zeolites and metal clusters as catalysts to render known hydrocarbon cracking and oxidation chemistry is more efficient. Decoration of such type of materials need proper invention, experimentation, and developing an understanding of the fundamentals of their structure, bonding and reactivity. Advances in theoretical methods are likely to play an increasing role in predicting the

features and synthetic viability of modified and novel catalyst structures. In this chapter we have given detail discussion of metal clusters, definition of catalyst, type of catalysts and the general overview on the use of these materials as the novel catalyst including their advantages and applications. We have also discussed in this chapter the reactivity descriptors, Hard Soft Acid Base (HSAB) principle and their application to the chemical problems in detail. We end the chapter by describing the motivation behind the research carried out herein and by presenting an outline of this thesis.

1.2 General Overview

The first quantum mechanical description of the electron pair bond was that given by Heitler and London for the hydrogen molecule in 1927[2]. This theory was further developed by Pauling and others in the 1930s, into a comprehensive theory of bonding called VBT[3–6]. This revolutionized the field of chemistry, encompassing all chemical structures from hydrogen molecule to DNA and to solids. In VBT the wavefunction is constructed in such a way that the two electrons can never be found on the same atom and hence their motion is correlated. Important chemical concepts of valence electrons such as resonance, octet rule and hybridization were first formulated as a part of VBT. However, in VBT the atomic orbitals are not orthogonal and hence the theory becomes more complicated as the number of atoms in the molecule increases. Moreover, Heitler and London wavefunction does not correspond to the virial theorem and is a poor approximation to the true wavefunction of the system. Parallel with the development of VBT, another type of quantum mechanical approach, the MOT was developed. MOT is based on the concept of LCAO, which involves the assignment of electrons to molecular orbital, which are in general delocalized over the whole molecule and are uncorrelated, unlike the electrons in VBT. Most of the problems of VBT, such as the virial theorem, excited states, orthogonality, etc. were solved by MOT in a much simpler form. Nevertheless, due to the localized electrons, VBT becomes more useful in describing reactions

and bond dissociation[7]. One can say that, VBT and MOT are two different but complementary models of the same phenomenon. However, nowadays most of the calculations are performed by MOT on account of its simplistic mathematical approach. Some of the theoretical models such as, HF, CI, DFT, CC, etc., based on MOT, have been successfully applied to study the electronic properties of systems containing few electrons[8]. Along with this, the development of the present day computer technology has made possible to apply the theory with ever greater accuracy to carry-out the simulations of more complex chemical systems. Hence, the results of the simulations are of great help to guide the experimental work. Among the theoretical methods, DFT has emerged as one of the most successful method to investigate large systems[9]. In DFT, the electron density is the basic variable instead of the wave function. This makes it computationally much more cheaper than the conventional *ab initio* methods, while retaining much of their accuracy. This feature is also a strong motivation to adopt DFT as a theoretical tool to study large molecules or clusters or even periodic solids.

In recent years, success of nanotechnology has made cluster science more interesting because large cluster sizes can eventually bridge with the nanosize materials in a more comprehensible way[10–12]. Secondly, with the advent of new experimental techniques, it has now become possible to produce and analyze clusters consisting of several hundred atoms while the lower limit for the size of nanoscale particles has reached less than 1 nm. Experiments have demonstrated that the properties of clusters depend uniquely on their size and composition and that they evolve differently[12]. This fundamental behavior has made researchers to use clusters as building blocks for new materials. One of the most well known ‘new’ clusters or nanostructures, are so called fullerenes which belongs to carbon family, discovered in 1985. The fullerenes are symmetrical hollow structures of carbon[13, 14]. This significant discovery explored a new field of carbon nanotubes and a new perspective to the research in the field of materials science[15, 16]. The exciting discovery of superconductivity at high temperature was achieved by doping K, Rb, Cs in C₆₀ fullerenes[17–19]. Other attempts of encapsulating atoms and molecules in C₆₀ had

been successfully carried out. Moreover, clusters have been shown to have technological importance in catalysis, photographic films, magnetic recordings, etc. Several types of clusters materials are familiar such as atomic clusters, molecular clusters, metallic clusters, organic clusters, quantum dots. Each clusters have their own specific features and properties. Metal clusters are among the more complex and interesting ones from both, fundamental and technological points of view. Indeed, metal clusters play an important role between the isolated atoms and bulk metal. Study on metal clusters address the evolution of shape sensitive behavior, properties with size, particularly those, such as structural, electronic, magnetic and optical properties[11–14]. As the dimension of the metal clusters goes on decreasing quantum effects becomes much more prominent and affect the behavior of e.g. the B. E., ionization potentials, polarizabilities, optical spectra, etc[20–22]. Such changes in the electronic structure can affect the bonding and other physical and chemical properties of metal clusters. With the advance of computational power, in the last few years, it has been possible to apply the theory to larger clusters. Since the clusters do not have the periodicity as in crystals, the same theoretical tools that are used to study molecules in gas phase can be used to study them. Lithium and sodium clusters are among the examples of metal clusters, which have been extensively studied in the last decade by experimental and theoretical methods[23, 24]. The reason for this is obviously the less computational effort. However, recently Li has been very important in the applications of Li batteries[25]. It has been found that some of the metal clusters are more abundant than the others due to exceptional stability as reflected in the mass spectra. These kinds of metal clusters have been referred to as ‘magic’ clusters[11, 12]. This was analogous to the shell filling in atoms and nuclei and the stability of these particular metal clusters was explained on the basis of electron shell filling. These kind of metal clusters were first observed in the mass spectra of Na. Pure boron is a large band–gap semiconductor. The allotropes of boron have been characterized on the different arrangement of the B₁₂ icosahedra. Hence, one might be interested in the properties of boron clusters leading to different structural arrangement. Although, boron and carbon are neighbors in

the periodic table, they vastly differ in their properties. Nevertheless, many studies have been carried out to show many chemical similarities between them. Recently Boron has been shown to form nanostructures similar to that of carbon nanostructures[26–28]. Boron clusters have been widely studied by Hanley and Anderson[26, 29, 30]. The other member belonging to the boron family is the Al. The important issue in the Al is that, unlike the alkali clusters the shell model does not hold for small Al clusters. Extensive theoretical and experimental research have been performed on Al clusters to explore their electronic and geometrical properties[31, 32]. Al_7^+ and Al_{14}^+ appear as magic clusters in some mass spectra of Al clusters. Cox *et al.* have investigated the reactions of neutral aluminum clusters with a number of different molecules[33]. Jarrold *et al.* have measured the activation barrier of the adsorption of D_2 on the Al clusters[34, 35]. It is believed that the transition metal atoms form the most reactive clusters, this is due to their unfilled d-orbitals, resulting in high coordination number[22]. The other way in which the metal clusters differ from their bulk is when they are alloyed. A single impurity in a metal cluster can create a drastic change in electronic and bonding properties. There are several reviews in which the stoichiometry of the different atoms have been related to the change in the chemical properties of the mixed metal clusters[36–39]. Recently, Li *et al.* showed that Al behaves as C of benzene in some Al–Li mixed clusters[40].

1.3 Metal Clusters

One of the fundamental goals of nanotechnology is to understand and characterize the properties at the atomic-scale. The study of metal clusters enables us to interpret such fundamental aspects and to explain the behavior of the nanoscale systems as their sizes and compositions are changed atom by atom.

1.3.1 General Features

Clusters are aggregates of atoms or molecules, intermediate in size between individual atom and bulk. Clusters are different from both molecules and solids, and for this reason can have very different properties. Molecules are characterized by having definite and unique structure and specific composition. On the other hand clusters may be composed of any number of particles and have a tendency to grow. As the number of particles of the cluster becomes larger, the number of locally stable structures (isomers) of the cluster grows rapidly. Some fundamental questions which can be raised about the clusters are, for e.g. (1) how does the physical property of a cluster change as the size of the cluster is evolved ?; (2) When does a transition from atomistic scale to a bulk scale take place ?; (3) Does the stability of the cluster increase monotonically with the size ?; (4) Does the cluster property suddenly change when it is doped with an impurity? For the last few years, an extensive experimental and theoretical research has been carried out to answer the above questions. The most interesting are the metal clusters where the transition from a localized (covalent or ionic) to a delocalized (metallic like) bonding occurs as the size of the cluster increases[10, 11, 13]. Therefore metal clusters are expected to show abundant peculiar and interesting behavior that are apparent from those of individual molecules or bulk solids materials. Structure and stability are the most important properties of the metal clusters, which can be correlated with the type of atom–atom bonds formed in the metal cluster. In general there are four types of bonds which can be distinguished within the metal clusters viz. covalent, ionic, metallic and van der Waal[13].

Among these clusters, covalent and ionic clusters are supposed to be the most stable clusters due to strong interatomic bonds.

1.3.2 Homoatomic and Heteroatomic Metal Clusters

Metal clusters can be classified as homoatomic and heteroatomic (or mixed) clusters according to their composition i.e. homoatomic metal clusters contain same type of atomic

species, on the otherhand heteroatomic clusters are made up of different type of atomic species. Several groups extensively have been carried out experimental and theoretical research on the structural and electronic properties of homoatomic metal clusters such as Li, Na, K, Al, Sn etc[20, 41–44]. Generally, the bonding in homoatomic clusters containing less than 10 atoms can be characterized as covalent. Thus, in these clusters the possibility of isomerization at a relatively low temperature is expected to be less. However, as the number of atoms increases, the delocalization of electrons within the cluster grows eventually, converting it into a metallic like behavior. It is worth mentioning that the delocalization occurring in the homoatomic covalent clusters such as carbon, resulting into graphite, is different from the delocalization due to metallic bonding in metals (Group Ia and IIb). The delocalization in the graphite is more directional than the delocalization in the Li or Na bulk. Among the elements of group 13, less work has been carried out on Ga, In and Th clusters[45]. Relatively, more detailed study has been done on Al and B clusters[30, 32, 34]. Some of the homoatomic metal clusters that have been studied are Be, Mg, Al, Sn, Si and transition metals[12, 21, 22]. In the last decade, similar investigations have been extended to study the heteroatomic clusters, but comparatively to a lesser extent than the homoatomic metal clusters. One of the reasons for this would be the complexity produced by the additional interactions of the unlike atoms (hetero interactions) within the heteroatomic clusters. Due to this reason, heteroatomic clusters are shown to have interesting properties. In small clusters, even a single impurity can significantly alter the geometrical and electronic properties. For example, an unstable homoatomic metal cluster can be converted to a stable ‘magic’ cluster by doping with a single impurity[46–48]. Zhao *et al.* have recently studied carbon doped aluminium clusters using mass spectrometric and *ab initio* methods[48]. They showed Al₇C–cluster to be magic with extremely high stability. Kumar and Sundararajan have shown that the substitutional doping of Al₁₃ cluster by a tetravalent atom leads to a more stable cluster[49]. Joshi *et al.* have studied the structural and electronic properties of Sn doped Li_n clusters using AIMD simulations[50].

Binary clusters such as A_xB_y also belong to the class of mixed clusters. Different kinds of alloys can be formed by changing the proportion of A and B of these binary clusters[51–53]. Changing the stoichiometry of different kinds of atoms provides another interesting way of improving the reactivity and selectivity of clusters possibly in the context of catalysis. Bonačić–Kouteck *et al.* have discussed the structural stability and ionization potential of some Ia–IIa mixed metal binary clusters[20]. Chacko *et al.* have worked on some Al_4X_4 mixed clusters where (X=Li, Na, K, Be, Mg, B and Si)[54]. Recently, in some interesting works, aluminum based alkali clusters were shown to exhibit aromaticity properties[40]. The other interesting works on mixed–metal clusters are on GaAs, AlAs and AuIn[55, 56].

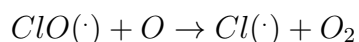
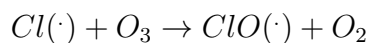
1.4 Catalysts and reaction energetics

One of the high impact industrial applications of catalyst is lowering the hard conditions of reaction processes. Catalysts facilitated chemical reactions to take place much faster rate or at lower temperatures by providing an alternative efficient reaction route of lower activation barrier for a reaction. This is done by inducing some changes in reactants while the catalyst remains chemically unchanged.

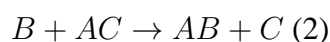
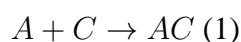
In short, catalysts reduce the total amount of energy require to start and complete a particular reaction. Reactants that would not have sufficient amount of energy to react or so that reaction probably would have taken a long time to form the product(s) are able to participate in chemical reaction in the presence of a catalyst with much faster rate. Catalyst is not adsorb in the reaction process so each catalyst can take part in several consecutive cycles. Therefore basically chemist needs only a pinch amount of catalyst molecule with respect to the reactants. catalyst's efficiency, measured in terms of turnover number (TON) is determined by the substrate/catalyst for a specific reaction.

1.5 Types of catalysts

Catalysts mainly are divided into two classes – homogeneous and heterogeneous. homogeneous catalysts participate in the same phase chemical reaction (e.g. a dissolved catalyst in a liquid reaction mixture) whereas heterogeneous catalysts are present in a different phase from that of the substrates (e.g. a solid catalyst in a liquid reaction mixture). A general model for heterogeneous catalysis involves the catalyst supplying a solid surface on which the substrates are temporarily adsorbed. For example, in industrial Haber–Bosch process which is used to production of ammonia, finely divided iron (iron surface) play a role of heterogeneous catalyst. The active site of finely divided iron aids in partial weak bonding interaction with the reactant gases. As a consequence, the bonding interactions within the molecules (reactants) are weakened, which allow to the reactants come close vicinity to each other. Following this way the strength of the very strong triple bond in nitrogen is reduced and easy to break. During this process hydrogen and nitrogen atoms are imported considerably closer than would be the case in the gas phase, thus the rate of reaction increases. It is important to mention, Turn Over Number (TON) and Turn Over Frequency (TOF) per active site, or per gram catalyst are the two important terms in heterogeneous catalysis. This is because one does not know exactly how many chemically active sites which participates in the process are on the surface. Several other such available and commonly used heterogeneous catalysts include nickel surface in the margarine production, vanadium oxide preparation in the contact process, production of alumina and silica in the cracking of alkanes and multi-metallic platinum, palladium and rhodium surfaces as a catalytic converters in car engines. A typical example of homogeneous catalysts are $H^+(aq)$, play a role as a catalyst in esterification reaction and chlorine free radicals (in the depletion of ozone layer). Chlorine free radicals are yields during the ultraviolet radiation on chlorofluorocarbons (CFCs). They combine with with transiently stable ozone molecule producing di-atomic oxygen molecules and recreating chlorine free radicals as follows:



In general homogenous catalysts react with one or more substrates yields a reaction intermediate which reacts to form the actual product of the reaction and in the end of each cycle the catalyst is regenerated for further use. Following is a typical reaction scheme, where C represents the homogeneous catalyst:



In homogeneous catalysis, the TON is the number of cycles that a catalyst can run through before it deactivates, i.e., the number of A molecules that one molecule of catalyst can convert into B molecules. The TOF is simply TON/time, i.e., the number of A molecules that one molecule of catalyst can convert into B molecules in one second, minute, or hour. Thus, the catalyst opens a selective route to the desired product. There are various kinds of product selectivity.

1.6 Applications, Advantages and Disadvantages

There are many different catalyst compounds. They range from the proton, H^+ , through Lewis acids, metal clusters, organic and inorganic polymers, organo-metallic complexes, and enzymes. However, their application is based on the type of reaction to be catalyzed. The main categories of reactions catalyzed by homogeneous catalysts are: oxidative addition; reductive elimination, dissociation and coordination; insertion and migration; de-insertion and β -elimination; and nucleophilic or electrophilic attack on a coordinated reactants. Several homogeneous catalysts are formed by metal atom mainly transition metal, which is stabilized by a various organic ligand, simply known as organo-metallic complexes. The ligand is mostly an organic molecule that coordinate with metal atom. The main advantage of an organo-metallic homogeneous catalyst is the tunability of catalyst's property by changing this ligand. It is very important to select the right metal

and the right ligand which enhance the reactivity selectivity, and stability of a catalyst (high TON). The most commonly used homogeneous organo-metallic compounds as catalyst include $\text{Rh}[\text{P}(\text{Ph})_3]_3\text{Cl}$, $\text{Cr}(\text{CO})_6$, $\text{IrCl}(\text{CO})[\text{P}(\text{C}_6\text{H}_5)_3]_2$, $\text{Ti}(\text{OiPr})_4$, $\text{Cu}(\text{OTf})_2$, $\text{Ni}[\text{P}(\text{Ph})_3]_3$, DIOP, BINAP, dpp-benzene, Xantphos, $\text{Ni}(\text{CO})_4$ and many more. Apart from this some species without metal co-ordination helps to speed up various organic reactions. This typically points the classic acid/base catalysis simply by H^+ and OH^- . Examples are aldol reactions, esterifications and trans-esterifications, and synthesis of nitroaromatics such as 2-methyl-1, 3, 5- trinitrobenzene. Brønsted acids catalyze reactions by protonating nucleophilic sites such as lone pairs on O or N atoms or alkene π -bonds. Another class of acid catalysis is organocatalysis. This type of catalysts are small organic molecules, primarily build with H, C, N, O, S, and P atoms. These molecules often acts as a Lewis acids or bases. Organocatalysts exhibit certain advantages over organometallic complexes: especially this class of catalyst are metal free, non-hazardous, in-toxic, inexpensive, readily available, and many of them are air- and water-stable. Metal free catalyst has significant advantage in itself: This type of catalyst are environment friendly. Metal separation and recovery are not required at the end of the reaction. Further more, organocatalysts are much less toxic and recyclable as compared to organo-metallic analogues. The typical examples of organocatalysts are piperidine praline, Cinchona alkaloid.

It is important to mention that, two of the seven Nobel Prizes in chemistry given this century were awarded for tremendous contribution in homogeneous catalysis: In 2001 William Knowles[57] and Ryoji Noyori[58] shared the prize with Barry Sharpless[59] for their contributions to asymmetric hydrogenation and oxidation catalysis, respectively. Four years later, Yves Chauvin[60], Robert Grubbs[61], and Richard Schrock[62] shared the prize for their contribution to metathesis catalysis. Significant advantage of homogeneous catalysis over heterogeneous part is the high reactivity and selectivity, which can be tuned by altering the molecular properties of catalyst. Moreover, the reactions, catalyzed by homogeneous catalyst are not impeded by the effects of solid surface, phase

transfer limitations or mass–transfer problems. Each and every catalytic reactive sites are available and all single metal atom is a potential active site. Despite these considerable advantages of homogeneous catalysis, the disadvantage is the difficulty of the process of catalyst separation, recovery and recycling.[63] Commonly used homogeneous catalysts are very sensible to heat, and decompose below 150ÅC. Thus distillation, even at reduced pressure, will lead to catalyst decomposition. Distillation at low pressure is also open to doubt, because a catalyst optimized for working under the condition of high pressure reaction may be subjected to unwanted side–reactions under reduced pressure. This often prevents their scientific successes from becoming commercial ones.

On the contrary, heterogeneous catalysis always take part in the catalytic reaction in the different phase with the substrates. Most commonly heterogeneous catalysis occurs to a chemical system where the catalyst is a solid thin surface and the substrates are either in gases or liquid phase. Heterogeneous catalysis mainly was used in the petrochemicals industries. Commonly used model catalyst systems contain glassy metals, oxide films[64, 65] and thin metal[66], supported catalysts based on chemical vapor deposition[67], and supported homometallic and bimetallic clusters and oxides[68–70]. Solid catalysts are also works well in clean and green energy applications such as solar energy conversion[71, 72] and fuel cells[73, 74]. The most preferred material for various chemical processes is the metallic surface[75–77]. Another such recently developed noticeable catalytic materials constitute clusters of various metallic and non–metallic elements. The cluster size varies from few to several hundred atoms combination. Experiments have demonstrated that the properties of clusters uniquely depend on their size and composition and that they evolve differently. These tiny surfaces exhibit the emphatic chemical and physical properties. This leads to potential applications of these materials in oxidation chemistry[78, 79]. Especially the melted analogues of these clusters are helpful in bringing down the tedious reaction. The latter characteristic of these clusters are hence useful to change the traditional high temperature, pressure demanding

processes in applications like hydrocarbon cracking, diffusion, polymerization etc. Heterogeneous catalysis process is much easy for catalyst separation, which is one of the major advantage to use this catalyst. In gas/solid systems the solid surface (catalyst) is easily removed and cleaned. On the other hand in liquid/solid systems, a simple filtration process can easily separate the catalyst from the reactants.

1.7 Motivation for Theoretical Investigation

At first glance, heterogeneous catalysis seems astounding. It is highly useful and the most sophisticated of the main two catalysis sub regimen, including inorganic, physical, organic, surface science, materials science and organo–metallic chemistry. Apparently heterogeneous catalysis seems strikingly simple: substrates passing through the reactor, form products and leave it. But inside mechanism is extremely complicated: reactants must diffuse through the catalyst pores, adsorb on its surface, travel to the active site, react there, and desorbs back to the gas phase. Each and every steps occurs at the microscopic level (molecular level). This microscopic behavior cause the main complicity of heterogeneous catalysis process. Unlike the homogeneous catalysis, bulk parameters such as particle size, shape, and mechanical strength are critical here. The interaction between reactants and catalyst surface determine the key to the catalysts efficiency, selectivity, and stability. Two other decisive dependency for catalytic activity are heat transfer and mass transfer. Metal crystal surfaces has several steps and kinks at the molecular level Thereby, the surface atoms cannot coordinate fully and thus have more options for interacting with reactant molecules[80–82]. However, one can predict the properties and performance of new catalysts by combining the data from high–throughput experimentation with statistical analysis and descriptor models (in–silico design)[79, 83]. The significant advancement of sophisticated chemical tools such as XRD, EXAFS, mass spectrometry, in situ IR and NMR analysis techniques allow to the modern chemist to investigate reaction kinetics, life time of catalytic intermediates under the actual reaction

conditions[84, 85]. Several class of of catalyst descriptors, ranging from very simple ones based on composition parameters to ones in the framework of *ab initio* quantum computations. Theoretical investigation give better insight of the reaction mechanisms and find out the possibility of new exciting reactions. Computer modeling can give a crude idea of the properties of new catalysts and materials. This theoretical molecular modeling has remarkable impact for ones that are difficult to synthesize in the laboratory. simulations are essential in industrial process design, where any changes in the reactor configuration are very costly. With increases the power and accuracy of computation, modern chemist can actually simulate any experimental conditions, together with reactions at very high or temperatures and pressures using *ab initio* molecular dynamics, which are almost impossible and risky to set up in the laboratory. Molecular modeling of such catalysts not only save much synthetic effort but also saves chemical and financial dissipation. In addition, Simulations let us observe reactions and species that are inaccessible by experiment, such as the transfer of single protons, intermediates and even the transition states. Thus main aim of the present thesis is to apply a combined, DFT and MD approach basically known as AIMD, to study the structural, bonding properties and hence finally reactivity of aluminum metal clusters.

1.8 Enhancement of catalyst by melting: Recent studies and advances

It is well known that in the nano regimen, small size metal clusters with 10–150 atoms can demonstrate phase transitions i. e. melting between solid–like and liquid–like states. This melting transition can be very sharp or flat and it obey first order characteristics. This have been observed experimentally from the peak of the heat capacity. Several research groups have experimentally investigate the phase transitions for a various metal cluster such as sodium[86–93], tin[94, 95], gallium[96–98] and aluminum[99–103] and

these measurements further supported by number of computational studies[104–108]. The experimental findings have affirmed considerable size dependent fluctuations in the melting temperatures. A century ago, Pawlow have anticipated that the melting transition of small molecules are considerably alter with the increase in the surface/volume ratio[109]. Sodium and aluminum clusters have been the most widely studied materials for the phase transition. The variation of melting temperature of sodium clusters are directly correlated with geometric shell configuration. On the other hand, for the aluminum clusters both electronic structure and geometry are highly sensitive[110–114]. Many recent *ab initio* simulations study have concluded that cluster melting can be anticipated by structural transitions[115–120]. For example Li *et al.* found that geometry change between low enthalpy structures occur for Au₅₅ at temperatures which is far below the melting temperature[121]. Cleveland *et al.* have concluded that for reasonably large clusters, Au₁₄₆ and Au₄₅₉ the melting phenomenon is interrupt by solid-to-solid geometry transformations between the ground state and higher energy icosahedral structures which are precursors to cluster melting[122]. However, experimental confirmation for structural change of an isolated metal clusters is insufficient. Ion mobility experiment have explored both aluminum and gold in some extent[123, 124]. Low temperature plunge in the heats capacities for Al₅₆⁺ – Al₆₂⁺ have been ascribed to harden of exothermic geometric transitions[99, 101]. The solid–liquid phase change, however, are not much sensitive strictly with size. That is, as size of cluster increases there are no linear rise in their melting temperature. For instance, the extensive first principle thermodynamic simulations on Al₁₃ and Ga₁₃ results higher melting temperature of nano size cluster than its bulk counter part[125]. On the other hand doping with carbon a considerably reduce the melting temperature. Thus doping of foreign impurity allows to tune finite temperature behavior of small clusters. Doping causes lot of structural rearrangement of atoms within the cluster enhancing its reactivity, whereas, melting induces less coordination enhancing the catalytic activity. In the last decade, various clusters of Au, Pt

and Pd are utilized vastly for their high catalytic reactivity[126, 127]. Bulk gold is well-known to be chemically inert; the metal does not react with oxygen in air. However, it is now well established that gold clusters differ from bulk as they have several surface and corner atoms that have low coordination and hence adopt geometries that are extremely active for catalyzing certain oxidation reactions[128, 129]. Some of the unique properties observed in these gold clusters are better response properties, and different melting behavior[130–133]. Several interesting findings on Au clusters have been summarized in a recent review on theoretical chemical calculations on gold[135]. One of the important applications of Au clusters has been for CO oxidation. In this context, the interaction of ground state geometry of Au clusters with O₂ and CO has been widely studied[136–144]. Moreover, it has now recently been reported that in some cases the higher energy conformations have better adsorption properties as compared to the ground state cluster[145]. Many additional reports have shown that this activity of neutral clusters which depends upon the type of sites exposed and their ability to absorb or donate electrons can be elevated by phase transitions. Although, no explicit study on phase transitions of Pt and Pd all-metal cluster is reported so far, these are well known catalysts in many applications. Considering the two critical issues, abundance and cost, the expensive materials like Au, Pt are best replaced by Al metal clusters. Many recent studies have proved the potential use of Al metal clusters as catalyst in varied applications[146–148]. A major breakthrough addressed by M. F. Jarrold motivated us to study the novel features of Al clusters, where they discuss the reactivity of N₂ on a Al₁₀₀ cluster[149]. They have determined the melting temperature of Al₁₀₀ using heat capacity measurements following which the ion beam experiments are used to investigate the reaction between the cluster and molecular N₂. They show above the melting transition, the activation barrier for N₂ adsorption decreases nearly by 1 eV. The significance of N₂ adsorption over Al-cluster has further motivated by Romanowski *et al.* to carried out a computational investigation of N₂ reaction with liquid Al metal[150]. Their study have concluded that the activation barrier for dissociative chemisorption of N₂ over Al metal to be around 3.0 eV. They

propose that the melting decreases the surface energy, and atoms in liquid are mobile and better able to adjust the N₂ molecule. Hence, previous studies on N₂ adsorption conclude that the atoms on the surface of the liquid cluster move to minimize their energy, lowering the activation barrier.

Apart from the enhanced mobility, detailed information on the reactivity of various Al clusters and the reacting sites within them has not yet been clearly obtained. A very little understanding is available concerning the role of structure and bonding of Al clusters on the adsorption reactivity of the cluster. The catalytic reactivity is always attributed to specific and precise structural rearrangement of atoms in the material. It is worthwhile to correlate the above two parameters to their reactivity. Thus, the interesting questions are: “Is the chemisorption of N₂ molecule a consequence of highly different structure of Al cluster following the phase transition? Do the changes in structure modify the chemical bonding property within the cluster thereby enhancing its reactivity or the higher reactivity is completely due the dynamical rearrangement of atoms within cluster? Does this reactivity vary as a function of cluster size?” and how we can tune the catalytic efficiency by doping of foreign particle? To answer the above questions, in this thesis, we have studied systematically the adsorption behavior of N₂ on pristine and doped (Si and P atom) Al cluster as a function of cluster size. We also address the issue of conformational changes following the phase transition and their impact on N₂ adsorption.

1.9 Characterization: Experiment and Theory

Cluster production is one of the most important steps in cluster studies. To produce them, one can either aggregate the particles or break them directly from a solid or in liquid. These can be produced in the form of colloidal particles. Mostly, the studies have been focused on the formation of clusters in the gaseous phase by using cluster sources. One of the most popular sources to produce metal cluster is the supersonic jet. The other two sources to produce clusters are the gas aggregation and the surface source.

However, in laser vaporization technique the clusters are produced from the surface of a solid material by particle or photon impact or by a high electric field. Smalley and coworkers were the first to combine a laser ablation method and a supersonic beam. In this source, metal vapor is produced by the pulsed–laser ablation of a rod of the material to be investigated. This source can be considered as the hybrid of the supersonic jet and the gas aggregation source[151]. All known spectroscopic techniques such as optical, infrared, photoelectron, have been applied to study the properties of clusters[151, 152]. Photodetachment and photodissociation techniques have allowed us to gain insight into the electronic properties of charged clusters.

Jarrold *et al.* have investigated the photodissociation of aluminum cluster ions[153]. The first attempt to measure the ionization energies of aluminium clusters by laser vaporization was by Cox *et al.*[154]. Information on the structural and bonding properties can be obtained through vibrational spectroscopy. Very recently, Fielicke *et al.* used far–infrared spectroscopy to determine the structures of cationic vanadium clusters containing 6 to 23 atoms[155]. Recently, structures of silver and gold cluster ions have been studied by collision cross section[156]. However, none of these experimental techniques or studies could reveal the evidence of catalytic nature of the gold clusters against their noble metallic phase. Gold clusters are the excellent demonstration, where theory has played a immodest role in determining their notabilities. Satya Bulusu *et al.* reported theoretical grounds of hollow golden cages. Their recent work has shown that gold cluster exhibit some unique properties such as strong aurophilic attraction and relativistic effects, which play a key role for the formation of several unusual golden cages. Small Au nano clusters (13 atoms or fewer) stable at planar structures, whereas Au₂₀ acquires a pyramidal shape and also examine the intermediate structures resulting in the high reactivity[157]. The same authors also demonstrate planar–to–tubular geometrical transition in boron clusters: B₂₀ as the nucleus of single–walled boron nanotubes considering *ab initio* simulations[158].

In this new era, a computer simulation has led to a novel way of doing science that

combines both theory and experiments. The finite number of atoms considered in the metal clusters makes these systems ideal for theoretical studies. They can also help and guide the experimental work. Theoretical approaches used to study cluster science are either based on the first principle methods, such as HF, CI, DFT or classical approximations such as jellium model, tight binding etc.

Classical Approaches

Jellium model is one of the simplest and widely used theoretical model to study the electronic properties of metal clusters. It is simple enough to be applied to spherical metal clusters ranging up to few thousand atoms. Jellium model completely ignores the ionic core structure and replaces it by an uniform positive charge as being smeared out over the entire volume of the cluster, while the valence electrons are free to move within this homogeneously distributed positively charged background. The electronic energies are calculated self-consistently to obtain the energy levels[151, 159]. This approach is thus particularly suitable for systems with rather delocalized valence electrons such as bulk metal. According to the jellium model clusters with closed electronic shells have the spherical shapes, while clusters with partially filled or opened electron shells are deformed. Hence, the background of the jellium model can be modified according to the shape of the cluster. The initial work by Ekardt has successfully shown that the jellium model can account for the experimentally observed properties[160]. A number of characteristic properties of metal clusters such as static polarizabilities, collective electronic excitations (plasmons), ionization potentials as well as the so called magic numbers can be explained in terms of jellium model and its extensions[159, 160]. The limitation of using the jellium model is obvious since it neglects the ionic perturbation. It fails to understand the properties of covalent and ionic solids, where the electrons are localized in the bonding region. Thus jellium model has a limited range of applications which include the group Ia metals, alkaline earth metals and to some extent the transition metals.

Nevertheless, the model cannot compete with the conventional *ab initio* quantum chemical methods to study the properties of less than 20 atoms cluster. Reviews by Brack and W. de Heer are suggested for the detailed study of the jellium model and its applications.

Ab initio Approaches

Although classical and semi-classical approaches are successful in describing the stability and structural properties of the metal clusters, very little information on the electronic structure and related properties such as polarizabilities, optical spectra and ionization potentials of small clusters is available through these approximations[159, 160]. Moreover, the hybridization taking place within the atoms cannot be explained on the grounds of classical and semi-classical theories. The most widely used *ab initio* method to calculate the ground state properties are the HF and DFT. The post HF method such as DFT, CI, CC have been used to calculate the excited state properties of metal clusters. Many techniques, such as simulated annealing, conjugate gradient, Newton-Raphson have been employed for searching the potential energy surface to find the lowest energy configuration. Simulated annealing technique begins by heating the cluster at a very high temperature and then cooling or quenching it slowly, hence probing the thermally accessible regions of the phase space[161, 162]. In a series of papers, the electronic structure of the clusters composed of Ia-group metal atoms and of IIa-group atoms have been investigated at the *ab initio* level[163]. Other studies on mixed metal clusters have also been carried out at the *ab initio* levels[164].

In the last decade combined approach of DFT and MD has been employed to study the ground state and dynamical properties of metal clusters[165]. In this approach the electronic potential derived from the DFT is combined with the classical MD equation, during the motion of nuclei to develop an efficient combined electronion minimization. This approach was first proposed by Car and Parrinello[166]. This technique also helps in studying the melting of clusters. Thermodynamical simulations are based on the concepts such as temperature, pressure, equipartition, phase transition, conformational search of

clusters etc[167–169]. These simulations are carried out in a micro–canonical ensemble (constant energy) or in a canonical ensemble (constant temperature)[170].

1.10 General Overview of Reactivity Descriptors

Chemical reaction can be understood and predicted by several theoretical quantities that have a direct correlation with the distinctive sets of substantial chemical properties. These important chemical quantities are known as descriptors. The reactivity descriptors (or reactivity indexes) are highly relevant to predicting the reactivity of the chemical systems and measure a qualitative and semi–quantitative way of the extent to which a particular site will be concerned in a given condition[171–181]. In the last centuries, several groups have attempted to analyze the reactivity and nature of bonding of various molecule based on some perceptive ideas, conceptual models and empirical theory based on reactivity descriptors. All are originally evolved from many experimental findings and several chemical phenomenon. This empirical methodologies led to the present perceptive and have contributed significantly to the problem of early chemistry. These concepts can explain few experimental facts rather than to be systematic in a general sense. It was thus, only partly favorable in explaining the chemical properties of the systems. So it is not very simple to formulation of a systematic generalization from these crude qualitative concepts and models. This conclusion is owing to the presence of the enormous number of different classes of molecule and consequently, the fascination as well as frustration started arising out among the modern chemist’s community.

Quantum mechanics in the framework of Molecular orbital theory (MO) tried to develop all the conceptual models and principles, and founded the mathematical foundations to it. The advancement of quantum chemical methods shed lights on the rigorous definition of several empirical concepts and has equipped a formulation for the calculation of the chemical properties of molecular systems[171–182]. Among all the significant developments of reactivity descriptors, many have been extraordinarily successful

in explaining the chemical and physical phenomenon molecular systems. In particular, the theory of the frontier molecular orbital theory (highest occupied molecular orbital (HOMO) and lowest unoccupied molecular orbital (LUMO)) proposed by Fukui[174], molecular orbital symmetry developed by Woodward–Hoffmann[183–185], Mulliken’s overlap and orientation principle[186–188] and Pearson’s hardness and softness concept (Hard–Soft Acid–Base principle)[189, 190]. All the concepts or principles have tremendous impact to explain experimental facts at the molecular level in an elegant way. Several other reactivity descriptors have also been proposed with these descriptors in parallel, such as Bader’s charge density of atoms in molecule (AIM), molecular electrostatic potential (MESP), electric field, etc[173, 191–194]. Thus, to explain the chemical process several such descriptors have been prescribed and each of them have their own domain of applicability. Hence, it is very crucial to know which parameters can explain molecular structure and reactivity, and which are the most appropriate representatives of the tendency of a given molecule to undergo a certain class of reactions. In the present thesis we have discussed elaborately the developments of the recently proposed density–based descriptors, such as chemical potential, hardness, softness, Fukui function and their derivatives. More importantly, we are interested in extending these concepts to investigate the reactivity of molecular systems in a semi–quantitative way.

1.11 The Concepts of Hardness and Softness Parameters: A Historical Perspective

Concepts such as hardness and softness have been part of the vocabulary of the chemists since the period of Berzelius, mainly to explain the occurrence of natural metal ores with several other groups or ligands, such as sulfides, oxides or carbonates[195]. The foundation for the concept of chemical hardness lies in the study of Ahrland and Chatt[196]. They showed that the metal ions are simply one group of electrophiles and which in turn

can be divided into two classes building upon on the relative affinities for ligands with various donor atoms. The class (a) metal ions react strongly with nucleophiles, which are normally basic to the protons. The class (b) metal ions react strongly with nucleophiles that can be easily oxidized. For instance, considering the affinity of some of the metal ions towards oxides and sulfides, the reactivity order for these metal ions has been given as, $\text{Mg}^{2+} > \text{Fe}^{2+} > \text{Ca}^{2+} > \text{Zn}^{2+} > \text{Pb}^{2+} > \text{Cu}^{2+} > \text{Cd}^{2+} > \text{Hg}^{2+}$. This order has been later shown to be in the increasing order of softness or decreasing order of hardness. Most of these works were focused to explain the reason for the preference of metal ions with some specific ligands. Although these classifications and explanations were satisfactory for the occurrence of many natural ores and other complexes in terms of the hardness and softness concepts, it was merely a conclusion from the observed results. However, there was no explanation for the variation in the stability of these complexes and it was probably due to the lack of knowledge of electronic structure of the systems and nature of the chemical bonds.

The first detailed explanation on the basis of electronic structure theory was given by Mulliken[186–188, 197, 198]. He suggested that the bond between the molecular systems, A and B, is predominantly ionic in character with a single electron transfer from the Lewis base B to the Lewis acid A. Mulliken also explained the stability or the strength of the molecular Lewis acid–base complex with the help of quantum mechanical formulation. He further argued that stability of the complex AB increases with the increasing heat of formation from system A and B, which in turn depends upon the resonance energy (i.e. resonance between the no bond and ionic bond structure of A and B). From the corresponding energy profiles of the no bond and ionic bond structures, he concluded that the lower the vertical ionization potential of B and higher the electron affinity of B, the more is the resonance, which implies greater strength of Lewis acid A and base B. Mulliken also showed that when both A and B are soft chemical species (by ‘soft’ he meant less exchange repulsion between the two systems) the resultant compound AB is more stable than the case when both of them are hard species (again by ‘hard’ he meant

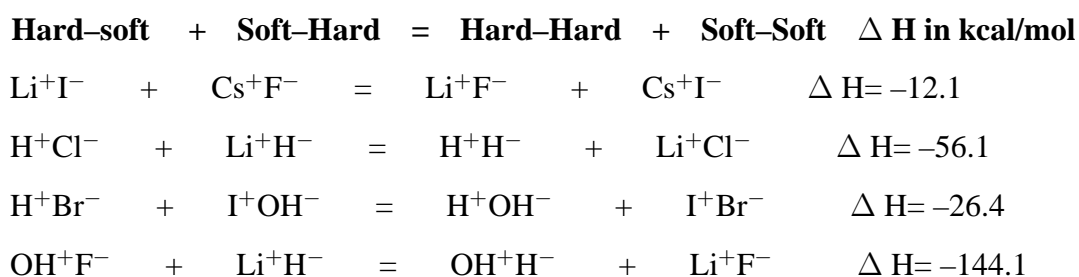
more exchange repulsion between two). So, according to him, softness in A or B should tend to make it a better acid or base, respectively,. On the basis of the above definition of “softness” or “hardness”, he also explained the “exothermicity” and “endothermicity” of the molecular compound AB.

This common idea of categorize chemical reagents with respect to their chemical nature stimulated further research on the physical properties of the complexes. Pearson’s study is considered to be one of the most significant works and it has been found to be very applicable for correlating and in depth understanding of a complex chemical systems in terms of the hard and soft parameters. More over, these concepts have gained further impetus and it became one of the most useful concepts among the chemist’s community after the proposition of HSAB principle by Pearson in 1963[199]. He has actually classified the molecular systems in terms of the hard–soft acid–base in a general way and the details are given below:

- (a) Hard acid (acceptors or nucleophiles): High positive charge, low polarizability and small in size. e.g. H^+ , Ca^{2+} , BF_3 etc
- (b) Soft acid: Low positive charge, high polarizability and larger in size e.g. Hg^{2+} , BH_3 , I^+
- (c) Hard base (donors or electrophiles): High electronegativity, difficult to oxidize and low polarizability. e.g. F^- , NH_3 , OH^-
- (d) Soft base: Low electronegativity, easily oxidizable and higher polarizability. e.g. H^- , I^- , C_2H_4 , CN^-

HSAB principle says that reaction of hard acid with hard base and soft acid with soft bases results addition stabilization of the systems. It is a concise statement of very large amount of chemical information from experimental observations. An account on the usefulness of the HSAB principle can be found in different areas through several proceedings and monographs or shorter overview articles. Some examples are given below that will explain the HSAB principle. For example, Li^+ is a hard acid, F^- a hard

base, Cs^+ a soft acid, and I^- a soft base. The exothermic nature of the reaction shows that hard–hard (Li and F) and soft–soft (Cs and I) interactions are preferred over hard–soft or soft–hard interactions. In a similar way, one can also explain the other reactions through the HSAB principle.



There are several possible factors that might influence the chemical strength of the hard–hard and soft–soft interactions. Indeed, these factors govern an important role depending upon the specific condition. Although the preceding discussion is inadequate, it compiles most of the important aspects, which seem likely to regulate the nature of hard–hard and soft–soft interactions. Because of the high intricacy of these factors, an elaborate analysis would scarcely be advocated. However, the theoretical proof for the HSAB principle will be discussed in the foregoing sections.

A more interesting idea is the one that relates the hard–hard and soft–soft character, respectively, to ionic and covalent interaction. A simple explanation for hard–hard interactions is by considering them to be primarily electrostatic or ionic interactions [199–204]. Most of the typical hard acids and bases are those that might be supposed to form ionic bonds such as Li^+ , Na^+ , etc and F^- , OH^- . As the electrostatic or Madelung energy of an ion pair is inversely proportional to the inter–atomic distance, the smaller the distance, the greater is the attraction between the hard acid and base. Since an electrostatic explanation cannot account for the apparent stability of the soft–soft interactions, it has been suggested that the predominant factor here is a covalent one. This would correlate well for transition metals, Ag, Hg, etc. It is usually assumed that bonds such as Ag–Cl are considerably more covalent than the corresponding ones of the alkali metals.

In this regard, the polarizing power and the polarizability of d orbital electrons becomes important. π -bonding has also been suggested for the soft-soft interactions. π -bonding occurs more readily in those metal ions that have low oxidation states and large number of d electrons and hence, these conditions favor the soft-soft type of interactions. We can conclude by two main conclusions. First one stated that soft molecules are more reactive in respect to the hard molecules in all reactions where rearrangement or electron transfer is essential. The second one tells about the hard molecules which resist to change, not only in the number of electrons, but also in the distribution among the nuclei.

An empirical equation was suggested by Drago to correlate heats of formation of acid-base complexes, such as $-\Delta H = E_A E_B + C_A C_B$, where the term E represents the susceptibility of the acid or the base to be subjected to electrostatic interaction. The term C measure the extent of participation in covalent bonding[205–208]. This equation seems to give superior agreement with experiment and compares in elegant way with that suggested by Pearson. However, empirical nature and the number of independent parameters involved in the calculations make it unrealistic to use. In addition, no physical reason or explanation for hard and soft behavior is provided by such an approach.

1.12 Reactivity descriptors: Application to the chemical problems

The objective for introduction of these reactivity descriptors is to quantify and analyze the conceptually important quantities such as chemical reactivity, selectivity and the stability of molecular systems from general theoretical view. The numerous works in terms of monographs and reviews in this field, brings out the utility of these descriptors in generalizing the chemical reactivity within the framework of DFT[209–215]. Based on proposition Zhou, Parr and Garst have proposed that both hardness and aromaticity are measures of high stability and low reactivity and absolute and relative hardness measures

the extent of aromaticity[216, 218–220]. Parr and co-workers have successfully correlated resonance energy per π electron, which is conventional valence-bond measure of aromaticity, with absolute hardness or relative hardness[216]. It has been shown that in electrophilic substitution reactions, the change in the hardness from reactant to the transition state, is the measure of activation energy of the system. They also argued that the absolute hardness is generally the most useful quantitative index for marking the closing of electronic shells and the closing of shells can be seen as consequence of MHP; the hardness of fully filled s-shells and half filled p-shells are seen to be local minima. Hardness has been shown as successful candidate in predicting the stability of different types of metal clusters[221, 222].

As we have discussed elaborately in the next chapter about the information contained in $f(r)$ and $s(r)$, these are extensively used to study intramolecular reactivity from local perspective[223, 224]. Langenaeker *et al.* have shown that more reliable reactivity order for intermolecular reactivity can be obtained by making use of local hardness, rather than FFs or local softness. Intermolecular interactions being charge controlled (hard-hard) interactions, are therefore, better described by hardness related descriptors, while the intramolecular interactions, being covalent, are better described by orbital related descriptors (like FF and $s(r)$).

Based on local HSAB principle, interpretation of orientation in organic reactions has also been studied in detail by various groups[223, 225]. LRDs have been reasonably successful in interpreting both regio-selectivity and mechanism of the Diels-Alder reactions[226–233]. In addition these have been extensively applied for problems of regio-selection in substituted benzyne and hexarynes and α, β -unsaturated aldehydes and ketones; and the nucleophilic and electrophilic substitution reactions of mono substituted benzenes[234–240, 242–244, 246, 247]. Recently, region-selectivity in fullerenes chemistry has been adequately rationalized by means of local softness[236]. The local hardness, in one or another approximate form, has also been studied on inter-molecular reactivity sequences, acidity of substituted acetic acids, hydrides, zeolites, alkyl alcohols

and reactivity of mono-substituted benzenes[237–240, 242, 243, 248].

There have been reported cases, where, these descriptors have failed in describing the experimentally observed reactivity trends[249–252]. Study by Mineva *et al.* has claimed that orbital FFs do not provide correct reactivity pattern for protonation sites of aniline in gas phase[254]. Roy *et al.* have reported some mismatches for α, β -unsaturated ketones on basis of local softness and FFs. They proposed relative electrophilicity and relative nucleophilicity as a more reliable descriptors over the condensed FFs[255]. Krishnamurty *et al.* studied intermolecular reactivity using concept of group softness, where, the group consists of reacting atoms and nearest neighbors of that atom[251].

Contreas *et al.* examined the usefulness of philicity in predicting region-selective isomers in Diels–Alder reaction[256–259]. Importance of philicity in describing global electrophilicity has been also discussed by few authors. Numerically, philicity has been tested to perform better than FFs in describing intermolecular reactivity.

As we have seen that there has been considerable success in describing the reactivity of the simple organic molecules, using the reactivity descriptors, the applicability of these descriptors has also been extended to more complex systems like zeolites. The acidity and basicity of different sites in zeolites lattice are the two important properties that determine the catalytic activity of zeolite. These properties have been extensively studied using these LRDs[260–266]. Recently, the influence of changes in the average framework electronegativity, (by the variations in the composition of the zeolites or by the isomorphous substitution of Si and Al atoms by other atoms), on the acidity of the bridging hydroxyl groups has been investigated using the reactivity descriptors by Geerlings *et al.*, Pal and co-workers, Deka *et al.* and Chatterjee *et al.*[257, 258, 263–266]

In addition to ground state description of reactivity, Chattaraj and co-workers also focused on extending the scope of these conceptual DFT tools of ground state to excited state[267–269]. These studies have led to significant understanding of excited state chemistry. They showed that hardness values for excited states are lower than those for

the ground state. On the other hand, the surface plots of local quantities FFs, charge density etc. show increase in reactivity for the excited states. They also revealed the linear relation between the $\alpha^{1/3}$ and the softness of the system even for the excited states.

1.13 Organization of the thesis

Motivation of the present thesis is to apply the advanced cost-effective DFT techniques to investigate the physical and chemical insight of metal clusters and catalysis at a microscopic level. Recent developments in the field of metal clusters has helped in understanding the evolution of the physical and chemical properties from an atomistic scale to nano and to a bulk scale. In addition to this, by doping with different kinds of metal atoms, new materials can be formed. One of the purposes of the present work is to use AIMD simulations to obtain the ground state properties of some doped metal clusters such as gallium doped aluminum based binary clusters.

The other purpose of the work is to develop charge transfer parameter to calculate interaction energy of several prototype organic molecules with multiple site based weak interactions using local hard – soft acid – base (HSAB) principle.

The outline of this thesis is as follows. In Chapter 2, we have presented an outline of the theoretical framework behind the methodology used in the most part of the work presented in the thesis. We begin with a brief introduction to the density functional theory (DFT) as an alternative route to perform reactivity and catalytic properties of molecule and metal clusters. A description of the concepts of molecular dynamics and *ab initio* molecular dynamics are given and also explain and compare the ideas and algorithms behind Born – Oppenheimer molecular dynamics and Car–Parrinello molecular dynamics. Lastly, we briefly review the earlier theoretical developments of chemical reactivity using the *ab initio* quantum chemical methods and properly describe how the empirical concepts (chemical potential, electronegativity, softness, hardness etc.) have been quantified theoretically within the domain of DFT. We have highlighted the energy – density

perturbation methods within the framework of DFT and the different semi – quantitative models, including local HSAB principle, in finding a one to one correspondent between the density based reactivity descriptors and the interaction energy of the complex.

In chapter 3, we calculate interaction energy of several prototype organic molecules with multiple site based weak interactions using local hard – soft acid – base (HSAB) principle. The local HSAB principle is semiquantitative in nature due to the presence of an *ad hoc* charge transfer parameter. We have derived the second – order approximation of ΔN (ΔN_{second}) as an *ad hoc* parameter for charge transfer to calculate interaction energies of multiple site based interactions using local hard soft acid base principle. The second – order approximation of ΔN has derived from Sandersons electronegativity equalization principle. We further discussed the advantages and limitations of the approach.

In the chapter 4, we have studied reactivity of aluminum clusters in the framework of density functional theory (DFT) – based reactivity descriptors to identify potential sites for adsorption and eventual chemical reaction. Depending on symmetry, susceptibility of various type of reactive sites within a cluster toward an impending electrophilic and/or nucleophilic attack are predicted using the reactivity descriptors and validated by performing an explicit adsorption of water molecule on Al clusters.

In chapter 5, we have studied di – nitrogen activation on the doped aluminum clusters. Density functional theory based calculations demonstrate doped aluminum clusters to be highly reactive toward molecular nitrogen and hence are prospective materials for its activation at low temperatures. Calculations on silicon and phosphorus doped aluminum clusters with 5 – 8 atoms reveal an enhanced N_2 activation with respect to their pristine ground state and high energy counterparts. *Ab initio* molecular – dynamics simulations further exhibit consequential efficiency of doped clusters toward dinitrogen activation at finite temperature.

In the chapter 6, we investigate structure and stability of aluminum clusters with successive substitution of gallium atom. We have carried out *ab initio* density functional theory (DFT) based molecular dynamics simulations (BOMD) on pure and successive gallium

doped on Al₈ clusters with an aim of understanding the thermodynamic properties of ground state conformations as a function of doping ratio. Structural and electronic properties are analyzed to explain factors leading to the stabilization.

In the last chapter, we have proposed to study energetics and mechanistic pathway of cross – coupling reaction over aluminium nanoclusters as catalyst. Density functional theory will be use to understand the facts. In spite of being an unconventional catalyst for radical polymerization, cross – coupling or similar type of reactions in bulk state, Al clusters can show significantly low activation barrier. To understand the insight into the reaction mechanism, mode of binding will be investigate with the *ab initio* Born Oppenheimer Molecular Dynamics (BOMD) simulation and the Natural Bond Orbital (NBO) analysis.

Bibliography

- [1] Rothenberg G. *Catalysis: Concepts and Green Applications* WILEY-VCH Verlag GmbH & Co. KGaA, Weinheim, **2008**
- [2] W. Heitler F. London *Z. Physik.* **1927**, *44*, 455.
- [3] Pauling L. *J. Am. Chem. Soc.* **1931**, *53*, 1367.
- [4] Pauling L. **The Nature of the Chemical Bond**, (3rd edn) Oxford and publishing co. **1960**.
- [5] Slater J. C. *Phys. Rev.* **1930**, *36*, 57.
- [6] Coulson C. A. *Proc. R. Soc. A.* **1939**, *169*, 413.
- [7] Mcweeny R. *Coulsons Valence*, (3rd edn) Oxford University Press. **1979**.
- [8] Levine I. N. *Quantum Chemistry*, (4th edn) PrenticeHall of India, **1995**.
- [9] Parr R. G.; Yang W. **Density Functional Theory of Atoms and Molecules**, Oxford University Press, **1989**.
- [10] *Physics and Chemistry of Finite Systems: From Clusters to Crystals*. edited by P. Jena P.; Khanna S. N.; Rao B. K. *Kluwer Academic, Dordrecht, Netherlands*, Vol. 1 and Vol. 2, **1992**.
- [11] *Clusters and Nanostructuredl Materials*, edited by P. Jena P.; Behera S. N. *Nova Science Publishers. Inc.*, **1996**.
- [12] *Clusters of Atoms and Molecules: Theory, Experiment, and Clusters of Atoms.*, edited by Haberland H., *Springer-Verlag, Heidelberg*, **1994**.
- [13] Kroto H. W. *Science.* **1988**, *242*, 1139.
- [14] Curl R. F.; Smalley R. E. *Science.* **1988**, *242*, 1017.

-
- [15] *Clusters and Fullerenes*. Edited by V. Kumar V.; T. P. martin T. P.; Tosatti E. *World Scientific*, **1993**.
- [16] Ijima S. *Nature*. **1992**, 359, 707.
- [17] A. F. Hebard A. F.; Rosseinsky M. J.; Haddon R. C.; Murphy D. W.; Glarum S. H.; Palstra T. M.; Kortan A. R.; Zahurak S. M.; Makhija A. V. *Phys. Rev. Lett.* **1991**, 66, 2830.
- [18] Chai Y.; Guo T.; Jin C.; Hauffer R. E.; Chibante L. P.; Fure J.; Wang L.; Alford J. M.; Smalley R. E. *J. Phys. Chem.* **1991**, 95, 7654.
- [19] Holczer K.; Klein O.; Huang S. M.; Kaner R. B.; Fu J.; Whetten R. L.; Diederich F. *Science*. **1991**, 252, 1154.
- [20] Bonacci-Koutecky V.; Fantucci P.; Koutecky J. *Chem. Rev.* **1991**, 91, 1035.
- [21] de Heer W. A. *Rev. Mod. Phys.* **1993**, 65, 611.
- [22] Alonso J. A. *Chem. Rev.* **2000**, 100, 637.
- [23] Knight W. D.; Clemenger K.; de Heer W. A.; Saunders W. A. *Phys. Rev. B.* **1985**, 31, 1539.
- [24] Bonacic-Koutecky V.; Boustani I.; Guest M. F.; Koutecky J. *J. Chem. Phys.* **1988**, 89, 4861.
- [25] *Lithium ion Batteries*, Edited by Balbuena.; Wang Y., *Imperial College Press*. **2004**.
- [26] Hanley L.; Witten J.; Anderson S. L. *J. Phys. Chem.* **1988**, 92, 5803.
- [27] Zhai H. J.; Wang L. S.; Alexandrova A. N.; Boldyrev A. I. *J. Chem. Phys.* **2002**, 208, 233.
- [28] Zhai H. J.; Alexandrova A. N.; Birch K. A.; Boldyrev A. I.; Wang L. S. *Angew. Chem. Int. Ed.* **2003**, 42, 6004.
-

-
- [29] Hanley L.; Anderson S. L. *J. Phys. Chem.* **1987**, *91*, 5161.
- [30] Hanley L.; Anderson S. L. *J. Chem. Phys.* **1988**, *89*, 2848.
- [31] Begemann W.; Meiwes-Broer K. H.; Lutz H. O. *Phys. Rev. Lett.* **1986**, *56*, 2248.
- [32] Chou M. Y.; Cohen M. L. *Phys. Lett. A.* **1986**, *113*, 420.
- [33] Cox D. M.; Trevor D. J.; Wheten R. L.; Kaldor A. *J. Phys. Chem.* **1988**, *92*, 421.
- [34] Jarrold M. F.; Bower J. E. *J. Am. Chem. Soc.* **1988**, *110*, 70.
- [35] Jarrold M. F.; Bower J. E. *Chem. Phys. Lett.* **1988**, *144*, 311.
- [36] Zhang S. B.; Cohen M. L.; Chou M. Y. *Phys. Rev. B.* **1987**, *36*, 3455.
- [37] Rothlisberger U.; Andreoni W. *Chem. Phys. Lett.* **1992**, *198*, 478.
- [38] Yannouleas C.; Jena P.; Khanna S. N. *Phys. Rev. B.* **1992**, *46*, 9751.
- [39] Lopez M. J.; Marcos P. A. J. A. Alonso J. A. *J. Chem. Phys.* **1996**, *104*, 1056.
- [40] Li X.; Kuznetsov A. E.; Zhang H. F.; Boldyrev A. I.; Wang L. S. *Science.* **2001**, *291*, 859.
- [41] Rao B. K.; Jena P. *Phys. Rev. B.* **1985**, *32*, 2058.
- [42] Jena P.; Rao B. K.; Nieminen R. M. *Solid State Commun.* **1986**, *59*, 509.
- [43] Fantucci P.; Koutecky J.; Pacchioni G. *J. Chem. Phys.* **1988**, *88*, 325.
- [44] P. Blaise, F. Spiegelmann, D. Maynau, J. P. Malrieu. *Phys. Rev. B.* **1990**, *41*, 5566.
- [45] King F. L.; Ross M. M. *Chem. Phys. Lett.* **1989**, *164*, 131.
- [46] Kumar V.; Kawazoe Y. *Appl. Phys. Lett.* **2003**, *83*, 2677.

-
- [47] Thomas C.; Zheng W. J.; Lippa T. P.; Xu S. J.; Lyapustina S. A.; Bowen Jr K. H.. *J. Chem. Phys.* **2001**, *114*, 9895.
- [48] Zhao J.; Liu B.; Zhai H.; Zhou R.; Ni G.; Xu Z. *Solid. State. Commun.* **2002**, *122*, 543, 2002.
- [49] V. Kumar, V. Sundarajan. *Phys. Rev. B.* **1988**, *57*, 4939.
- [50] Joshi K.; Kanhere D. G. *Phys. Rev. A.* **2002**, *65*, 043203.
- [51] Hunsicker S.; Jones R. O. *J. Chem. Phys.* **1996**, *105*, 5048.
- [52] Alonso J. A.; Molina L. M.; Lopez M. J.; Rubio A.; Stott M. J. *Chem. Phys. Lett.* **1998**, *289*, 451.
- [53] Wang B.; Stott M. J. Alonso J. A. *Phys. Rev. B.* **2002**, *65*, 045410.
- [54] Chacko S.; Deshpande M.; Kanhere D. G. *Phys. Rev. B.* **2003**, *64*, 155409.
- [55] Andreoni W. *Phys. Rev. B.* **1992**, *45*, 4203.
- [56] Heinebrodt M.; Malinowski N.; Tast F.; Branz W.; Billas I. M. L.; Martin T. P. *J. Chem. Phys.* **1999**, *110*, 9915.
- [57] Knowles W.S. Asymmetric hydrogenations (Nobel Lecture). *Angew. Chem. Int. Ed.* **2002**, *41*, 1998
- [58] Noyori R. Asymmetric catalysis: science and opportunities (Nobel Lecture) *Adv. Synth. Catal.* **2003**, *345*, 15
- [59] Sharpless K. B. Searching for new reactivity (Nobel Lecture) *Angew. Chem. Int. Ed.* **2002**, *41*, 2024
- [60] Chauvin Y. Olefin metathesis: the early days (Nobel Lecture) *Angew. Chem. Int. Ed.* **2006**, *45*, 3740
-

-
- [61] Grubbs R. H. Olefin–metathesis catalysts for the preparation of molecules and materials (Nobel Lecture) *Angew. Chem. Int. Ed.* **2006**, *45*, 3760
- [62] Schrock R. R. Multiple metal–carbon bonds for catalytic metathesis reactions (Nobel Lecture) *Angew. Chem. Int. Ed.* **2006**, *45*, 3748
- [63] Cornils B.; Herrmann W. A. *J. Catal.* **2003**, *216*, 23
- [64] Friend C.M.; Queeney K. T.; Chen D. A.(b)
Appl. Surf. Sci. **1999**, *142*, 99
- [65] Rainer D. R.; Goodman D. W. *NATO ASI Ser. E: Appl. Sci* **1997**, *331*, 27
- [66] Baiker A. *Faraday Discuss. Chem. Soc.* **1989**, *87*, 239
- [67] Kim S. H.; Somorjai G. A. *Proc. Natl. Acad. Sci., USA* **2006**, *103*, 15289
- [68] Frank M.; Baumer M. *Phys. Chem. Chem. Phys.* **2000**, *2*, 3723
- [69] Wallace W. T.; Min B. K. *Top. Catal.* **2005**, *34*, 17
- [70] Rainer D. R.; Xu C.; Goodman D. W. *J. Mol. Catal. A: Chem.* **1997**, *119*, 307
- [71] Kamat P. V.; Dimitrijevic N. M. *Solar Energy* **1990**, *44*, 83
- [72] Serpone N. *Res. Chem. Intermed.* **1994**, *20*, 953
- [73] Chuang S. S. C. *Catalysis* **2005**, *18*, 186
- [74] Carrette L.; Friedrich K. A.; Stimming U. *Chem. Phys. Chem.* **2000**, *1*, 163
- [75] Zaidman B.; Wiener H.; Sasson Y. *Int. J. Hydr. Energy* **1986**, *11*, 341
- [76] Wiener H.; Zaidman B.; Sasson Y. *Solar Energy* **1989**, *43*, 291
- [77] Haberland H. Clusters of Atoms and Molecules: Theory, Experiment, and Clusters of Atoms. *Springer–Verlag, Heidelberg* **1994**
-

-
- [78] Okuhara T. *Chem. Rev.* **2002**, *102*, 3641
- [79] Harmer M. A.; Sun Q. *Appl. Catal. A: Gen.* **2001**, *221*, 45
- [80] Taylor H. S. *J. Ind. Eng. Chem.* **1920**, *13*, 75
- [81] Taylor H. S. *Proc. R. Soc. (London)* **1925**, *108A*, 105
- [82] Taylor H. S. *Proc. R. Soc. (London)* **1926**, *113A*, 105
- [83] Corma A.; Nemeth L. T.; Renz M.; Valencia S. *Nature* **2001**, *412*, 423
- [84] Corma A. *Chem. Rev.* **1995**, *95*, 559
- [85] Chang C. D.; Silvestri A. J. *J. Catal.* **1977**, *43*, 249
- [86] Schmidt M.; Kusche R.; Kronmüller W.; Issendorf von. B.; Haberland H. *Phys. Rev. Lett.* **1997**, *79*, 99
- [87] M. Schmidt M.; R. Kusche R.; Issendorf von. B.; Haberland H. *Nature London* **1998**, *393*, 238
- [88] Schmidt M.; Kusche R.; Hippler T.; Donges J.; Kronmüller W.; Issendorff von B.; Haberland H. *Phys. Rev. Lett.* **2001**, *86*, 1191
- [89] Schmidt M.; Haberland H. *C. R. Phys.* **2002**, *3*, 327
- [90] Schmidt M.; Donges J.; Hippler Th.; Haberland H. *Phys. Rev. Lett.* **2003**, *90*, 103401
- [91] Haberland H.; Hippler T.; Donges J.; Kostko O.; Schmidt M.; Issendorff von B. *Phys. Rev. Lett.* **2005**, *94*, 035701
- [92] Chirot F.; Feiden P.; Zamith S.; Labastie P.; LHermite J. M. *J. Chem. Phys.* **2008**, *129*, 164514

-
- [93] C. Hock C.; S. Strassburg S.; Haberland H.; Issendorff von B.; Aguado A.; Schmidt M. *Phys. Rev. Lett.* **2008**, *101*, 023401
- [94] Shvartsburg A. A.; Jarrold M. F. *Phys. Rev. Lett.* **2000**, *85*, 2530
- [95] G. A. Breaux G. A.; Neal C. M.; Cao B.; Jarrold M. F. *Phys. Rev. B* **2005**, *71*, 073410
- [96] Breaux G. A.; Benirschke R. C.; Sugai T.; Kinnear B. S.; Jarrold M. F. *Phys. Rev. Lett.* **2003**, *91*, 215508
- [97] Breaux G. A.; Hillman D. A.; Neal C. M.; Benirschke R. C.; Jarrold M. F. *J. Am. Chem. Soc.* **2004**, *126*, 8628
- [98] Breaux G. A.; Cao B.; Jarrold M. F. *J. Phys. Chem. B* **2005**, *109*, 16575
- [99] Breaux G. A.; Neal C. M.; Cao B.; Jarrold M. F. *Phys. Rev. Lett.* **2005**, *94*, 173401
- [100] Neal C. M.; Starace A. K.; Jarrold M. F.; Joshi K.; Krishnamurty S.; Kanhere D. *G. J. Phys. Chem. C* **2007**, *111*, 17788
- [101] Neal C. M.; Starace A. K.; Jarrold M. F. *Phys. Rev. B* **2007**, *76*, 054113
- [102] Jarrold M. F.; Cao B.; Starace A. K.; Neal C. M.; Judd O. H. *J. Chem. Phys.* **2008**, *129*, 014503
- [103] Starace A. K.; Neal C. M.; Cao B.; Jarrold M. F.; Aguado A.; López J. M. *J. Chem. Phys.* **2008**, *129*, 144702
- [104] W. Zhang W.; Zhang F.; Zhu Z. *Phys. Rev. B* **2006**, *74*, 033412
- [105] Li Z. H.; Truhlar D. G. *J. Am. Chem. Soc.* **2008**, *130*, 12698
- [106] Hsu P. J.; Luo J. S.; Lai S. K.; Wax J. F.; Bretonnet J. L. *J. Chem. Phys.* **2008**, *129*, 194302

-
- [107] Ojwang J. G. O.; Santen van R.; Kramer G. J.; van Duin A. C. T.; Goddard W. A. *J. Chem. Phys.* **2008**, *129*, 244506
- [108] Ghazi S. M.; Zorriasatein S.; Kanhere D. G. *J. Phys. Chem. A* **2009**, *113*, 2659
- [109] Pawlow Z. P. *Phys. Chem.* **1909**, *65*, 1
- [110] Haberland H.; Hippler T.; Donges J.; Kostko O.; Schmidt M.; Issendorff B. V. *Phys. Rev. Lett.* **2005**, *94*, 035701
- [111] Aguado A.; López J. M. *Phys. Rev. Lett.* **2005**, *94*, 233401
- [112] Aguado A. *J. Phys. Chem. B* **2005**, *109*, 13043
- [113] Noya E. G.; Doye J. P. K.; Wales D. J.; Aguado A. *Eur. Phys. J.* **2007**, *43*, 57
- [114] Starace A. K.; Neal C. M.; Cao B.; Jarrold M. F.; Aguado A.; López J. M. *J. Chem. Phys.* **2009**, *131*, 044307
- [115] Neal C. M.; Starace A. K.; Jarrold M. F. *J. Phys. Chem. A* **2007**, *111*, 8056
- [116] Chirot F.; Feiden P.; Zamith S.; Labastie P.; Hermite J. M. L. *J. Chem. Phys.* **2008**, *129*, 164514
- [117] Jarrold. M. F; Honea E. C. *J. Phys. Chem.* **1991**, *95*, 9181
- [118] Neal C. M.; Breaux G. A.; Cao B.; Starace A. K.; Jarrold M. F. *Rev. Sci. Instrum.* **2007**, *78*, 075108
- [119] Bohr J. *Int. J. Quantum Chem.* **2001**, *84*, 249
- [120] D. Poland *J. Chem. Phys.* **2007**, *126*, 054507
- [121] Li T. X.; Lee S. M.; Han S. J.; Wang G. H. *Phys. Lett. A* **2002**, *86*, 300
- [122] Cleveland C. L.; Luedtke W. D.; Landman U. *Phys. Rev. Lett.* **1998**, *81*, 2036
-

-
- [123] Jarrold M. F.; Bower J. E. *J. Chem. Phys.* **1993**, *98*, 2399
- [124] P. Weis P.; Bierweiler T.; Vollmer E.; Kappes M. M. *J. Chem. Phys.* **2002**, *117*, 9293
- [125] Chandrachud P.; Joshi K.; Kanhere D. G. *Phys. Rev. B* **2007**, *76*, 235423
- [126] De H. S.; Krishnamurty S.; Pal S. *J. Phys. Chem. C* **2009**, *113*, 7101
- [127] De H. S.; Krishnamurty S.; Pal S. *J. Phys. Chem. C* **2010**, *114*, 6690
- [128] Haruta M. *Gold Bull* **2004**, *37*, 27
- [129] M. Haruta M.; Date M. *Appl. Catal.* **2001**, *222*, 427
- [130] Landman U.; Luedtke W. D.; Burnham N. A.; Colton R. *Science* **1990**, *248*, 454
- [131] Yang Y.; Chen S. *Nano Lett.* **2003**, *3*, 75
- [132] Pyykko P. *Inorg. Chim. Acta* **2005**, *358*, 4113
- [133] Krishnamurty S.; Shafai G. S.; Kanhere D. G.; Soule de Bas B.; Ford M. J. *J. Phys. Chem. A* **2007**, *111*, 10769
- [134] *Solar Energy* **1989**, *43*, 291
- [135] Pyykko P. *Chem. Rev.* **2008**, *37*, 1967
- [136] Wallace W. T.; Wyrwas R. B.; Wheten R. L.; Mitric R.; Bonacic-Koutecky V. *J. Am. Chem. Soc.* **2003**, *125*, 8408
- [137] Issendorff von B.; Hakkinen H.; Moseler M.; Landman U. *Chem. Phys. Chem.* **2007**, *8*, 157
- [138] Luo C.; Fa W.; Dong J. *J. Chem. Phys.* **2006**, *125*, 84707
- [139] Barton D. G.; Podkolzin S. *J. Phys. Chem. B* **2005**, *109*, 2262

-
- [140] Barrio L.; Lui P.; Rodriguez J.; Campos-Martin M.; Fierro J. L. G. *J. Phys. Chem. C* **2007**, *111*, 19001
- [141] W. T. Wallace W. T.; Wheten R. L. *J. Am. Chem. Soc.* **2002**, *124*, 7499
- [142] Okumura M.; Haruta M.; Kitagawa Y.; Yamaguchi K. *Gold. Bull.* **2007**, *40*, 40
- [143] S. Chretien S.; Metiu H. *J. Chem. Phys.* **2007**, *126*, 104701
- [144] Naresh J. K.; Chandrakumar K. R. S.; Ghosh S. K. *J. Phys. Chem. C* **2009**, *113*, 17885
- [145] Shafai G.; Hong S.; Bertino M.; Rahman T. S. *J. Phys. Chem. C* **2009**, *113*, 12072
- [146] Ferrando R.; Jellinek J.; Johnston R. L.; Washington D. C. *Chem. Rev.* **2008**, *108*, 845
- [147] Orlov A. O.; Amlani I.; Bernstein G. H.; Lent C. S.; Snider G. L. *Science* **1997**, *277*, 928
- [148] Valden M.; Lai X.; Goodman D. W. *Science* **1998**, *281*, 1647
- [149] Cao B.; Starace A. K.; Judd O. H.; Jarrold M. F. *J. Am. Chem. Soc.* **2009**, *131*, 2446
- [150] Romanowski Z.; Krukowski S.; Grzegory I.; Porowski S. *J. Chem. Phys.* **2001**, *114*, 6353
- [151] Haberland H. *Clusters of Atoms and Molecules: Theory, Experiment, and Clusters of Atoms.* Springer-Verlag, Heidelberg **1994**
- [152] Mann D. M.; Broida H. P. *J. Appl. Phys.* **1973**, *44*, 4950
- [153] Ray U.; Jarrold M. F.; Bower J. E.; Kraus J. S. *Chem. Phys. Lett.* **1989**, *159*, 221
- [154] Cox D. M.; Trevor D. J.; Wheten R. L.; Kaldor A. *J. Phys. Chem.* **1988**, *92*, 421
-

-
- [155] Fielicke A.; Kirilyuk A.; Ratsch C.; Behler J.; Scheffler M.; Helden von G.; Meijer G. *Phys. Rev. Lett.* **2004**, *93*, 023401
- [156] Weis P.; Bierweiler T.; Glib S.; Kappes M. M. *Chem. Phys. Lett.* **2002**, *355*, 355
- [157] Bulusu S.; Li X.; Wang L. S.; Zeng X. C. *Proc. Natn. Acad. Sci.* **2006**, *103*, 8326
- [158] Kran B.; Bulusu S.; Zhai H. J.; Yoo S.; Zeng X. C.; Wang L. S. *Proc. Natn. Acad. Sci.* **2005**, *102*, 961
- [159] Knight W. D.; De Heer W. A.; Saunders W. A.; Clemenger K.; Chou M. Y.; Cohen M. L. *Chem. Phys. Lett.* **1987**, *134*, 1
- [160] Ekardt W. *Phys. Rev. B* **1984**, *29*, 1558
- [161] Brack M. *Rev. Mod. Phys.* **1993**, *65*, 677
- [162] Kirkpatrick S.; Gelatt. C. D.; Vecchi M. P. *Science* **1983**, *220*, 671
- [163] Boustani I.; Pewestorf W.; Fantucci P.; Bonacic-Koutecky V.; Koutecky J. *Phys. Rev. B* **1987**, *B35*, 9437
- [164] Jena P.; Khanna S. N.; Rao B. K.; **Microclusters**. Edited by Sugano S.; Nishina Y.; Ohnishi S. *Springer-Verlag, Heidelberg* **1987**
- [165] Shetty S. *Ph. D. Thesis, Pune University* **2005**, *43*, 291
- [166] Car R.; Parrinello M. *Phys. Rev. Lett.* **1985**, *55*, 2471
- [167] Galli G.; Martin R.; Car R. M.; Parrinello M. *Science* **1990**, *250*, 1547
- [168] Ballone P.; Andreoni W.; Car R.; Parrinello M. *Phys. Rev. Lett.* **1988**, *60*, 271
- [169] Hohl D.; Jones R. O.; Car R.; Parrinello M. *Phys. rev. Lett.* **1987**, *139*, 540
- [170] Allen M. P.; Tildesley D. J. **Computer Simulation of Liquids**. *Clarendon Press, Oxford* **1987**
-

-
- [171] Pauling L. *The Nature of Chemical Bond and Structure of Molecule and Crystals; Oxford and IBH: New Delhi 1967*
- [172] Weeny Mc. R. Coulson's Valence *Oxford University Press, Oxford 1979*
- [173] Theoretical Models of Chemical Bonding: The Concept of the Chemical Bond; Maksic, Z. B. Ed. *Springer-Verlag: Berlin 1990*
- [174] Fukui K. Theory of Orientation and Stereo Selection *Springer-Verlag, Berlin 1975*
- [175] Stretwieser Jr. A. Molecular Orbital Theory for Organic Chemists; *John-Wiley & Sons, New York 1961, 43, 291*
- [176] Dewar M. J. S. The Molecular Orbital Theory of Organic Chemistry *McGraw-Hill, New York 1969*
- [177] Dewar M. J. S. *Trans. Faraday Soc 1946, 42, 764*
- [178] Coulson C. A. *Discussions Faraday Soc 1947, 2, 9*
- [179] Coulson C. A. *J. Chem. Phys. 1948, 45, 243*
- [180] Coulson C. A.; Longuet-Higgins, H. C. *Proc. Roy. Soc. A (London) 1947, 191, 39*
- [181] Wheland G. W. *J. Am. Chem. Soc. 1942, 64, 900*
- [182] *Conceptual Trends in Quantum Chemistry*, Ed. by Kryachko E. S. ; Clais J. L. *Kluwar Academic Publishers, Netherlands 1994*
- [183] Woodward R. B.; Hoffmann R. *J. Am. Chem. Soc. 1965, 87, 395*
- [184] Woodward R. B.; Hoffmann R. *Acc. Chem. Res. 1968, 1, 17*
- [185] Woodward R. B.; Hoffmann R. **The Conservation of Orbital Symmetry**, *New York, Academic Press 1989*
-

-
- [186] Mulliken R. S. *J. Am. Chem. Soc.* **1952**, 74, 811
- [187] Orgel, L. E.; Mulliken, R. *J. Am. Chem. Soc.* **1957**, 79, 4839
- [188] Tsubomura, H.; Mulliken R. S. *J. Am. Chem. Soc.* **1960**, 82, 5966
- [189] Pearson R. G. **Hard and Soft Acids and Bases** Dowden, Hutchinson, and Ross, Stroudsburg, PA **1973**
- [190] Pearson R. G. **Chemical Hardness: Applications from Molecules to Solids** Wiley-VCH Verlag GMBH: Weinheim **1997**
- [191] Politzer, P.; Truhlar, D. G. Ed. **Chemical Applications of Atomic and Molecular Potentials** Plenum, New York **1981**
- [192] Murray J. N; Sen K. D. Ed. **Molecular Electrostatic Potential: Concepts and Applications:** , . Elsevier, Amsterdam **1996**
- [193] Gadre S. R.; Shirsat R. N. **Electrostatics of atoms and Molecules** Universities Press, Hyderabad, India **2000**
- [194] Bader R. F. W. **Atoms in Molecules: A Quantum Theory** Clarendon Press, Oxford. **1990**
- [195] Pearson, R. G. In K. D. Sen Ed. *Structure and Bonding*; Springer, Berlin **1993**
- [196] Ahrland S.; Chatt J.; Davies N. *Quart. Revs. (London)* **1958**, 12, 265
- [197] Mulliken R. S. *J. m. Chem. Soc.* **1955**, 77, 884
- [198] Mulliken R. S. *J. Phys. Chem.* **1952**, 56, 801
- [199] Pearson R. G. *J. Am. Chem. Soc.* **1963**, 85, 3533
- [200] Pearson R. G. *Science* **1966**, 151, 172

-
- [201] Pearson, R. G. *Coord. Chem. Rev.* **1990**, *100*, 403
- [202] Huheey J. E. **Inorganic Chemistry: Principles of Structure and Reactivity**
Harper and Row: New York 1983
- [203] Klopman G. **Chemical Reactivity and Reaction Path** *Wiley, New York 1974*
- [204] Fleming I. **Frontier Orbitals and Organic Chemical Reactions** *Wiley, New York 1976*
- [205] Drago R. S. *Structure and Bonding* **1973**, *15*, 73
- [206] Drago R. S.; Wayland B. B. *J. Am. Chem. Soc* **1965**, *87*, 3571
- [207] Drago, R. S.; Kabler, R. A. *Inorg. Chem.* **1972**, *11*, 3144
- [208] Drago R. S. *Inorg. Chem.* **1973**, *12*, 2211
- [209] Parr R. G; Yang W. **Density Functional Theory of Atoms and Molecules**, *Oxford University Press: New York. 1989*
- [210] De Proft F.; Geerlings P. *Chem. Rev.* **2001**, *101*, 1451
- [211] Geerlings P.; De Proft F.; Langenaeker W. *Chem. Rev.* **2003**, *103*, 1793.
- [212] Mendez F.; Tamariz J.; Geerlings P. *J. Phys. Chem. A* **1993**, *97*, 4059.
- [213] Pearson R. G. **Hard and Soft Acids and Bases**, *Dowden, Hutchinson, and Ross: Stroudsburg, PA 1973*
- [214] Pearson R. G. *J. Chem. Educ.* **1987**, *64*, 561.
- [215] Pearson, R. G. *J. Am. Chem. Soc.* **1963**, *85*, 3533.
- [216] Parr R. G.; Zhou Z. *Acc. Chem. Res.* **1993**, *26*, 256.
- [217] Zhou, Z.; Parr, R. G.; Garst, J. F. *Tetrahedron Lett.* **1988**, *29*, 4843.
-

-
- [218] Zhou Z.; Parr R. G. *J. Am. Chem. Soc.* **1989**, *111*, 7371.
- [219] Zhou Z.; Navangul H. V. *J. Phys. Org. Chem.* **1990**, *3*, 784.
- [220] Zhou, Z. *J. Phys. Org. Chem.* **1995**, *8*, 103.
- [221] Harbola M. K. *Proc. Natl. Acad. Sci. USA* **1992**, *82*, 264.
- [222] Alonso J. A.; Balbas L. C.; *in Structure and Bonding, Ed. by Sen. K. D.* **80**, 229, 1993.
- [223] Geerlings P.; De Proft F. *Int. J. Mol. Sci.* **2002**, *3*, 276.
- [224] Roy R. K.; Tajima N.; Hirao K. *J. Phys. Chem. A* **2001**, *105*, 2117.
- [225] Geerlings P.; De Proft F.; Langenaeker W. *Adv. Quant. Chem.* **1999**, *33*, 303.
- [226] Langenaeker W.; De Proft F. Geerlings P. *J. Phys. Chem.* **1995**, *99*, 6424.
- [227] Geerlings P.; De Proft F. *Int. J. Quantum. Chem.* **2000**, *80*, 227.
- [228] Baeten A.; De Proft F. Geerlings P. *Chem. Phys. Lett.* **1995**, *235*, 17.
- [229] Nguyen L. T.; De Proft F.; Nguyen M. T.; Geerlings P. *J. Org. Chem.* **2001**, *66*, 4316.
- [230] Nguyen L. T.; De Proft F.; Chandra A. K.; Uchimarui T.; Nguyen M. T.; Geerlings P. *J. Org. Chem.* **2001**, *66*, 6096.
- [231] Sengupta D.; Chandra A. K.; Nguyen M. T. *J. Org. Chem.* **1999**, *62*, 6404.
- [232] Damoun S.; Van de Woude G.; Mendez F.; Geerlings P. *J. Phys. Chem., A* **1997**, *101*, 886.
- [233] Ponti, A. *J. Phys. Chem. A* **2000**, *104*, 8843
-

-
- [234] Tielemans M.; Areschka V.; Colomer J.; Promel R.; Langenaeker W.; Geerlings P. *Tetrahedron*, **1992**, *48*, 10575.
- [235] Langenaeker W.; Demel K.; Geerlings P. *J. Mol. Struct. THEOCHEM*. **1991**, *234*, 329.
- [236] Choho K.; Langenaeker W.; Van De Woude G.; Geerlings P. *J. Mol. Struct. THEOCHEM*. **1996**, *305*, 362.
- [237] Ghosh S. K. *Chem. Phys. Lett.* **1990**, *172*, 77.
- [238] De Proft F.; Amira S.; Choho K.; Geerlings P. *J. Phys. Chem.* **1994**, *98*, 5227.
- [239] Langenaeker W.; Coussement N.; De Proft F.; Geerlings P. *J. Phys. Chem.* **1994**, *98*, 3010.
- [240] Chandra A. K.; Nguyen M. T. *J. Chem. Soc. Perkin. Trans.* **1997**, *2* 1415.
- [241] Perez P.; Toro-Labbe A.; Contreras R. *J. Phys. Chem. A* **2000**, *104*, 5882
- [242] Roy R. K.; De Proft F.; Geerlings P. *J. Phys. Chem. A* **1998**, *102*, 7035.
- [243] Van Lier G.; Fowler P. W.; De Proft F.; Geerlings P. *J. Phys. Chem. A* **2002**, *106*, 5128.
- [244] Damoun S.; Van de Woude G.; Choho K.; Geerlings P. *J. Phys. Chem. A* **1999**, *103*, 7861.
- [245] Mendez F.; Tamariz,; Geerlings P. *J. Phys. Chem. A* **1998**, *102*, 6292
- [246] Patricia P.; Toro-Labbe A.; Contreras R. *J. Phys. Chem. A* **2001**, *105*, 4272.
- [247] P. Perez, Simon-Manso Y.; Aizman A.; Fuentealba P.; Contreras R. *J. Am. Chem. Soc.* **2000**, *122*, 4756.
- [248] Langenaeker W.; De Proft F.; Geerlings P. *J. Phys. Chem. A* **1998**, *102*, 5944.
-

-
- [249] Anane H.; Jarid A.; Boutalib A.; Nebot-Gill I.; Toma F. *Chem. Phys. Lett.* **2000**, 324, 156
- [250] Jonos V.; Renking G.; Reetz M. T. *J. Am. Chem. Soc.* **1994**, 116, 8741.
- [251] Krishnamurty S.; Pal S. *J. Phys. Chem. A* **2000**, 104, 7639.
- [252] Deka R. C.; Hirao K. *J. Mol. Cata. A*, **2002**, 181, 275.
- [253] Deka R. C.; Roy R. K.; Hirao K. *Chem. Phys. Lett.* **2000**, 332, 576.
- [254] Russo N.; Toscano M.; Grand A.; Mineva T. *J. Phys. Chem. A* **2000**, 104, 4017.
- [255] Roy R. K.; Krishnamurti S.; Geerlings P.; Pal S. *J. Phys. Chem. A* **1998**, 102, 3746.
- [256] Perez P.; Toro-Labbe A.; Aizman A.; Contreras R. *J. Org. Chem.* **2002**, 67, 4747.
- [257] Domingo L. R.; Aurell M. J.; Perez P.; Contreras R. *J. Phys. Chem. A*. **2002**, 106, 6871
- [258] Perez P.; Toro-Labbe A.; Contreras R. *J. Am. Chem. Soc.* **2001** 123, 5527.
- [259] Perez P.; Aizman A.; Contreras R., *J. Phys. Chem. A*. **2002**, 106, 3964.
- [260] Corma A.; Llopis F.; Viruela P. *J. Am. Chem. Soc.* **1994**, 116, 134.
- [261] Langenaeker W.; De Decker M.; Geerlings P.; Raeymaekers P. *J. Mol. Struct. THEOCHEM.* **1990**, 207, 115.
- [262] Damoun S.; Langenaeker W.; Geerlings P. *J. Phys. Chem. A*. **1997**, 101, 6951.
- [263] Damoun S.; Langenaeker W.; Van de Woude G. Geerlings P. *J. Phys. Chem.* **1995**, 99, 12151.
- [264] Baekelandt B. G.; Mortier W. J.; Schoonheydt R. A. **Structure and Bonding**, Vol.80, Ed. by Sen, K. D.; Springer-Verlag, Berlin, 187, **1993**.
-

-
- [265] Krishnamurthy S.; Roy R. K.; Vetrivel R.; Iwata S.; Pal S. *J. Phys. Chem. A* **1997**, *101*, 7253.
- [266] Deka R. C.; Pal S.; Goursot A.; Vetrivel R. *Catalysis Today*, **1999**, *49*, 221.
- [267] Chattaraj P. K.; Poddar A. *J. Phys. Chem. A* **1998**, *102*, 9944.
- [268] Chattaraj P. K.; Poddar A. *J. Phys. Chem. A* **1999**, *103*, 1274.
- [269] Chattaraj P. K.; Poddar A. *J. Phys. Chem. A* **1999**, *103*, 8691.

CHAPTER 2

**Theoretical Methods and
Computational Aspects**

2.1 The Schrödinger Equation

The time independent non-relativistic Schrödinger equation

$$\hat{H}\Psi = E\Psi \quad (2.1)$$

provides a theoretical foundation for the solution of virtually all problems in chemistry. \hat{H} is the Hamiltonian operator, Ψ is a many-particle wave function, and E is the energy of the system. The set of wave functions Ψ_i , ($i = 1, 2, \dots$), which are the solutions of this equation, represent the set of possible quantum states of the system with the wave function Ψ_i containing all information for the state i . However, the analytic solution of the Schrödinger equation has only been possible to date for atoms and molecules with only one electron. In atomic units the Hamiltonian for N electrons and M nuclei is

$$\hat{H} = - \sum_{i=1}^N \frac{1}{2} \Delta_i^2 - \sum_A \frac{1}{2M_A} \Delta_A^2 - \sum_{i=1}^N \sum_{A=1}^M \frac{Z_A}{r_{iA}} + \sum_{i=1}^N \sum_{j>i}^N \frac{1}{r_{ij}} + \sum_{A=1}^M \sum_{A>B}^M \frac{Z_A Z_B}{R_{AB}} \quad (2.2)$$

In the above equation M_A and Z_A are the mass and the charge of the nucleus A , $r_{iA} = |\mathbf{r}_i - \mathbf{R}_A|$ is the distance between the i^{th} and the A^{th} nucleus, $r_{ij} = |\mathbf{r}_i - \mathbf{r}_j|$ is the distance between the i^{th} and the j^{th} electron and $R_{AB} = |\mathbf{R}_A - \mathbf{R}_B|$ is the distance between the A^{th} and the B^{th} nucleus. For molecules, the first approximation made in all the calculations is the Born-Oppenheimer approximation, in which the nuclear and the electronic wave functions are considered separately.

2.2 The Born – Oppenheimer Approximation

Since nuclei are much heavier as compared to electrons, they move very slowly. Hence, to a quality approximation, one can consider the electrons in a molecule to be moving in the field of fixed nuclei. Within the approximation, the kinetic energy of the nuclei is neglected and the repulsion between the nuclei is taken to be constant. Hence, electronic Hamiltonian describing the motion of N electrons in the field of M nuclei, is given as,[1]

$$\hat{H} = - \sum_{i=1}^N \frac{1}{2} \Delta_i^2 - \sum_{i=1}^N \sum_{A=1}^M \frac{Z_A}{r_{iA}} + \sum_{i=1}^N \sum_{j>i}^N \frac{1}{r_{ij}} + \sum_{A=1}^M \sum_{A>B}^M \frac{Z_A Z_B}{R_{AB}} \quad (2.3)$$

Electronic structure methods solve the eigenvalue equations of the electronic Hamiltonian and the total energy is obtained as a sum of the electronic energy and the constant nuclear repulsion. There are many theoretical methods which can be used to solve the Schrödinger equation such as HF, CI, CC, etc.[1] One such method is the DFT which uses the electron density instead of the wavefunction. This method is not only easy to derive but also computationally cheaper than the other ab initio methods. Moreover, DFT considers the electron–electron correlation unlike the HF. DFT has been explicitly used in the present thesis.

2.3 Density Functional Theory

DFT has long been an extremely useful method for the electronic structure calculations in quantum chemistry. It has been successfully applied to calculate the ground state properties of atoms, molecules, metals, semiconductors, etc. DFT is a rigorous way of circumventing the interacting problem of ground state by a more trivial non-interacting problem. The breakthrough idea of DFT is to describe an interacting system of N –electrons through its electron density and not via its many–body wave function. The fact that the ground state properties are functionals of the electron density, $\rho(r)$, was proved

by Hohenberg and Kohn and it implements the basic framework for modern DFT.[2]

2.3.1 Hohenberg–Kohn Theorems

The first HK theorem states that the external potential $v(r)$ (second term in the eqn 2.3) is determined, within a trivial additive constant, by the electron density $\rho(r)$. [2] Since ρ determines the number of electrons, it follows that $\rho(r)$ also determines the ground state wave function Ψ and all other electronic properties of the system.

$$\rho(r) \longrightarrow N \longrightarrow \Psi_i \longrightarrow \text{all properties}$$

The second HK theorem provides the energy variational principle. It states that, for a trial density $\rho'(r)$ such that $\rho'(r) \geq 0$ and $\int \rho'(r) dr = N$

$$E_0 \leq E_v[\rho'] \tag{2.4}$$

E_0 is the energy which corresponds to the ground state electron density. The above equation presents a search for the ground state electron density and corresponding ground state energy through the minimization of the energy functional $E[\rho]$. However, the trial densities should satisfy the necessary criteria of N–representability, i.e. the trial density should be associated with an anti–symmetric wavefunction. More importantly, the density should also have some external potential and satisfying the v–representability condition. The N–representability condition is necessary for the v–representability condition. Levy has shown that there are some densities which are not v–representable i.e. the densities do not map to any external potential. [4] Therefore, such non–v–representable densities would not correspond to any ground state.

2.3.2 Kohn–Sham Method

KS introduced a method based on the HK theorem that enables minimization of $E[\rho(r)]$ by varying $\rho(r)$ over all densities containing N electrons.[3] The total electronic energy

in the KS approach, $E[\rho(r)]$ can be partitioned as follows

$$E_{total}[\rho(r), RI] = -\frac{1}{2} \sum_i \langle \psi_i(r) | \Delta_i^2 | \psi_i(r) \rangle + \frac{1}{2} \int \int \frac{\rho(r)\rho(r')}{|r-r'|} dr dr' + E_{xc}[\rho(r)] + \int V_{nuc}(r)\rho(r)dr \quad (2.5)$$

In the above eqn 2.5, the first term is the kinetic energy of electrons in a model non-interacting system which has the same electron density as the real system. The second term is the pure Coulomb interaction between the electrons. The third term is the exchange–correlation energy, which includes the electron exchange, the difference of the non–interacting and the interacting kinetic energy and the correction for the self interaction due to the Coulomb potential, and the last term is the external potential, i.e., potential coming from nuclei. The minimum of the KS functional is obtained by varying the energy functional (eqn. 2.5) with respect to the electron density. This leads to the KS orbital equations

$$[-\frac{1}{2}\Delta_i^2 + v_{eff}] \psi_i = \epsilon_i \psi_i \quad (2.6)$$

$$v_{eff}(r) = v(r) + \int \frac{\rho(r')}{|r-r'|} dr' + V_{xc}(r) \quad (2.7)$$

$$\rho(r) = \sum_{i=1}^n |\psi_i(r)|^2 \quad (2.8)$$

Eqn 2.8 is the electron density. Since the sum of the orbital energies is not equal to the total electronic energy. Hence, the total electronic energy can be derived as

$$E = \sum_{i=1}^n \epsilon_i - \frac{1}{2} \int \int \frac{\rho(r)\rho(r')}{|r-r'|} dr dr' + E_{xc}[\rho(r)] - \int V_{xc}\rho(r)dr \quad (2.9)$$

The exchange–correlation functional as defined by KS remains unknown. However, there exist several approximations. LDA is the simplest possible density functional approximation where the exchange and correlation of an interacting but homogeneous electron gas at the density given by the local density $\rho(r)$ at space point r in the inhomogeneous system.[3] It is defined as

$$E_{xc}^{LDA}[\rho(r)] = \int \rho(r)\epsilon_{xc}\rho(r)dr \quad (2.10)$$

More sophisticated is the GGA approximation, where the unknown functional is approximated by an integral over a function that depends only on the density and its gradient at a given point in space.

$$E_{xc}^{GGA}[\rho(r)] = \int dr \rho(r) \epsilon_{xc}^{GGA}(\rho(r); \Delta\rho(r)) \quad (2.11)$$

Some of the GGA functional for example, are the BLYP,[5, 6] the PW91,[7] or the PBE exchange–correlation density functionals.

2.4 Classical Molecular Dynamics

In classical MD, the nuclear motion in a molecular system is treated by the classical equations of motion interacting via a potential. The potential used to derive the forces on the atoms are classical such as Lennard–Jones, Buckingham, etc. These potentials do not account the electronic motion and hence, classical MD becomes computationally much cheap. In MD, successive configurations of the system are generated by integrating the Newtons equation of motion. The result is the trajectory that specifies how the positions and velocities of the atoms in the system vary with respect to time. Hence, MD is a deterministic approach, in which the state of the system at any future time can be predicted from its current state.[8] The trajectory is obtained by solving the differential equations involved in the Newtons second law. Given a set of atoms of masses M_I at position R_I , one can write

$$F_I = M_I \ddot{\mathbf{R}}_I \quad (2.12)$$

where the force on the atom I is given by F_I , which can be related to the potential E_{R_I} as

$$F_I = \frac{\delta E(\mathbf{R}_I)}{\delta \mathbf{R}_I} \quad (2.13)$$

Various algorithms have been devised to solve the above equations. Perhaps the most widely used method is the Verlet algorithm.[8] The method is based on the atomic positions $\mathbf{R}_I(t)$, accelerations $\mathbf{A}_I(t)$ and the atomic positions of the previous step $\mathbf{R}_I(t + \Delta t)$.

The equation for the next step is calculated from the Taylor expansion

$$\mathbf{R}_I(t + \Delta t) = \mathbf{R}_I(t) + \Delta t \mathbf{V}_I(t) + \frac{1}{2} \Delta t^2 \mathbf{A}_I(t) + \dots \quad (2.14)$$

$$\mathbf{R}_I(t - \Delta t) = \mathbf{R}_I(t) - \Delta t \mathbf{V}_I(t) + \frac{1}{2} \Delta t^2 \mathbf{A}_I(t) - \dots \quad (2.15)$$

Adding 2.14 and 2.15 we have

$$\mathbf{R}_I(t + \Delta t) = 2\mathbf{R}_I(t) - \mathbf{R}_I(t - \Delta t) + \frac{\Delta t^2}{M_I} F_I \quad (2.16)$$

where F_I is given by Eqn 2.13 The velocities are not needed to compute the trajectories, but they are useful to calculate the kinetic energy. They may be obtained as

$$\mathbf{V}_I(t) = \frac{\mathbf{R}_I(t + \Delta t) - \mathbf{R}_I(t - \Delta t)}{2\Delta t} \quad (2.17)$$

In MD simulations, it is very important to store the information of the system after every Δt step, such as, velocities, forces and the instantaneous values of all the calculated properties. The information stored in an MD simulation is time ordered and can be used to calculate time correlation function, and thus, can be used to calculate the transport properties such as diffusion coefficient, viscosity coefficient, etc. Moreover, the temperature dependent properties can also be calculated from the equipartition law

$$\frac{3}{2} N K_B T = \left\langle \sum_{i=1}^N \frac{1}{2} m_i^2 v_i^2 \right\rangle \quad (2.18)$$

Although many systems have successfully been investigated with model potentials like for eg. Lennard–Jones potentials. In classical MD it is difficult to account for the local atomic properties such as, chemical bonding, including the chemical reactions which form and break bonds in a quantum mechanical fashion. On the other hand, quantum dynamics of the nuclear motion of a large molecular system becomes highly computationally expensive. These difficulties can be accomplished by the use of AIMD.

2.5 *Ab Initio* Molecular Dynamics

AIMD method allows to simulate the motion of the individual atoms based on forces which are calculated quantum mechanically.[9, 10] The basic idea behind AIMD is that,

since the nuclei are much heavier than the electrons should be moved classically using the Newtons equation of motion under the electronic potential derived from quantum mechanical approach. In 1985, in a seminal paper, Car and Parrinello initiated the field of AIMD by combining the conventional MD technique with the DFT and were termed to be CPMD.[11] This allows one to study, formation and breaking of chemical bonds in contrast to the conventional MD. A number of other techniques have been developed which are based on minimization of the electronic orbitals to their ground state at each time step. These techniques were referred to as BOMD.

2.5.1 Car Parrinello Molecular Dynamics

Car and Parrinello proposed a scheme based on MD and DFT.[11] They postulated the following Lagrangian

$$\mathcal{L}_{CP} = \frac{1}{2} \sum_i \mu \int |\dot{\psi}_i(\mathbf{r})|^2 dr + \frac{1}{2} \sum_I M_I \dot{\mathbf{R}}_I^2 - E_{total}[\psi_i, \mathbf{R}_I] + \sum_{ij} \Lambda_{ij} \left(\int dr \psi_i^*(\mathbf{r}) \psi_j(\mathbf{r}) - \delta_{ij} \right) \quad (2.19)$$

\mathcal{L} does not depend explicitly on time, and is a functional of two states of classical degrees of freedom, the ψ_i and the \mathbf{R}_I , which depend on time. The μ_i are arbitrary parameters which play the generalized masses for the electronic degrees of freedom. The first and the second term in Eqn.2.19 are the kinetic energy of the electronic (K_e) and ionic degrees of freedom (K_I), respectively. E is the potential energy of the coupled electron-ion fictitious system. The Lagrangian multipliers Λ_{ij} are used to impose orthonormality conditions on the ψ_i .

The Euler equations associated with the Eqn.2.19 are

$$\mu \ddot{\psi}_i = -\frac{\delta E}{\delta \psi_i^*} + \sum_j \Lambda_{ij} \psi_j \quad (2.20)$$

$$M_I \ddot{\mathbf{R}}_I = -\frac{\delta E}{\delta \mathbf{R}_I} \quad (2.21)$$

According to the Car–Parrinello equations of motion, the nuclei evolve in time at a certain physical temperature $\propto K_I$, whereas a fictitious temperature $\propto K_e$ is associated to the electronic degrees of freedom. Thus, a groundstate wavefunction optimized for the initial configuration of the nuclei will stay close to its ground state also during time evolution if it is kept at a sufficiently low temperature and need not be optimized after each time step.

2.5.2 Born Oppenheimer Molecular Dynamics

An alternative approach to include the electronic structure in molecular dynamics simulations consists in straightforwardly solving the static electronic structure problem in each molecular dynamics step, given the set of fixed nuclear positions at that instance of time.[12] Thus, the electronic structure part is reduced to solving a time independent quantum problem, e.g. by solving the time independent Schrödinger equation, concurrently to propagating the nuclei via classical molecular dynamics. Thus, the BOMD equation is given by

$$\mathcal{L}_{BO} = \frac{1}{2} \sum_I M_I \dot{\mathbf{R}}_I^2 - \min_{\{\psi_i\}} E_{total}[\{\psi_i\}, \{\dot{\mathbf{R}}_I\}] \quad (2.22)$$

and the minimization is constraint to orthogonal sets of $\{\phi_i\}$. The equations of motion are

$$M_I \ddot{\mathbf{R}}_I = -\Delta_I [\min_{\{\psi_i\}} E[\{\psi_i\}; \{\mathbf{R}_I\}]] \quad (2.23)$$

The above Eqn. ensures that the minimization of the electronic energy is done at each MD step.

2.5.3 Comparison of CPMD and BOMD

It is very important to ask which AIMD method would be the most computationally efficient? One of the advantage of CPMD over BOMD is that no diagonalization of the Hamiltonian (or the equivalent minimization of an energy functional) is necessary,

except at the very first step in order to obtain the initial wavefunction. In CPMD, the explicitly treated electron dynamics does not allow one to take a larger time-step that can be used in order to integrate the coupled equations of motion for nuclei and electrons. Since, in BOMD there is no explicit dependence on the electronic motion the maximum time-step is given by the nuclear motion only. However, the time gained in BOMD due to the larger time step is lost in the orthogonalization. But it is seen that BOMD is an order of magnitude faster than the CPMD. For a more detailed comparison between the CPMD and BOMD, one can refer to [13]. In the present thesis we have used the BOMD approach for obtaining the ground state structures of metal clusters. The BOMD method has been used to drive the system in a minimum energy configuration by using the simulated annealing technique (Section 2.6). The details of BOMD and CPMD are discussed in several reviews and thesis[12, 14–16].

2.6 Optimization Techniques

Optimization techniques are used to drive the system in the minimum energy configuration. Once the initial configuration is defined the next step is to find its minimum energy structure. A variety of optimization techniques have been suggested. Basically, there are two kinds of optimizations, one is the electronic energy optimizations at a fixed nuclei and the other is the geometrical optimization. The final ground state geometry is considered only when the ions and the electrons are in their minimum energy configurations.

Conjugate gradient

The conjugate gradient method provides simple and efficient way to locate the minimum of a particular system[17]. The initial direction is taken to be the negative of the gradient at the starting point. A subsequent conjugate direction is then constructed from a linear combination of the new gradient and the previous direction that minimized the function.

It should be noted that at each point the gradients are orthogonal but the directions are conjugate. Since the minimization along the conjugate directions are independent, the dimensionality of the vector space explored in this technique reduces by one at each iterations. When the dimensionality of the function has been reduced to zero, there are no directions left in which to minimize the function, so the trial vector must be at the minimum. In this technique, the search direction is generated using the information from all the sampling points along the conjugate gradient path. This method works very well for the systems lying close to the minima.

Simulated Annealing

Annealing is the process in which the temperature of a system is increased till it melts and then it is slowly reduced until the material crystallizes. Simulated annealing is a computational method which uses the same approach as this, in order to find the minimum of a particular system[18].

For a system containing many ions will have several ionic configurations that are minimas. The simulated annealing procedure has to explore all these minimas to locate the lowest energy minima. At a given temperature the system is allowed to reach thermal equilibrium using a AIMD technique. At high temperatures, the system is able to occupy high energy regions of conformational space and to pass over high energy barriers. As the temperature is lowered, the lower energy becomes more probable in accordance with the Boltzmann distribution. At absolute zero the system should occupy the lowest energy state(i.e. the global energy conformation). Simulated annealing is ideal for the systems having small difference between the local and the global minima. This is often difficult to acheive in practice. Thus, simulated annealing cannot guarantee to find the global minimum. This technique has been very useful in obtaining the ground state geometries of metal clusters and to study their thermodynamical properties[19].

In the present thesis we use the simulated annealing technique to obtain the lowest

energy state structures of the metal clusters.

Finding the Minimum using AIMD

Initially the charge density is obtained from Eqn.2.8 to calculate the KS energy functional (Eqn.2.12) by solving the KS equations (Eqn.2.5) self-consistently as discussed in the section 2.3.2. Reaching the minimum of the energy is only the first step in an AIMD simulation. In the next step, the force on the ions are computed according to the Hellman–Feynman theorem. The ions are then moved by solving the Newtons equation of motion (Eqn. 2.21) by Eqn. 2.16. As the ions are moved, the KS energy functional is minimized again, in order to calculate the Hellman–Feynman forces at every point in the MD trajectory.

2.7 Conceptual DFT

2.7.1 Global Reactivity Descriptors

As already mentioned, electron density $\rho(r)$ is the fundamental variable in DFT. It contains all the information about the system. $\rho(r)$ determines external potential due to nuclei, $v(r)$. Determination of $v(r)$ implies fixing of the Hamiltonian H of the system. It also determines N , the total number of electrons, via its normalization.

$$\int \rho(r) dr = N \quad (2.24)$$

Since, it determines number of electrons, it follows that $\rho(r)$ also determines the wavefunction and all other electronic properties. This theorem is also known as first Hohenberg–Kohn theorem[20].

$$E = E_v(\rho) \quad (2.25)$$

The second HK theorem provides the energy variational principle i.e. looking for $\rho(r)$ what minimizes the energy functional $E_v(\rho)$. For optimal $\rho(r)$ the energy doesnt change

with variation of $\rho(r)$, provided the $\rho(r)$ integrates to N. This constraint can be introduced by method of Lagrangian multipliers, yielding the variational condition:

$$\delta\{E - \mu(\int \rho(r)dr - N)\} = 0 \quad (2.26)$$

where, μ is the corresponding Lagrangian multiplier.

One finally obtains Euler–Lagrange equation:

$$\mu = \frac{\delta E_v(\rho)}{\delta \rho(r)} = v(r) + \frac{\delta F_{HK}}{\delta \rho(r)} \quad (2.27)$$

F_{HK} is universal Hohenberg–Kohn functional (now onwards we will use notation F instead of F_{HK}) comprising of electronic kinetic energy functional, $T[\rho]$ and the electron–electron interaction functional, $V_{ee}[\rho]$.

In the landmark paper by Parr and coworkers[21], they provided interpretation of Lagrangian multiplier μ . They showed that under “N representability assumption”[22] and “V representability assumption”[23] if the density is derived from anti–symmetric wavefunctions, the following stationary principle holds.

$$\delta\{E[\rho'] - \mu N[\rho']\} = 0 \quad (2.28)$$

where, ρ' is some approximation to exact ground state density ρ , normalized to total number of electrons, $N[\rho']=N$. The Lagrangian multiplier μ associated with Eq.2.28 is the derivative w.r.t. the value of constraint, N, of the minimum of the functional $E_v[\rho']$

$$\mu = \left(\frac{\partial E}{\partial N}\right)_{v(r)} \quad (2.29)$$

In analogy to thermodynamic chemical potential

$$\mu_{therm} = \left(\frac{\partial G}{\partial N}\right)_{P,T} \quad (2.30)$$

where, G represents Gibbs free energy and n the number of moles, μ is commonly termed as electronic chemical potential and measures the escaping tendency of the electrons

from the molecule. Based on Iczkowski and Margrave[24] formulation of electronegativity formula $\chi = -(\frac{\partial E}{\partial N})_{n=0}$, where $n=N-Z$, Z being atomic number of the nucleus; they made identification of this abstract Lagrange multiplier as

$$\chi = -\mu = -(\frac{\partial E}{\partial N})_{v(r)} \quad (2.31)$$

The Mullikens definition of electronegativity, which is given by,

$$\chi_M = \frac{I + A}{2} \quad (2.32)$$

where, I and A are the ionization potential and electron affinity respectively, which are nothing but the finite difference approximation to the Eq.2.31

Parr and Pearson[25] demonstrated the importance of second derivative of the energy with respect to number of electrons and termed it as absolute hardness (η).

$$\eta = \frac{1}{2}(\frac{\partial^2 E}{\partial N^2})_{v(r)} = \frac{1}{2}(\frac{\partial \mu}{\partial N})_{v(r)} \quad (2.33)$$

From Eq.2.33, chemical hardness can be interpreted as resistance of chemical potential to the change in number of electrons. The operational definition of the same was provided by the finite difference approximation to the above equation and can be expressed as,

$$\eta = \frac{I - A}{2} \quad (2.34)$$

They further theoretically deduced the HSAB principle (section 2.8), later, using concept of hardness and electronegativity equalization principle[26].

Another molecular property, softness (S), is also defined as,

$$S = \frac{1}{2\eta} = (\frac{\partial N}{\partial \mu})_{v(r)} \quad (2.35)$$

Recently Parr, Von Szentpaly and Liu, introduced another reactivity descriptor viz. electrophilicity index by combining electronegativity and hardness. To propose an electrophilicity index, Parr *et al.* assumed electrophile immersed in a sea of free electron gas at zero temperature and zero chemical potential[27]. For calculation of change in

binding energy due to partial electron transfer from the sea to the electrophile, energy change to the second order at constant external potential is considered.

$$\Delta E = \mu\Delta N + \frac{1}{2}\eta\Delta N^2 \quad (2.36)$$

The saturation point of the ligand for electron inflow was characterized by putting,

$$\frac{\Delta E}{\Delta N} = 0 \quad (2.37)$$

Combining Eqs.2.36 and 2.37 yields the amount of partial electron transfer as,

$$\Delta N = -\frac{\mu}{\eta} \quad (2.38)$$

and corresponding stabilization energy as,

$$\Delta E = -\frac{\mu^2}{2\eta} \quad (2.39)$$

The quantity $\frac{\mu^2}{\eta}$, is described as electrophilicity index (W) and considered to be a measure of electrophilicity of the ligand. In analogy to the equation of power ($W = \frac{V^2}{R}$) in classical electricity, it is also considered to be measure of “electrophilic power”. Under finite difference approximation, electrophilicity index can be written as,

$$W = \frac{\mu^2}{2\eta} = \frac{(I + A)^2}{8(I - A)} \quad (2.40)$$

The above descriptors can also be related to frontier orbital energies by making use of Koopmans approximation within the molecular orbital theory, where in I and A can be expressed in terms of HOMO and LUMO energies[28–30].

$$I = -\varepsilon_{HOMO} \quad (2.41)$$

$$A = -\varepsilon_{LUMO} \quad (2.42)$$

Since, all these parameters (chemical potential, hardness, softness and electrophilicity index) are obtained by averaging over molecular space these are called GRDs. Though, they are quite capable of describing overall reactivity of the system, they do not have any information about the nature of active atoms or group that constitutes the molecule.

2.7.2 Local Reactivity Descriptors

The most chemical reactions are generally associated with the expressed properties of the atoms or groups of atoms in the molecule and not to the molecule itself. Inability of the GRDs in identifying the reactive site in the molecule that has high proclivity to undergo chemical reaction is a matter of concern for understanding of reactivity in such systems. Concerning chemical reactivity, an important aspect is how the charge or density fluctuations in chemical systems affect, and are related to the observed reactivity trends. Since the electron density distribution, $\rho(r)$, contains all of the information on the system in its ground state, it is thought that the chemical reactivity should be reflected in its sensitivity to perturbations. These facts have necessitated or demanded the proposition of some descriptors that are local or non-local in nature, so called LRDs.

The concept of using electron density for description of reactivity was initiated by Fukui 1(a)-(b), when he introduced the role of frontier orbitals in describing reactivity of aromatic systems leading to three principles[31, 32]. He proposed that the site of attack is described by the highest electron density of two electrons in the frontier-orbitals. For electrophilic attack, the frontier orbitals are considered to be HOMO, for nucleophilic attack, the frontier orbitals are considered to be LUMO, whereas, for radical attack, one electron is assumed to be in HOMO and other in LUMO.

Parr and collaborators showed how Fukuis frontier-orbitals concept could be grounded in DFT[33–36]. They used ensemble formulation of DFT to introduce the expectation value N of total electron number as continuous variable and defined FFs (or the frontier function) as,

$$f(r) = \left(\frac{\partial\mu}{\partial v(r)}\right)_N = \left(\frac{\partial\rho(r)}{\partial N}\right)_{v(r)} \quad (2.43)$$

Considering the Fundamental equations for change in energy,

$$dE = \mu dN + \int \rho(\vec{r}) dv(\vec{r}) dr \quad (2.44)$$

$$d\mu = 2\eta dN + \int f(\vec{r}) dv(\vec{r}) dr \quad (2.45)$$

The quantity $d\mu$ in Eq. 2.45 measures the extent of the reaction. The preferred direction is the one for which the initial $|d\mu|$ for the species is a maximum. The first term on the right side of Eq. 2.45 involves only global quantities and at large distances, is ordinarily less direction sensitive than the second term. The preferred direction is the one with largest $f(r)$ at the reaction site[37].

Like $E(N)$, $\rho(r)$ being function of N , also has discontinuity at integral N ; Eq. 2.43 in fact provides two reaction indices as left- and right- hand-side derivatives, to be considered at a given number of electrons, $N=N_0$.

$$f^-(r) = \left(\frac{\partial\rho(r)}{\partial N}\right)_{v(r)}^- \quad (2.46)$$

for an electrophilic attack, provoking an electron increase in the system, and

$$f^+(r) = \left(\frac{\partial\rho(r)}{\partial N}\right)_{v(r)}^+ \quad (2.47)$$

for a nucleophilic attack, provoking an electron decrease in the system.

Under the frozen core approximation $d\rho = d\rho_{valence}$ in each case and therefore governing electrophilic attack,

$$f(r)^- = \rho_{HOMO} \quad (2.48)$$

governing nucleophilic attack,

$$f(r)^+ = \rho_{LUMO} \quad (2.49)$$

and the third function governing radical attack, as arithmetic mean of the above two.

$$f(r)^0 = \frac{1}{2}(\rho_{HOMO} + \rho_{LUMO}) \quad (2.50)$$

FF is normalized to unity,

$$\int f^a(r)dr = 1 \quad \forall a = +, -, 0 \quad (2.51)$$

Thus, FF contains the relative information about different regions in a given molecule; it doesn't describe the local intensity of the response. When comparing across different molecules, local softness $s(r)$, defined by Yang and Parr turns out to describe the

intensity of the response[38]:

$$s(r) = \left(\frac{\partial \rho(r)}{\partial \mu} \right)_{v(r)} \quad (2.52)$$

$s(r)$ is local analogous to global softness S (see Eq. 1.20). By applying chain rule, local softness can be written as the product of total softness and the FF,

$$s(r) = \left(\frac{\partial \rho(r)}{\partial \mu} \right)_{v(r)} = \left(\frac{\partial \rho(r)}{\partial N} \right)_{v(r)} \left(\frac{\partial N}{\partial \mu} \right)_{v(r)} = f(r)S \quad (2.53)$$

indicating that $f(r)$ redistributes the global softness among different parts of molecules, and that $s(r)$ integrates to S . The above equation can also be written as following to explicitly describe the electrophilicity, nucleophilicity or radical type attack.

$$\int s^a(r) dr = f^a(r)S \quad \forall a = +, -, 0 \quad (2.54)$$

$$S = \int s^a(r) dr \quad \forall a = +, -, 0 \quad (2.55)$$

2.7.3 Atom Condensed Local Descriptors

The formal definition of the FF as introduced by Parr and Yang, is a function of position r in the given molecular space, varying from one position to another[37]. By plotting these functions one can get idea about the reactive centers. However, to describe reactivity quantitatively, with reference to atomic centers, is difficult to interpret. Hence, it is necessary, to condense the values of $f(r)$ and $s(r)$ around each atomic site into a single value that characterizes the atomic contribution in molecule to describe the site selectivity or site reactivity of an atom in a molecule. Yang and Mortier introduced Atom condensed FFs, based on the idea of electronic population over atomic regions, similar to procedure followed in population analysis technique[39].

$$f_A^+ = q_{A,N_0+1} - q_{A,N_0} \quad (2.56)$$

$$f_A^- = q_{A,N_0} - q_{A,N_0-1} \quad (2.57)$$

$$f_A^0 = \frac{1}{2}(q_{A,N_0+1} - q_{A,N_0-1}) \quad (2.58)$$

where, $q_{A,N}$ denotes the electronic population of atom A of a system with N-electrons. They used Mullikens population scheme[40] to describe the reactivity associated with the respective atoms. Other population schemes, such as, Löwdin population[41], natural population analysis[42], Bader's atoms-in-molecules (AIM) partitioning method[43], the charges derived from molecular electrostatic potential[44, 45] and electronegativity equalization methods[46, 47], are also employed for calculation of atom condensed FFs. Using Eqs. 2.54, 2.55 and 2.56, – 2.58, various condensed local softnesses of an atom can be defined.

$$s_A^a = f_A^a S \quad \forall a = +, -, 0 \quad (2.59)$$

where, +, – and 0 indicate electrophilicity, nucleophilicity and tendency for radical attack respectively.

Pal and co-workers, introduced concepts of “relative electrophilicity” (R.E.) and “relative nucleophilicity” (R.N.)[48]. These descriptors were shown to be reliable descriptors for intramolecular reactivity as they contain information about both electrophilic and nucleophilic character. They defined these descriptors as

$$R.E = \frac{s_A^+}{s_A^-} \quad (2.60)$$

$$R.N = \frac{s_A^-}{s_A^+} \quad (2.61)$$

Based on additive rule, $S = \sum s_A^+$ and Eq. 2.40, local electrophilicity (w_A^+) was introduced

$$W = \frac{\mu^2}{2\eta} = \frac{\mu^2}{2} S = \frac{\mu^2}{2} \sum s_A^+ = \sum w_A^+ \quad (2.62)$$

From this, Perez *et al.* proposed a regional electrophilicity power condensed value on atom A[49].

$$w_A = \frac{\mu^2}{2} s_A^+ \quad (2.63)$$

Considering the existence of some function $w(r)$ that integrates to the global philicity (W), Chattaraj and co-workers[50], presented a generalized version of above equation

through the resolution of the identity associated with FFs, as,

$$W = W \int f(r) = \int W f(r) = \int w(r) \quad (2.64)$$

They argued that $w(r)$ contains information about both $f(r)$ and W (which in turn also provide information of chemical potential and softness), thereby, it is the most powerful concept of reactivity and selectivity when compared to other descriptors. This was, later criticized by Roy and others by numerically testing the reliability of philicity[51, 52]. Their argument is that the philicity index does not provide any extra reliability over other descriptors as the main contribution comes from FFs. Atom condensed philicity can be written as:

$$w_A^a = W f_A^a \quad \forall a = +, -, 0 \quad (2.65)$$

2.8 Hard Soft Acid Base principle (HSAB)

As said earlier, the Pearsons original formulation of HSAB lacks the sharp definitions of the hardness and softness. Parr and Pearsons introduction of hardness as second derivative of energy of atomic or molecular system with respect to number of electrons, paved the way for formal proof of HSAB principle[25]. They made use of the Taylor series energy expansion in terms of the number of electron (N) as a perturbation variable. Assuming the systems A and B are the interacting systems, the energy expression for each system is expressed as,

$$E_A = E_A^0 + \mu_A(N_A - N_A^0) + \eta_A(N_A - N_A^0)^2 + \dots \quad (2.66)$$

$$E_B = E_B^0 + \mu_B(N_B - N_B^0) + \eta_B(N_B - N_B^0)^2 + \dots \quad (2.67)$$

If one ignores all other effects, except, the second order, the total change in energy will have the form as,

$$\Delta E = (\mu_A - \mu_B)\Delta N + (\eta_A - \eta_B)\Delta N^2 \quad (2.68)$$

where,

$$\Delta N = N_B^0 - N_B = N_A - N_A^0 \quad (2.69)$$

In a molecule μ_A and μ_B are equal. Thus ΔN is such that,

$$\mu_A = \mu_A^0 + 2\eta_A \Delta N = \mu_B = \mu_B^0 + 2\eta_B \Delta N \quad (2.70)$$

or,

$$\Delta N = \frac{\mu_B - \mu_A}{2(\eta_A + \eta_B)} \quad (2.71)$$

On substituting the expression for ΔN , the interaction energy can be expressed as,

$$\Delta E_{AB} = -\frac{(\mu_B - \mu_A)^2}{4(\eta_A + \eta_B)} \quad (2.72)$$

It can be observed from the Eq. 2.72, that the energy lowering results from electron transfer and the differences in electronegativity or chemical potential drive the electron transfer. This process is assumed to take place continuously till the equilibrium is attained and it is referred as the chemical potential or electronegativity equalization process. If both acid and base are soft, $\eta_A + \eta_B$ is a small number, and for a reasonable difference in electronegativity, ΔE is substantial and stabilizing. This explains the HSAB principle, in part: soft prefers soft. It does not explain, however, the hard–hard preference (large denominator).

Chattaraj, Lee, and Parr gave two proofs for HSAB principle[53]. In the first proof, the interaction process between an acid A and a base B is dissected into two steps: a charge–transfer process, resulting in a common chemical potential at a fixed external potential, and a reshuffling process at a fixed chemical potential. While the energy change transfer process is taken as provided by Eq. 2.72, MHP was invoked in qualitative sense for reshuffling of charge at constant chemical potential[54].

If the above Eq. 2.72 is rewritten in terms of softness parameter, the expression for ΔE becomes,

$$\Delta E_{AB} = -\frac{(\Delta\mu)^2 S_A S_B}{2(S_A + S_B)} \quad (2.73)$$

This implies that for a given S_A , larger value of S_B is better. While MHP implies exactly reverse. Opposing tendencies in two steps are reconciled by compromise

$$S_A = S_B \quad (2.74)$$

In the second proof, one casts Eq. 2.72 into the form,

$$\Delta E_{AB} = \Delta\Omega_A + \Delta\Omega_B \quad (2.75)$$

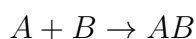
introducing the grand potentials, Ω_A and Ω_B , of the interacting systems as the natural “thermodynamic” quantities for an atom, functional group, or any other sub-unit of the molecule due to their “open” nature. $\Delta\Omega_A$ is given as,

$$\Delta\Omega_A = \frac{(\mu_B - \mu_A)^2 \eta_A}{4(\eta_A + \eta_B)^2} \quad (2.76)$$

with an analogous expression for Ω_B . For a given $\mu_B - \mu_A$ and η_B , minimization of Ω_A with respect to η_A yields

$$\eta_A = \eta_B \quad (2.77)$$

The same result is obtained when Ω_B is minimized with respect to η_B , for a given η_A , yielding HSAB principle. If one considers the general molecular interaction case, where A interacts with B to give third species AB,



Energy change associated with the process can be written as,

$$\Delta E_{int} = E[\rho_{AB}] - E[\rho_A] - E[\rho_B] \quad (2.78)$$

where, $\rho_{AB}(r)$ is the electron density of the system AB at equilibrium and $\rho_A(r)$ and $\rho_B(r)$ are the electronic densities of the isolated systems.

Gazquez tried to validate the HSAB principle based on the old assumption that the interaction can be divided into two steps[55]. In the first step, when A and B are located far apart from each other, their chemical potentials, μ_A and μ_B , change to reach a common value of μ_{AB} at constant external potential. The energy change associated with this

step can be written as,

$$\Delta E_v = \Delta E_v(A) + \Delta E_v(B) \quad (2.79)$$

where,

$$\Delta E_v(A) = E[\rho_A^*] - E[\rho_A^0] \quad (2.80)$$

and

$$\Delta E_v(B) = E[\rho_B^*] - E[\rho_B^0] \quad (2.81)$$

Here $\rho_A^*(r)$ corresponds to system A with v_A and μ_{AB} and $\rho_B^*(r)$ corresponds to system B with v_B and μ_{AB} .

In the second step, A and B evolve towards the equilibrium state through changes in the electronic density of the global system AB produced by changes in the external potential v_{AB} . This step occurs under conditions of constant chemical potential, and can be expressed in the form,

$$\Delta E_\mu = E[\rho_{AB}] - E[\rho_{AB}^*] \quad (2.82)$$

where, $\rho_{AB}^*(r) = \rho_A^*(r) + \rho_B^*(r)$ is the electronic density of the system AB with μ_{AB} , when A and B are far away from each other. Adding Eqs. 2.80 – 2.83, one can find that,

$$\Delta E_{int} = \Delta E_v + \Delta E_\mu \quad (2.83)$$

expression for ΔE_v can be presented in the form as given by Eqs. 2.72 and 2.73.

$$\Delta E_v = \frac{(\mu_B - \mu_A)^2}{4(\eta_A + \eta_B)} = -\frac{(\mu_B - \mu_A)^2}{2(S_A + S_B)} S_A S_B \quad (2.84)$$

Since, much of the work presented in the thesis is based on working at constant chemical potential, we will not go much into the details on discussion of ΔE_v . What is of our interest is in the step, which involves reshuffling of density at constant chemical potential. We shall now derive the expression of ΔE_μ .

2.8.1 Expression for ΔE_μ

[56] From Hohenberg–Kohn Equation and its corresponding Euler–Lagrange equation, one can write

$$E[\rho] = F[\rho] + \mu N - \int dr \frac{\delta F[\rho]}{\delta \rho(r)} \rho(r) \quad (2.85)$$

The energy difference between a ground state characterized by $\mu_i, \rho_i(r), N_i, v_i(r)$ and another ground state characterized by $\mu_f, \rho_f(r), N_f, v_f(r)$, may be expressed by, from the expression 2.85, Let ,

$$\Delta E = E[\rho_f] - E[\rho_i] \quad (2.86)$$

$$\Delta E = N_f \mu_f - N_i \mu_i - F[\rho_f] - F[\rho_i] + \int \rho_i(r) \frac{\delta F}{\delta \rho(r)} \Big|_{\rho_i(r)} + \int \rho_f(r) \frac{\delta F}{\delta \rho(r)} \Big|_{\rho_f(r)} \quad (2.87)$$

Now, if one performs a Taylor series functional expansion of $F[f]$ around $F[i]$, and of $\frac{\delta F}{\delta \rho(r)} \Big|_{\rho_f(r)}$ around $\frac{\delta E}{\delta \rho(r)} \Big|_{\rho_i(r)}$, the above expression for ΔE can be written as,

$$\Delta E = (N_f \mu_f - N_i \mu_i) - \frac{1}{2} \int \int dr dr' \eta_f(r, r') \rho_f(r) \rho_f(r) + 2 \int \int dr dr' \eta(r, r') \rho_i(r) \rho_i(r') \quad (2.88)$$

where, the expression for $\eta(r, r')$ is used, and in the first integral $\eta_i(r, r')$ has been replaced by $\eta_f(r, r')$, and the higher order terms are neglected.

If electronic densities of anion and cation are approximated as renormalized N–electron system density, and FF under a finite difference approximation can be shown as $f(r) \approx \rho(r)$, one can write,

$$\Delta E \approx (N_f \mu_f - N_i \mu_i) - \frac{1}{2} N_f^2 \eta_f + \frac{1}{2} N_i^2 \eta_i \quad (2.89)$$

Now, if we assume that the total number of electrons are not changing, i.e. $N_i = N_f = N$ and if the two ground states have the same chemical potential, $\mu_i = \mu_f$, then Eq. 2.89 becomes,

$$\Delta E_\mu \approx -\frac{1}{2} N^2 \Delta \eta \quad (2.90)$$

from Eqs. 2.83, 2.84 and 2.90 [55]

$$\Delta E_{int} \approx -\frac{(\mu_B - \mu_A)^2}{2(S_A + S_B)} S_A S_B - \frac{1}{2} N^2 \Delta \eta \quad (2.91)$$

Gazquez *et al.* put forward another equation which is widely used to study HSAB and lays foundations of Local HSAB principle[57, 58].

$$\Delta E_{AB} \approx -\frac{(\mu_B - \mu_A)^2}{2(S_A + S_B)} S_A S_B - \frac{1}{2} \frac{\lambda}{(S_A + S_B)} \quad (2.92)$$

where, λ is constant related to effective number of valence electrons.

2.8.2 Local HSAB Principle

Local version of HSAB was put forward by Mendez and Gazquez,[57] in which A interacts with B via its k^{th} atom and thus transforming Eq. (1.76b)

$$\Delta E_{AB,k} \approx -\frac{(\mu_B - \mu_A)^2}{2(S_A f_{Ak} + S_B)} S_A S_B f_{Ak} - \frac{1}{2} \frac{\lambda}{(S_A f_{Ak} + S_B)} \quad (2.93)$$

where, authors introduced FF f_{ak} for atom k in acid A. Further, if interaction from B is considered to be from lth atom of B. S_B can be replaced by $S_B f_{Bl}$, leading to the situation similar to HSAB principle[59]. Here, one infers that the interaction is more favored from the sites whose local softnesses are similar.

Bibliography

- [1] Levine I. N. *Quantum Chemistry*, (4th edn) Prentice–Hall of India, **1995**.
- [2] Parr, R. G.; Yang, W. *Density Functional Theory of Atoms and Molecules*; Oxford University Press: New York, **1989**
- [3] Pal, S.; Roy, R.; Chandra, A. K. *J. Phys. Chem.* **1994**, 98, 2314
- [4] M. Levy. *Phys. Rev. A* **1982**, 26, 1200
- [5] A. D. Becke. *Phys. Rev. A* **1988**, 38, 3098
- [6] C. Lee, W. Yang. *Phys. Rev. B* **1988**, 37, 785
- [7] J. Perdew, K. Burke, Y. Wang. *Phys. Rev. B* **1996**, 54, 16533
- [8] M. P. Allen, D. J. Tildesley. *Computer Simulation of Liquids*. Clarendon Press, Oxford **1987**
- [9] M. C. Payne, M. P. Teter, D. C. Allan, T. A. Arias, J. D. Joannopoulos. *Rev. Mod. Phys.* **1992**, 64, 1045
- [10] M. E. Tuckerman, P. J. Ungar, T. von Rosenvinge, M. L. Klein. *J. Phys. Chem.* **1996**, 100, 12878
- [11] R. Car, M. Parrinello. *Phys. Rev. Lett.* **1985**, 55, 2471
- [12] D. Marx, J. Hütter. *Ab Initio Molecular Dynamics: Theory and Implementation published in Modern Methods and Algorithms of Quantum Chemistry, Edited by J. Grotendorst, NIC series* **2000**, 3
- [13] D. Gibson, I. V. Ionova, E. A. Carter *Chem. Phys. Lett.* **1995**, 240, 261
- [14] Ph. D. Thesis, Mrinalini Deshpande, *Pune University*, **2004**

-
- [15] M. C. Payne, M. P. Teter, D. C. Allan, T. A. Arias, J. D. Joannopoulos. *Rev. Mod. Phys.* **1992**, 64, 1045
- [16] G. Galli, A. Pasquarello. Computer Simulation in chemical Physics. Edited by M. P. Allen, D. J. Tildesley *Kluwer Academic Publishers*. **1993**, 261
- [17] Payne M. C.; Teter M. P.; Allan D. C.; Arias T. A.; Joannopoulos J. D. *Rev. Mod. Phys.* **1992**, 64, 1045.
- [18] Kirkpatrick S.; Gelatt C. D.; Vecchi M. P. *Science*. **1983**, 220, 671.
- [19] **Ph. D. Thesis**, Deshpande M., *Pune University*, 2004.
- [20] Hohenberg P.; Kohn W. *Phys. Rev.* **1964**, 136, B864.
- [21] Parr R. G.; Donnelly R. A.; Levy M.; Palke W. E. *J. Chem. Phys.* **1978**, 68, 3801.
- [22] Gerbert T. L. *Phys. Rev. B.* **1975**, 12, 2111.
- [23] footnote **12** of ref. **20**
- [24] Iczkowski R. P.; Margrave J. L. *J. Am. Chem. Soc.* **1961**, 83, 3547.
- [25] Parr R. G.; Pearson R. G. *J. Am. Chem. Soc.* **1983**, 105, 7512.
- [26] Sanderson R. T. *Science*, **1951**, 114, 670.
- [27] Parr R.G.; Szentpaly L. V.; Liu S. *J. Am. Chem. Soc.* **1999**, 121, 1922
- [28] Pearson R. G. *J. Chem. Educ.* **1987**, 64, 561.
- [29] Koopmans T. A. *Physica*, **1933**, 1, 104.
- [30] Pearson R. G. *Proc. Natl. Acad. Sci. USA*, **1986**, 83, 8440.
- [31] Fukui K.; Yonezawa T.; Shingu H. *J. Chem. Phys.* **1952**, 20, 722.
- [32] Fukui K.; Yonezawa T.; Nagata C.; Shingu H. *J. Chem. Phys.* **1954**, 22, 1433.
-

-
- [33] Parr R. G; Yang W. **Density Functional Theory of Atoms and Molecules**, Oxford University Press: New York, **1989**.
- [34] Parr R. G; Pearson R. G. *J. Am. Chem. Soc.* **1983**, *105*, 7512.
- [35] Parr R. G.; Yang W. *J. Am. Chem. Soc.* **1984**, *106*, 4049.
- [36] Yang W.; Parr R.G. *Proc. Natl. Acad. Sci.* **1985**, *82*, 6723.
- [37] Taylor P. R. **Lecture Notes in Quantum Chemistry: European Summer School**, Springer-Verlag, Berlin, **1994**, 125.
- [38] Geerlings P.; De Proft F.; Langenaeker W. *Chem. Rev.* **2003**, *103*, 1793.
- [39] Parr R. G.; Szentpaly L. V.; Liu S. *J. Am. Chem. Soc.* **1999**, *121*, 1922.
- [40] Mulliken R. S. *J. Chem. Phys.* **1955**, *23*, 1833.
- [41] Lowdin P. O. *Phys. Rev.* **1955**, *97*, 1475.
- [42] Reed A. E.; Weinstock R. B.; Weinhold F. *J. Chem. Phys.* **1985**, *83*, 73.
- [43] Bader R. F. W. *Chem. Rev.* **1991**, *91*, 893.
- [44] Singh U. C.; Kollman P. A. *J. Comput. Chem.* **1984**, *5*, 129.
- [45] Bayly, C. I.; Cieplak, P. Cornell, W. D.; Kollman, P. A. *J. Phys. Chem.* **1993**, *97*, 10269.
- [46] Gasteiger J.; Marsili M. *Tetrahedron*, **1980**, *36*, 3219.
- [47] De Proft F.; Langenaeker W.; Geerlings P. *J. Mol. Struct. (THEOCHEM)*, **1995**, *339*, 45.
- [48] Roy R. K.; Krishnamurti S.; Geerlings P.; Pal S. *J. Phys. Chem. A.* **1998**, *102*, 3746.
- [49] Perez P.; Toro-Labbe A.; Aizman A.; Contreras R. *J. Org. Chem.* **2002**, *67*,4747.

-
- [50] Chattaraj P.K.; Maiti B.; Sarkar U. *J. Phys. Chem.* **2003**, *107*, 4973.
- [51] Roy R. K. *J. Phys. Chem. A.* **2004**, *108*, 4934.
- [52] Roy R. K.; Usha V.; Paulovic J.; Hirao K. *J. Phys. Chem. A.* **2005**, *109*, 4601.
- [53] Chattaraj P. K.; Lee H.; Parr R. G. *J. Am. Chem. Soc.* **1991**, *113*, 1855.
- [54] Parr R. G.; Chattaraj P. K. *J. Am. Chem. Soc.* **1991**, *131*, 1854.
- [55] Gazquez J. L. **In Chemical Hardness**; Sen K.D. ed. *Structure and Bonding*; Vol. 80 Springer-Verlag: Berlin, **1993**.
- [56] Gazquez J. L.; Martinez A.; Mendez F. *J. Phys. Chem.* **1993**, *97*, 4059.
- [57] Gazquez J. L.; Mendez F. *J. Am. Chem. Soc.* **1994**, *116*, 9298.
- [58] Gazquez J. L.; Mendez F. *J. Phys. Chem.* **1994**, *98*, 4591.
- [59] Mendez F.; Gazquez J. L. *Proc. Indian. Acad. Sci.* **1994**, *106*, 183.

Critical Study of the Charge Transfer Parameter for the Calculation of Interaction Energy Using the Local Hard–Soft Acid–Base Principle

Local hard–soft acid–base (HSAB) principle is semiquantitative in nature due to the presence of an ad hoc charge transfer parameter. The accuracy of HSAB principle significantly depends on the definition of this ad hoc parameter. In this paper, for the first time we have introduced the second–order approximation of ΔN (ΔN_{second}) as an ad hoc parameter for charge transfer to calculate interaction energies of multiple site based interactions using local hard soft acid base principle. The second-order approximation of ΔN has been derived from Sandersons electronegativity equalization principle. To validate our approach, we have studied interaction energies of some prototype molecules. The interaction energies obtained from our approach have been further compared with the interaction energies of those obtained using other charge transfer parameters (ΔN_{first} and λ) and the conventional methods. We have also discussed the advantages and limitations of the approach.

3.1 Introduction

Density functional theory (DFT) is popular due to its success in studying the molecular structure, chemical bonding[1–11], interaction energy (IE), reactivity, and selectivity of molecules[12–22]. In recent years, DFT based reactivity descriptors have been extensively used to study the aromaticity, the intra- and intermolecular reactivity, regioselectivity, electrophilicity, nucleophilicity[23] of organic reactions, and prediction of the reactive site of various molecular systems[24, 25]. DFT has also provided theoretical basis for concepts such as electronic chemical potential, electronegativity, hardness and softness, collectively known as global reactivity descriptors (GRD)[26–30]. The global reactivity descriptors describe the molecule as a whole. These descriptors essentially determine the response of the energy of a system to the change of number of electrons at fixed external potential. The chemical potential of the two systems determines the flow of electrons. Global hardness talks about the inertness of the whole molecule and can be seen as reluctance to the charge transfer[31, 32]. However, the interaction between molecules occurs through particular atoms (definite site) within the molecule, and thus, the interaction is always local. Therefore, to explain the interactions between molecules, we need local reactivity descriptors (LRD)[33–36] such as Fukui function and local softness. The Fukui function and local softness relate the change of electron density to the number of electrons and chemical potential respectively. LRDs have a direct relation with the Fukui frontier molecular orbitals, and the relevance has been verified in identifying electrophilic and nucleophilic reactive centers in a molecule. From the value of Fukui function of every atom in a molecule, we can predict the reactive atom of the system and higher the value of Fukui function, higher is the reactivity[34, 37]. Various theoretical approaches exist for correlating the reactivity of molecular system based on different quantities like molecular orbital theory, charge on the atom, bond order, etc.

Pearson introduced hardness and softness parameter in the context to explain the reactivity of acids and bases[41]. He has tabulated reactivity trends of acids and bases in terms of hard soft acid base parameter. This concept is called Pearsons hard–soft acid–base (HSAB) principle. The principle says that soft acid-soft base and hard acid–hard base combination is more favorable than hard–soft combination. It became very popular among the chemists because of its simplicity and wide range of applicabilities. However, the theoretical quantification of qualitative HSAB principle is difficult. Many groups are working on this issue for explaining the relative bond strengths of acid–base complex. Li and Evans have proposed a reactivity scheme by using energy perturbation method within the framework of density functional theory[42]. They have shown that the Fukui function is an important quantity, which relates frontier molecular orbital (FMO) theory to HSAB principle[26, 43, 44]. Later, Gazquez and Mendez also proposed the local HSAB principle, which states that the interaction between two molecules will occur not necessarily through their softest atoms but rather through those atoms which have similar Fukui function values[45]. Pal and co–workers have shown failure of Fukui function and local softness to describe intramolecular reactivity trend in several organic carbonyl compounds. They have proposed a new reactivity descriptor called relative electrophilicity and relative nucleophilicity to explain the reactivity of a particular site[46]. Nguyen and co–workers also noticed the failure of Fukui indices in rationalizing the regioselectivity of protonation in fluoro– and chloro–substituted phenol[47]. Roy *et al.* have observed difficulty to obtain rank ordering of the reactivity of atoms in molecules where Fukui function becomes negative[48, 49]. They have prescribed the Hirshfeld population scheme to obtain the non–negative Fukui functions[50]. Fuentealba *et al.* have also discussed the possible existence of negative value of Fukui indices by computing Kohn–Sham frontier orbital density[51]. Chattaraj and co–workers have extended the applicability of these descriptors to describe the molecular excited states[52–54]. Toro–Labbé calculated bond energy of hydrogen bonded complexes by using Sandersons principle of electronegativity equalization[55]. The working equations of local HSAB principle are

based on the perturbative theory and the local descriptors of the reacting system. The local HSAB principle is semiquantitative in nature due to presence of an ad hoc parameter (K)[56]. This principle works well for weak interacting systems viz. hydrogen bonded complexes, Lewis acid–base complexes, etc. Earlier, Gazquez and Mendez have studied the reactivity of enolate anions and pyridine derivatives using an arbitrary value of $K = 0.5$ [45, 57]. Similarly, Geerlings and co-workers have studied the reactivity of benzonitrile oxides using the value of $K = 1.0$ [58]. The authors could relate the reactivity of various sites of a given molecule with the energy only at the qualitative level. Pal and co-workers have made a critical study on the applicability of local reactive descriptors in the case of weak interactions[12]. They have used the charge transfer parameter defined by Sanderson for the calculation of multiple site interaction energies[59]. This parameter is derived from the electronegativity equalization principle by truncating Taylor series expansion of energy at the second order. The interaction energy can be calculated by using another ad hoc charge transfer parameter denoted as λ . This parameter is defined as the net difference of the sum of the condensed electron population of each atom present in the system A having p -number of atoms, before and after the interaction[12, 59, 60]. Thus, to calculate λ , the actual geometry of reactants before and after interaction should be known. Therefore, it is difficult to calculate interaction energy using parameter λ , for the systems having a large number of interaction sites that interact simultaneously. Most of the biological interactions occur via multiple sites and are complex in nature. Thus, in that case the parameter λ cannot be useful. This has motivated us to extend our approach of calculation of interaction energy using second–order approximation of δN . In this paper, we have derived the second–order charge transfer parameter by truncating Taylor series expansion of energy up to third order. The calculation of δN requires information of reactant molecules only before interaction. Hence, it can be explicitly useful for any kind of interaction pattern. Recently, Anton used it for adsorbates and metal surface[61]. Theoretically, δN_{second} is supposed to be more accurate than δN_{first} because it includes

higher order terms of the Taylor series expansion of energy. Therefore, we have investigated multiple site based interactions of prototype biological molecules using δN_{second} as an ad hoc parameter. We have further studied the IE of the same molecules using δN_{first} , as well as λ , and compared the results with the IE obtained using δN_{second} . The paper is organized as follows. In section 2, we present some important definitions of the reactivity descriptors and derivation of second-order approximation of δN . Section 3 provides the details about the computational methodology we have used. The elaborate discussion about the results obtained is provided in section 4. The important conclusions are drawn in section 5.

3.2 Theory

3.2.1 Derivation for Charge Transfer Parameter

Suppose reactants A and B are reacting to form a product AB. The energy of the reactants A and B can be written in Taylor series expansion as[1]

$$E_A = E_A^0 + \left(\frac{\delta E_A}{\delta N_A}\right)_{v(r)}(N_A - N_A^0) + \frac{1}{2!}\left(\frac{\delta^2 E_A}{\delta N^2}\right)_{v(r)}(N_A - N_A^0)^2 + \frac{1}{3!}\left(\frac{\delta^3 E_A}{\delta N^3}\right)_{v(r)}(N_A - N_A^0)^3 + \dots \quad (3.1)$$

$$E_B = E_B^0 + \left(\frac{\delta E_B}{\delta N_B}\right)_{v(r)}(N_B - N_B^0) + \frac{1}{2!}\left(\frac{\delta^2 E_B}{\delta N^2}\right)_{v(r)}(N_B - N_B^0)^2 + \frac{1}{3!}\left(\frac{\delta^3 E_B}{\delta N^3}\right)_{v(r)}(N_B - N_B^0)^3 + \dots \quad (3.2)$$

The term $\left(\frac{\delta E}{\delta N}\right)_{v(r)}$ is called the chemical potential, which is defined as μ , $\frac{1}{2!}\left(\frac{\delta^2 E}{\delta N^2}\right)_{v(r)} = \eta$ is the hardness and $\frac{1}{3!}\left(\frac{\delta^3 E}{\delta N^3}\right)_{v(r)}$ is known as the hyperhardness, denoted by γ and so on[64–67]. Rewriting eqs (3.1) and (3.2) in terms of μ , η , and γ

$$E_A = E_A^0 + \mu_A^0 \Delta N + \eta_A^0 \Delta N^2 + \gamma_A^0 \Delta N^3 \dots \quad (3.3)$$

$$E_B = E_B^0 + \mu_B^0 \Delta N + \eta_B^0 \Delta N^2 + \gamma_B^0 \Delta N^3 \dots \quad (3.4)$$

If all other effects are ignored, then the total energy will have following form

$$E_A + E_B = E_A^0 + E_B^0 + (\mu_A^0 - \mu_B^0)\Delta N + (\eta_A^0 + \eta_B^0)\Delta N^2 + (\gamma_A^0 - \gamma_B^0)\Delta N^3 + \dots \quad (3.5)$$

where

$$\Delta N = (N_B^0 - N_B) = (N_A - N_A^0) \quad (3.6)$$

When a reaction takes place between two reactants with different chemical potentials, one of the reactants donates electrons and the other accepts electrons, leading to a change in the chemical potential. If $\mu_B^0 > \mu_A^0$ and ΔN is positive, electrons will flow from B to A. At equilibrium

$$\mu_A = \mu_B \quad (3.7)$$

where

$$\mu_A = \left(\frac{\delta E_A}{\delta N_A}\right)_{v(r)} = \mu_A^0 + 2\eta_A \Delta N + 3\gamma_A \Delta N^2 \dots \quad (3.8)$$

$$\mu_B = \left(\frac{\delta E_B}{\delta N_B}\right)_{v(r)} = \mu_B^0 + 2\eta_B \Delta N + 3\gamma_B \Delta N^2 \dots \quad (3.9)$$

Considering terms up to second order of eqs (3.8) and (3.9), we have from eq (3.7)

$$\mu_A^0 + 2\eta_A \Delta N = \mu_B^0 - 2\eta_B \Delta N \quad (3.10)$$

Consequently, the first-order approximation of charge transfer parameter will be

$$\Delta N_{first} = \frac{\mu_A^0 - \mu_B^0}{2(\eta_A + \eta_B)} \quad (3.11)$$

The second-order approximation of charge transfer parameter is obtained from eqs (3.8) and (3.9), by considering terms up to third order.

$$\mu_A^0 + 2\eta_A \Delta N + 3\gamma_A \Delta N^2 = \mu_B^0 - 2\eta_B \Delta N + 3\gamma_B \Delta N^2 \quad (3.12)$$

So,

$$(3\gamma_A - 3\gamma_B)\Delta N^2 + (2\eta_A + 2\eta_B)\Delta N + (\mu_A^0 - \mu_B^0) = 0 \quad (3.13)$$

Equation (3.13) is a quadratic equation. It gives the second-order approximation of charge transfer parameter,

$$\Delta N_{second} = \frac{-(2\eta_A + 2\eta_B) \pm \sqrt{(2\eta_A + 2\eta_B)^2 - 4(3\gamma_A - 3\gamma_B)(\mu_A^0 - \mu_B^0)}}{2(3\gamma_A - 3\gamma_B)} \quad (3.14)$$

Equation (3.13) has two roots; thus, eq (3.14) gives two values of ΔN_{second} . However, physically, ΔN is the amount of charge transfer from one molecule to another in the process of complex formation between two molecules. In this thesis we have studied multiple site based hydrogen bonding interaction. The H-bonding interactions are weak interactions; thus the amount of charge transfer from one molecule to another during the complex formation is very small (<1). In such a case, out of possible root the acceptable value of ΔN_{second} is one that is less than 1. In Table 1, we have reported the acceptable value of ΔN_{second} .

3.2.2 Global and Local Reactivity Descriptors

In DFT, the ground state energy of an atom or molecule is written in terms of electron density, $\rho(\vec{r})$ as[62]

$$E[\rho] = F[\rho] + \int dr \rho(\vec{r})v(\vec{r}) \quad (3.15)$$

$F[\rho]$ is the universal Hohenberg–Kohn functional. It contains electronic kinetic energy and electron–electron repulsion term. $v(\vec{r})$ is the external potential which includes the nuclear potential. The first and second partial derivatives of $E[\rho]$ with respect to the number of electrons N under the constant external potential $v(\vec{r})$ are defined as the chemical potential μ and the global hardness η of the system respectively[26–30]

$$\mu = \left(\frac{\delta E}{\delta N}\right)_{v(\vec{r})} \quad (3.16)$$

$$\eta = \frac{1}{2} \left(\frac{\delta^2 E}{\delta N^2}\right)_{v(\vec{r})} \quad (3.17)$$

The inverse of the global hardness is called global softness and it is denoted by letter S .

$$S = \frac{1}{\eta} \quad (3.18)$$

The global descriptor, hardness, measures the overall stability of the system. It is customary to use a finite difference approximation for μ and η [43, 63]. By using the energies of

N , $(N + 1)$, and $(N - 1)$ electronic systems, we get the operational definition of μ and η [1],

$$\mu = \frac{E_{N+1} - E_{N-1}}{2} = \frac{IP - EA}{2} \quad (3.19)$$

$$\eta = \frac{E_{N+1} + E_{N-1} - 2E_N}{2} = \frac{IP - EA}{2} \quad (3.20)$$

where IP and EA are the first vertical ionization energy and electron affinity of the chemical species, respectively. The third term is γ , which is hyperhardness, and it is the third derivative of energy with respect to total number of electrons

$$\gamma = \frac{1}{6} \left(\frac{\delta^3 E}{\delta N^3} \right)_{v(\vec{r})} \quad (3.21)$$

Equation (3.21) has been defined by Fuentealba and Paar[64]. The value of hyperhardness is usually small and the reason behind the small value of γ is that the energy, E , often has nearly quadratic dependence on the number of electrons, N . By using finite difference approximation of energy and using the energies of $(N + 2)$, $(N + 1)$, N , $(N - 1)$, and $(N - 2)$ systems, we obtain the expression for γ .

$$\gamma = \frac{1}{12} (E_{N+2} - 2E_{N+1} + 2E_{N-1} - E_{N-2})_{v(\vec{r})} \quad (3.22)$$

The detailed derivation of γ has been given in the **Appendix**.

The site selectivity of a chemical reaction cannot be described by global reactivity descriptor. Thus, the appropriate local quantities need to be defined. Local softness is defined as[34, 37]

$$s(\vec{r}) = \left(\frac{\delta \rho(\vec{r})}{\delta \mu} \right)_{v(\vec{r})} \quad (3.23)$$

where

$$\int s(\vec{r}) dr = S \quad (3.24)$$

Rewriting eq (3.23) we have

$$s(\vec{r}) = \left(\frac{\delta \rho(\vec{r})}{\delta N} \right)_{v(\vec{r})} \left(\frac{\delta N}{\delta \mu} \right)_{v(\vec{r})} \quad (3.25)$$

By using the definition of the global softness in eq (3.18), we can write

$$s(\vec{r}) = f(\vec{r})S \quad (3.26)$$

where $f(\vec{r})$ is defined as the Fukui function (FF)[34, 37–40]. It can be defined as

$$f(\vec{r}) = \left(\frac{\delta \rho(\vec{r})}{\delta N} \right)_{v(\vec{r})} \quad (3.27)$$

To describe the site selectivity or reactivity of an atom in a molecule, it is necessary to condense the values of $f(\vec{r})$ and $s(\vec{r})$ around each atomic site into a single value that characterizes the atom in a molecule. This can be achieved by electronic population analysis. Depending upon the type of electron transfer, we have three different types of condensed Fukui function of the atom k[35],

for nucleophilic attack,

$$f_k^+ = [\rho_k(N+1) - \rho_k(N)] \quad (3.28)$$

for electrophilic attack,

$$f_k^- = [\rho_k(N) - \rho_k(N-1)] \quad (3.29)$$

for radical attack,

$$f_k^0 = \frac{1}{2}[\rho_k(N+1) - \rho_k(N-1)] \quad (3.30)$$

where $\rho_k(N)$, $\rho_k(N+1)$, and $\rho_k(N-1)$ are defined as a gross electronic population of the atom k in neutral, anionic, and cationic system, respectively. Corresponding condensed local softness can be defined as

$$s_k^+ = f_k^+ S \quad (3.31)$$

$$s_k^- = f_k^- S \quad (3.32)$$

$$s_k^0 = f_k^0 S \quad (3.33)$$

3.2.3 Expression for the Interaction Energy (IE)

Multiple sites based interaction essentially, found to have two limiting cases, so-called localized reactive model (LRM) (Figure 1) and global (smeared) reactive models (SRM) (Figure 2). The expression for interaction energy of LRM is given as[59, 60, 69]

$$\Delta E_{int} \approx -\frac{(\mu_A - \mu_B)^2}{2} \left(\frac{S_A S_B f_{Ax} f_{Bk}}{S_A f_{Ax} + S_B f_{Bx}} + \frac{S_A S_B f_{Ay} f_{Bl}}{S_A f_{Ay} + S_B f_{Bl}} + \frac{S_A S_B f_{Az} f_{Bm}}{S_A f_{Az} + S_B f_{Bm}} + \dots \right)_{v(\vec{r})} - \frac{K}{4} \left(\frac{1}{S_A f_{Ax} + S_B f_{Bx}} + \frac{1}{S_A f_{Ay} + S_B f_{Bl}} + \frac{1}{S_A f_{Az} + S_B f_{Bm}} + \dots \right)_{\mu} \quad (3.34)$$

Here the distinctive reactive sites of A and B are designated x, y, z, etc. and k, l, m, etc. respectively. It has been assumed that the interaction is taking place simultaneously between different pairs of reactive sites of the two systems as x-k, y-l, z-m, etc. Similarly, the IE of SRM is

$$\Delta E_{Ax-Bk} \approx -\frac{(\mu_A - \mu_B)^2}{2} \left[\frac{(\sum_{i=1}^n S_{A_{x_i}})(\sum_{j=1}^m S_{B_{k_j}})}{(\sum_{i=1}^n S_{A_{x_i}}) + (\sum_{j=1}^m S_{B_{k_j}})} \right]_{v(\vec{r})} - \frac{K}{4} \left[\frac{1}{(\sum_{i=1}^n S_{A_{x_i}}) + (\sum_{j=1}^m S_{B_{k_j}})} \right]_{\mu} \quad (3.35)$$

where there are n participating atoms x_1, x_2, \dots, x_n in the site A_x , similarly, there are m atoms k_1, k_2, \dots, k_m in the site B_k . The detailed derivation of LRM and SRM are given in ref **69**. In eqs (3.34) and (3.35) parameter K is a charge transfer parameter. It can be defined in various ways and in the literature K has been defined arbitrarily. To calculate IE by eqs (3.34) and (3.35), Pal and co-workers have replaced this ad hoc parameter K by λ which is the change in the electron densities at the interacting site before and after the interaction process. Thus, the expression for the term λ can be written for the system A as

$$\lambda_A = \sum_{i=1}^p \rho_{A_i}^{eq} - \sum_{i=1}^p \rho_{A_i}^0 \quad (3.36)$$

Similarly, the term λ can be defined for the system B,

$$\lambda_B = \sum_{j=1}^q \rho_{B_j}^{eq} - \sum_{j=1}^q \rho_{B_j}^0 \quad (3.37)$$

where the first terms of the right hand sides of eqs (3.36) and (3.37) refer to the sum of the electron densities of each atom in A and B in the molecule AB at equilibrium, respectively, and the second terms in eqs (3.36) and (3.37) refer to electron densities of each atom in the isolated systems A and B, respectively. The indices p and q are

the number of atoms of the systems A and B, respectively. The ad hoc parameter K in eqs (3.34) and (3.35) is replaced in three different ways: (1) first-order approximation of ΔN (eq (3.11)), second-order approximation of ΔN (eq (3.14)) and parameter λ (eqs (3.36) and (3.37)).

3.3 Methodology and Computational Details

In this study we have chosen various prototype molecules viz., succinamide (SUC), butyrolactam (BUTL), formamidine (FD), formic acid (FA), acetic acid (AA), formamide (FRM), N-methylformamide (NFRM), acetamide (ATM), N-methylacetamide (NATM). To investigate the charge transfer parameter in smeared reactive models (SRM), we have considered acetylene (ACT), butylene (BUTY), HCl (HCL), and LiCl (LICL) molecules. All the structures are optimized at MP2[70]/6-311G(d,p) and DFT[71-73]/B3LYP[75, 76]/6-311G(d,p)[77] level of theory using Gaussian 09 software package[74]. The three-parameter hybrid functional of Becke and Lee, Yang, and Parr correlation potential has been used for DFT calculations[75, 76]. We have checked our geometries for nonimaginary vibrational frequencies. Single point calculations to calculate reactivity descriptors have been performed at DFT, MP2, and CCSD(T) level of theory. Optimized geometries of MP2 level are used for the single point calculations in CCSD(T) method. RHF calculations are carried out for all the neutral system with spin multiplicity 1. For the cationic (charge +1.0) and anionic (charge -1.0) systems, single point ROHF calculations are carried out with spin multiplicity 2. The optimized geometry of the neutral system was used to perform calculations on the cationic and anionic systems to satisfy the condition of constant external potential. The condensed Fukui function and local softness for each reactive atom are computed via eqs (3.28) to (3.33) using Mulliken population analysis[78]. The reactive atoms in our study are hydrogen atom (electrophilic center) and oxygen atom (nucleophilic center). The parameter λ is calculated using eqs (3.36) and (3.37) through Mulliken population analysis scheme. In conventional methods, the

interaction energy will be evaluated from the difference between the energy of the complex AB and sum of the energy of the monomer A and B,

$$\Delta E_{AB} = E_{AB} - E_A - E_B \quad (3.38)$$

We have taken care of BSSE-counterpoise correction to calculate IE by conventional method.

3.4 Results and Discussions

Hydrogen bonding interactions are extremely important in biological systems[79–81, 83]. The helical structure of DNA molecule is due to the H–bonding between base pairs. In biological molecules such as proteins, polysaccharides, and lipids etc. the interactions are largely determined by multiple intra and intermolecular H–bonding. To study such interactions, we have considered prototype complexes of formamide, acetamide, formic acid, acetic acid and their derivative with formamidine (FD) molecule as a simple nucleic acid base model. The amide–formamidine complex has been studied earlier by Bertran *et al.*, Sponer *et al.*, Kim *et al.*, and Galetich *et al.*[84–87]. They found that this is an important model complex having many features similar to those of the actual nucleic–acid base pair model. These complexes have two types of H–bonds: (a) –C=O group in amide and acid with formamidine –NH group; (b) amide –NH, acid –OH with formamidine N–C. The interaction between succinamide and butyrolactum has been studied by Uchamaru and co–workers[88]. Along with the above–mentioned complexes, we have also studied some multiple bonded interactions between π –electronic and electrophilic molecules. These molecules also show hydrogen–bonding interactions. The complexes formed between acetylene and butylene with HCl and LiCl are the examples of such multiple hydrogen bonded interactions[89]. Here H^+ of HCl and Li^+ of LiCl act as an electrophile interacting with the π –electron cloud of acetylene and butylene.

In Table 2, the global properties of all prototype molecules are presented. These properties are calculated with DFT/B3LYP/6-311G(d,p), MP2/6-311G(d,p), and CCSD(T)/6-311G(d,p) levels of theory. For all the molecules the chemical potential (μ) obtained from DFT is higher than that of MP2 and CCSD(T) levels. Compared to chemical potentials for all other molecules, the chemical potential of HCl and LiCl calculated through DFT are much higher than that of MP2 and CCSD(T) methods. In the case of amide and acid complexes, the chemical potential difference is marginal in the range ≈ 0.012 to ≈ 0.027 . However, hardness (η) does not follow a similar trend. The CCSD(T) values of hardness are higher for most of the molecules compared to DFT values. The MP2 values of hardness for acid molecules (viz. acetic acid and formic acid) are higher than those obtained with DFT and those of HCl and LiCl obtained from DFT are higher than those obtained with MP2 and CCSD(T) methods. In the case of hyperhardness, some molecules show higher values of γ at the CCSD(T) level and others show larger values at the DFT method. As per our observation, the values of γ are much lower than the chemical potential whereas μ and η values are in comparable magnitude for the all three methods. In 1991, Fuentealba and Parr have also shown that in the case of atoms and their ions, the values of γ are smaller compared to μ and η [90]. In contrast, Ordon and Tachibana have shown in the case of diatomic molecules that γ can have a higher value than μ and η using maximum hardness principle[91]. Thus, γ is not always lower than μ and η , and it varies from system to system. For the systems where γ is higher than μ and η , second-order approximation of ΔN will be more important to calculate the interaction energies. It is important to mention here that the sign of the γ can be either positive or negative. In the Table 2, all molecules have negative values of γ computed through three different methods viz. DFT, MP2, and CCSD(T). The μ and η values are positive and negative respectively for all the molecules. The γ values obtained using all the methods are significantly low and thus face a low profile existence in the interpretation of chemical bonding and reactivity[67].

Table 3 shows the values of local softness (S_k^\pm) of all monomers calculated by DFT,

MP2, and CCSD(T) levels of theory using the 6–311G(d,p) basis. The molecules reacting through the localized reactive model and smeared reactive model (Figures 1 and 2) have two and one reactive atoms, respectively. The local softness value for the reactive atom A of the molecules SUC, FD, FA, AA, ACT, and HCL are higher at the CCSD(T) level than at DFT and MP2. On the other hand, FRM, NFRM, ATM, NATM, BUTL, and LICL have higher values of S_k^\pm for atom A at the MP2 level. In the case of reactive atom B, DFT gives larger values of S_k^\pm for most of the molecules except FRM, NFRM, and BUTY, which have higher values at the MP2 level. Compared to values for other molecules, the LRD values (S_k^+) of HCl and LiCl are exceptionally high, which confirms the higher reactivity of HCl and LiCl. The effect of methylation to the amide –NH₂ group on μ and η can be seen from Table 2. The same effect is observed on the condensed local softness value of carbonyl oxygen (S_k^-) and hydrogen (S_k^+). The condensed local softness of reactive atoms A and B of FRM and ATM molecules are greater than their N–methyl derivative. Due to the +I effect of the methyl group, methylation leads to depletion of positive charge on the reactive H atom, which results into the lowering of GRD and LRD values of the reactive O–atom and H–atom. Hence, the reactivity of the methylated system is reduced and the corresponding value of IE is expected to be lower than those of the unsubstituted amide complex.

The first–order and second–order approximation of ΔN calculated through DFT, MP2, and CCSD(T) using eqs (3.11) and (3.14), respectively, are reported in Table 1. We have also presented DFT results of λ using eqs (3.36) and (3.37). The CCSD(T) values of ΔN_{first} and ΔN_{second} for all the complexes are higher than those of other two methods. The difference between first–order and second–order approximation of the charge transfer parameter has been discussed in section 2.1. We note in the present study that the values of ΔN_{second} are slightly different from the ΔN_{first} . However, DFT results of ΔN_{first} and ΔN_{second} are higher for most of the complexes compared to CCSD(T) results except for the complexes 1, 2, 9, and 11 (Table 1). It should be mentioned here that the third term, γ , is very small for all the molecules we studied here. Hence, ΔN_{second}

does not show significant improvement in IE in our study. However, the ΔN_{second} will be very useful to calculate IE for the molecules that have a larger value of γ . Further, we see that the charge transfer is less in the methylated $-NH_2$ group than in the unmethylated species. In the case of the LiCl interaction with acetylene and butylene, the value of charge transfer parameters (ΔN_{first} , ΔN_{second} , and λ) are greater than those for the corresponding HCl complex. This observation is consistent with our earlier discussion on the value of GRD and LRD (Tables 2 and 3). However, among the acetylene and butylene complexes, butylene complexes (BUTY-HCL and BUTY-LICL) show higher charge transfer during the complexation. This is due to the +I effect of $-CH_3$ group, which increases electron density of adjacent triple bonded C atoms, resulting in greater affinity of butylene toward H^+ and Li^+ .

Tables 4 and 5 show the IEs obtained from the DFT and the MP2 methods, respectively. Three different charge transfer parameters, viz. ΔN_{first} , ΔN_{second} , and λ are used for the calculation of the IEs. Looking at the results, it is observed that the MP2 IEs are lower than those of the DFT IEs. In light of the HSAB principle, the interaction between the molecules takes place in two steps: (a) step 1 (referred to as ΔE_v) occurs at a constant external potential leading to equilibration of chemical potential; (b) step 2 (referred to as ΔE_μ) involves the change in the electron density of the complex leading to an equilibrium state with constant chemical potential. The charge transfer parameter is involved in the ΔE_μ , which is the dominating term in the total IE and is computed through eq (3.34) (SUC-BUTL to NATM-FD) and eq (3.35) (ACT-HCL to BUTY-LICL), known as LRM and SRM, respectively. In the case of amide-formamidine (FRM-FD, NFRM-FD, ATM-FD, and NATM-FD), acid-formamidine (FA-FD and AA-FD), and succinamide-butyrolam (SUC-BUTL), the reactive atoms are not directly connected to each other and thus the reactivity of each atom will be more or less independent of each other. For such complexes, the IE can be considered as a sum of the IE arising from each pair of reactive atoms and that is the reason LRM (eq (3.34)) gives reasonable results. The results are further compared with the interaction energy calculated

by the conventional method using eq (3.38). Because the reactive C atom in acetylene and butylene are directly connected through a triple bond and act as a group, the IE of these molecules with HCl and LiCl have been calculated by SRM (eq (3.35)). It is gratifying to note that the IE of LiCl with this triply bonded system is greater compared to the IE of the HCl complex. The IE values of the ACT–HCL complex are -3.5141 kcal/mol (by ΔN_{first}), -3.5127 kcal/mol (by ΔN_{second}), and -2.1556 kcal/mol (by λ) obtained from DFT calculations. and conventionally (using DFT) they are -2.1773 kcal/mol, whereas the IE values of the ACT–LICL complex computed through ΔN_{first} , ΔN_{second} , and λ are -3.5449 , -3.5462 , and -7.4412 kcal/mol, respectively, and conventional IE is -5.5990 kcal/mol. The higher IE of ACT–LICL is due to the higher electron affinity of Li^+ as compared to that of the H^+ ion. As mentioned earlier, the effect of methylation reduces the reactivity of the molecule. This is also supported by values of IE that are -4.1128 and -2.5550 kcal/mol using ΔN_{second} for FRM–FD and ACT–FD complexes, respectively, whereas their N–methyl derivative, i.e., NFRM–FD and NATM–FD complexes, have -2.4116 and -1.4202 kcal/mol for IE values, respectively. A similar trend is observed in IE calculated using other charge transfer parameters (ΔN_{first} and λ). As per our expectations, complexes of butylene with HCl and/or LiCl have higher values of IE than the corresponding complexes of acetylene. In an earlier study by Pal and co-workers, ΔN_{first} and λ have been used to calculate the IE of multiple site based interactions. Here we have chosen the same molecules but the calculations are performed with a higher level of theory and bigger basis set, which leads to better results of IE compared to the values reported by Pal and co-workers. As an example, for SUC–BUTL and ACT–HCL complexes, the reported values of ΔN_{first} are 0.099 and 0.079, respectively, and the corresponding IEs are -49.71 and -6.37 kcal/mol, respectively, using the HF/3–21g* level of theory. Our results for the ΔN_{first} and IE are better as compared to the previously reported values by Pal and co-workers. In our study, the CCSD(T)/6–311G(d,p) level of theory gives 0.0415 and 0.0365 values of ΔN_{first} for SUC–BUTL and ACT–HCL, respectively, and the IEs are -14.9963 and -2.7350 kcal/mol, respectively.

The actual IEs are -8.58 and -1.50 kcal/mol, respectively.

3.5 Conclusion

In this work, we have calculated the hydrogen bonding interaction energy of various complexes using the local HSAB principle. We have derived ΔN_{second} and applied it as an ad hoc parameter in the calculation of the IE. Two different ad hoc charge transfer parameters (ΔN_{first} and λ) are also used to calculate the IE, and additionally, the advantage of using ΔN_{first} and ΔN_{second} over λ is highlighted. It is very hard to obtain theoretical information (optimized structure) due to complexity in the interaction in a biological environment. Therefore, to study this kind of interaction, higher order approximations of ΔN should be investigated. To compute ΔN (ΔN_{first} or ΔN_{second}), it is sufficient to have the information of only the reacting species, which is a tremendous advantage over λ where the actual structure of the supermolecule (complex product) is necessary. However, we have observed in our study using all the three methods, viz. DFT, MP2, and CCSD(T), ΔN_{second} does not improve the IE as compared to the ΔN_{first} , which is good enough to study the weak interactions. It must be mentioned here that among all three methods, CCSD(T), the most correlated method gives the minimum deviation of IE calculated through local HSAB and conventional method. Hence, higher correlated methods should be the choice to deal with multiple site based weak interactions. The local HSAB principle is based on the second-order perturbation method and the descriptors of the isolated reactants. Both the approximations make this model applicable only to weak interacting systems. In the case of weak interacting molecules, the influence of one monomer on another is comparatively less. Hence, the formula of local HSAB interaction energy more accurately describes the interaction process. On the other hand, the influence of one molecule on the other in the case of strong interactions can be high and in addition, higher orders of perturbation term can become more predominant when

the equation is derived using the perturbation method. Therefore, one can modify the local HSAB formula by adding the higher orders of perturbation terms and use for various strong interaction cases.

Appendix

Evaluation of γ

For a given function $f(x)$, the derivative function is defined as,

$$\frac{df(x)}{dx} = \lim_{x \rightarrow 0} \left(\frac{f(x + \frac{\Delta x}{2}) - f(x - \frac{\Delta x}{2})}{\Delta x} \right) \quad (\text{A})$$

Let, $(\frac{df(x)}{dx}) = f'(x)$, $(\frac{d^2f(x)}{dx^2}) = f''(x)$ and $(\frac{d^3f(x)}{dx^3}) = f'''(x)$. Hence,

$$f''(x) = \lim_{x \rightarrow 0} \left(\frac{f'(x + \frac{\Delta x}{2}) - f'(x - \frac{\Delta x}{2})}{\Delta x} \right) \quad (\text{B})$$

Similarly,

$$f'''(x) = \lim_{x \rightarrow 0} \left(\frac{f''(x + \frac{\Delta x}{2}) - f''(x - \frac{\Delta x}{2})}{\Delta x} \right) \quad (\text{C})$$

Taking the value of $x = 1$ and comparing eqs (A), (B), and (C) finally we have

$$f'''(x) = \frac{1}{2} [f(x+2) - 2f(x+1) + 2f(x-1) - f(x-2)] \quad (\text{D})$$

Therefore we can write,

$$\gamma = \frac{1}{6} \left(\frac{d^3E}{dN^3} \right) = \frac{1}{12} [E(N+2) - 2E(N+1) + 2E(N-1) - E(N-2)] \quad (\text{E})$$

Table 3.1: Value of Charge Transfer Parameters for the Multiple Bonded Complexes. Values are in Atomic Units.

Complex	ΔN_{1st}			ΔN_{2nd}			λ
	DFT*	MP2*	CCSD(T)*	DFT*	MP2*	CCSD(T)*	DFT*
SUC-BUTL(1)	0.02940	0.01421	0.04151	0.02938	0.01420	0.04161	0.02142
FA-FD(2)	0.03092	0.02538	0.03307	0.03093	0.02536	0.03302	0.07620
AA-FD(3)	0.02570	0.01699	0.02488	0.02571	0.01697	0.02486	0.06871
FRM-FD(4)	0.01395	0.00805	0.00342	0.01396	0.00805	0.00342	0.02531
NFRM-FD(5)	0.00977	0.00204	0.00261	0.00982	0.00224	0.00261	0.01724
ATM-FD(6)	0.01114	0.00385	0.00121	0.01127	0.00385	0.00121	0.04448
NATM-FD(7)	0.00543	0.00095	0.00449	0.00552	0.00095	0.00449	0.12151
ACT-HCL(8)	0.05162	0.04440	0.03650	0.05165	0.04439	0.03647	0.02797
ACT-LICL(9)	0.06414	0.06320	0.06517	0.06417	0.06325	0.06513	0.02766
BUTY-HCL(10)	0.07564	0.06083	0.07449	0.07572	0.06085	0.07441	0.02766
BUTY-LICL(11)	0.09557	0.08588	0.10412	0.09593	0.08612	0.10417	0.02435

DFT* = DFT / 6-311G(d,p) / B3LYP

MP2* = MP2 / 6-311G(d,p)

CCSD(T)* = CCSD(T) / 6-311G(d,p)

Table 3.2: Values of the Chemical Potential (μ), Hardness (η), and Hyperhardness (γ) of all Monomers Calculated at the DFT, MP2, and CCSD(T) Levels. Values are in Atomic Units.

Reactants Molecule	chemical potential, μ			DFT*	hardness, η			hyperhardness, γ		
	DFT*	MP2*	CCSD(T)*		MP2*	CCSD(T)*	DFT*	MP2*	CCSD(T)*	
Succinamide (SUC)	-0.1517	-0.1345	-0.1400	0.2078	0.2100	0.2203	-0.0055	-0.0001	-0.0313	
Butyrolactam (BUTL)	-0.1268	-0.1220	-0.1022	0.2146	0.2309	0.2345	-0.0103	-0.0096	-0.0137	
Formamidine (FD)	-0.1232	-0.1213	-0.1068	0.2464	0.2483	0.2555	-0.0128	-0.0184	-0.0207	
Formic acid (FA)	-0.1548	-0.1479	-0.1414	0.2648	0.2756	0.2682	-0.0167	-0.0076	-0.0069	
Acetic acid (AA)	-0.1485	-0.1387	-0.1322	0.2460	0.2638	0.2556	-0.0158	-0.0103	-0.0107	
Formamide (FRM)	-0.1368	-0.1293	-0.1103	0.2404	0.2523	0.2567	-0.0146	-0.0129	-0.0081	
N-methylformamide (NFRM)	-0.1320	-0.1191	-0.1042	0.2335	0.2402	0.2461	-0.0106	-0.0064	-0.0114	
Acetamide (ATM)	-0.1337	-0.1250	-0.1056	0.2251	0.2390	0.2452	-0.0147	-0.0075	-0.0140	
N-methylacetamide (NATM)	-0.1283	-0.1222	-0.1023	0.2174	0.2335	0.2384	-0.0113	-0.0107	-0.0178	
Acetylene (ACT)	-0.1401	-0.1277	-0.1254	0.2785	0.2925	0.4150	-0.0201	-0.0184	-0.0237	
Butylene (BUTY)	-0.1212	-0.1147	-0.0966	0.2272	0.2460	0.2570	-0.0121	-0.0132	-0.0196	
HCl (HCL)	-0.1973	-0.1782	-0.1758	0.2755	0.2755	0.2749	-0.0165	-0.0159	-0.0146	
LiCl (LICL)	-0.1985	-0.1862	-0.1851	0.1769	0.1701	0.1683	-0.0225	-0.0220	-0.0211	

DFT* = DFT / 6-311G(d,p) / B3LYP

MP2* = MP2 / 6-311G(d,p)

CCSD(T)* = CCSD(T) / 6-311G(d,p)

Table 3.3: Condensed Local Softness (S_k^+ and S_k^-)^a of the Reactive Atoms. Values are in Atomic Units.

Reactant Molecule			DFT*		MP2		CCSD(T)	
	A	B	A	B	A	B	A	B
Succinamide (SUC)	O	H	0.5239	0.1890	0.5890	0.1641	0.6001	0.1549
Butyrolactam(BUTL)	O	H	0.7140	0.5897	1.0106	0.2845	0.8416	0.1808
Formamidine (FD)	N	H	0.6300	0.6513	0.6589	0.2326	0.6679	0.1873
formic acid (FA)	O	H	0.8346	1.4177	0.9496	0.1714	0.9825	0.1767
acetic acid (AA)	O	H	0.8119	1.0852	0.9494	0.1543	0.9853	0.1605
formamide (FRM)	O	H	0.8793	0.1955	1.0030	0.3490	0.9934	0.1973
N-methylformamide (NFRM)	O	H	0.8771	0.4714	0.9447	0.5379	0.6876	0.1691
acetamide (ATM)	O	H	0.8760	0.6299	1.0263	0.3488	1.0068	0.1785
N-methylacetamide (NATM)	O	H	0.7171	0.4430	1.0227	0.2040	1.0014	0.1612
acetylene (ACT) C	C		0.6637	0.6637	0.6492	0.6492	0.6564	0.6564
butylene (BUTY) C	C		0.4472	0.4472	0.5507	0.5507	0.5272	0.5272
HCl (HCL) H	H		1.5986		1.6013		1.6032	
LiCl(LICL) Li	Li		2.5216		2.6515		2.6055	

DFT* = DFT / 6-311G(d,p) / B3LYP

MP2* = MP2 / 6-311G(d,p)

CCSD(T)* = CCSD(T) / 6-311G(d,p)

^aFor oxygen and nitrogen atoms S_k^- and for hydrogen and lithium atoms S_k^+ has been calculated. S_k^+ and S_k^- are same for the carbon atom.

Table 3.4: ΔE_v , ΔE_μ , and Total Interaction Energy of all the Complexes as Described in the Text, Calculated by the Parameters ΔN_{1st} and ΔN_{2nd} using the DFT/6-311G(d,p) Method^b

Complex	ΔE_v			ΔE_μ			ΔE_{tot}			ΔE_{geom}
	ΔN_{1st}	ΔN_{2nd}	λ	ΔN_{1st}	ΔN_{2nd}	λ	ΔN_{1st}	ΔN_{2nd}	λ	
SUC – BUTL(1)	-0.0826	-0.0826	-0.0826	-9.2480	-9.2434	-6.7387	-9.3306	-9.3260	-6.8215	-14.8663
FA – FD(2)	-0.2513	-0.2513	-0.2513	-5.6326	-5.6347	-13.8829	-5.8859	-5.8839	-14.1343	-20.6473
AA – FD(3)	-0.1527	-0.1527	-0.1527	-5.1059	-5.1071	-13.6514	-5.2586	-5.2598	-13.8041	-19.8042
FRM – FD(4)	-0.0303	-0.0303	-0.0303	-4.0822	-4.0825	-8.1825	-4.1125	-4.1128	-8.2128	-16.2580
NFRM – FD(5)	-0.0177	-0.0177	-0.0177	-2.3940	-2.3939	-6.7789	-2.4118	-2.4116	-6.7966	-16.3290
ATM – FD(6)	-0.0238	-0.0238	-0.0238	-2.5310	-2.5312	-6.2852	-2.5548	-2.5550	-6.3090	-15.9840
NATM – FD(7)	-0.0048	-0.0048	-0.0048	-1.4154	-1.4154	-6.3517	-1.4202	-1.4202	-6.3565	-15.9421
ACT – HCL(8)	-0.7450	-0.7450	-0.7450	-2.7691	-2.7677	-1.4107	-3.5141	-3.5127	-2.1556	-2.1773
ACT – LICL(9)	-0.9307	-0.9307	-0.9307	-2.6143	-2.6156	-6.5106	-3.5449	-3.5463	-7.4412	-5.5990
BUTY – HCL(10)	-1.0409	-1.0409	-1.0409	-4.7599	-4.7648	-2.7990	-5.8008	-5.8056	-3.8399	-4.2221
BUTY – LICL(11)	-1.2358	-1.2358	-1.2358	-4.3893	-4.4057	-5.5804	-5.6251	-5.6415	-6.8162	-14.9459

^bEnergy values are in kcal/mol. The corresponding values of ΔN_{1st} and ΔN_{2nd} are given in Table 5.4. LRM (eq (3.34)) and SRM (eq (3.35)) have been used to calculate the IE of the complexes SUC – BUTL(1) to NATM – FD(7) and ACT – HCL(8) to BUTY – LICL(11), respectively.

Table 3.5: ΔE_v , ΔE_μ and Total Interaction Energies (ΔE_{tot}) of all Complexes as Described in the Text, Calculated by the Parameters ΔN_{1st} and ΔN_{2nd} using the MP2/6-311G(d,p) Method^c

Complex	ΔE_v		ΔE_μ		ΔE_{tot}		ΔE_{geom}
	ΔN_{1st}	ΔN_{2nd}	ΔN_{1st}	ΔN_{2nd}	ΔN_{1st}	ΔN_{2nd}	
SUC – BUTL(1)	-0.0164	-0.0164	-4.4483	-4.4463	-4.4647	-4.4626	-10.9489
FA – FD(2)	-0.0717	-0.0717	-8.1643	-8.1579	-8.2360	-8.2296	-13.4694
AA – FD(3)	-0.0296	-0.0296	-5.5336	-5.5314	-5.5633	-5.5610	-12.9607
FRM – FD(4)	-0.0085	-0.0085	-2.2762	-2.2759	-2.2847	-2.2844	-10.5835
NFRM – FD(5)	-0.0008	-0.0008	-0.6741	-0.6741	-0.6749	-0.6749	-11.0741
ATM – FD(6)	-0.0019	-0.0019	-1.0794	-1.0793	-1.0813	-1.0811	-10.7523
NATM – FD(7)	-0.0009	-0.0009	-0.2918	-0.2918	-0.2919	-0.2919	-10.1012
ACT – HCL(8)	-0.5725	-0.5725	-2.4023	-2.4016	-2.9748	-2.9741	-1.5980
ACT – LICL(9)	-0.9350	-0.9350	-2.5102	-2.5120	-3.4452	-3.4470	-4.3785
BUTY – HCL(10)	-0.8240	-0.8240	-3.5306	-3.5322	-4.3546	-4.3563	-3.4168
BUTY – LICL(11)	-1.2471	-1.2471	-3.5902	-3.6000	-4.8373	-4.8471	-12.9545

^cEnergy values are in kcal/mol. The corresponding values of ΔN_{1st} and ΔN_{2nd} are given in Table 1. LRM (eq (3.34)) and SRM (eq (3.35)) have been used to calculate the IE of the complexes SUC–BUTL(1) to NATM–FD(7) and ACT–HCL(8) to BUTY–LICL(11), respectively.

Table 3.6: ΔE_v , ΔE_μ and Total Interaction Energy of all the Complexes as Described in the Text, Calculated by the Parameters ΔN_{1st} and ΔN_{2nd} using the CCSD(T)/6-311G(d,p) Method^d

Complex	ΔE_v		ΔE_μ		ΔE_{tot}		ΔE_{geom}
	ΔN_{1st}	ΔN_{2nd}	ΔN_{1st}	ΔN_{2nd}	ΔN_{1st}	ΔN_{2nd}	
SUC – BUTL(1)	-0.1207	-0.1207	-14.8756	-14.9117	-14.9963	-15.0364	-14.8035
FA – FD(2)	-0.1118	-0.1118	-10.5770	-10.5633	-10.6888	-10.6751	-12.6066
AA – FD(3)	-0.0582	-0.0582	-8.0401	-8.0343	-8.0983	-8.0924	-12.2465
FRM – FD(4)	-0.0012	-0.0012	-1.0755	-1.0754	-1.0767	-1.0766	-10.3826
NFRM – FD(5)	-0.0006	-0.0006	-0.9555	-0.9556	-0.9562	-0.9562	-10.1929
ATM – FD(6)	-0.0001	-0.0001	-0.3837	-0.3837	-0.3838	-0.3838	-10.3182
NATM – FD(7)	-0.0018	-0.0018	-1.4382	-1.4382	-1.4400	-1.4400	-10.3338
ACT – HCL(8)	-0.4638	-0.4638	-2.2728	-2.2712	-2.7350	-2.7366	-1.1971
ACT – LICL(9)	-0.9755	-0.9755	-2.6091	-2.6077	-3.5846	-3.5832	-4.0198
BUTY – HCL(10)	-1.2529	-1.2529	-4.3970	-4.3924	-5.6499	-5.6453	-3.0173
BUTY – LICL(11)	-1.8470	-1.8470	-4.4627	-4.4652	-6.3096	-6.3121	-10.8380

^dEnergy values are in kcal/mol. The corresponding values of ΔN_{1st} and ΔN_{2nd} are given in Table 1. LRM (eq (3.34)) and SRM (eq (3.35)) have been used to calculate the IE of the complexes SUC–BUTL(1) to NATM–FD(7) and ACT–HCL(8) to BUTY–LICL(11), respectively.

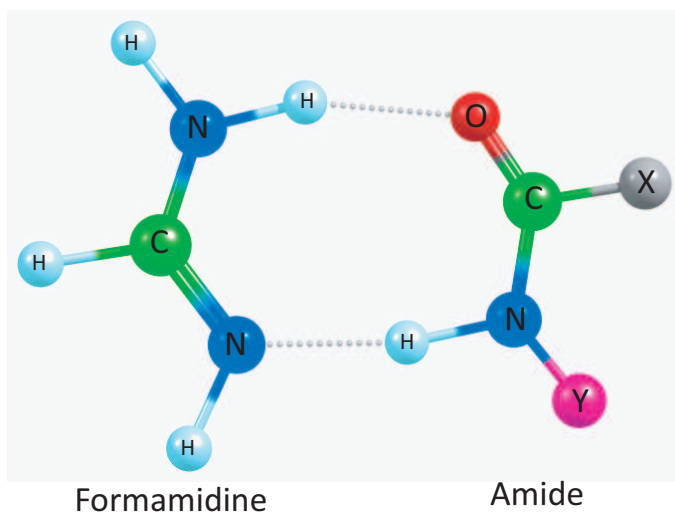


Figure 3.1: Multiple site based interactions pattern by localized reactive model (LRM) between acid, amide, and formamide, where $X = -H, -CH_3$ refer to formamide and acetamide, respectively, and in all cases Y is $-H$. In the case of N -methyl derivatives, Y is $-CH_3$.

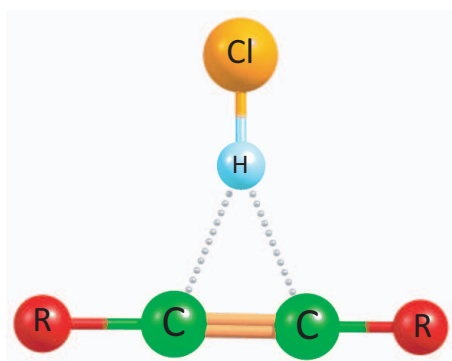


Figure 3.2: Multiple site based interactions pattern by smeared reactive models (SRM) between acetylene, butylene, H^+ , and Li^+ , where $R = -H$ and $-CH_3$ refer to acetylene and butylene, respectively.

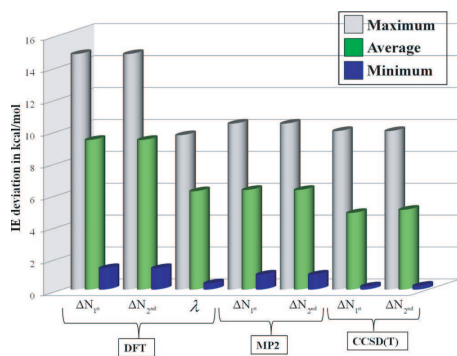


Figure 3.3: Maximum, average, and minimum deviation of interaction energy calculated through local HSAB (eqs (3.34) and (3.35)) and conventional methods (eq (3.38)).

Bibliography

- [1] Parr, R. G.; Yang, W. *Density Functional Theory of Atoms and Molecules*; Oxford University Press: New York, **1989**
- [2] Cohen, M. H. *In Theory of Chemical Reactivity*; Nalejwajski, R. F., Ed.; Topics in Current Chemistry; Springer-Verlag: Berlin, **1996**; Vol. 183, pp 143.
- [3] Geerlings, P.; De Proft, F.; Langenaeker, W. *In Advances in Quantum Chemistry*; Per-Olov, L., Ed.; Academic Press: New York, 1998; Vol. 33, pp 303.
- [4] Pal, S.; Roy, R.; Chandra, A. K. *J. Phys. Chem.* **1994**, 98, 2314.
- [5] Gazquez, J. L. *J. Phys. Chem. A* **1997**, 101, 8967.
- [6] Gazquez, J. L. *J. Phys. Chem. A* **1997**, 101, 9464.
- [7] Ghanty, T. K.; Ghosh, S. K. *J. Am. Chem. Soc.* **1994**, 116, 3943.
- [8] Ghanty, T. K.; Ghosh, S. K. *J. Phys. Chem.* **1996**, 100, 12295.
- [9] Ghanty, T. K.; Ghosh, S. K. *Inorg. Chem.* **1992**, 31, 1951.
- [10] Ghanty, T. K.; Ghosh, S. K. *J. Phys. Chem.* **1994**, 98, 1840.
- [11] Putz, M. V. *J. Mol. Struct: THEOCHEM.* **2009**, 900, 64.
- [12] Pal, S.; Chandrakumar, K. R. S. *J. Am. Chem. Soc.* **2000**, 122, 4145.
- [13] Pérez, P.; Simón-Manso, Y.; Aizman, A.; Fuentealba, P.; Contreras, R. *J. Am. Chem. Soc.* **2000**, 122, 4756.
- [14] *J. Am. Chem. Soc.* **2000**, 122, 2010.
- [15] Chattaraj, P. K.; Fuentealba, P.; Gómez, B.; Contreras, R. *J. Am. Chem. Soc.* **1999**, 122, 348.

-
- [16] Krishnamurty, S.; Pal, S. *J. Phys. Chem. A* **2000**, 104, 7639.
- [17] Parr, R. G.; Szentpály, L.; Liu, S. *J. Am. Chem. Soc.* **1999**, 121, 1922.
- [18] Pérez, P.; Toro-Labbé, A.; Contreras, R. *J. Phys. Chem. A* **1999**, 103, 11246.
- [19] Russo, N.; Toscano, M.; Grand, A.; Mineva, T. *J. Phys. Chem. A* **2000**, 104, 4017.
- [20] Mineva, T.; Sicilia, E.; Russo, N. *J. Am. Chem. Soc.* **1998**, 120, 9053.
- [21] Castro, R.; Berardi, M. J.; Córdova, E.; Ochoa de Olza, M.; Kaifer, A. E.; Evanseck, J. D. *J. Am. Chem. Soc.* **1996**, 118, 10257.
- [22] Soliman, S. M. *Comput. Theor. Chem.* **2012**, 994, 105.
- [23] Jaramillo, P.; Patricia Pérez, P. *J. Phys. Chem. A* **2009**, 113, 6812.
- [24] Geerlings, P.; De Proft, F.; Langenaeker, W. *Chem. Rev.* **2003**, 103, 1793.
- [25] Matito, E.; Putz, M. V. *J. Phys. Chem. A* **2011**, 115, 12459.
- [26] Pearson, R. G. *J. Am. Chem. Soc.* **1963**, 85, 3533.
- [27] Gazquez, J. L. *In Structure and Bonding (Berlin)*; Sen, K. D, Ed.; Springer – Verlag: Berlin, **1993**; Vol. 80, pp 27.
- [28] Parr, R. G.; Pearson, R. G. *J. Am. Chem. Soc.* **1983**, 105, 7512.
- [29] Parr, R. G.; Donnelly, R. A.; Levy, M.; Palke, W. E. *J. Chem. Phys.* **1978**, 68, 3801.
- [30] Pearson, R. G. *J. Am. Chem. Soc.* **1985**, 107, 6801.
- [31] Miquel, T. S.; Salvador, P.; Geerlings, P.; Solá, M. *J. Comput. Chem.* **2007**, 28, 574.
- [32] Miquel, T. S.; Salvador, P.; Solá, M.; Geerlings, P. *J. Comput. Chem.* **2008**, 29, 1064.
- [33] Parr, R. G.; Yang, W. *J. Am. Chem. Soc.* **1984**, 106, 4049.
-

-
- [34] Yang, W.; Parr, R. G. *Proc. Natl. Acad. Sci. U. S. A.* **1985**, 82, 6273.
- [35] Yang, W.; Mortier, W. J. *J. Am. Chem. Soc.* **1986**, 108, 5708.
- [36] Szarek, P.; Komorowski, L. *J. Comput. Chem.* **2011**, 32, 1721.
- [37] Parr, R. G.; Yang, W. *J. Am. Chem. Soc.* **1984**, 106, 4049.
- [38] Szarek, P.; Komorowski, L.; Lipiński, J. *Int. J. Quantum Chem.* **2010**, 110, 2315.
- [39] Komorowski, L.; Lipiński, J.; Szarek, P. *J. Chem. Phys.* **2009**, 131, 124120.
- [40] Yang, W.; Cohen, A. J.; Proft, F. D.; Geerlings, P. *J. Chem. Phys.* **2012**, 136, 144110.
- [41] Pearson, R. G. *Hard and Soft Acids and Bases*; Dowden, Hutchinson, and Ross: Stroudsburg, PA, **1973**.
- [42] Li, Y.; Evans, J. N. S. *J. Am. Chem. Soc.* **1995**, 117, 7756.
- [43] Pearson, R. G. *J. Chem. Edu.* **1987**, 64, 561.
- [44] Pearson, R. G. *Inorg. Chim. Acta* **1995**, 240, 93.
- [45] Mendez, F.; Gazquez, J. L. *J. Am. Chem. Soc.* **1994**, 116, 9298.
- [46] Roy, R. K.; Krishnamurthy, S.; Geerlings, P.; Pal, S. *J. Phys. Chem. A* **1998**, 102, 3746.
- [47] Tishchenko, O.; Pham – Tran, N.–N.; Kryachko, E. S.; Nguyen, M. T. *J. Phys. Chem. A* **2001**, 105, 8709.
- [48] Roy, R. K.; Pal, S.; Hirao, K. *J. Chem. Phys.* **1999**, 110, 8236.
- [49] Roy, R. K.; Hirao, K.; Pal, S. *J. Chem. Phys.* **2000**, 113, 1372.

-
- [50] Verstraelen, T.; Ayers, P. W.; Speybroeck, V.; Waroquier, M. *J. Chem. Theory Comput.* **2013**, *9*, 2221.
- [51] Fuentealba, P.; Perez, P.; Contreras, R. *J. Chem. Phys.* **2000**, *113*, 2544.
- [52] Chattaraj, P. K.; Poddar, A. *J. Phys. Chem. A* **1999**, *103*, 1274.
- [53] Chattaraj, P. K.; Poddar, A. *J. Phys. Chem. A* **1998**, *102*, 9944.
- [54] Chattaraj, P. K.; Poddar, A. *J. Phys. Chem. A* **1999**, *103*, 8691.
- [55] Gutiérrez – Oliva, S.; Jaque, P.; Toro-Labbé, A. *J. Phys. Chem. A* **2000**, *104*, 8955.
- [56] Chandrakumar, K. R. S.; Kar, R.; Pal, S. *Semiquantitative Aspects of Density – Based Descriptors and Molecular Interactions: A More Generalized Local Hard – Soft Acid – Base Principle. In Concepts and Methods in Modern Theoretical Chemistry: Electronic Structure and Reactivity*; Ghosh, S. K.; Chattaraj, P. K., Eds.; Taylor and Francis, CRC Press: Boca Raton, FL, **2013**; Chapter 19, pp 391.
- [57] Mendez, F.; Gazquez, J. L. *Proc. Indian Acad. Sci.* 1994, *106*, 183.
- [58] Menendez, F.; Tamariz, J.; Geerlings, P. *J. Phys. Chem. A* **1998**, *102*, 6292.
- [59] Chandrakumar, K. R. S.; Pal, S. *J. Phys. Chem. A* **2002**, *106*, 5737.
- [60] Chandrakumar, K. R. S.; Pal, S. *Int. J. Mol. Sci.* **2002**, *3*, 324.
- [61] Kokalj, A. *Chem. Phys.* **2012**, *393*, 1.
- [62] Hohenberg, P.; Kohn, W. *Phys. Rev.* **1964**, *136*, B864.
- [63] Parr, R. G.; Chattaraj, P. K. *J. Am. Chem. Soc.* **1991**, *113*, 1854.
- [64] Fuentealba, P.; Parr, R. G. *J. Chem. Phys.* **1991**, *94*, 5559.
- [65] Cárdenas, C.; Rabi, N.; Ayers, P. W.; Morell, C.; Jaramillo, P.; Fuentealba, P. *J. Phys. Chem. A* **2009**, *113*, 8660.
-

-
- [66] Sablon, N.; Proft, F. D.; Ayers, P. W.; Geerlings, P. *J. Chem. Theory Comput.* **2010**, *6*, 3671.
- [67] Geerlings, P.; De Proft, F. *Phys. Chem. Chem. Phys.* **2008**, *10*, 3028.
- [68] Ayers, P. W.; Parr, R. G. *J. Chem. Phys.* **2008**, *128*, 184108.
- [69] Chandrakumar, K. R. S.; Pal, S. *J. Phys. Chem. B* **2001**, *105*, 4541.
- [70] Møller, C.; Plesset, M. S. *Phys. Rev.* **1934**, *46*, 618.
- [71] Kohn, W.; Sham, L. J. *Phys. Rev.* **1965**, *137*, A1697.
- [72] Kohn, W.; Sham, L. J. *Phys. Rev.* **1965**, *140*, A1133.
- [73] Sham, L. J.; Kohn, W. *Phys. Rev.* **1966**, *145*, 561.
- [74] Frisch, M. J.; Trucks, G. W.; Schlegel, H. B.; Scuseria, G. E.; Robb, M. A.; Cheeseman, J. R.; Scalmani, G.; Barone, V.; Mennucci, B.; Petersson, G. A.; Nakatsuji, H.; *Gaussian 09*; Gaussian, Inc.: Wallingford, CT, **2009**
- [75] Becke, A. D. *J. Chem. Phys.* **1993**, *98*, 5648.
- [76] Lee, C.; Yang, W.; Parr, R. G. *Phys. Rev. B* **1988**, *37*, 785.
- [77] Wiberg, K. B. *J. Comput. Chem.* **1986**, *7*, 379.
- [78] Mulliken, R. S. *J. Chem. Phys.* **1955**, *23*, 1833.
- [79] Parish, J. H. *Bio. Educ.* **1985**, *13*, 92.
- [80] Watson, J. D.; Crick, F. H. C. *Nature* **1953**, *171*, 737.
- [81] Desiraju, G. R. *Acc. Chem. Res.* **1996**, *29*, 441.
- [82] Desiraju, G. R. *Science* **1997**, *278*, 404.
- [83] Hobza, P.; Šponer, J. *Chem. Rev.* **1999**, *99*, 3247.
-

-
- [84] Bertran, J.; Oliva, A.; Rodríguez – Santiago, L.; Sodupe, M. *J. Am. Chem. Soc.* **1998**, 120, 8159.
- [85] Šponer, J.; Hobza, P. *J. Phys. Chem. A* **2000**, 104, 4592.
- [86] Kim, Y.; Lim, S.; Kim, Y. *J. Phys. Chem. A* **1999**, 103, 6632.
- [87] Galetich, I.; Stepanian, S. G.; Shelkovsky, V.; Kosevich, M.; Blagoi Adamowicz, L. *J. Phys. Chem. B* **1999**, 103, 11211.
- [88] Uchimaru, T.; Korchowicz, J.; Tsuzuki, S.; Matsumura, K.; Kawahara, S. I. *Chem. Phys. Lett.* **2000**, 318, 203.
- [89] Mootz, D.; Deeg, A. *J. Am. Chem. Soc.* **1992**, 114, 5887.
- [90] Fuentealba, P.; Parr, R. G. *J. Chem. Phys.* **1991**, 94, 5559.
- [91] Ordon, P.; Tachibana, A. *J. Chem. Phys.* **2007**, 126, 234115.

**Understanding the Site Selectivity in
Small-Sized Neutral and Charged Al_n
($4 \leq n \leq 7$) Clusters Using Density
Functional Theory Based Reactivity
Descriptors: A Validation Study on
Water Molecule Adsorption**

Aluminum clusters are now technologically important due to their high catalytic activity. Our present study on the small-sized aluminum clusters applies density functional theory (DFT)-based reactivity descriptors to identify potential sites for adsorption and eventual chemical reaction. Depending on symmetry, susceptibility of various type of reactive sites within a cluster toward an impending electrophilic and/or nucleophilic attack is predicted using the reactivity descriptors. In addition, the study devises general rules as to how the size, shape, and charge of the cluster influences the number of available sites for an electrophilic and/or nucleophilic attack. The predictions by reactivity descriptors

are validated by performing an explicit adsorption of water molecule on Al clusters with four atoms. The adsorption studies demonstrate that the most stable watercluster complex is obtained when the molecule is adsorbed through an oxygen atom on the site with the highest relative electrophilicity.

4.1 Introduction

During the last two decades aluminum based clusters have attracted considerable amount of interest due to their catalytic properties.[1–5] Their catalytic properties are comparable with those of transition metal clusters such as Au, Pt, Pd etc.[6–10] These properties are specifically seen in small sized Al clusters viz., between 2–50 atoms.[11–15] In this size range, the catalytic property is seen to be size specific and this makes them attractive especially in the area of nanocatalysis.[16, 17] Aluminum nanoclusters[18–20] and aluminum nitrides[21] are the most prominent and well studied systems among the aluminum based clusters for the catalytic properties. Interestingly, small sized aluminum nanoclusters are also reported to behave as super atoms[22, 23] which can potentially lead to a huge impact in the area of nanoscience.[24–26] Following this understanding, many experimental and theoretical studies have attempted to address or investigate the structure-property (catalytic property) correlation within the aluminum clusters.[27–32] Khanna *et al.* have shown that some of the aluminum clusters are reactive towards even less reactive hydrocarbons.[43, 44] Several diatomic molecules such as H₂,[31, 34, 35] D₂,[36, 37] O₂[14, 38] etc. are seen to adsorb very strongly on aluminum clusters. Oxidation and photochemical reactions[39–41] on aluminum cluster anions are also being explored experimentally as well as theoretically and a tendency to form alumina-oxides is noted.[42] One of the significant experimental and theoretical study is a report by Johnson *et al.*[33] which clearly demonstrates that the oxidation behavior of metal cluster depends upon size, stoichiometry and ionic charge. However, a more surprising result is that a high energy bond in N₂ molecule is cleaved following a chemisorption on aluminum clusters in the size range of 44 to 100 atoms.[45] The N₂ adsorption has also been theoretically studied by Romanowski *et al.*[46] and Pal and co-workers.[47] Important conclusion of the above studies is that the reactivity of aluminum clusters critically depends on not only cluster size but also on its shape. The highlight of this finding is

that a high energy conformation can at times be more catalytically active as compared to the ground state conformation. This increases the complexity in identifying the most catalytically active conformation within a given size. Hence, there is now a necessity to diagnose some leads in identifying catalytically most promising cluster.

In a recent paper, Khanna et al.[48] have brought out factors that make a cluster reactive or other wise. They have, in their work analyzed the mechanism behind the dissociative chemisorption of water to produce hydrogen gas in various neutral and charged aluminum clusters.[48] They examined the reactions of $Al_n^- + H_2O$ where $n= 7-18$, and have shown that the complementary active sites[49] play a predominant role in the chemisorption. In other words, clusters with pair of adjacent sites, which behave as Lewis acid and Lewis base, redistribute the charge within a cluster and hence are responsible for the remarkable reactivity exhibited by it. Following their work, Henry *et al.* also noticed the same on charged and neutral aluminum clusters and determined the comparative reaction barriers and enthalpies for both neutral and singly charged clusters.[50] Few other groups have also theoretically addressed the Al-H₂O reaction mechanisms.[51, 52]

Thus, if a cluster with complementary active sites is identified, it will help greatly in potential applications of aluminum clusters in nanocatalysis.[53, 54] Hence, in this work, we aim to identify the aluminum clusters with complementary reactive sites. For this purpose, we have chosen clusters with 4-7 atoms in neutral, cationic and anionic states. One of the approaches to identify complementary active sites is by using density functional based reactivity descriptors.[55] We have discussed in detail the response of various sites in clusters toward an impending an electrophilic or a nucleophilic attack. For this purpose, relative nucleophilicity and electrophilicity of the various aluminum-clusters are calculated and an analysis of this is presented in section IV-A. Following the identification of potential reactive cluster, we carry out an explicit water molecule adsorption on few of the clusters and validate the results obtained from the reactivity descriptor based studies.

4.2 Theoretical Methods

The ground-state energy of an atom or a molecule, in DFT, is expressed in terms of electron density $\rho(\vec{r})$. [56] The response of $\rho(\vec{r})$ to the number of electrons is called as Fukui function $f(\vec{r})$. [55] Thus, $f(\vec{r})$ is defined as,

$$f(\vec{r}) \equiv \left(\frac{\delta\mu}{\delta v(\vec{r})}\right)_N = \left(\frac{\delta\rho(\vec{r})}{\delta N}\right)_{v(\vec{r})} \quad (4.1)$$

Here μ and N represent the chemical potential and the total number of electrons of the system respectively. $v(\vec{r})$ is the external potential (i.e., the potential due to the positions of the nuclei plus applied external field, if any) at position \vec{r} of the chemical species. $f(\vec{r})$ is called as the Fukui function (FF). The middle term i.e. $\left(\frac{\delta\mu}{\delta v(\vec{r})}\right)_N$ of equation 1 measures the sensitivity of a chemical potential to an external perturbation at a particular point. $\left(\frac{\delta\rho(\vec{r})}{\delta N}\right)_{v(\vec{r})}$ shows change of electron density for a system with N number of electrons. The N discontinuity problem of atoms and molecules in eq. 1 leads to the introduction of both right and left hand side derivatives at a given number of electrons [57–59], $N_0 (= N)$. By the finite difference method, using electron densities of N_0 , (N_0+1) and (N_0-1) electron systems, FF's for nucleophilic and electrophilic attack can be defined respectively as,

$$f^+(\vec{r}) \equiv \rho_{N_0+1}(\vec{r}) - \rho_{N_0}(\vec{r}) \quad (4.2)$$

$$f^-(\vec{r}) \approx \rho_{N_0}(\vec{r}) - \rho_{N_0-1}(\vec{r}) \quad (4.3)$$

and for radical attack

$$f^0(\vec{r}) \approx \frac{1}{2}(\rho_{N_0+1}(\vec{r}) - \rho_{N_0-1}(\vec{r})) \quad (4.4)$$

Here, $\rho_{N_0}(\vec{r})$, $\rho_{N_0+1}(\vec{r})$ and $\rho_{N_0-1}(\vec{r})$ are the electron densities of N_0 , (N_0+1) and (N_0-1) electronic systems at a particular point \vec{r} . $f^+(\vec{r})$ and $f^-(\vec{r})$ are known as local electrophilicity and nucleophilicity respectively.

Parr pointed out, in the frozen core approximation, $f^+(\vec{r})$ and $f^-(\vec{r})$ can be approximated with the density of lowest unoccupied molecular orbital (LUMO) and highest occupied molecular orbital (HOMO).

$$f^+(\vec{r}) \approx \rho^{LUMO}(\vec{r}) \quad (4.5)$$

measures the reactivity toward a nucleophilic reagent

$$f^-(\vec{r}) \approx \rho^{HOMO}(\vec{r}) \quad (4.6)$$

measures the reactivity toward a electrophilic reagent and

$$f^0(\vec{r}) \approx \frac{1}{2}(\rho^{HOMO}(\vec{r}) + \rho^{LUMO}(\vec{r})) \quad (4.7)$$

measures the reactivity toward a radical reagent. Here, $\rho^{HOMO}(\vec{r})$ and $\rho^{LUMO}(\vec{r})$ are the densities of HOMO and LUMO respectively.

To describe the site reactivity or site selectivity, Yang and Mortier[60] proposed the condensed FF's for an atom k. The condensed electrophilicity for an atom k is defined as,

$$f_k^+ \approx q_k^{N_0+1} - q_k^{N_0} \quad (4.8)$$

similarly condensed nucleophilicity for an atom k is defined as,

$$f_k^- \approx q_k^{N_0} - q_k^{N_0-1} \quad (4.9)$$

The condensed reactivity descriptor of the site, appropriate for the radical attack is f_k^0 and can be defined as,

$$f_k^0 \approx \frac{1}{2}(q_k^{N_0+1} - q_k^{N_0-1}) \quad (4.10)$$

where, $q_k^{N_0}$, $q_k^{N_0+1}$ and $q_k^{N_0-1}$ are the electronic populations on the atom k for N_0 , $(N_0 + 1)$ and $(N_0 - 1)$ electron systems, respectively.

Roy *et al.* proposed a new set of relative indices which are more appropriate for intra molecular reactivity[61, 65]. The condensed relative electrophilicity of an atom k can be defined as,

$$f_k^{el} \approx \frac{f_k^+}{f_k^-} \quad (4.11)$$

similarly relative nucleophilicity

$$f_k^{nu} \approx \frac{f_k^-}{f_k^+} \quad (4.12)$$

f_k^{el} or f_k^{nu} are found to be very effective in comparing site reactivity across the molecule. A site with $f_k^{el} > f_k^{nu}$ is favorable for a nucleophilic attack, while a site with $f_k^{nu} > f_k^{el}$ is clearly a site favorable towards an electrophilic attack. A site with f_k^{el} is nearly equal to f_k^{nu} is likely to both give or take electrons with equal ease making it an amphiphilic site, likely to participate in both oxidation and reduction chemical reactions.

4.3 Computational Details

Various conformations of Al₄, Al₅, Al₆, and Al₇ are generated and optimized in mono positive, neutral and mono negative charge states. All the structures are optimized at DFT[62, 63] level of theory using Gaussian 09 software package[64] with aug-cc-PVTZ[66, 67] basis set and B3PW91 functional.[68–71] This functional has proved to be suitable to describe such kind of systems.[72–74] Harmonic vibrational frequencies and binding energies are computed for all the conformations at the end of optimization. Before calculating the relative reactivity descriptor the total binding energy of each cluster is calculated as,

$$E_{B.E} = nE_{Al} - E_{Al_n} \quad (4.13)$$

Here nE_{Al} is total energy of free atoms and E_{Al_n} is energy of the cluster.

Only conformations with all positive frequencies are taken for further study of site selectivity using reactivity descriptors. To obtain the reactivity descriptor at a given site, single point energy calculation is done at DFT/B3PW91/aug-cc-PVTZ level on the charged counterparts by maintaining them at the optimized geometry of the neutral conformation. Finite difference approximation is considered to calculate Fukui functions as discussed in the Section II. The condensed Fukui functions are calculated with Hirshfeld population analysis.[75] The relative reactivity descriptors are calculated from the FF's to evaluate the electrophilicity and nucleophilicity of various sites. Following the reactivity descriptor calculations, water molecule is adsorbed at various sites of few Al₄ clusters. Interaction energy of cluster–water complex is calculated as,

$$E_{AB}^{int} = E_A + E_B - E_{AB} \quad (4.14)$$

Where E_A and E_B is the energy of monomer and E_{AB} is the energy of complex.

4.4 Results and Discussion

4.4.1 Site selectivity of aluminum clusters using relative reactivity descriptors

1. Al₄ : The structure, electronic properties and the reactivity parameters for all the Al₄ clusters are given in Table I and Table II. We begin our discussion with conformation I which is stable in all three viz. neutral, positive and negative states. This conformation has the highest binding energy for an Al₄ cluster in neutral, cationic and anionic states. All three conformations have two sites, viz., A and B which have distinct chemical environment and are situated alternatively. Sites A and B are bonded to each other of 2.49Å and 2.65Å in neutral state. This structure does not show much charge redistribution among both the sites. Site A has higher relative electrophilicity (1.30) while site B has higher relative nucleophilicity (1.25) value. Hence, sites A behaves as the site most

probable for attack by nucleophile whereas sites B is most likely to be attacked by an electrophile. In positive and negative states, inter atomic bond distances are uniform as shown in Table I. In both these conformations, there is a small amount of charge localization on site B, with respect to site A. In positively charged conformation, the site A is electrophilic and site B is nucleophilic. In the negatively charged conformation, both sites act as electrophilic centers as seen from the reactivity descriptor values which are 2.54 and 1.41 for sites A and B, respectively.

The next conformation (II) is a pendant, which is also stable in all three charged states. All three conformations have three chemically distinct sites, viz., A, B and C. Site B is bonded to A and C and the two equivalent atoms of site A are connected to each other. Compared to the neutral and negative conformations, the B–C and A–A bonds of positively charged conformation are slightly elongated, while the trend is reverse for A and B inter atomic distances. Site C is most positively charged atom in the neutral and positively charged conformations, whereas, in negatively charged conformation, charge enriched sites are A atoms (–0.316). Sites A are electrophilic centers and site B is a nucleophilic center in neutral and positively charged state. Site C is a nucleophilic center in neutral cluster while in positively charged one relative electrophilicity and relative nucleophilicity are nearly equal on this site. Such a site has been referred to as an amphiphilic site in one of the earlier papers.[76] it is an amphiphilic site. Sites B and C are highly electrophilic centers in the negatively charge cluster.

Conformation III is tetrahedral in shape and is stable only in neutral and negatively charged state. In case of positively charged conformation, one of the vibrational mode is imaginary. Negatively charged conformation III is as equally stable as the negatively charged conformation I. Binding energy of this conformation is 8.09 eV. Both the states of conformation III have two distinct sites viz. A and B. It is seen from the Table II, that the neutral conformation does not have much charged redistribution among both the sites. However, in case of negatively charged conformation there is a small amount of charged localization on site B, with respect to site A. Analysis of the relative reactivity descriptors

reveals that site A is electrophilic and site B is nucleophilic in neutral conformation. On the other hand, in the negatively charged conformation, both the sites behave as a electrophilic centers.

Other two conformations we have studied here are stable only in one of the states with the other two states have imaginary vibrational frequencies. Conformation IV is linear and is stable in positively charged state. It has two distinct reactive sites viz. A and B. There is a charge redistribution in the conformation IV. Site B has higher charge localization as compared to site A. Site B is electrophilic center (with relative electrophilicity of 1.38) while site A is nucleophilic in nature (relative nucleophilicity is 1.31). Conformation V has a zigzag form and is stable in neutral state. It also has two chemically distinct reactive sites viz. A and B. These two sites are situated alternatively. Compared to A–A, A–B bond distance is higher by 0.06 Å. Hirshfeld charge shows that A is negatively charged (-0.108) while B is positively charged (0.108). Site A is amphiphilic in nature and site B is electrophilic as seen from the values of relative reactivity descriptors.

2. Al₅ : The structure, electronic properties and the reactivity parameters for all the studied Al₅ clusters are given in Tables III and IV. We have optimized several conformations for Al₅ cluster. However, only few of them had all positive frequencies. We here discuss the reactivity patterns in the clusters with all positive vibrational modes. Conformation I is stable in two state viz., neutral, negative. Both the conformations have three chemically distinct sites viz. A, B and C. In the neutral state, site A and site B are bonded to each other with an inter atomic distance of 2.60 Å. Sites B and C are bonded through a distance of 2.87 Å. Sites C and A are 2.49 Å apart from each other. Two equivalent atoms(B) are connected by a bond distance of 2.57 Å. In negative state, distance between site A and site C is larger by 0.07 Å, whereas other inter atomic distances decrease slightly as shown in Figure (second column of Table III). The neutral conformation does not show much charge redistribution among all the sites. However, in case of negatively charged conformation, charge distribution is unequal. There is a small amount of charge

localization on site A, with respect to other two. In neutral conformation, all the sites have nearly equal relative reactivity descriptors. Thus, all sites are amphiphilic in nature. On the other hand, in negatively charged conformation, site B has higher relative electrophilicity (2.38) while site C has higher relative nucleophilicity (1.52) value. Thus, site B behaves as an electrophilic center and site C as a nucleophilic center. Site A is a weaker electrophilic center as compared to site B.

Conformation II is stable in neutral and positively charged states. In negatively charged conformation, one of the vibrational modes is imaginary. This conformation has higher number of chemically distinct reactive sites. Both the states have four distinct reactive sites viz. A, B, C and D. Site B is connected to two equivalent atoms viz., A which are in turn is connected to site C. Site C connected to site D. Compared to the neutral conformation the C–D and A–B inter atomic distance of positively charged conformation is larger by 0.19Å and 0.23Å respectively. The reverse is observed in the other bonds. It has been shown from the Table II that there is a charge localization in site B in both the states. However, greater charge localization is seen for the positively charged conformation. Relative reactivity analysis indicates that sites D and B are electrophilic in the order $D > B$. Sites A and C are nucleophilic in the order of $A > C$. On the other hand, in the positively charge conformation, site C and site D have higher relative electrophilicity (1.38 and 1.12 respectively) values. Site A is amphiphilic in nature, while site B is nucleophilic, as predicted by the relative reactivity descriptors.

Other two conformations are stable in only one of the charged states. Other states have imaginary vibrational frequencies. Binding energy analysis shows that among the all Al_5 conformations these two clusters are most stable with binding energy values of 8.28 eV and 32.45 eV for conformation III and conformation IV respectively. However, we present their reactivity descriptors for the sake of completeness. Conformation III is stable in neutral state. It has three unique sites viz. A,B and C. A–B, A–C, B–C and B–B inter atomic distances are 2.60Å, 2.51Å, 2.78Å, are 2.47Å respectively. There is a very little charge distribution in the conformation III. Site A is electrophilic and site

B are amphiphilic in nature according to the relative reactivity descriptor analysis. Site C acts as a nucleophilic site. Conformation IV is stable in positively charged state. It also has three distinct reactive sites viz. A, B and C. Inter atomic distance between site A and site B is comparatively higher than in other bonds. Site A and site B are electrophilic in nature, whereas, site C behaves as an nucleophilic site due to its higher relative nucleophilicity value.

3. Al₆ : Structure, electronic properties and the reactivity parameters for all Al₆ clusters are given in the Table V and Table VI. We have chosen two conformations for this cluster size. Conformation I is octahedral and is stable in three states viz., neutral, positive, and negative states. All the states of this conformation have higher binding energies as compared to the other conformations. In neutral and negative states, all the atoms are equivalent i.e it has one chemically distinct site viz., A. In both these states bond distance is identical. Interestingly, in both these conformations, charge is uniformly distributed among the all six atoms. The reactivity descriptors indicate that in the neutral conformations all the sites are amphiphilic in nature. On the other hand, in the negatively charged conformation all the sites are electrophilic in nature. In the positively charge conformation, the cluster modifies marginally to result in two chemically distinct sites viz., A and B. In this conformation, alternate inter atomic distance between sites A are 3.19Å and 2.52Å, respectively, while the alternate bond distances between sites A and site B are 2.95Å and 2.66Å respectively. This leads to a charge redistribution within the cluster, as seen from the Table V. Site A of positively charged conformation is amphiphilic and site B is weakly electrophilic.

Conformation II also stable in all the three states. Neutral conformation is unsymmetrical leading to six chemically distinct sites, viz., A, B, C, D, E and F. A-B and D-E inter atomic distances are equal (2.52Å). Positive and negatively charged conformations have four distinct sites viz. A, B, C and D. The A–A and A–B inter atomic distance are larger (0.2Å) in positively charged conformation than negative one. On the other hand, other bonds distances are lower by 0.18 Å Neutral and positive conformations do

not exhibit much charge redistribution unlike the negatively charged conformation which has 0.24 electrons localized (-0.24) on site D. Analysis of relative reactivity descriptors reveals that in the unsymmetrical neutral conformation, electrophilic sites are B, C, E and F in the order of $E > C > F > B$. Site D behaves as a nucleophilic center (relative nucleophilicity 1.54). Site A is very weakly nucleophilic. However, in case of positively charged conformation sites A and D are strong electrophilic centers followed by site B. Site C is only nucleophilic site. In the negatively charged conformation, all sites are electrophilic in nature.

4. Al_7 : Table VII describes the structure, electronic properties and the reactivity parameters for the studied Al_7 cluster. Conformation I is stable in the neutral and negatively charged states. Both the structures have five chemically distinct sites viz A, B, C, D and E. In the negatively charged conformation most of the inter atomic distances are higher as compared to the neutral one except for A–E and B–C bonds. Charge in the neutral conformation is almost equally distributed on all the seven atoms. On the other hand, more charge is localized on site D (-0.23) in the negative conformation. According to above discussion, sites A and C are nucleophilic and site D is electrophilic in neutral state. B and C are amphiphilic centers. In the negative conformation all sites are electrophilic with the exception of site C which is amphiphilic. Binding energies of neutral and negatively charged clusters are 14.51 eV and 16.92 eV, respectively.

It is important to note here that the reactivity trends within above studied atomic clusters (relative electrophilicity or nucleophilicity) are in some cases different to the trend implied by the atomic charges. Relative reactivity descriptors for a given site (f_k^{el} and f_k^{nu}) are a ratio of two individual descriptors viz. nucleophilic Fukui function ($f^+(\vec{r})$) and electrophilic Fukui function ($f^-(\vec{r})$) of that particular site. The individual descriptors are, in turn, calculated from the difference of the electronic population between charged states for a particular site. Hence, as compared to the absolute atomic charge, it is more reliable reactivity descriptor of a chemical environment. In other words, a negatively charged site may be more prone to accept electrons and behave as a electrophilic site

as indicated by the higher relative electrophilicity values. Similarly in spite of being positively charged, a particular site can be more prone to electrophilic attack as indicated by its higher relative nucleophilicity.

4.4.2 Understanding the site selectivity in aluminum clusters using explicit water molecule adsorption: Case study on Al_4

A case study of water molecule adsorption has been carried out on Al_4 cyclic and pendent conformations. It is expected that a site with higher value of relative electrophilicity will form a stronger bond with the oxygen atom of water molecule (or alternatively, the site with higher relative nucleophilicity will form stronger bond with one of the hydrogen atoms of the water molecule). Neutral and positive conformations of cyclic Al_4 have two chemically distinct sites each viz., A and B. Site A (Table I) has higher relative electrophilicity in both cases. As seen from the Table VIII, neutral cyclic conformation-water molecule complex has an interaction energy of 0.75 eV for the site A as compared to the 0.27 eV for the site B. Similar observation is seen in case of positive cyclic Al_4 conformation-water complexes. Interestingly, in case of both neutral and positively charged cyclic Al_4 conformations, we have alternating electrophilic and nucleophilic sites. In case of negatively charged cyclic Al_4 conformation, water molecule adsorbs strongly on both the sites. However, upon adsorption the structure modifies itself into a square conformation. The water molecule dissociates into OH^- and H^+ . Thus, while the high electrophilicity on both the sites favors the adsorption of H_2O via O atom, absence of adjacent nucleophilic sites makes the conformation unstable after adsorption. On the other hand, in case of neutral Al_4 pendent conformation, electrophilic site A adsorbs water molecule with an interaction energy of 0.29 eV. This is much less than the corresponding value for cyclic Al_4 conformation (site A), a cluster with alternating nucleophilic and electrophilic sites. Similar consistent observations are also noted for other Al clusters whose results are not reported here.

4.5 Conclusion

In the above work, we have attempted to understand the site selective reactivity patterns in Al clusters with 4–7 atoms. Our work shows that reactivity changes as function of both size, and charge of the clusters. Reactivity descriptors can effectively be used as screening tool to isolate clusters with higher reactivity as well as clusters with alternating lewis acid base sites. Among neutral, positive and negatively charged clusters, negatively charged Al clusters are seen to have strongest electrophilic centers. Positively charged and neutral clusters have alternating electrophilic and nucleophilic centers. The water molecule is expected to adsorb strongly on all the electrophilic centers via the oxygen atom and this is validated in our water adsorption case studies. While the water molecule adsorbs strongly on the electrophilic centers of positive and neutral clusters, the adsorption is followed by water molecule dissociation in the negatively charged clusters. However, due to the absence of adjacent nucleophilic centers in the negatively charged clusters the cluster is seen to undergo structural fluxionality. This is consistent with observations in earlier reports that negatively charged Al clusters are more catalytically active clusters for the case of water splitting.

Table 4.1: Structural, Electronic and Reactivity Parameters of Al_4 conformations. The values given next to the conformations in column II of the table correspond to the inter-atomic distances (in Å) between various unique sites.

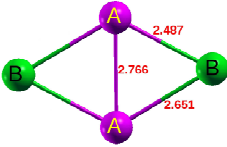
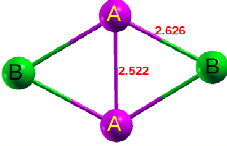
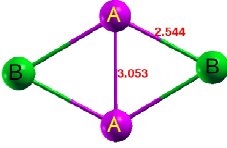
State	Structure	Total Binding energy (eV)	Sites	Hirshfeld	f_k^{el}	f_k^{nu}
Neutral (I)		5.51	A	0.009	1.300	0.770
			B	-0.009	0.800	1.254
Positive (I)		23.63	A	0.225	1.027	0.9734
			B	0.275	0.966	1.035
Negative (I)		8.09	A	-0.239	2.536	0.394
			B	-0.260	1.416	0.706

Table 4.2: Structural, Electronic and Reactivity Parameters of Al_4 conformations. The values given next to the conformations in column II of the table correspond to the inter-atomic distances (in Å) between various unique sites.

State	Structure	Total Binding energy (eV)	Sites	Hirshfeld	f_k^{el}	f_k^{nu}
Neutral (II)		5.21	A	-0.015	1.272	0.786
			B	-0.100	0.706	1.418
			C	0.131	0.917	1.090
Positive (II)		23.47	A	0.240	1.023	0.977
			B	0.0317	0.945	1.058
			C	0.488	0.998	1.002
Negative (II)		7.27	A	-0.316	0.943	1.061
			B	-0.202	1.774	0.564
			C	-0.165	5.993	0.167

Table 4.3: Structural, Electronic and Reactivity Parameters of Al_4 conformations. The values given next to the conformations in column II of the table correspond to the inter-atomic distances (in Å) between various unique sites.

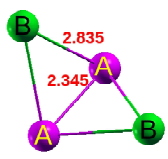
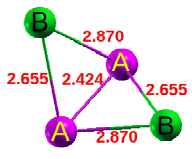
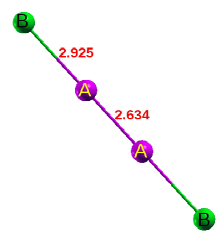
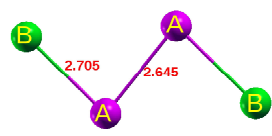
State	Structure	Total Binding Energy (eV)	Sites	Hirshfeld	f_k^{el}	f_k^{nu}
Neutral (III)		5.31	A	-0.006	1.396	0.716
			B	0.006	0.763	1.310
Negative (III)		8.09	A	-0.239	2.542	0.393
			B	-0.257	1.415	0.707
Positive (IV)		23.28	A	0.138	0.762	1.312
			B	0.363	1.387	0.721
Neutral (V)		4.17	A	-0.108	1.001	0.999
			B	0.108	1.098	0.911

Table 4.4: Structural, Electronic and Reactivity Parameters of Al_5 conformations. The values given next to the conformations in column II of the table correspond to the inter-atomic distances (in Å) between various unique sites.

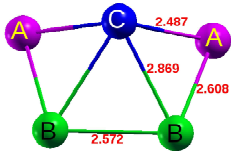
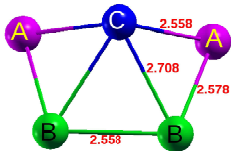
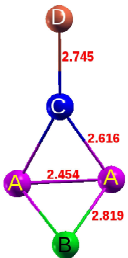
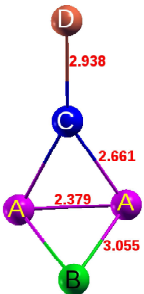
State	Structure	Total Binding Energy (eV)	Sites	Hirshfeld	f_k^{el}	f_k^{nu}
Neutral (I)		8.24	A	0.016	1.043	0.959
			B	0.007	1.070	0.934
			C	-0.045	0.954	1.049
Negative (I)		10.60	A	-0.242	1.543	0.648
			B	-0.161	2.380	0.420
			C	-0.192	0.655	1.526
Neutral (II)		7.13	A	-0.041	0.808	1.238
			B	0.026	1.167	0.859
			C	-0.059	0.936	1.069
			D	0.122	1.424	0.702
Positive (II)		31.88	A	0.147	0.995	1.006
			B	0.260	0.704	1.420
			C	0.078	1.389	0.720
			D	0.368	1.127	0.887

Table 4.5: Structural, Electronic and Reactivity Parameters of Al_5 conformations. The values given next to the conformations in column II of the table correspond to the inter-atomic distances (in Å) between various unique sites.

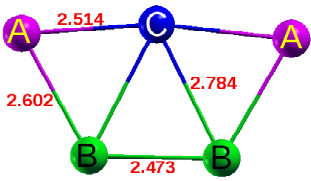
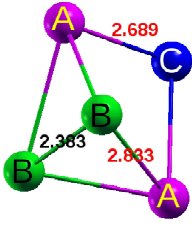
State	Structure	Total Binding Energy (eV)	Sites	Hirshfeld	f_k^{el}	f_k^{nu}
Neutral (III)		8.28	A	0.036	1.088	0.919
			B	0.000	0.980	1.020
			C	-0.073	0.850	1.177
Positive (IV)		32.45	A	0.155	1.049	0.954
			B	0.222	1.046	0.956
			C	0.246	0.807	1.243

Table 4.6: Structural, Electronic and Reactivity Parameters of Al_6 conformations. The values given next to the conformations in column II of the table correspond to the inter-atomic distances (in \AA) between various unique sites.

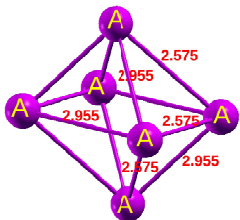
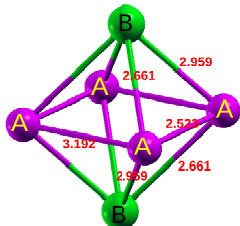
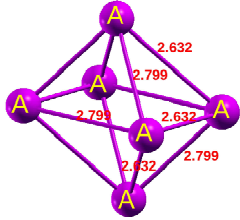
State	Structure	Total Binding Energy (eV)	Sites	Hirshfeld	f_k^{el}	f_k^{nu}
Neutral (I)		11.13	A	0.000	1.019	0.982
Positive (I)		41.24	A B	0.179 0.141	0.994 1.023	1.006 0.977
Negative (I)		13.92	A	-0.167	1.300	0.769

Table 4.7: Structural, Electronic and Reactivity Parameters of Al₆ conformations. The values given next to the conformations in column II of the table correspond to the inter-atomic distances (in Å) between various unique sites.

State	Structure	Total Binding Energy (eV)	Sites	Hirshfeld	f_k^{el}	f_k^{nu}
Neutral (II)		10.39	A B C D E F	-0.008 0.005 0.002 0.008 0.0136 -0.020	0.973 1.035 1.226 0.648 1.676 1.181	1.028 0.966 0.816 1.544 0.597 0.847
Positive (II)		41.02	A B C D	0.189 0.122 0.190 0.188	1.144 1.050 0.908 1.137	0.874 0.952 1.101 0.887
Negative (II)		13.04	A B C D	-0.186 -0.125 -0.133 -0.243	1.634 1.482 1.051 1.838	0.612 0.675 0.951 0.544

Table 4.8: Structural, Electronic and Reactivity Parameters of Al_7 conformations. The values given next to the conformations in column II of the table correspond to the inter-atomic distances (in Å) between various unique sites.

State	Structure	Total Binding Energy (eV)	Sites	Hirshfeld	f_k^{el}	f_k^{nu}
Neutral (I)		41.51	A	-0.007	0.876	1.142
			B	0.006	1.010	0.990
			C	0.006	1.013	0.987
			D	0.0038	1.258	0.795
			E	-0.007	0.877	1.140
Negative (I)		16.92	A	-0.141	3.250	0.308
			B	-0.115	2.116	0.4727
			C	-0.140	0.996	1.004
			D	-0.231	1.042	0.960
			E	-0.115	1.081	0.925

Table 4.9: Interaction energy of water adsorption on Al₄ conformations.

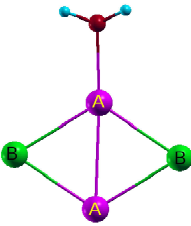
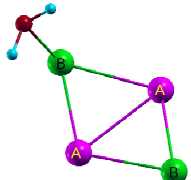
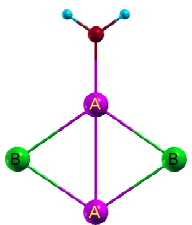
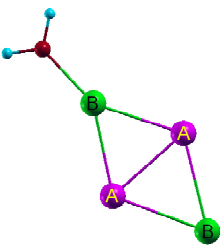
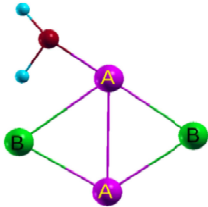
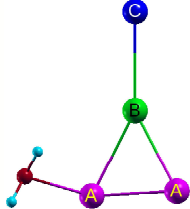
State	Structure	Water adsorption site	Interaction energy (eV)
Neutral		A	0.75
Neutral		B	0.27
Positive		A	1.72
Positive		B	1.56

Table 4.10: Interaction energy of water adsorption on Al₄ conformations.

State	Structure	Water adsorption site	Interaction energy (eV)
Negative*		A	1.81
Neutral		A	0.29

*This conformation undergo structural fluxionality. Optimize geometry is a square structure.

Bibliography

- [1] S. N. Khanna ; P. Jena. *Phys. Rev. B.* **1992**, *69*, 1664-1667.
- [2] Shiv N. Khanna ; P. Jena. *Phys. Rev. B.* **1995**, *51*, 13705-13716.
- [3] Ashman C; Shiv N Khanna; Liu Feng; Jena P.; Kaplan T.; Mostoller M. *Phys. Rev. B.* **1997**, *55*, 15868-15873.
- [4] B. Medrano; Victor G.; Farin Benjamin; Gaigneaux Eric M. *ACS Catalysis.* **2012**, *2*, 322-336.
- [5] N. O. Jones; J. Ulises Reveles; S. N. Khanna; D. E. Bergeron; P. J. Roach *J. Chem. Phys.* **2006**, *124*, 154311-154327.
- [6] M. Haruta; N. Yamada; T. Kobayashi; S. Iijima. *J. Catal.* **1989**, *115*, 301-309.
- [7] Hannu Hakkinen; Michael Moseler; Uzi Landman. *Phys. Rev. Lett.* **2002**, *89*, 33401-33405.
- [8] Lichang Wang; Qingfeng Ge. *Chem. Phys. Lett.* **2002**, *366*, 368-376.
- [9] G. Gantefor; M. Gausa; K-H. Meiwes-Broer; H. O. Lutz. *J. Chem. Soc., Faraday Trans.* **1990**, *86*, 2483-2488.
- [10] Kiyotomi Kaneda; Yoko Fujie; Kohki Ebitani. *Tetrahedron Letters.* **1997**, *38*, 9023-9026.
- [11] B.N.J. Persson; J.E. Müller. *Surface Science.* **1986**, *171*, 219-225.
- [12] R. E. Leuchtner; A. C. Harms; and A. W. Castleman. *J. Chem. Phys.* **1991**, *94*, 1093-1102.
- [13] Martin Beyer; Christian Berg; Hans W. Görlitzer; Thomas Schindler; Uwe Achatz; Gerhard Albert; *J. Am. Chem. Soc.* **1996**, *118*, 7386-7389.

-
- [14] Arthur C. Reber; Shiv N. Khanna; Patrick J. Roach; William H. Woodward; A. Welford Castleman Jr. *J. Am. Chem. Soc.* **2007**, *129*, 16098-16101.
- [15] D.L. Trimm; A. Stanislaus. *Applied Catalysis.* **1986**, *21*, 215-238.
- [16] M. Valden; X. Lai; D. W. Goodman. *Science.* **1998**, *281*, 1647-1650.
- [17] Polshettiwar Vivek; Varma Rajender S. *Green Chemistry.* **2010**, *12*, 743-754.
- [18] Andrés Aguado; José M. López. *J. Chem. Phys.* **2009**, *130*, 64704-64713.
- [19] S.N. Khanna; P. Jena. *Chem. Phys. Lett.* **1994**, *219*, 479-483.
- [20] Mojtaba Alipour; Afshan Mohajeri. *J. Phys. Chem. A.* **2010**, *114*, 12709-12715.
- [21] Aurora Costales; M. A. Blanco; E. Francisco; A. Martín Pendás; Ravindra Pandey. *J. Phys. Chem. B.* **2006**, *110*, 4092-4098.
- [22] Minoru Akutsu; Kiichirou Koyasu; Junko Atobe; Natsuki Hosoya; Ken Miyajima; Masaaki Mitsui; Atsushi Nakajima. *J. Phys. Chem. A.* **2006**, *110*, 12073-12076.
- [23] Arthur C. Reber; Shiv N. Khanna; A. Welford Castleman , Jr. *J. Am. Chem. Soc.* **2007**, *129*, 10189-10194.
- [24] Helley A. Claridge; A. W. Castleman; Shiv N. Khanna; Christopher B. Murray; Ayusman Sen; Paul S. Weiss. *ACS Nano.* **2009**, *3*, 244-255.
- [25] Abhay N. Pasupathy; Radoslaw C. Bialczak; Jan Martinek; Jacob E. Grose; Luke A. K. Donev; Paul L. McEuen; Daniel C. Ralph. *Science.* **2004**, *306*, 86-89.
- [26] Nakamura, S. *Proceedings of International Symposium on Blue Laser and Light Emitting Diodes.* Yoshikawa, A.; Kishino, K.; Kobayashi, M.; Yasuda, T., Eds.; Chiba University Press: Japan, 1996; p 119.
- [27] A. Chatterjee; T. Iwasaki; H. Hayashi; T. Ebina; K. Torii *J. Mol. Catal. A: Chemical.* **1998**, *136*, 195-202.
-

-
- [28] Peter V. Liddicoat; Xiao-Zhou Liao; Yonghao Zhao; Yuntian Zhu; Maxim Y. Murashkin; Enrique J. Lavernia; Ruslan Z. Valiev; Simon P. Ringer. *Nat. Commun.* **2010**, *1*, 1062-1062.
- [29] B. K. Rao; P. Jena. *J. Chem. Phys.* **1999**, *111*, 1890-1905.
- [30] Ahlrichs Reinhart; Elliott Simon D. *Phys. Chem. Chem. Phys.* **1999**, *1*, 13-21.
- [31] D. M. Cox; D. J. Trevor; R. L. Whetten; A. Kaldor. *J. Phys. Chem.* **1988**, *92*, 421-429.
- [32] K.J. Taylor; C.L. Pettiette; M.J. Craycraft; O. Chesnovsky; R.E. Smalley. *Chem. Phys. Lett.* **1988**, *152*, 347-352.
- [33] Grant E. Johnson; Roland Mitrić; Vlasta Bonačić-Koutecký; A.W. Castleman Jr. *Chem. Phys. Lett.* **2009**, *475*, 1-9.
- [34] Z.J. Li, J.H. Li. *Solid State Commun.* **2009**, *149*, 375-378.
- [35] J. Moc *J. Eur. Phys. J. D.* **2007**, *45*, 247-252.
- [36] Jarrold M. F.; Bower J. E. *J. Am. Chem. Soc.* **1988**, *110*, 70-78.
- [37] Cui L.-Feng.; Li X.; Wang L.Sheng. *J. Chem. Phys.* **2006**, *124*, 54308-54313.
- [38] W. H. Woodward; Nicole Eyt; Nicholas S. Shuman; Jordan C. Smith; Albert A. Viggiano; A. W. Castleman Jr. *J. Phys. Chem. C.* **2011**, *115*, 99039908.
- [39] Jennifer Schuttlefield; Gayan Rubasinghege; Mohamed El-Maazawi; Jason Bone; Vicki H. Grassian. *J. Am. Chem. Soc.* **2008**, *130*, 1221012211.
- [40] Brian T. Cooper, Denise Parent, Steven W. Buckner. *Chem. Phys. Lett.* **1998**, *284*, 401406.
- [41] D.H. Paik; N.J. Kim; A.H. Zewail. *J. Chem. Phys.* **2001**, *111*, 612-617.
-

-
- [42] R. E. Leuchtner; A. C. Harms; A. W. Castleman. *J. Chem. Phys.* **1989**, *91*, 2753-2755.
- [43] Denis E. Bergeron; A. Welford Castleman Jr.; Naiche O. Jones; Shiv N. Khanna. *Chem.Phys. Lett.* **2005**, *415*, 230-233.
- [44] Arthur C. Reber; Patrick J. Roach; W.Hunter Woodward; Shiv N. Khanna; A. W. Castleman Jr. *J. Phys. Chem. A.* **2012**, *116*, 8085-8091.
- [45] Baopeng Cao; Anne K. Starace; Oscar H. Judd; Indrani Bhattacharyya; Martin F. Jarrold; José M. López; Andrés Aguado. *J. Am. Chem. Soc.* **2010**, *132*, 12906-12918.
- [46] Romanowski, Z.; Krukowski, S.; Grzegory, I.; Porowski, S. *J. Chem. Phys.* **2001**, *114*, 6353-6366.
- [47] Bhakti S. Kulkarni; Sailaja Krishnamurty; Sourav Pal. *J. Phys. Chem. C.* **2011**, *115*, 14615-14623.
- [48] Patrick J. Roach; W. Hunter Woodward; A. W. Castleman Jr.; Arthur C. Reber; Shiv N. Khanna. *Science.* **2009**, *323*, 492-495.
- [49] Arthur C. Reber; S. N. Khanna. *J. Phys. Chem. A.* **2010**, *114*, 60716081.
- [50] David J. Henry; Irene Yarovsky. *J. Phys. Chem. A.* **2009**, *113*, 2565-2571.
- [51] W.Mou.; S.Ohmura.; A.Hemeryck.; F.Shimojo.; Rajiv K. Kalia.; A.Nakano.; P.Vashishta. *AIP Advances.* **2011**, *1*, 42149-42162.
- [52] Sonia Álvarez-Barcia; Jesús R. Flores. *J. Phys. Chem. A.* **2012**, *116*, 8040-8050.
- [53] Duca Dario; Giuffrida Sergio; Fontana Alberta; Varga Zsuzsanna. *Nanocatalysis, Ed. Murzin, Dmitry Yu.* **2006**, 177-229.

-
- [54] Abbet S.; Ferrari A. M.; Giordano L.; Pacchioni G.; Häkkinen H.; Landman U.; Heiz U. *Surface Science*. **2002**, *514*, 249-255.
- [55] Parr, R. G.; Yang, W. *J. Am. Chem. Soc.* **1984**, *106*, 4049-4051.
- [56] Hohenberg, P.; Kohn, W. *Phys. Rev.* **1964**, *136*, B864-B871.
- [57] Perdew John P.; Parr Robert G.; Levy Mel; Balduz Jose L. Jr. *Phys. Rev. Lett.* **1982**, *49*, 1691-1695.
- [58] Zhang, Y.; Yang, W. *Theor. Chem. Acc.* **2000**, *103*, 346-348.
- [59] De Proft, F.; Amira, S.; Choho, K.; Geerlings, P. *J. Phys. Chem.* **1994**, *98*, 5227-5233.
- [60] Yang, W.; Mortier, W. *J. Am. Chem. Soc.* **1986**, *108*, 5708-5711.
- [61] Roy, R. K.; Krishnamurti, S.; Geerlings, P.; Pal, S. *J. Phys. Chem. A*. **1998**, *102*, 3746-3755.
- [62] Kohn W; Sham L. J. *Phys. Rev.* **1965**, *137*, A1697-A1705.
- [63] Kohn W; Sham L.J. *Phys. Rev.* **1965**, *140*, A1133-A1138.
- [64] **Gaussian 09, Revision A.1**, M. J. Frisch GWT; H. B. Schlegel; G. E. Scuseria; M. A. Robb; J.R. Cheeseman; G. Scalmani; V. Barone; B. Mennucci; G. A. Petersson; H. Nakatsuji *et al.* **2009**. Gaussian, Inc, Wallingford CT.
- [65] Roy R. K.; Proft F. de; Geerlings P. *J. Phys. Chem. A*. **1998** *102* 7035-7040.
- [66] Rick A. Kendall; Thom H. Dunning; Robert J. Harrison. *J. Chem. Phys.* **1992**, *96*, 6796-6807.
- [67] Kirk A. Peterson; Thom H. Dunning. *J. Chem. Phys.* **2002**, *117*, 10548-10561.
- [68] Axel D. Becke. *J. Chem. Phys.* **1993**, *98*, 5648-5653.
-

-
- [69] Stephens P. J.; Devlin F. J.; Chabalowski C. F.; Frisch M. J. *J. Phys. Chem.* **1994**, *98*, 11623-11627.
- [70] Chengteh Lee; Weitao Yang; Robert G. Parr. *J. Phys. Rev.B.* **1988**, *37*, 785-789.
- [71] Perdew J. P.; Chevary J. A.; Vosko S. H.; Jackson K. A.; Pederson M. R.; Singh D. J.; Fiolhas C. *J. Phys. Rev.B.* **1992**, *46*, 6671-6687.
- [72] Magdolna Hargittai; Balazs Reffy; Maria Kolonits. *J. Phys. Chem. A.* **2006**, *110*, 3770-3777.
- [73] Brian G. Willis; Klavs F. Jensen. *J. Phys. Chem. A.* **1998**, *102*, 2613-2623.
- [74] Li–juan Fu; Lin Jin; Chang–bin Shao; Yi–hong Ding. *Inorg. Chem.* **2010**, *49*, 5276-5284.
- [75] Hirshfeld F. L. *Theor. Chim. Acta.* **1977**, *44*, 129-138
- [76] Himadri Sekhar De; Sailaja Krishnamurty; Sourav Pal. *J. Phys. Chem. C.* **2010**, *114*, 6690-6703.

Dinitrogen Activation by Silicon and Phosphorus Doped Aluminum Clusters

N₂ reduction is crucial for life and very few catalysts are currently available to carry out this process at ambient temperature and pressure. In the present work, density functional theory based calculations reveal doped aluminum clusters to be highly reactive towards molecular nitrogen and hence are prospective materials for its activation at low temperatures. Calculations on silicon and phosphorus doped aluminum clusters with 5–8 atoms demonstrate an enhanced N₂ activation with respect to their pristine ground state and high energy counterparts. This increased efficiency of N₂ activation by doped ground state Al clusters is corroborated by an increment of the N≡N bond length, red shift in N≡N bond stretching frequency and adsorption energy (E_{ad}). Ab initio molecular dynamical simulations demonstrate consequential efficiency of doped clusters towards dinitrogen activation at finite temperature. The ability of doped clusters towards activation of molecular nitrogen is site and shape sensitive. In short, this theoretical study highlights the critical role of doping foreign impurities for future endeavors in the design of a cost-effective, and efficient catalysts for N₂ activation at ambient temperatures. This observation may spur further studies in the field of aluminum nanocatalysis by doping silicon and phosphorus atom in aluminum clusters.

5.1 Introduction

Since the first discovery of a dinitrogen complex $[\text{Ru}(\text{NH}_3)_5\text{N}_2]^{2+}$ in 1965, many experimental and theoretical groups have attempted to study dinitrogen activation on various systems[1–10]. The activation of N_2 (nitrogen fixation) is tremendously challenging due to its large bond dissociation energy (9.79 eV), HOMO/LUMO energy gap (22.90 eV) and high electron affinity (1.80 eV). Moreover, N_2 has a large ionization potential (15.00 eV) and does not donate electrons either. Hence, cleaving of N_2 bond to produce NO_x demands high temperature and particularly, occurs in a flash of lightning and as a side product of combustion. The conversion of N_2 into NH_3 is a basic process for life as fixed nitrogen is essential for the synthesis of nucleic acids and proteins. The catalytic NH_3 formation from N_2 is an important industrial process and also requires N_2 bond activation. The most productive method remains the Haber–Bosch process, which requires both high pressure and temperature (150 to 350 atm and 350°C to 550°C).[11]

In this context, N_2 activation on metal clusters is an emerging area as it offers a possibility of lower pressure and working temperature.[12–29] Fielicke and co-workers have demonstrated N_2 activation on neutral ruthenium clusters with 5 to 16 atoms.[30] They observed a red shift of the $\text{N}\equiv\text{N}$ bond stretch up to 1300 cm^{-1} and concluded that the activation of N_2 is highly structure sensitive and molecular binding is a major channel for N_2 adsorption on Ru surfaces. With the help of laser spectroscopic measurements, Mankelevich *et al.* have produced vibrationally excited N_2 on the heated tungsten surface.[31] Theoretically, very recently, Roy *et al.*[32] have modeled the dinitrogen activation by solid Li_n ($n = 2, 4, 6, \text{ and } 8$) clusters with a red shift of the $\text{N}\equiv\text{N}$ bond stretching frequency up to 810 cm^{-1} . They found that Li_8 is the smallest cluster, able to cleave the $\text{N}\equiv\text{N}$ bond of the N_2 molecule in a highly exothermic process. However, Li being the lightest metal, solid Li clusters display properties such as a unusual spin state,[33] structural fluxionality and complicated dynamics.[34]

Among various metal clusters, it is seen that aluminum clusters are highly promising catalysts for ammonia formation from N_2 and H_2 . [35–37] In one of the first experimental works by Jarrold and co-workers, it is demonstrated that when a Al_{100}^+ cluster melts, the activation barrier towards N_2 molecule decreases by nearly 1 eV. [37] This work is followed by a more detailed experimental and theoretical study by the same research group on $Al_{44}^{+/-}$ where it is seen that threshold energies for N_2 decrease by 1 eV after the cluster melts. [35] In other words, the cluster reactivity is seen to increase on melting due to the volume change and atomic disorder. At 600K, the N_2 embeds into the cluster with an average $N\equiv N$ bond increment up to 1.65 Å. This essentially means that $Al_{44}^{+/-}$ is one of the most reactive clusters towards N_2 molecule.

Theoretically, N_2 adsorption on Al clusters has been studied by few groups, such as Romanowski *et al.* [38] and Pal and co-workers. [39] Important conclusions of the above studies are: (i) Geometry and electronic structure of excited Al clusters play an important role in N_2 dissociation. (ii) Dissociative chemisorption of N_2 is an exothermic reaction and, (iii) Catalytic ammonia formation on Al clusters turns out to be a shape and size sensitive reaction. In another work, Boo *et al.* [36] have investigated structure and energetics of low-lying AlN_3 , Al_3N , and Al_2N_2 . Their results (MP2/cc-pVDZ level) show that the $N\equiv N$ bond length elongation is about 1.139 Å with respect to its gas phase value of 1.098 Å. In short, pristine aluminum clusters which show catalytic activity towards N_2 adsorption are high energy conformations (Excited State Conformations) in different sizes which are obtained after heating the Ground State (GS) conformation. Hence, it is a very natural demand to synthesize stable and catalytically active cluster in ground state.

Doping is known to be an excellent way to enhance the catalytic properties of pure clusters. [40–44] It is now possible to dope quantum dots with an exact, stoichiometric number of dopant and that such control of the chemical structure is necessary to develop future functional materials. [45, 46] Doping significantly affects charge localization within the clusters and hence it is an elegant way of tuning the electronic environment

of atomic clusters. Doped aluminum clusters are in particular very promising candidates for catalytic applications. In this respect, Khanna and co-workers.[47] reported an interesting study on structure, stability and reactivity of magnesium doped aluminum clusters towards oxygen. Their results showed that Al_nMg_m^- ($4 \leq n + m \leq 15; 0 \leq m \leq 3$) clusters activate oxygen and HOMO–LUMO energy gap controls their reactivity with O_2 . Doping of copper in aluminum cluster (Al_nCu^- ; $n= 11–34$) has also been studied by the same group.[48] In another work, Jiang *et al.* indicated that the mixed Al–B clusters exhibit peculiar aromatic behaviors.[49] Bergeron *et al.* reported that the Al_{13}I_2 cluster behaves chemically like the triiodide ion, and in terms of stability, Al_{13}I_x clusters are exceptionally stable for even number of I atoms, while Al_{14}I_x exhibits stability for odd number of I atoms.[50, 51] Kurkina *et al.* found that the Fe, Co, and Ni impurities may be magnetic or non magnetic depending on the size of the Al_n cluster.[52] Yoshiyuki and co-workers have reported the stability of silicon doped Al_{13} , Al_{19} and Al_{21} using *ab initio* molecular–dynamics method.[53] Apart from the above mentioned studies, the effect of doping on the reactivity and catalytic activity of aluminum clusters remains largely unexplored.

In this paper, we set out to investigate the dinitrogen activation using silicon and phosphorus doped aluminum clusters as catalyst. It is reported earlier that small–sized Al clusters with 2 to 50 atoms are catalytically active and importantly, their behavior is seen to be size and shape sensitive, making them as attractive candidate in nanocatalysis.[54–56] Hence, we have chosen Al clusters with 5–8 atoms. The reasons for considering silicon and phosphorus as dopant in the aluminum clusters are:

- (i) to design cost effective catalyst and
- (ii) substitutional doping of Si and P atom in Al clusters is highly exothermic,[57] indicating higher stability of doped cluster as compared to its pristine analogue.

Various sites in a GS conformations are doped by either Si or P atom. Dinitrogen molecule activation by the doped conformations is compared with the catalytic activity of the pristine GS conformation as well as two representative Excited State (ES) pristine conformations towards N_2 molecule. *Ab initio* molecular dynamical studies are also carried out at two representative temperatures (300K and 450K) on cluster– N_2 complexes (Al_8) to validate the results obtained by geometry optimizations.

5.2 Computational Details

The ground state (GS) and Excited State (ES) conformations for Al clusters with 5–8 atoms are well reported in the literature.[58–60] We have taken 6 representative conformations for each cluster size (5–8 atoms) and optimized them. Optimizations revealed that our ground state for Al₅, Al₆, Al₇, and Al₈ is consistent with the ones reported in the literature. We have chosen the GS and two ES in each cluster size for further study. The ES are chosen such that one of ES lies within 1 eV above GS and the second ES lies between 1 eV–2 eV above the ground state. The aim is to sample ES lying in different energy levels above the GS geometry. In order, to evaluate the effect of doping on the catalytic activity, only the GS Al clusters are considered with 5–8 atoms. Various atomic positions in each GS conformation are replaced with the either Si or P atoms in order to have a doped Al conformation. As consequence, at least 4–5 doped conformations are obtained for each GS aluminum cluster. N₂ molecule is adsorbed in linear and parallel modes on various atomic sites of a given cluster (GS, ES and doped cluster). Doped clusters with highest adsorption energies towards N₂ molecule and highest activation towards N₂ molecule are highlighted during the discussion. In order to facilitate easy understanding, we highlighted various definitions and abbreviations used the later part of the text. GS refers to the ground state conformation of Al cluster of a given size. ES refers to the excited state (high energy) conformations of Al cluster in a given size. Doped–GS refers to the ground state conformation of Al where one of the atoms has been substituted by either Si or P atom.

The electronic structure of all the clusters and their corresponding N₂ complexes is investigated using first–principles molecular orbital approach wherein the wave function is expressed as a linear combination of atomic orbitals located on the atomic sites. All calculations are performed using deMon.2.2.6 code.[61] All the geometries are optimized using the 1996 gradient–corrected correlation functional of Perdew, Burke and Ernzerhof (PBE).[62] Aluminum, silicon, phosphorus and nitrogen atoms are described using a DZVP basis set.[63] The auxiliary density is expanded in primitive Hermite Gaussian function by using the GEN–A2 auxiliary basis set.[64] Harmonic vibrational frequencies are computed for the optimized geometries and all the frequencies are found to be positive, confirming the structure to be a minima. Only the lowest spin state is considered for pristine as well as doped clusters.

Ab initio Born–Oppenheimer Molecular Dynamical (BOMD) simulations are performed with the most stable cluster–N₂ complex at 300K and 450K on clusters with 8 atoms. Auxiliary density functional theory is employed for the BOMD simulations.[65] At each temperature, the complex is equilibrated for a time period of 10 ps followed by a simulation time of 40 ps. The temperature of the complex is maintained using the Berendsens thermostat (= 0.5 ps) in an NVT ensemble.[66] It is well known that Berendsen thermostat does not produce an accurate NVT phase space distribution.[67] However, the aim of the present work is to evaluate the extent of N–N bond stretch at finite temperatures rather than have an accurate NVT space distribution. The nuclear positions are updated using velocity Verlet algorithm with a time step of 1 fs. We hold the total angular momentum of the cluster to zero, thereby suppressing the cluster rotation.

Adsorption energy of cluster–N₂ complex is calculated as,

$$E_{AB}^{ad} = -(E_{AB} - E_A - E_B)$$

where E_A and E_B are the energies of the cluster and N₂ molecule, respectively. E_{AB} is the energy of the cluster–N₂ complex. Further, we have taken care of basis set superposition error (BSSE) correction to calculate E_{ad} by conventional method.

5.3 Results and Discussions

We begin our discussion with note on the ground state (viz. Al₈¹) and two characteristic high energy conformations (viz. Al₈^{2†} and Al₈^{3†}) of pristine Al₈ cluster (see Table 1). Al–Al bond lengths in isolated clusters and within N₂ complexes, Al–N bond lengths in Al₈–N₂ complexes with their adsorption energies, E_{ad} is also given in the same Table. The high energy structures chosen, differ nearly by 0.214 eV and 1.90 eV in energy respectively with respect to their ground state analogue. The bond length and stretching frequency of isolated N₂ molecule is 1.121 Å and 2333 cm⁻¹ respectively. On adsorbing N₂ molecule in parallel mode on Al₈¹ cluster, the N≡N bond is activated to 1.318 Å with a red shift of the N≡N stretching frequency to 1235 cm⁻¹. The Al–N bond distances vary from 1.903 Å to 2.998 Å. The E_{ad} of N₂ on Al₈¹ is 1.821 eV. Excited state conformations result in higher N≡N bond elongation as compared to ground state conformation. The N≡N bond enhancement in Al₈^{2†} and Al₈^{3†} is 1.353 Å and 1.348 Å respectively and corresponding red shift of stretching frequencies are ~1169 cm⁻¹ and ~1154

cm⁻¹ respectively. As compared to GS conformation, excited state (ES) conformations show enhanced binding, towards dinitrogen with an E_{ad} of 2.865 eV and 1.881 eV respectively. This is further characterized by shorter Al–N bond lengths in ES–N₂ complexes as compared to GS–N₂ complex. In Al₈^{2†}–N₂ and Al₈^{3†}–N₂ complexes the Al–N bond lengths lie between 1.838 Å to 2.325 Å and 1.918 Å to 2.344 Å respectively. Thus, it prevails that ES pristine conformations act as a better catalysts for the N≡N bond activation as compared to GS pristine conformations.

Tables 2 and 3 give trends of N₂ adsorption on Si and P doped GS–Al₈ conformations. Si and P atoms are doped at A, B, C sites of Al₈¹. Among the three different sites, cluster with Si doped in site C (Al₇¹Si_C) and P doped in site B (Al₇¹P_B) are the most effective catalysts as they activate the N≡N bond by 0.080 Å and 0.030 Å larger as compared to the pristine Al₈¹ conformation (see Table 1). Further, the activation of N≡N bond by Al₇¹Si_C is also larger as compared to the activation by Al₈^{2†} (0.045 Å) and Al₈^{3†} (0.048 Å) clusters respectively. The significant activation of the N₂ molecule is also corroborated by an appreciable red shift in N≡N stretching frequency (Al₇¹Si_C–N₂ and Al₇¹P_B–N₂ complexes show $\sim 220\text{cm}^{-1}$ and $\sim 55\text{cm}^{-1}$) as compared to ES–N₂ complexes. Such elongated bonds with a red shift in IR stretching frequency have higher potential for activation as seen in the literature.[21, 32, 68, 69] Notably, in doped clusters the Al–N bond lengths are shorter than in pristine counterpart, indicating a strong adsorption of N₂. In particular, the Al–N bond lengths of Al₇¹Si_C–N₂ and Al₇¹P_B–N₂ complexes lie between 1.856 Å to 2.180 Å and 1.830 Å to 2.422 Å respectively. The Si–N bond and P–N bond in Al₇¹Si_C–N₂ and Al₇¹P_B–N₂ complexes are 1.848 Å and 1.849 Å respectively. Strong binding of N₂ with doped clusters as compared to its pristine analogue is further characterized by high adsorption energy (2.517 eV and 2.218 eV respectively) in Al₇¹Si_C and Al₇¹P_B clusters. In short, we observe a significant enhancement in catalytic efficiency of GS–Al cluster after doping it with a single Si or P atom. However, doping the other two sites (sites A and B for Si and sites A and C for P) does not result in the same activation of N₂ molecule. In Al₇¹Si_A–N₂ complex, the N≡N bond elongates to 1.300 Å and stretching frequency is 1265 cm⁻¹. N₂ adsorbs in parallel mode on Al₇¹Si_A–N₂ with an E_{ad} of 1.026 eV. Another cluster with Si dopant, Al₇¹Si_B significantly also activates dinitrogen molecule (N≡=1.380 Å and $\nu_{N\equiv N} = 1086\text{cm}^{-1}$). This doped cluster–N₂ complex has the highest adsorption energy among the doped clusters. On the other hand, other P doped clusters, Al₇¹P_A and Al₇¹P_C activate the N≡N bond to 1.206 Å and 1.262 Å respectively, with

E_{ad} of 2.108 eV and 2.218 eV respectively. The stretching frequencies are 1737 cm^{-1} and 1180 cm^{-1} respectively as shown in Table 3. However, during absorption of N_2 molecule, pristine $\text{Al}_8^{2\dagger}$ and $\text{Al}_8^{3\dagger}$, clusters with Si-dopant (Al_7^1Si_C), and P-dopant (Al_7^1P_A , Al_7^1P_B and Al_7^1P_C) undergo structural fluctuation.

Ab initio BOMD simulations are performed to understand the cluster stability and activation barriers of N_2 adsorption in aluminum clusters at finite temperature. Simulations have been performed at two different temperatures, 300K and 450K on pristine $\text{Al}_8^1\text{-N}_2$ complex and catalytically efficient doped clusters ($\text{Al}_7^1\text{Si}_C\text{-N}_2$ and $\text{Al}_7^1\text{P}_B\text{-N}_2$ complexes). Table 4 reports the $\text{N}\equiv\text{N}$ bond length fluctuation in $\text{Al}_8^1\text{-N}_2$, $\text{Al}_7^1\text{Si}_C\text{-N}_2$ and $\text{Al}_7^1\text{P}_B\text{-N}_2$ complexes at the two temperatures. At 300K, in $\text{Al}_8^1\text{-N}_2$ complex, the average $\text{N}\equiv\text{N}$ bond length is 1.361 \AA with a fluctuation of $\pm 0.2\text{ \AA}$. On the other hand, in $\text{Al}_7^1\text{Si}_C\text{-N}_2$ and $\text{Al}_7^1\text{P}_B\text{-N}_2$ complexes the $\text{N}\equiv\text{N}$ bond has larger fluctuations. The average $\text{N}\equiv\text{N}$ bond lengths are 1.632 \AA and 1.526 \AA (Fig. 1) with the fluctuation of $\pm 0.4\text{ \AA}$ and $\pm 0.3\text{ \AA}$ respectively. Interestingly, these average $\text{N}\equiv\text{N}$ bond lengths are very close to the ones seen in $\text{Al}_{44}^{+/-}\text{-N}_2$ complexes by Jarrold and co-workers.[35] At 450K, fluctuations are higher and Al_7^1Si_C cluster (cluster with largest potential towards dinitrogen activation as shown in Table 2), cleaves the $\text{N}\equiv\text{N}$ bond. Thus, Si as a dopant in aluminum clusters (in particular, Al_7^1Si_C) generates catalytically sound clusters towards dinitrogen activation.

Molecular orbital (MO) analysis is done to understand the interaction of N_2 with pristine and doped 8 atom clusters qualitatively. All the HOMO-1, HOMO and LUMO pictures are presented in the supporting information. Within the complex, N_2 acts as an electron acceptor while cluster is an electron donor. HOMO-1, HOMO (Table S1) show a considerable overlap between p-orbital of Al and N in $\text{Al}_8^1\text{-N}_2$ complex resulting in a strong Al-N bond. On the other hand, greater molecular orbital overlap is expected in catalytically active doped cluster- N_2 complexes (viz., $\text{Al}_7^1\text{Si}_C\text{-N}_2$ and $\text{Al}_7^1\text{P}_B\text{-N}_2$) as compared to their pristine analogue, $\text{Al}_8^1\text{-N}_2$ complex. Accordingly, it is seen from Table S1 that Si and P doped clusters show a more significant overlap of p orbital of Al and Si (or P) with p orbital of N. Greater overlap in doped complex is in line with the Al-N bond lengths which are shorter in the $\text{Al}_7^1\text{Si}_C\text{-N}_2$ and $\text{Al}_7^1\text{P}_B\text{-N}_2$ complexes as compared to $\text{Al}_8^1\text{-N}_2$ complex (see Tables 1 and 2). In contrast, similar type of MO overlap is absent in the complexes in which fail to generate vibrationally excited N_2 molecule (see Table S2).

Finally, Mulliken charge analysis gives a clear indication of the extent of N₂ activation in different cluster–N₂ complexes. In cluster–N₂ complexes, there is a charge transfer from cluster to the anti bonding orbital of N₂ molecule leading to an elongation of the N≡N bond. A larger charge transfer results in a larger increment of the N≡N bond. The amount of electron transfer from Al₈¹ cluster to N₂ molecule during the complexation is 0.584, resulting increment of the N≡N bond length to 1.318 Å as shown in Table 5. On the other hand, there is a substantial increase of charge transfer in ES–N₂ (Al₈^{2†}–N₂ and Al₈^{3†}–N₂) complexes as compared to GS–N₂ complex. Among the doped clusters, there is a larger charge separation in Al₇¹Si_C–N₂ complex (amount of electron transfer is 0.689) leading to maximum elongation of the N≡N bond length (1.398 Å), yielding potentially efficient Al₇¹Si_C cluster toward N₂ activation. Other cluster–N₂ complexes also show similar trend of N≡N bond elongation with charge separation between cluster and N₂ fragments of cluster–N₂ complex.

Studies on Al₇, Al₆¹Si and Al₆¹P also exhibit similar trends as Al₈, Al₇¹Si and Al₇¹P clusters. The results of seven atoms clusters, pristine GS, Al₇¹ and ES, Al₇^{2†}, and Al₇^{3†} clusters and their N₂ adsorbed complexes are compiled in the Table 6. Relative energies of this chosen ES conformations are 1.884 eV and 1.903 eV, respectively. Ground state conformation (Al₇¹) with the E_{ad} of 1.648 eV, elongates the N≡N bond to 1.353 Å which is also evident from a red shift in the stretching frequency of N≡N bond to 1089 cm⁻¹. As compared to the GS conformation, adsorption on Al₇^{2†} and Al₇^{3†} leads to an additional increment of N≡N bond length by 0.032 Å and 0.055 Å respectively with a larger red shift of N≡N stretching frequencies (975 cm⁻¹ and 916 cm⁻¹ respectively). Moreover, higher energy conformations, Al₇^{2†} and Al₇^{3†}, bind strongly with N₂ (E_{ad} are 1.654 eV and 3.459 eV respectively). Similar to Al₈ clusters, doping of single Si and P atom on the pristine Al₇ cluster yield more catalytically efficient clusters towards N₂ activation as shown in Tables 7 and 8. In particular, Si and P atoms as a dopant on site B, among the three sites, viz., A, B, and C (of Al₇ GS) substantially activate the N≡N to 1.413 Å and 1.483 Å respectively. The red shift of N≡N stretching frequency in Al₆¹Si_B–N₂ and Al₆¹P_B–N₂ complexes are also (~133 cm⁻¹ and ~168 cm⁻¹ respectively) larger than their pristine counterpart. The E_{ad} of doped clusters with N₂ are 3.404 eV and 3.836 eV respectively. Interestingly, doping on the other two sites (viz. Al₆¹Si_A, Al₆¹Si_C, Al₆¹P_A and Al₆¹P_B) also generates vibrationally excited N₂ molecule though to a lesser extent as compared to Al₆¹Si_B and Al₆¹P_B.

Catalytic behavior of Al₆ clusters and the role of doping on the same are abstracted in Tables 9, 10 and 11. As case of other clusters we have considered ground state (viz. Al₆¹) and two high energy conformations, Al₆^{2†} and Al₆^{3†}. N₂ adsorbs only in a linear mode on Al₆ GS conformation. Due to linear mode of adsorption, N₂ binds weakly as compared to Al₈¹, Al₇¹ and Al₅¹ clusters. Contrastingly, ES conformations with less symmetry have stronger affinity to bind with dinitrogen. The N≡ bond activation and stretching frequencies in Al₆^{2†}-N₂ and Al₆^{3†}-N₂ complexes are 1.388 Å, 953 cm⁻¹ and 1.394 Å, 922 cm⁻¹ respectively. Strong adsorption of N₂ is confirmed by large E_{ad} which is 3.464 eV and -4.207 eV, respectively. Doping a single Si or P atoms in GS Al₆¹, Al₅¹Si_C and Al₅¹P_B show higher catalytic potential than all pristine analogues. Both the clusters adsorb N₂ in parallel mode with a red shift of stretching frequencies viz., ~593 cm⁻¹ and ~706 cm⁻¹. In summary, efficiency to produce vibrationally excited N₂ among 6 atom clusters is as follows: Al₆^{3†} > Al₆^{2†} > Al₅¹P_B > Al₅¹P_C > Al₅¹Si_C > Al₅¹P_A > Al₅¹Si_A > Al₆¹ > Al₅¹Si_B.

Tables 12, 13 and 14 describe the catalytic efficiency of Al₅ clusters towards N₂ activation. On parallel mode of adsorption, the N≡N bond is elongated in Al₅¹-N₂ complex by 0.084 Å and red shift of N≡N bond stretching frequency is ~674 cm⁻¹ as compared to isolated N₂ molecule. On the other hand, as expected, other two high energy(ES) conformations (viz. Al₅^{2†} and Al₅^{3†}), show larger potential to activate N₂ molecule as clearly seen from the N≡N bond length elongation and red shift of N-N stretching frequency (see Table 12). Additionally, N₂ E_{ad} on Al₅^{3†} is reasonably higher (E_{ad} is 2.130 eV). In this context, Al₄¹Si_C and Al₄¹P_B are the most effective doped clusters within 5 atom clusters. Both the clusters have tendency to adsorb N₂ on parallel mode leading to a stable cluster-N₂ adduct. The N≡N bond elongation, red shift of the N≡N bond stretching frequency and the adsorption energy on both the doped clusters are 1.248 Å, 1408 cm⁻¹, 1.143 eV and 1.183 Å, 1761 cm⁻¹, 1.183 eV, respectively. This once again reveals that a single Si and P atom doping significantly enhances catalytic potential of a pristine conformation towards N₂ activation, the most challenging step for NH₃ synthesis. However, doping on site A (Al₄¹Si_A and Al₄¹P_A) does not generate a catalytically sound cluster as site B and site C do. The possible reason could be the linear mode of adsorption of N₂ in this site, resulting weak interaction between cluster and N₂ (0.369 eV and 0.016 eV of E_{ad} for Al₄¹Si_A and Al₄¹P_A respectively).

5.4 Conclusions

In conclusion, our combined DFT and BOMD calculations reveal that ground state aluminum clusters when doped with a single Si or P atom are highly reactive and are capable of activating nature's most inert molecule viz., N_2 . Further, this activation of dinitrogen by doped Al clusters is remarkably higher as compared to the pristine Al clusters (ground as well as excited state conformations). N_2 activation and its strong binding towards doped cluster is reflected by an increment of $N\equiv N$ bond length, red shift in $N\equiv N$ bond stretching frequency, increase of $N\equiv N$ bond length fluctuations in N_2 molecule at finite temperatures and moreover adsorption energy of in cluster- N_2 complex. Interestingly, the catalytic activity of doped cluster is site and shape selective. The higher efficiency of doped cluster in conjunction with their preferential activation of the nitrogen molecule once again demonstrates the overwhelmingly important contribution of multi-metallic clusters in the area of nanocatalysis. The only other atomic clusters capable of better N_2 activation among so far reported in literature are Li clusters. However, greater thermal and structural stability of doped Al clusters make them best possible catalysts for N_2 activation among the atomic clusters.

Average of the N-N bond length fluctuations

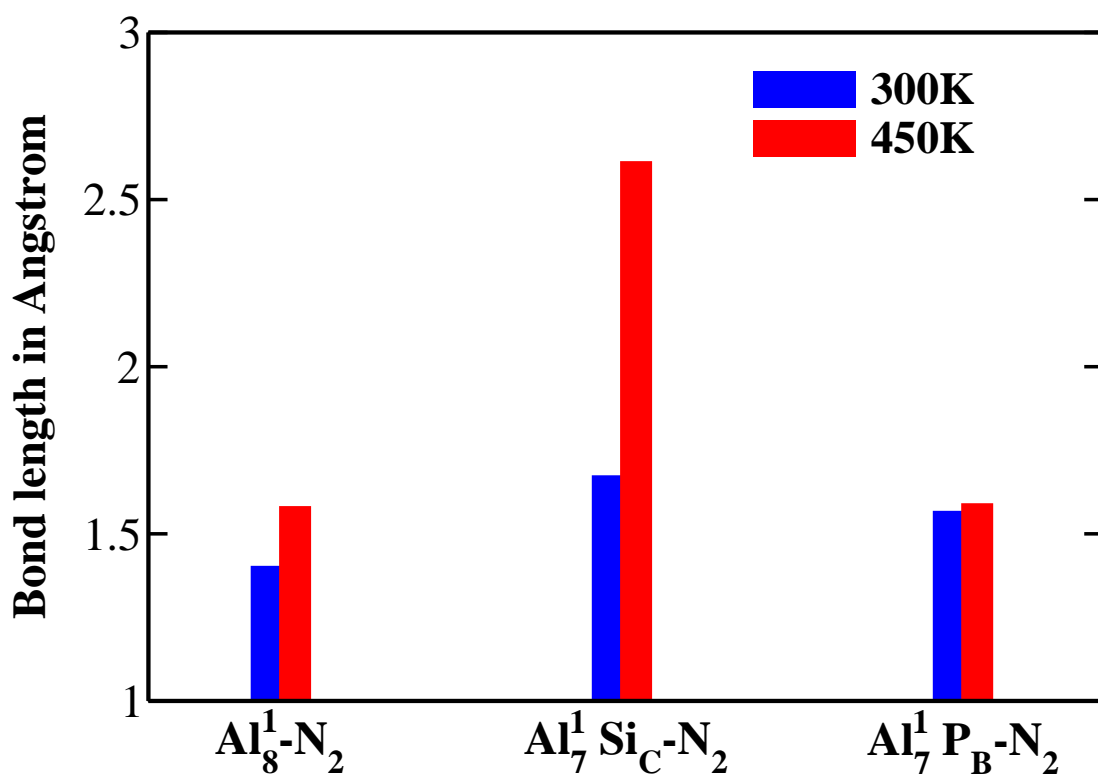


Figure 5.1: Average of the N≡N bond length fluctuations in $Al_8^1-N_2$, $Al_7^1 Si_C^1-N_2$ and $Al_7^1 P_B^1-N_2$ complexes at 300K and 450K.

Table 5.1: Ground and excited state conformations of Al_8 and their corresponding N_2 complexes.

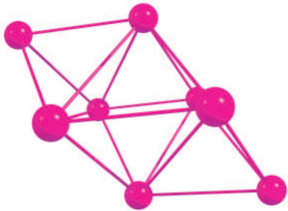
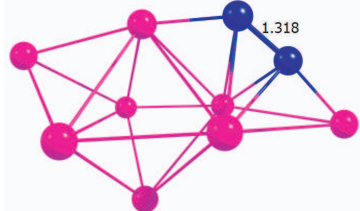
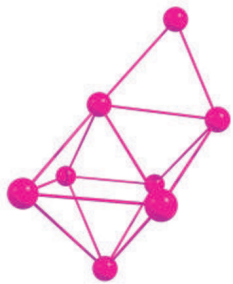
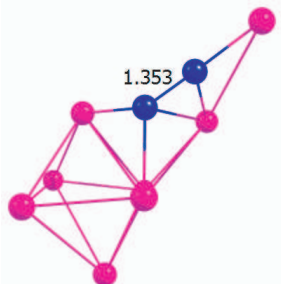
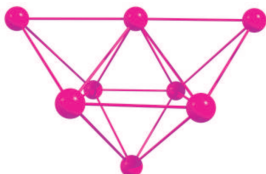
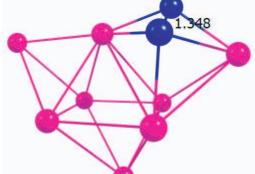

Al_8^1	$\nu_{\text{N}\equiv\text{N}} = 1235 \text{ cm}^{-1}$
	
RE = 0.000 eV Al-Al = 2.542–2.852 Å	$E_{ad} = 1.821 \text{ eV}$ Al-N = 1.903–2.998 Å Al-Al = 2.638–3.336 Å
$\text{Al}_8^{2\ddagger}$	$\nu_{\text{N}\equiv\text{N}} = 1164 \text{ cm}^{-1}$
	
RE = 0.214 eV Al-Al = 2.613–2.891 Å	$E_{ad} = 2.865 \text{ eV}$ Al-N = 1.838–2.325 Å Al-Al = 2.595–2.964 Å
$\text{Al}_8^{3\ddagger}$	$\nu_{\text{N}\equiv\text{N}} = 1179 \text{ cm}^{-1}$
	
RE = 1.902 eV Al-Al = 2.591–2.901 Å	$E_{ad} = 1.881 \text{ eV}$ Al-N = 1.918–2.344 Å Al-Al = 2.591–2.949 Å
	

Table 5.2: Most effective site of Al_7^1Si and Al_7^1P clusters towards N_2 activation.

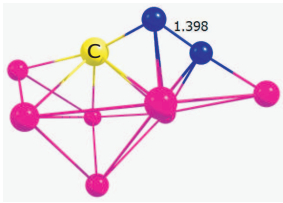
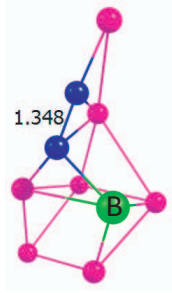

Al_7^1Si_C $\nu_{\text{N}\equiv\text{N}} = 1014 \text{ cm}^{-1}$	Al_7^1P_B $\nu_{\text{N}\equiv\text{N}} = 1180 \text{ cm}^{-1}$
	
$E_{ad} = 2.517 \text{ eV}$ $\text{Al-N} = 1.856\text{--}2.180 \text{ \AA}$ $\text{Si-N} = 1.848 \text{ \AA}$ $\text{Al-Si} = 2.574\text{--}2.594 \text{ \AA}$ $\text{Al-Al} = 2.568\text{--}3.362 \text{ \AA}$	$E_{ad} = 2.218 \text{ eV}$ $\text{Al-N} = 1.830\text{--}2.422 \text{ \AA}$ $\text{P-N} = 1.849 \text{ \AA}$ $\text{Al-P} = 2.448\text{--}2.741 \text{ \AA}$ $\text{Al-Al} = 2.532\text{--}2.953 \text{ \AA}$
	

Table 5.3: Other potential sites for N₂ adsorption on Al₇¹Si and Al₇¹P clusters.

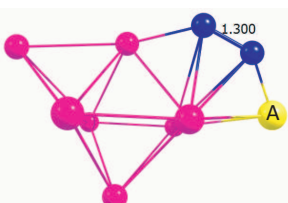
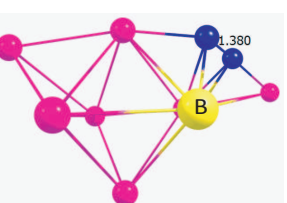
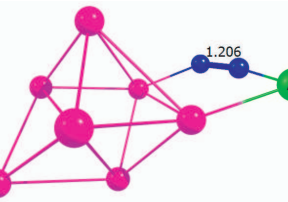
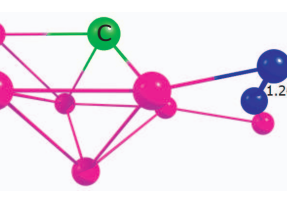
<p>Al₇¹Si_A $\nu_{N\equiv N} = 1265 \text{ cm}^{-1}$</p>	<p>Al₇¹Si_B $\nu_{N\equiv N} = 1086 \text{ cm}^{-1}$</p>
	
<p>$E_{ad} = 1.026 \text{ eV}$ Al-N = 1.921–2.112 Å Si-N = 1.774 Å Al-Si = 2.588–2.690 Å Al-Al = 2.598–2.827 Å</p>	<p>$E_{ad} = 2.652 \text{ eV}$ Al-N = 1.823–2.381 Å Si-N = 1.863 Å Al-Si = 2.504–2.821 Å Al-Al = 2.581–2.934 Å</p>
<p>Al₇¹P_A $\nu_{N\equiv N} = 1737 \text{ cm}^{-1}$</p>	<p>Al₇¹P_C $\nu_{N\equiv N} = 1180 \text{ cm}^{-1}$</p>
	
<p>$E_{ad} = 2.108 \text{ eV}$ Al-N = 2.009 Å P-N = 1.624 Å Al-P = 2.540 Å Al-Al = 2.561–3.084 Å</p>	<p>$E_{ad} = 2.218 \text{ eV}$ Al-N = 1.893–2.242 Å Al-P = 2.430–2.597 Å Al-Al = 2.556–2.973 Å</p>
<p>Al Si P N</p>	

Table 5.4: The N≡N bond length fluctuations in $\text{Al}_8^1\text{-N}_2$, $\text{Al}_7^1\text{Si-N}_2$ and $\text{Al}_7^1\text{P-N}_2$ complexes at 300K and 450K.

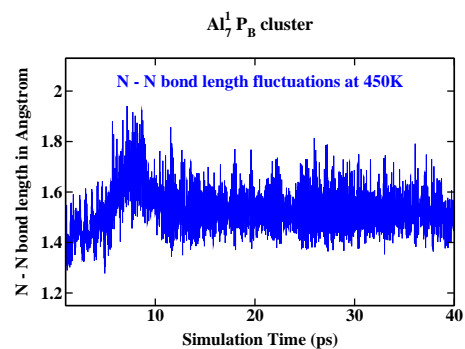
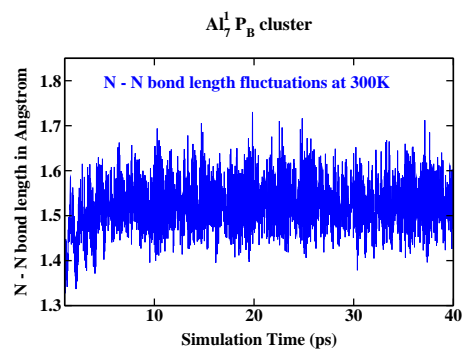
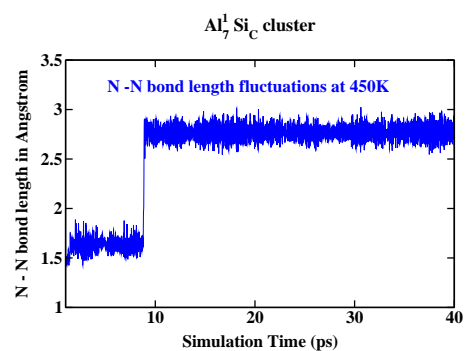
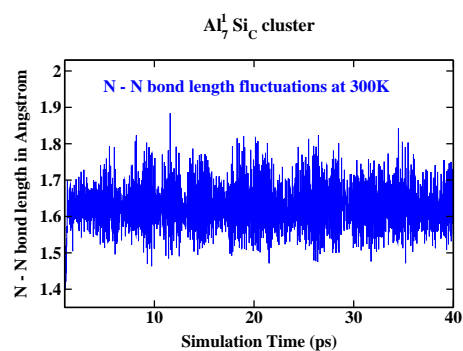
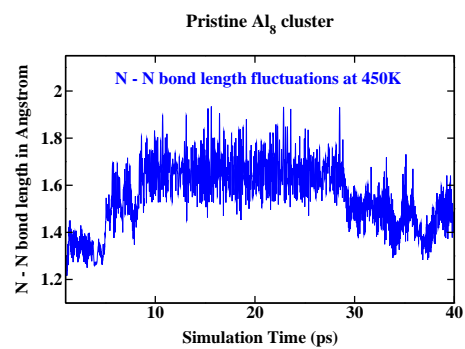
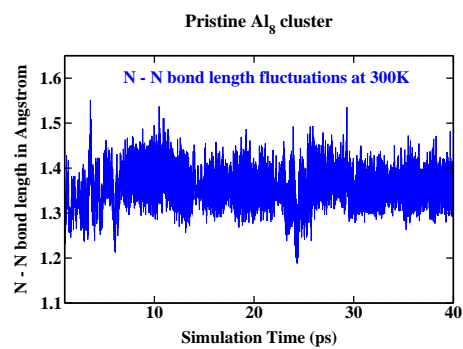


Table 5.5: Mulliken charge analysis of the complexes in ground, excited and doped clusters with N₂ molecule

Cluster-N ₂ complex	Charge on the cluster fragment	Charge on the N ₂ fragment	N≡N bond elongation (Å)
Al ₈ ¹ -N ₂	0.584	-0.584	1.318
Al ₈ ^{2†} -N ₂	0.669	-0.669	1.353
Al ₈ ^{3†} -N ₂	0.657	-0.657	1.348
Al ₇ ¹ Si _A -N ₂	0.481	-0.481	1.300
Al ₇ ¹ Si _B -N ₂	0.664	-0.664	1.380
Al ₇ ¹ Si _C -N ₂	0.689	-0.689	1.398
Al ₇ ¹ P _A -N ₂	0.266	-0.266	1.206
Al ₇ ¹ P _B -N ₂	0.666	-0.666	1.348
Al ₇ ¹ P _C -N ₂	0.441	-0.441	1.262

Table 5.6: Ground and excited state conformations of Al_7 and their corresponding N_2 complexes.

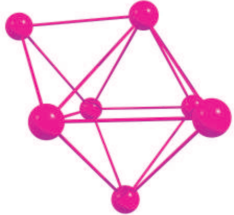
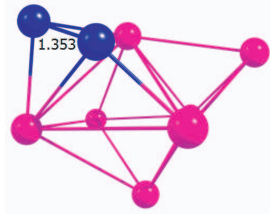
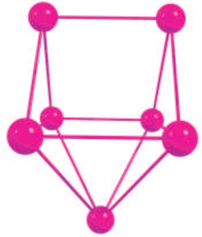
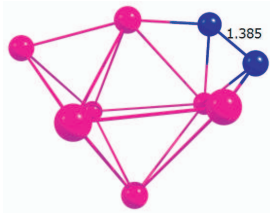
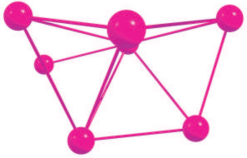
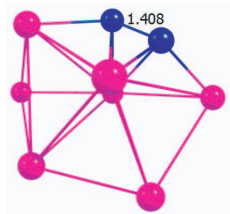

Al_7^1	$\nu_{N-N} = 1089 \text{ cm}^{-1}$
	
RE = 0.000 eV Al-Al = 2.580–2.933 Å	$E_{ad} = 1.648 \text{ eV}$ Al-N = 1.858–2.347 Å Al-Al = 2.614–2.948 Å
$Al_7^{2\dagger}$	$\nu_{N-N} = 975 \text{ cm}^{-1}$
	
RE = 1.884 eV Al-Al = 2.532–2.842 Å	$E_{ad} = 1.654 \text{ eV}$ Al-N = 1.929–2.014 Å Al-Al = 2.565–2.925 Å
$Al_7^{3\dagger}$	$\nu_{N-N} = 916 \text{ cm}^{-1}$
	
RE = 1.903 eV Al-Al = 2.528–2.920 Å	$E_{ad} = 3.459 \text{ eV}$ Al-N = 1.923–1.966 Å Al-Al = 2.592–3.079 Å
	

Table 5.7: Most effective sites of Al_6^1Si and Al_6^1P clusters towards N_2 activation

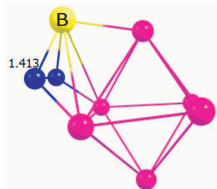
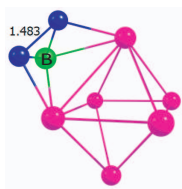

Al_6^1Si_B $\nu_{N-N} = 956 \text{ cm}^{-1}$	Al_6^1P_B $\nu_{N-N} = 921 \text{ cm}^{-1}$
	
$E_{ad} = 3.404 \text{ eV}$ $\text{Al-N} = 1.956\text{--}1.960 \text{ \AA}$ $\text{Si-N} = 1.856\text{--}1.860 \text{ \AA}$ $\text{Al-Al} = 2.535\text{--}3.064 \text{ \AA}$ $\text{Al-Si} = 2.631\text{--}3.287 \text{ \AA}$	$E_{ad} = 3.836 \text{ eV}$ $\text{Al-N} = 1.944\text{--}1.953 \text{ \AA}$ $\text{P-N} = 1.780\text{--}1.798 \text{ \AA}$ $\text{Al-Al} = 2.571\text{--}3.005 \text{ \AA}$ $\text{Al-P} = 2.544\text{--}3.043 \text{ \AA}$
	

Table 5.8: Other potential sites for N₂ adsorption on Al₆¹Si and Al₆¹P clusters.

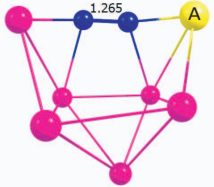
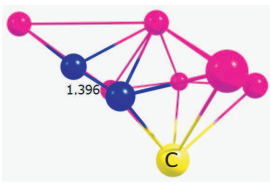
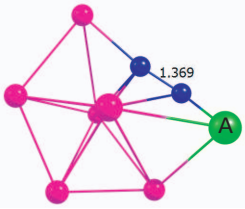
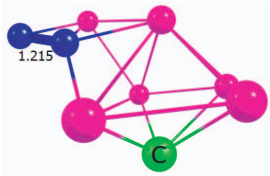

<p>Al₆¹Si_A $\nu_{N-N} = 1396 \text{ cm}^{-1}$</p>  <p>$E_{ad} = 1.611 \text{ eV}$ Al-N = 2.005–2.227 Å Si-N = 1.708 Å Al-Si = 2.591–2.681 Å Al-Al = 2.566–2.791 Å</p>	<p>Al₆¹Si_C $\nu_{N-N} = 1062 \text{ cm}^{-1}$</p>  <p>$E_{ad} = 4.131 \text{ eV}$ Al-N = 1.860–2.269 Å Si-N = 1.905 Å Al-Si = 2.545–2.905 Å Al-Al = 2.696–2.908 Å</p>
<p>Al₆¹P_A $\nu_{N-N} = 1050 \text{ cm}^{-1}$</p>  <p>$E_{ad} = 2.429 \text{ eV}$ Al-N = 1.875–2.522 Å P-N = 1.824 Å Al-P = 2.399–2.401 Å Al-Al = 2.601–2.976 Å</p>	<p>Al₆¹P_C $\nu_{N-N} = 1574 \text{ cm}^{-1}$</p>  <p>$E_{ad} = 0.658 \text{ eV}$ Al-N = 2.009–2.352 Å Al-P = 2.416–2.748 Å Al-Al = 2.599–3.040 Å</p>
	

Table 5.9: Ground and excited state conformations of Al_6 and their corresponding N_2 complexes.

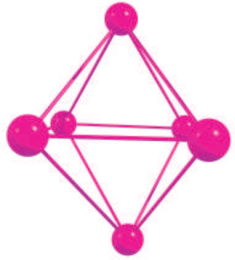
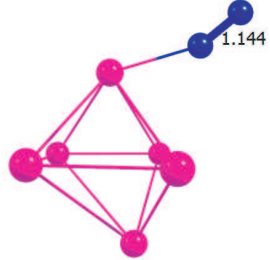
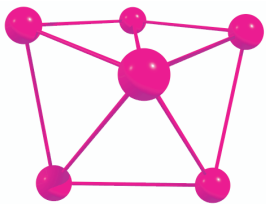
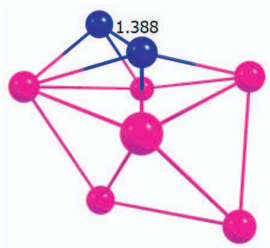
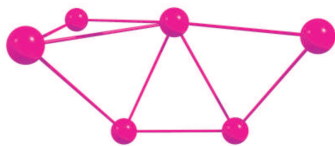
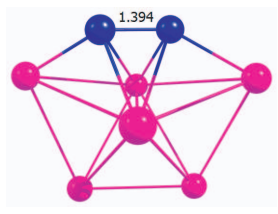
Al_6^1  RE = 0.000 eV Al-Al = 2.575–2.956 Å	$\nu_{\text{N-N}} = 2042 \text{ cm}^{-1}$  $E_{ad} = 0.335 \text{ eV}$ Al-N = 2.044 Å Al-Al = 2.550–3.051 Å
$\text{Al}_6^{2\dagger}$  RE = 0.342 eV Al-Al = 2.543–2.766 Å	$\nu_{\text{N-N}} = 953 \text{ cm}^{-1}$  $E_{ad} = 3.464 \text{ eV}$ Al-N = 1.911–2.326 Å Al-Al = 2.694–2.891 Å
$\text{Al}_6^{3\dagger}$  RE = 0.856 eV Al-Al = 2.512–2.974 Å	$\nu_{\text{N-N}} = 922 \text{ cm}^{-1}$  $E_{ad} = 4.207 \text{ eV}$ Al-N = 1.927–2.275 Å Al-Al = 2.662–2.896 Å



Table 5.10: Most effective site of Al_5^1Si and Al_5^1P clusters towards N_2 activation.

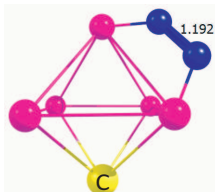
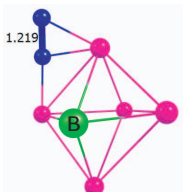

Al_5^1Si_C $\nu_{N-N} = 1739 \text{ cm}^{-1}$	Al_5^1P_B $\nu_{N-N} = 1627 \text{ cm}^{-1}$
	
$E_{ad} = 1.092 \text{ eV}$ $\text{Al-N} = 2.152\text{--}2.171 \text{ \AA}$ $\text{Al-Si} = 2.555\text{--}2.577 \text{ \AA}$ $\text{Al-Al} = 2.693\text{--}2.737 \text{ \AA}$	$E_{ad} = 0.053 \text{ eV}$ $\text{Al-N} = 1.913\text{--}2.100 \text{ \AA}$ $\text{Al-P} = 2.487\text{--}2.568 \text{ \AA}$ $\text{Al-Al} = 2.698\text{--}2.867 \text{ \AA}$
	

Table 5.11: Other potential sites for N₂ absorption on Al₅Si and Al₅P clusters.

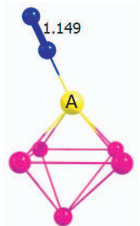
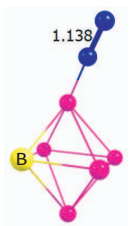
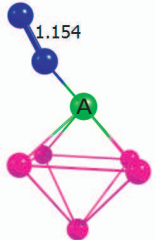
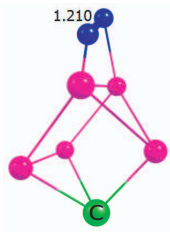
<p>Al₅Si_A $\nu_{N-N} = 2015 \text{ cm}^{-1}$</p>  <p>$E_{ad} = 0.874 \text{ eV}$ Si-N = 1.186 Å Al-Si = 2.551–2.581 Å Al-Al = 2.627–2.965 Å</p>	<p>Al₅Si_B $\nu_{N-N} = 2088 \text{ cm}^{-1}$</p>  <p>$E_{ad} = 0.355 \text{ eV}$ Al-N = 2.025 Å Al-Si = 2.508–2.628 Å Al-Al = 2.623–2.830 Å</p>
<p>Al₅P_A $\nu_{N-N} = 2085 \text{ cm}^{-1}$</p>  <p>$E_{ad} = 0.464 \text{ eV}$ P-N = 1.823 Å Al-P = 2.431–2.475 Å Al-Al = 2.711–2.786 Å</p>	<p>Al₅P_C $\nu_{N-N} = 1656 \text{ cm}^{-1}$</p>  <p>$E_{ad} = 0.617 \text{ eV}$ Al-N = 1.949–2.191 Å Al-P = 2.338–2.453 Å Al-Al = 2.586–2.673 Å</p>
<p>Al Si P N</p>	

Table 5.12: Ground and excited state conformations of Al_5 and their corresponding N_2 complexes.

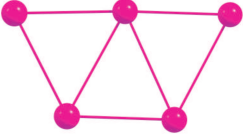
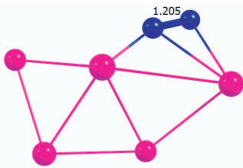
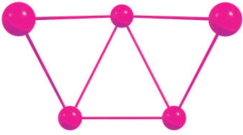
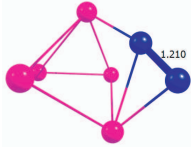

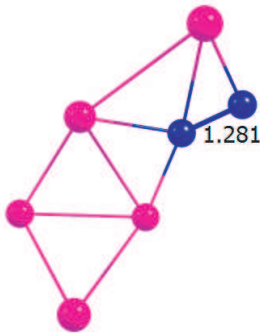

Al_5^1	$\nu_{N-N} = 1659 \text{ cm}^{-1}$
 <p>RE = 0.000 eV Al-Al = 2.483–2.780 Å</p>	 <p>$E_{ad} = 0.600 \text{ eV}$ Al-N = 1.891–2.349 Å Al-Al = 2.610–3.031 Å</p>
$\text{Al}_5^{2\ddagger}$	$\nu_{N-N} = 1610 \text{ cm}^{-1}$
 <p>RE = 0.035 eV Al-Al = 2.489–2.866 Å</p>	 <p>$E_{ad} = 0.715 \text{ eV}$ Al-N = 1.889–2.115 Å Al-Al = 2.678–2.760 Å</p>
$\text{Al}_5^{3\ddagger}$	$\nu_{N-N} = 1255 \text{ cm}^{-1}$
 <p>RE = 1.196 eV Al-Al = 2.441–2.997 Å</p>	 <p>$E_{ad} = 2.130 \text{ eV}$ Al-N = 1.988–2.268 Å Al-Al = 2.593–2.734 Å</p>
	

Table 5.13: Most effective site of Al_4^1Si and Al_4^1P clusters towards N_2 activation.

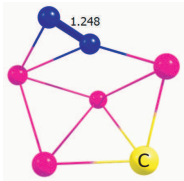
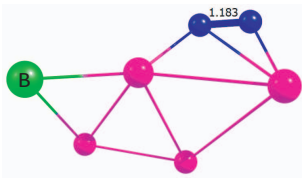

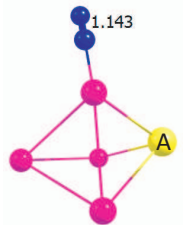
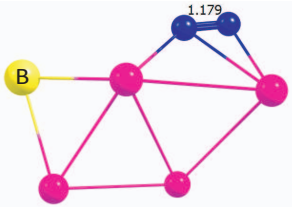
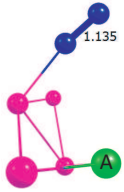
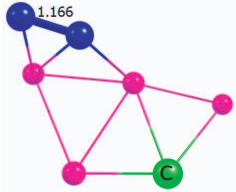
Al_4^1Si_C $\nu_{N-N} = 1408 \text{ cm}^{-1}$	Al_4^1P_B $\nu_{N-N} = 1761 \text{ cm}^{-1}$
	
$E_{ad} = 1.423 \text{ eV}$ $\text{Al-N} = 2.029\text{--}2.125 \text{ \AA}$ $\text{Al-Si} = 2.467\text{--}2.522 \text{ \AA}$ $\text{Al-Al} = 2.658\text{--}2.923 \text{ \AA}$	$E_{ad} = 0.153 \text{ eV}$ $\text{Al-N} = 2.136\text{--}2.281 \text{ \AA}$ $\text{Al-P} = 2.276\text{--}2.278 \text{ \AA}$ $\text{Al-Al} = 2.649\text{--}2.822 \text{ \AA}$
	

Table 5.14: Other potential sites for N₂ absorption on Al₄¹Si and Al₄¹P clusters.

<p>Al₄¹Si_A $\nu_{N-N} = 2061 \text{ cm}^{-1}$</p>  <p>$E_{ad} = 0.369 \text{ eV}$ Al-N = 1.984 Å Al-Si = 2.464–2.492 Å Al-Al = 2.599–2.757 Å</p>	<p>Al₄¹Si_B $\nu_{N-N} = 1798 \text{ cm}^{-1}$</p>  <p>$E_{ad} = 0.073 \text{ eV}$ Al-N = 1.972–2.333 Å Al-Si = 2.389–2.414 Å Al-Al = 2.616–2.885 Å</p>
<p>Al₄¹P_A $\nu_{N-N} = 2114 \text{ cm}^{-1}$</p>  <p>$E_{ad} = 0.016 \text{ eV}$ Al-N = 2.087 Å Al-P = 2.343–2.286 Å Al-Al = 2.620–2.765 Å</p>	<p>Al₄¹P_C $\nu_{N-N} = 1882 \text{ cm}^{-1}$</p>  <p>$E_{ad} = 0.189 \text{ eV}$ Al-N = 2.339–2.373 Å Al-P = 2.305–2.469 Å Al-Al = 2.640–2.879 Å</p>
<p>Al Si P N</p>	

Bibliography

- [1] Evans, W. J.; Lee, S. D.; Rego, B.D.; Perotti, J.M.; Kozimor, S. A.; Moore, E. K.; Ziller, J. *W. J. Am. Chem. Soc.* **2004**, *126*, 14574–14582.
- [2] MacKay, A. B.; Fryzuk, D. M. *Chem. Rev.* **2004**, *104*, 385–402.
- [3] Yandulov, D. V.; Schrock, R. R. *Science* **2003**, *301*, 76–78.
- [4] Rodriguez, M. M.; Bill, E.; Brennessel, W. W.; Holland, P. L. *Science* **2011**, *334*, 780–783.
- [5] Avenier, P.; Taoufik, M.; Lesage, A.; Solans–Monfort, X.; Baudouin, A.; de Mallmann, A.; Veyre, L.; Basset, J. M.; Eisenstein, O.; Emsley, L.; Quadrelli, E. A. *Science* **2007**, *317*, 1056–1060.
- [6] Hendrich, P. M.; Gunderson, W.; Behan, R. K.; Green, M. T.; Mehn, M. P.; Betley, T. A.; Connie, C. Lu.; Peters, J. C. *Proc. Natl. Acad. Sci.* **2006**, *103*, 17107–17112.
- [7] Gambarotta, S.; Jennifer, S. J. *Angew. Chem. Int. Ed.* **2004**, *43*, 5298–5308.
- [8] Himmel, H–J.; Reiher, M. *Angew. Chem. Int. Ed.* **2006**, *45*, 6264–6288.
- [9] Pool, J. A.; Lobkovsky, E.; Chirik, P. J. *Nature* **2003**, *427*, 527–530.
- [10] Knobloch, D. J.; Lobkovsky, E.; Chirik, P. J. *Nature Chemistry* **2010**, *2*, 30–35.
- [11] Smil, V. *The MIT Press: Cambridge, MA* **2001**
- [12] Bolin, J. T.; Ronco, A. E.; Morgan, T. V.; Mortenson, L. E.; Xuong, N. H. *Proc. Natl. Acad. Sci.* **1993**, *90*, 1078–1082.
- [13] Hintz, P.A.; Sowa, M. B.; Ruatta, S. A.; Anderson, S. L. *J. Chem. Phys.* **1991**, *94*, 6446–6453.
- [14] Deng, H.; Hoffmann, R. *Angew. Chem. Int. Ed.* **1993**, *32*, 1062–1065.
- [15] Kim, D. Y.; Stolcic, D.; Fischer, M.; Ganteför, G. *J. Chem. Phys.* **2003**, *119*, 10307–10314.

-
- [16] Berces, A.; Hackett, P. A.; Lian, Li; Mitchell, S. A.; Rayner, D. M. *J. Chem. Phys.* **1998**, *108*, 5476–5490.
- [17] Hidai M. *Coord. Chem. Rev.* **1999**, *185–186*, 99–108.
- [18] Leigh, G. J. *Acc. Chem. Res.* **1992**, *25*, 177–181.
- [19] Eady, R. R. *Chem. Rev.* **1996**, *96*, 3013–3030.
- [20] MacKey, B. A.; Fryzuk, M. D. *Chem. Rev.* **2004**, *104*, 385–401.
- [21] Studt, F.; Tuzek, F. *J. Comput. Chem.* **2006**, *27*, 1278–1291.
- [22] Gambarotta S. *J. Organomet. Chem.* **1995**, *500*, 117–126.
- [23] Gambarotta, S.; Scott, J. *Angew. Chem., Int. Ed.* **2004**, *43*, 5298–5308.
- [24] Schrock, R. R. *Angew. Chem., Int. Ed.* **2008**, *47*, 5512–5522.
- [25] Curley, J. J.; Cook, T. R.; Reece, S. Y.; Müller, P.; and Cummins, C. C. *J. Am. Chem. Soc.* **2008**, *130*, 9394–9405.
- [26] Tanaka, H.; Mori, H.; Seino, H.; Hidai, M.; Mizobe, Y.; and Yoshizawa, K. *J. Am. Chem. Soc.* **2008**, *130*, 9037–9047.
- [27] Fryzuk, M. D. *Acc. Chem. Res.* **2009**, *42*, 127–133.
- [28] Schenk, S.; Reiher, M. *Inorg. Chem.* **2009**, *48*, 1638–1648.
- [29] Christian, G.; Stranger, R.; and Yates, B. F. *Chem.–Eur. J.* **2009**, *15*, 646–655.
- [30] Kerpál, C.; Harding, J. D.; Lyon, T. J.; Meijer, G.; Fielicke, A. *J. Phys. Chem. C* **2013**, *117*, 12153–12158.
- [31] Umemoto, H.; Funae, T.; Yuri A. Mankelevich, A. Y. *J. Phys. Chem. C* **2011**, *115*, 6748–6756.
- [32] Roy, D.; A. Navarro–Vazquez, A.; Schleyer, P. v. R. *J. Am. Chem. Soc.* **2009**, *131*, 13045–13053.

-
- [33] Sung, M-W.; Kawai, R.; Weare J. H. *Phys. Rev. Lett.* **1994**, *73*, 3552–3555.
- [34] Rousseau, R.; Marx, D. *Phys. Rev. Lett.* **1998**, *80*, 2574–2577.
- [35] Cao, B.; Starace, A. K.; Judd, O. H.; Bhattacharyya, I.; Jarrold, M. F.; López, J. M.; Aguado, A. *J. Am. Chem. Soc.* **2010**, *132*, 12906–12918.
- [36] Boo, B. H.; Liu, Z. *J. Phys. Chem. A* **1999**, *103*, 1250–1254.
- [37] Cao, B.; Starace, A. K.; Judd, O. H.; Jarrold, M. F. *J. Am. Chem. Soc.* **2009**, *131*, 2446–2447.
- [38] Romanowski, Z.; Krukowski, S.; Grzegory, I.; Porowski, S. *J. Chem. Phys.* **2001**, *114*, 6353–6366.
- [39] Kulkarni, B. S.; Krishnamurty, S.; Pal, S. *J. Phys. Chem. C* **2011**, *115*, 14615–14623.
- [40] Andrews, L.; Zhou, M.; Chertihin, G. V.; Bare, W. D.; Hannachi, Y. J. *J. Phys. Chem. A* **2000**, *104*, 1656–1661.
- [41] Kandalam, A. K.; Pandey, R.; Blanco, M. A.; Costales, A.; Recio, J. M.; Newsam, J. M. *J. Phys. Chem.* **2000**, *104*, 4361–4367.
- [42] Hua, Y.; Liu, Y.; Jiang, G.; Du, J.; Jun Chen, J. *J. Phys. Chem. A* **2013**, *117*, 2590–2597.
- [43] Lang, S. M.; Claes, P.; Neukermans, S.; Janssens, E. *J. Am. Soc. Mass Spec.* **2011**, *22*, 1508–1514.
- [44] Datta, A.; Pati S. K. *J. Phys. Chem. A*, **2004**, *108*, 9527–9530.
- [45] Tyrakowski, C. M.; Snee, P. T. *Phys. Chem. Chem. Phys.*, **2014**, *16*, 837–855.
- [46] Sun, K.; Vasudev, M.; Jung, H.-S.; Yang, J.; Kar, A.; Li, Y.; Reinhardt, K.; Snee, P. T.; Stroschio, M. A.; Dutta, M. *Microelectron. J.* **2009**, *40*, 644–649.
- [47] Luo, Z.; Grover, C. J.; Reber, C. A.; Khanna, S. N.; Castleman, Jr. A. W. *J. Am. Chem. Soc.* **2013**, *135*, 4307–4313.
-

-
- [48] Roach, P. J.; Woodward, W. H.; Reber, A. C.; Khanna, S. N.; Castleman, Jr. A. W. *Phys. Rev. B* **2010**, *81*, 195404–195409.
- [49] Jiang, Z–Y.; Luob, X–M.; Lic, S–T.; Chud, S–Y. *Int. J. Mass Spectrom.* **2006**, *252*, 197–203.
- [50] Bergeron, D. E.; Castleman, Jr. A. W.; Morisato, T.; Khanna S. N. *Science* **2004**, *304*, 84–87.
- [51] Bergeron, D. E.; Roach, P. J.; Castleman, A. W., Jr.; Jones, N.; Khanna, S. N. *Science* **2005**, *307*, 231–235.
- [52] Kurkina, L. I.; Farberovich, V.; Gorbunovt, V. A. *J. Phys.: Condens. Matter* **1993**, *5*, 6029–6042.
- [53] Kumar, V.; Bhattacharjee, S.; Kawazoe, Y. *Phys. Rev. B* **2000**, *61*, 8541–8547.
- [54] Polshettiwar, V.; Varma, S. R. *Green Chem.* **2010**, *12*, 743–754.
- [55] Alipour, M.; Mohajeri, J. *Phys. Chem. A* **2010**, *114*, 12709–12715.
- [56] Aguado, A.; López, J. M. *J. Chem. Phys.* **2009**, *130*, 64704–64713.
- [57] Gong, G. X.; Vijay Kumar, V. *Phys. Rev. Lett.* **1993**, *70*, 2078–2081.
- [58] Chuang, F. C.; C. Z. Wang, C.Z.; Ho, K. H. *Phys. Rev. B* **2006**, *73*, 125431–125437.
- [59] Fournier R. *J. Chem. Theory. Comput.* **2007**, *3*, 921–929.
- [60] Paranthaman, S.; Kiryong, Hong K.; Kim, J.; Kim, D. E.; Kim T. K. *J. Phys. Chem. A* **2013**, *117*, 9293–9303.
- [61] Köster, A. M.; Calaminici, P.; Casida, M. E.; Dominguez, V. D.; Flores-Moreno, R.; Geudtner, G.; Goursot, A.; Heine, T.; Ipatov, A.; Janetzko, F.; del Campo, J. M.; Reveles, J. U.; Vela, A.; Zuniga– Gutierrez, B.; Salahb, D. R. deMon2k; The deMon developers Cinvestav: Mexico City, 2006.
- [62] Perdew, J. P.; Burke, K.; Ernzerhof, M. *Phys. Rev. Lett.* **1996**, *77*, 3865–3868.

-
- [63] Godbout N.; Salahub, D. R.; Andzelm, J.; Wimmer, E. *Can. J. Chem.* **1992**, *70*, 560–571.
- [64] Calaminici, P.; Janetzko, F.; Köster, A. M.; Mejia-Olvera, R.; Zuñiga-Gutierrez, B. *J. Chem. Phys.* **2007**, *126*, 44108–44118.
- [65] Köster, A.M.; Reveles, U.J.; del Campo, J.M. *J. Chem. Phys.* **2004**, *121*, 3417–3424.
- [66] Berendsen, H. J. C.; Postma, J. P. M.; van Gunsteren, W. F.; DiNola, A.; Haak, J. R. *J. Chem. Phys.* **1984**, *81*, 3684–3689.
- [67] Gamboa, G. U.; José, M.; Pérez, V.; Calaminici, P.; Köster A. M. *Int. J. Quant. Chem* **2010**, *110*, 2172–2178.
- [68] Jena, N. K., Chandrakumar, K.R.S.; Ghosh, S. K. *J. Phys. Chem. Lett.* **2011**, *2*, 1476–1480.
- [69] Mondal, K.; Banerjee, A.; Ghanty, T. K. *J. Phys. Chem. C* **2014**, *118*, 11935–11945.

Effect on Structure and Stability of Aluminum Cluster with the Successive Gallium Substitution

Conformation and electronic charge on a aluminum cluster are two main factors governs its catalytic property. However, little is known on the finite temperature behavior of various aluminum cluster conformations. Much less is known the effect of doping with successive increasing ratio. In this work, we have carried out ab initio density functional theory (DFT) based molecular dynamical simulations on pure and gallium doped with different proportion of Al_8 clusters with an aim of understanding the thermodynamic properties of ground state conformations as a function of doping ratio. Our simulations reveal that cluster properties does not follow a monotonic relation with the increasing doping percentage. 12.5%, 25% and 37.5% doping of gallium (i.e Al_7Ga , Al_6Ga_2 , and Al_5Ga_3) become liquidlike at much lower temperature (200 – 250K) than its pristine Al_8 analogue (450K). On the other hand cluster with 50% gallium doping (i.e Al_4Ga_4) remarkably stable (solidlike upto 600K) as compared to its pristine counterpart. In order to look into the factors leading to the stabilization structural and electronic properties are analyzed. Factors such as charge redistribution within the atoms and composition of molecular orbitals are seen to contribute towards stronger Al–Ga bonds in Al_4Ga_4 thereby stabilizing it considerably.

6.1 Introduction

Small size clusters in the size range of $N=2-150$, where N is number of atoms, are well known to behave surprisingly different in respect to their bulk counterparts[1–7]. The finite size behavior are reflected in most of their properties, like optical properties, energetics and equilibrium geometries, ionization potential, polarizabilities, etc. Stability of a class of clusters depends on the filling up of geometric or electronic shell. The filled electronic shell yield magic number cluster[8, 9]. Further, addition of an impurity significantly alter the finite temperature properties of homogeneous clusters which makes them attractive in nanoscience[10, 11]. In the past decade, few work are reported on the impurity doped metal clusters[12, 13]. Our *ab initio* molecular dynamics (BOMD) investigation shed light on a number of interesting aspects like modifications in the equilibrium structures, trapping of an impurity, changes in the bonding characteristics due to electron transfer and enhancement in the stability and catalytic property. Many of these properties get influenced by the relative difference in the valence, ionic radii, and electro–negativity.

Small clusters have large number of active coordinate site, unlike periodic surfaces, making them tremendous applicability in the field of catalysis[14, 15]. Moreover, these small size clusters are highly effective in the area of nanoscience due to the alteration of active sites with the size and shape of the cluster and the catalytic reaction on the active site happen at different finite temperature. This isomorphism confirm that there is a correlation between shape of the cluster and its temperature. Hence, it is significant to understand the stability of a particular geometry at its working temperature. This information is incomplete in the literature still date and therefore a limitation in its practical applications.

The analysis on heterogeneous clusters mainly dealing with the ground state properties. A number of experimental work have been reported about the thermal properties of the metallic clusters[16–26]. Haberland and co–workers has studied the oxidation behavior of sodium clusters[16]. They have concluded that the oxidization of Na clusters with 135–192 atoms by a single oxygen molecule significantly lower both the melting points and the latent heats and interaction between the pure and oxidized part of the cluster is responsible for the effect. In an another combined experimental and theoretical investigation on $Al_{44}^{+/-}N_2$ clusters by Jarrold and

co-workers revealed that the above statement is not valid on this cluster[17]. They concluded that the thermal behavior of the impurity doped systems is unpredictable for small clusters. The same group further investigated the heat capacities for $Al_{n-1}Cu^-$ clusters ($n = 49-62$) and equate the findings with pristine Al_n^+ clusters[18]. It is concluded from their study that a single atom Cu doping is responsible for either decrease or increase the melting points of the doped materials.

In the literature most of the studies of thermodynamic properties are reported on homogeneous clusters[27–38]. Computational investigation of heterogeneous clusters is much challenging due to the demand of higher length of configuration space for optimization of geometry. A cluster with a few number of impurities can be seen as a simpler version of heterogeneous materials which has a substantial interest. Major issues laying on the effect of doped atoms on the thermodynamic properties[39–44]. *Ab initio* molecular dynamics simulations based on density functional theory or classical potentials based study are describe in this area. Joshi *et al.* have described elaborately a representative system of Li_6Sn in which there is a competition between covalent and ionic bonding, makes finite temperature behavior of this doped species much different in respect to its pristine analogue, Li_7 cluster[45]. Lee *et al.* have reported the electronic structure, equilibrium geometries, and the bonding nature in Li–Sn, and the thermodynamic properties of Li clusters doping with Al atoms[46, 47]. Their conclusion is that the geometries of Li clusters change drastically by adding of few impurities of Sn. Chandrachud *et al.* have explored the thermodynamic properties of aluminum and gallium clusters doping with few carbon impurities[48]. Their important studies highlights the significant reduction in the melting temperature of the host clusters upon doping there and, in the case of gallium, the carbon impurities alter the geometry to icosahedral from decahedral. Krishnamurty *et al.* conclude that the small clusters of Si_n ($n = 15$ and 20) become very unstable and fragment with heating up to approximately 1600 K[49]. Interestingly, Kumar *et al.* tuned the stability of a caged structure of Si cluster using a several class of dopants. Specifically, they propose that a single impurity of transition metal atoms such as Ti, Zr, and Hf increases the binding energy of Si_{16} and alter the geometry to a caged one, very similar to cages of carbon[50–53]. Zorriasatein *et al.* have performed the fragmentation process in Si_{16} prohibited by adding impurity of Ti atom[54]. A significant work by Ferrando and co-workers in the frame work of classical inter-atomic potentials concluded that a single impurity of Ni or Cu can able to shift dramatically the melting temperature of icosahedral zg clusters with

tens to hundreds of atoms[55]. They observed that a few impurities in the central position causes a significant relaxation of the strained icosahedral structure resulting better stability against thermal disordering. All the theoretical studies prescribed a strong and direct correlation between the geometric structure and the behavior of the heat capacity. Das *et al.* have investigated di-nitrogen activation on Si and P atom doped aluminum clusters and they have concluded that a single impurity of Si and P atom enhanced catalytic property of aluminum clusters dramatically as compared to its pristine analogue[56].

Recently, Calvo and co-workers have studied the heat capacity of pristine and heterogeneous water clusters with the help of exchange Monte Carlo simulations with several intermolecular potentials[57]. They further observed that a small amount of impurity has tendency to shift the melting point to a higher temperature in the small cluster ($n=21$) but the effect is considerably reduced in the larger species having 50 molecules. The work of Lyalin *et al.* shows that the addition of a carbon impurity in Ni_{147} lowers its melting temperature by 30 K[58]. This is mainly due to excessive stress produced on the cluster lattice. The distortion of the system lattice leads to the change in energetics as well as entropy of the cluster. The reduction of the melting temperature of magic Lennard-Jones clusters due to a single impurity has also been observed.

Quite clearly the effect of a few impurities on the properties of host cluster can be quite dramatic. In the present work, we investigate the finite temperature behavior of pristine Al_8 and gallium doped Al_7Ga , Al_6Ga_2 , Al_5Ga_3 and Al_4Ga_4 clusters. Since the impurity is known to change the geometry as well as bonding substantially in the pristine cluster it is also expected to change the finite temperature properties of the pristine analogue. In the doped cluster, there is a finite amount of charge transfer from aluminum to gallium atom(s), resulting nature of bonding changes metallic like to predominantly ionic like. This charge transfer has remarkable effect in the finite temperature behavior of doped clusters hence, its effect on catalytic efficiency. We have demonstrated that percentage of impurity has dramatic impact on the host cluster. 12.5%, 25% and 37.5% doping of gallium significantly lower the melting temperature but 50% gallium doping enhance the melting temperature of the cluster. Root mean square bond length fluctuation (δ_{rms}) of gallium doped clusters is considerably lower than that of pristine Al_8 implying that expansion of volume upon melting is reasonably less in that cluster. However, it is difficult to conclude a direct correlation between the properties of the bulk alloys and small clusters but physics is

originally same originating from the charge transfer which results into the strong ionic bond.

The paper is organized as follows. In Sec. 2 we describe briefly our computational and statistical approaches. Results for the equilibrium geometries, nature of bonding and finite temperature properties of pristine Al, Al–Ga and pristine Ga are given in Sec. 3, and the conclusions are given in Sec. 4.

6.2 Computational Details

All calculations are performed in the framework of density functional theory (DFT), using a linear combination of Gaussian orbitals as implemented in deMon2k code[59]. All the pure and doped clusters are optimized using the Perdew–Burke–Ernzerhof (PBE) exchange and correlation functional[60] with DZVP basis set[61]. The A2 auxiliary functions are used to fit the charge density[62]. The convergence of the geometries is based on gradient and displacement criteria with a threshold value of 10^5 au and the criteria for convergence of an SCF cycle was set to 10^9 . Only the lowest spin state is considered for all the Al clusters. Thus, the spin multiplicity for an even electron (odd number of Al atoms) cluster is singlet and doublet for odd electron (even number of Al atoms) clusters. Following the geometry optimization, harmonic vibrational frequencies are computed for each cluster. All of the frequencies are found to be positive, thereby indicating the conformations to be a local minima.

The optimized, lowest energy conformation is chosen as the starting conformation for all of the molecular dynamical (MD) simulations. The finite temperature simulation for each cluster is carried out implementing (ab initio) Born–Oppenheimer molecular dynamics (BOMD) using the same exchange–correlation functionals and basis set described above[63]. The simulations are carried out between 200K and 1600K. At each temperature, the cluster is equilibrated for a time period of 10 ps followed by a simulation time of 40 ps. The temperature of the cluster is maintained using Berendsens thermostat ($\tau = 0.5$ ps)[64]. The nuclear positions are updated using a velocity Verlet algorithm with a time step of 1 fs. The atomic positions and bond length fluctuations of atoms are analyzed using traditional parameters such as root mean square bond length fluctuations (δ_{rms}) and the mean square ionic displacements (MSDs). The δ_{rms} is defined

as

$$\delta_{rms} = \frac{2}{N(N-1)} \sum_{i < j} \sqrt{\frac{\langle R_{ij}^2 \rangle_t - \langle R_{ij} \rangle_t^2}{\langle R_{ij} \rangle_t}} \quad (6.1)$$

where N is the number of particles in the system, r_{ij} is the distance between the i^{th} and j^{th} particle in the system and $\langle \dots \rangle_t$ denotes a time average over the entire trajectory. The MSD of an individual atom is defined as

$$\langle R_i^2 \rangle = \frac{1}{M} \sum_{m=1}^M [R_i(t_{0m} + t) - R_i(t_{0m})]^2 \quad (6.2)$$

where $R_i(t_{0m})$ is the instantaneous position of atom i at t_0 and $R_i(t_{0m} + t)$ is the corresponding position of atom i after a time interval t .

6.3 Results and Discussion

6.3.1 Equilibrium geometries

We begin our discussion with the equilibrium geometries of pristine Al_8 , gallium doped Al_7Ga_1 , Al_6Ga_2 , Al_5Ga_3 and Al_4Ga_4 and pristine Ga_8 clusters as shown in figure 1. In each case of doping, we first doped gallium impurity and then optimized. Optimized geometry of pristine Al_8 clusters is a capped octahedral with the shortest bond length of 2.56 Å and longest bond length of 2.88 Å. Doping with 1, 2, 3, and 4 atoms does not change the shape of the cluster but bond lengths alter significantly. In Al_7Ga_1 cluster, the Al–Al bond lengths vary between 2.55 Å to 2.85 Å. The Al–Ga bond length is 2.54 Å. On the other hand, in Al_6Ga_2 , the Al–Al and Al–Ga bond lengths vary from 2.56 – 2.86 Å and 2.54 Å respectively. In Al_5Ga_3 the Al–Al and Al–Ga bond lengths are 2.57 – 2.84 Å and 2.52 – 2.92 Å. Similarly in Al_4Ga_4 , the Al–Al and Al–Ga bond lengths are 2.57 – 3.27 Å and 2.54 – 2.90 Å. The Ga–Ga bond lengths vary between 2.51 – 2.73 Å in pristine Ga_8 clusters.

6.3.2 Thermodynamics

In this section we investigate the insight of the stability of pristine and Ga-atom doped aluminum clusters. Moreover we have also investigated the structure and stability of 8 atoms Ga cluster. We begin with pristine Al_8 clusters which vibrate around equilibrium position, called solid like ('I') up to 550K. With increase the temperature vibration frequency of atoms increases which leads to interconversion between several low energy conformations. This region is called structural fluctuance ('II') state and it is observed up to 850K. Atomic movement further increases rapidly with temperature and produces large number of high energy isomers called as liquid like ('III') region. Pristine Al_8 became liquid like as clearly seen from δ_{rms} and MSD values (figure 6.3 and 6.4 respectively). The δ_{rms} values up to 550K (solid region) is 0.15\AA then it increases to 0.25\AA in the region 'II'. Above the temperature of 850K δ_{rms} became steady confirms liquid like region of this cluster. Figure 6.4 highlights the MSD values of each atom at 400K, 600K, 1000K and 1200K. At 400K (solid like region) the MSD of each atom is quite small as in this temperature atoms vibrate around equilibrium position. MSD at 600K which is the region 'II' rapidly increases up to 12\AA and then slowly increase with temperature. Several conformations (ground state and high energy conformations) obtained during the simulation between 200K to 1600K are compiled in Figure 6.5.

Doping with one Ga atom alter the thermodynamic properties dramatically. Al_7Ga_1 cluster became liquid like much earlier temperature as compared to its pristine analogue. It vibrate around equilibrium position up to 240K ('I') which is much less (300K) as compared to its pristine analogue. Above 240K it start transforming between different conformations (region 'II'). Al_7Ga_1 cluster became liquid like at 560K ('III'). δ_{rms} (figure 6.6) gives clear indication of the three different states of Al_7Ga_1 cluster. In the solid like region up to 240K, δ_{rms} is reasonably low ($\approx 0.1\text{\AA}$). At 560K (region 'II') it has the values 0.2\AA and slowly increase in the region 'III'. MSD values of each atom as shown in table also explain the same. Mulliken charge distribution (figure 6.2) indicate that there is a charge transfer from Al atoms to Ga atom in Al_7Ga_1 cluster. Although charge transfer from Al to Ga atom make Al-Ga bond ionic in nature but unsymmetrical charge distribution produces considerable stress in the system which is the source of instability. Hence, Al_7Ga_1 became liquid like much earlier temperature as compared to its pristine analogue,

Al₈ cluster. Various isomers generated during the simulation between 200K to 1600K are shown in figure 6.8.

Now we want to discuss the thermodynamic properties of Al₈Ga₂ cluster. Doping with two Ga atoms yield the cluster Al₈Ga₂ which is slightly more stable as compared to Al₇Ga₁. Al₆Ga₂ cluster stable up to 360K. Unlike Al₇Ga₁ cluster, structural fluctuation region is reasonably large (360K – 1500K) of Al₆Ga₂ cluster. Above 1500K it became liquid like. δ_{rms} and MSD of each atom in various temperature are given in figure 6.9 and figure 6.10 respectively. The δ_{rms} is less than 0.1 Å below 360K and it is increases up to 0.5 Å at 1600K. MSD values also give clear indications of the three region. Several conformations obtained during the simulation steps are given in the figure 6.11.

The two gallium atoms doping in the two edge of Al₈ makes a symmetrical Al₈Ga₂ cluster (figure 6.1). Hence, charge redistribution is comparatively symmetrical in respect to one Ga atom doped cluster. The Ga atoms of the upper and lower edge have the charge of –0.215 and –0.200 respectively. All the Al atoms in the square planer position consist of positive charge and the other two Al atoms which are nearest to upper and lower edge Ga atoms respectively are negatively charge. This symmetrical charge redistribution enhance the stability of the Al₈Ga₂ cluster. On the other hand stability is enhanced by 70k of Al₅Ga₃ cluster in respect to Al₆Ga₂ but it is less stable than pristine analogue. Al₅Ga₃ cluster shows liquid like behavior above 750 K. The corresponding δ_{rms} and MSD values are compiles in figure 6.12 and 6.13 respectively. Different conformations obtained during the simulation between 200 – 1600K are compiled in figure 6.14

Doping with 50%, i.e 4 gallium atoms enhanced the cluster stability significantly. Aluminum and gallium moves around equilibrium position up to 580k which is 30K higher than its pristine analogue. δ_{rms} (figure 6.15) at 580k is >0.2 Å. MSD value of each atoms at 400K (solid region) is >0.1Å. Region ‘II’ survives up to 1100K. Several low energy conformations observed in this region. δ_{rms} is >3 Å and MSD at 600K is >4 Å. MSD increases rapidly as atoms vibrates more frequently with the temperature. Above 1100K, Al₄Ga₄ became liquid like which is evident from δ_{rms} and MSD values.

We have also investigate the structure and stability of Ga₈ cluster. This cluster has highest stability among the considerate clusters in this thesis. Pristine Ga₈ is stable up to 770K (δ_{rms} and

MSD values are $>1.5 \text{ \AA}$ and 0.6 \AA respectively) which is 220K higher in respect to pristine Al_8 cluster. Above this temperature vibration amplitude start increasing and cluster inter-converts between several low energy isomers. the span of structural fluctuation region is around 350K ($770 - 1120\text{K}$). It goes to liquid like region beyond 1120K . δ_{rms} and MSD values are compiled in figures 6.18 and 6.19 respectively. Selected conformations including low and high energies during the simulation up to 40ps are given in the figure 6.20

It is well known that clusters are transit from a solid-like state to liquid-like state as a function of temperature. Clusters evolves from solid to liquid like state via a structural fluctuation state where atoms vibrate moderately and yields several low energy conformations. Every states carry their own significance. The solid-like region is significant owing to the structural stability (atoms moves around equilibrium position) and an affirmation of a constant electronic and geometric configuration. This state is highly significant for applications where the clusters are applied for their response properties, which are shape and size sensitive. The liquid-like region is a more dynamic (atoms have large vibration in this state), which is significant for the synthesis of larger nanoclusters where a soft electronic and geometric structure is essential. Interestingly, all the clusters (pristine as well as doped) studied in the present thesis exhibit a conformational rearrangement state (where they transit through several isomers) before they enter into a liquid-like region. This intermediate region is known as structural fluctuation region which is highly significant for catalysis.

Fig 6.2 shows the Mulliken charge distribution on all the clusters as they undergo the above structural rearrangement. It is clearly noticeable from the values of Mulliken charge on each atoms that a structural rearrangement between various conformations leads to a moderate to considerable charge redistribution. For example, the Al_4Ga_4 analogue undergoes a significant charge depletion from Al atoms to Ga atoms. So if a ligand molecule such as CO is adsorbed on Ga atom through carbon atom, the presence of a more negatively charged Ga atom adjacent to it will help in an easier reduction process of CO. Similar analysis can be drawn for other ligand molecules such as O_2 , CH_3OH , etc. Hence, the presence such a structural rearrangement appears to be important for many catalytic purpose. The three regions are demarcated by dashed line and shown in all the δ_{rms} plot.

6.4 Conclusions

We have presented the equilibrium geometries, energetics, and bonding characteristics of pristine Al, successive Ga doped Al clusters, and pristine Ga cluster obtained by *ab initio* molecular dynamics. Our BOMD simulations shed light on the effect doping on the finite temperature behavior of the Al₈ cluster. Doping of Ga impurity alter the thermodynamic property of the cluster considerably. Al₄Ga₄ is the most stable cluster, and a significant charge transfer from Al to Ga is observed and over all charge distributed symmetrically. A dynamic transition between several isomers or conformations is observed in all the clusters between the solid-like state and liquid-like state. This conformational fluctuation is seen to be cluster-specific and transition called thermally driven structural fluctuation, which has remarkable impact and contribute positively to catalytic property of the doped clusters.

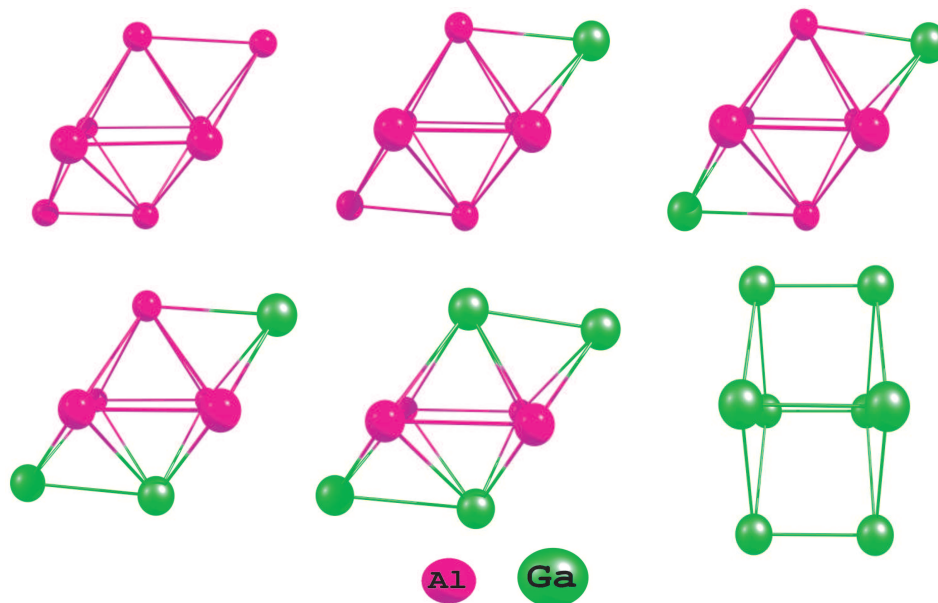


Figure 6.1: Optimized geometry of Al₈, Al₇Ga₁, Al₆Ga₂, Al₅Ga₃, Al₄Ga₄ and Ga₈ clusters

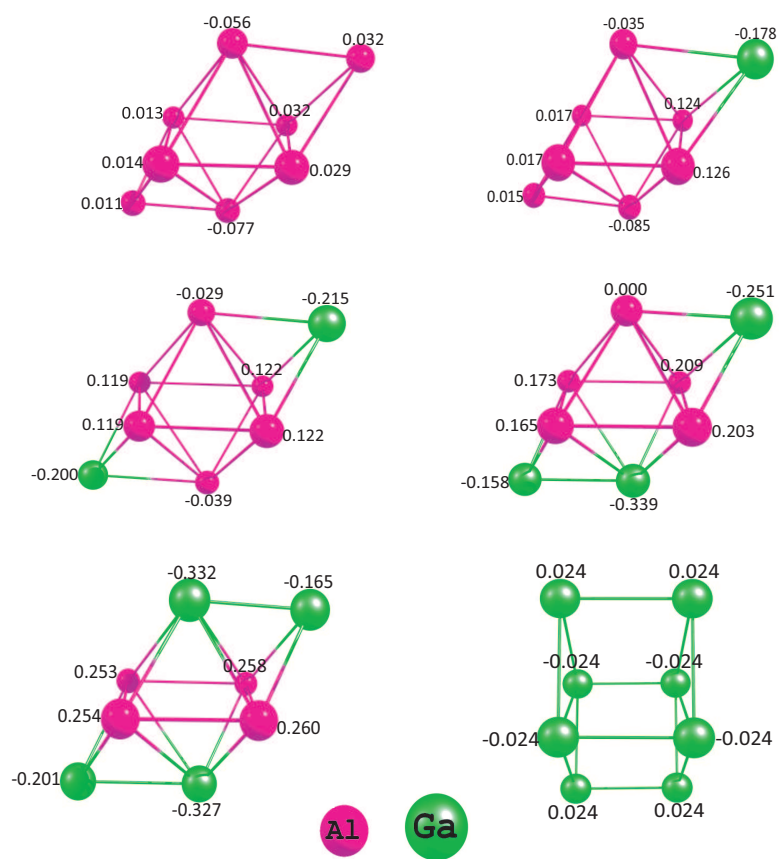


Figure 6.2: Mulliken charge on each atom of Al₈, Al₇Ga₁, Al₆Ga₂, Al₅Ga₃, Al₄Ga₄ and Ga₈ clusters

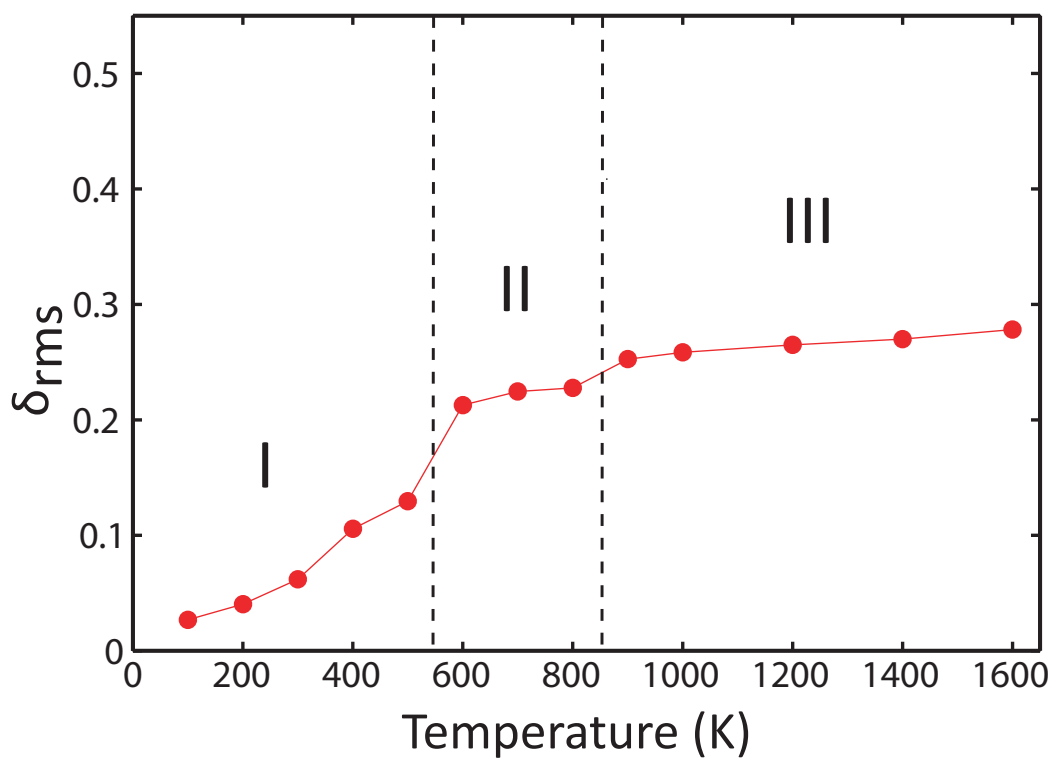


Figure 6.3: Bond length fluctuation (δ_{rms}) as a function of temperature in Al_8 cluster

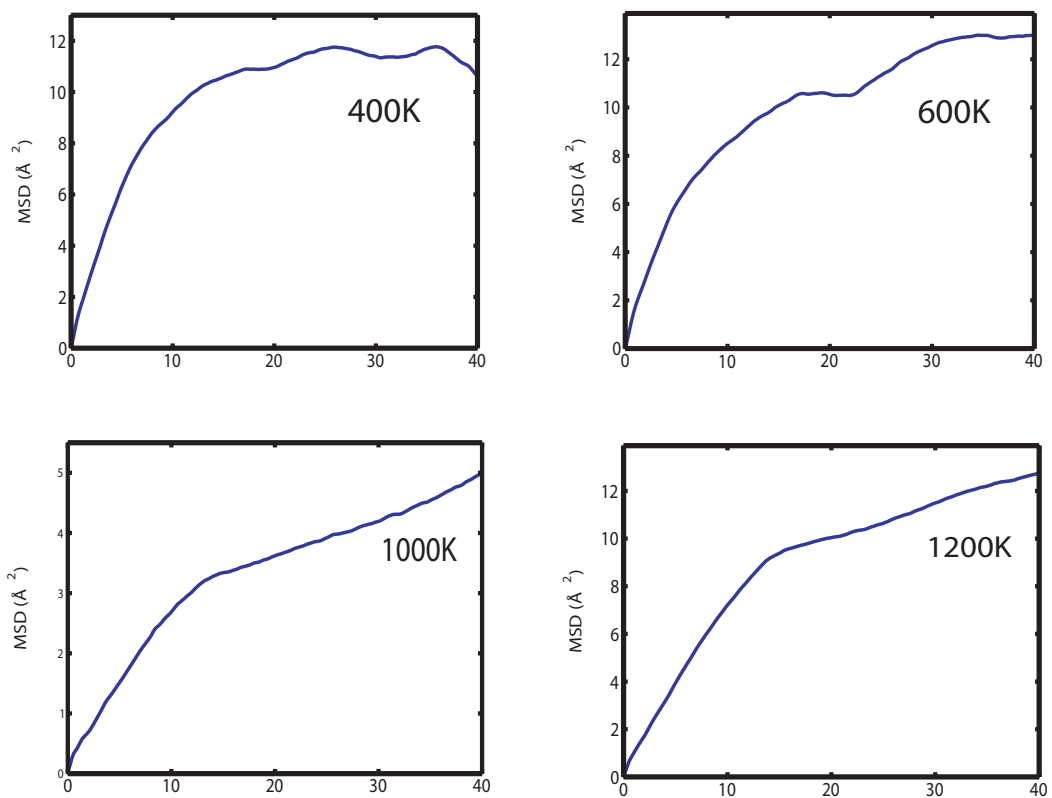


Figure 6.4: MSD of atoms in Al_8 cluster between 200K to 1600K.

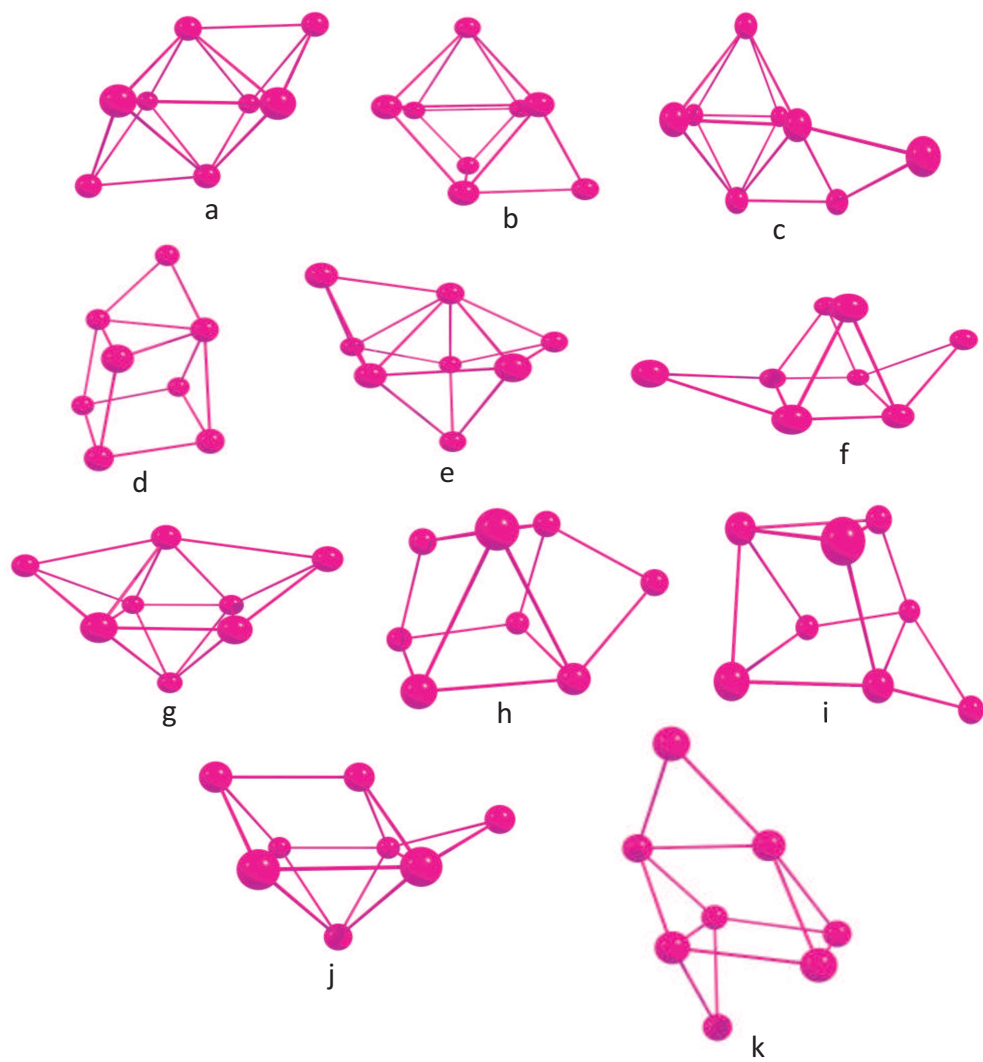


Figure 6.5: Various conformations of Al_8 observed during an MD simulation. (a) corresponds to the ground state conformation.

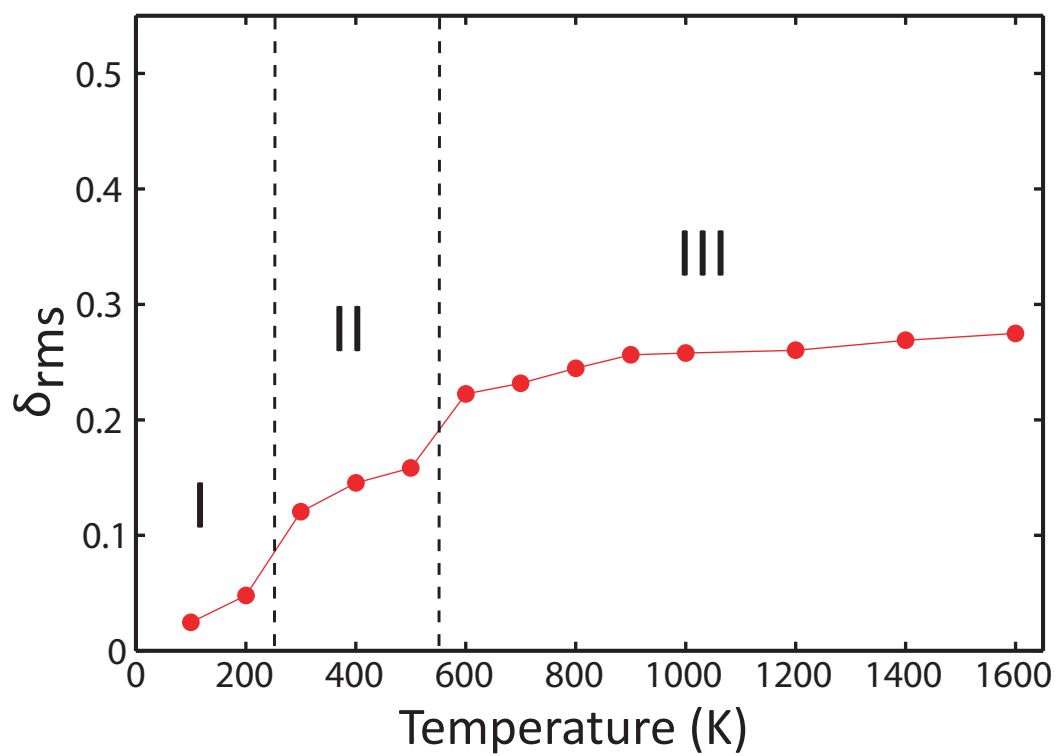


Figure 6.6: Bond length fluctuation (δ_{rms}) as a function of temperature in Al_7Ga_1 cluster

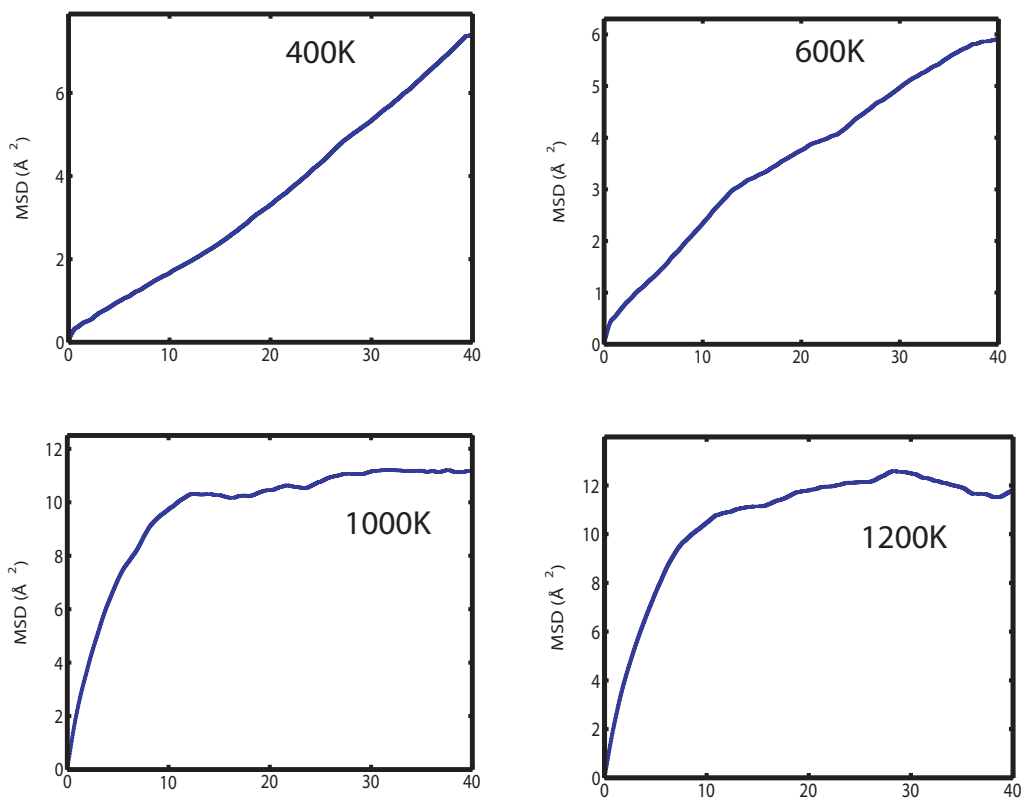


Figure 6.7: MSD of atoms in Al_7Ga_1 cluster between 200K to 1600K.

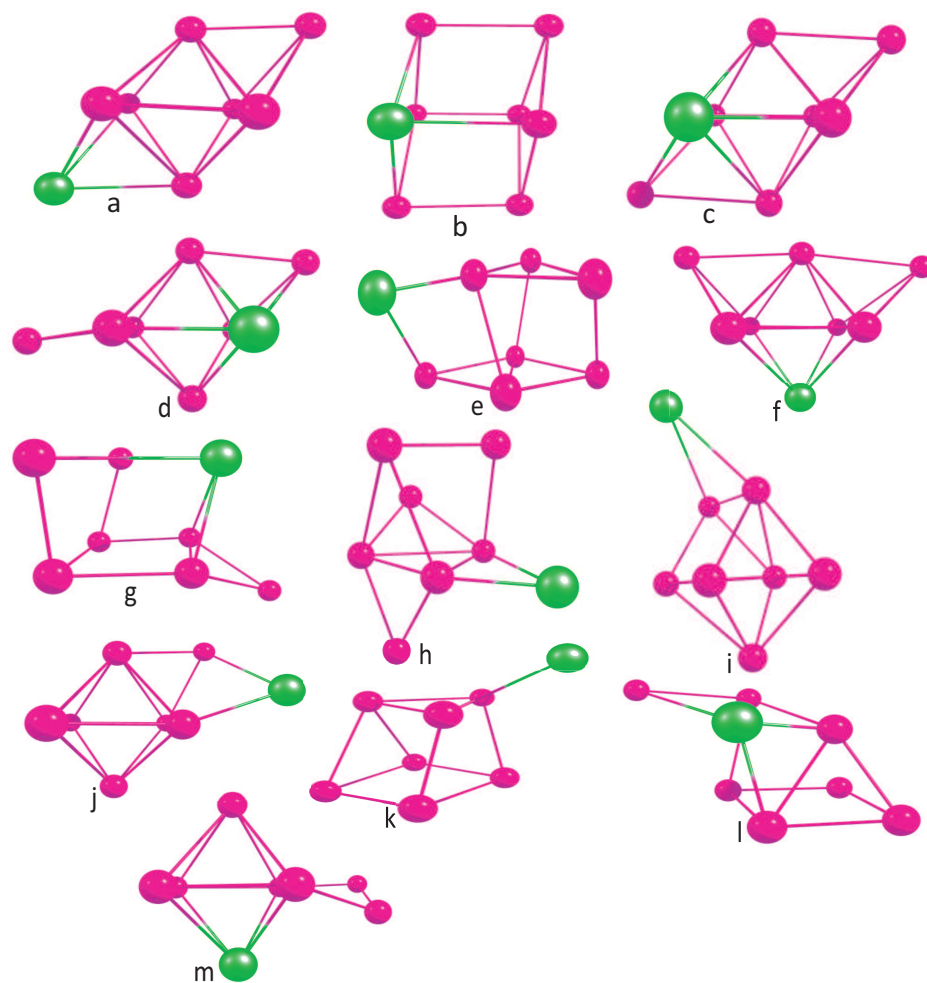


Figure 6.8: Various conformations of Al_7Ga_1 observed during an MD simulation. (a) corresponds to the ground state conformation.

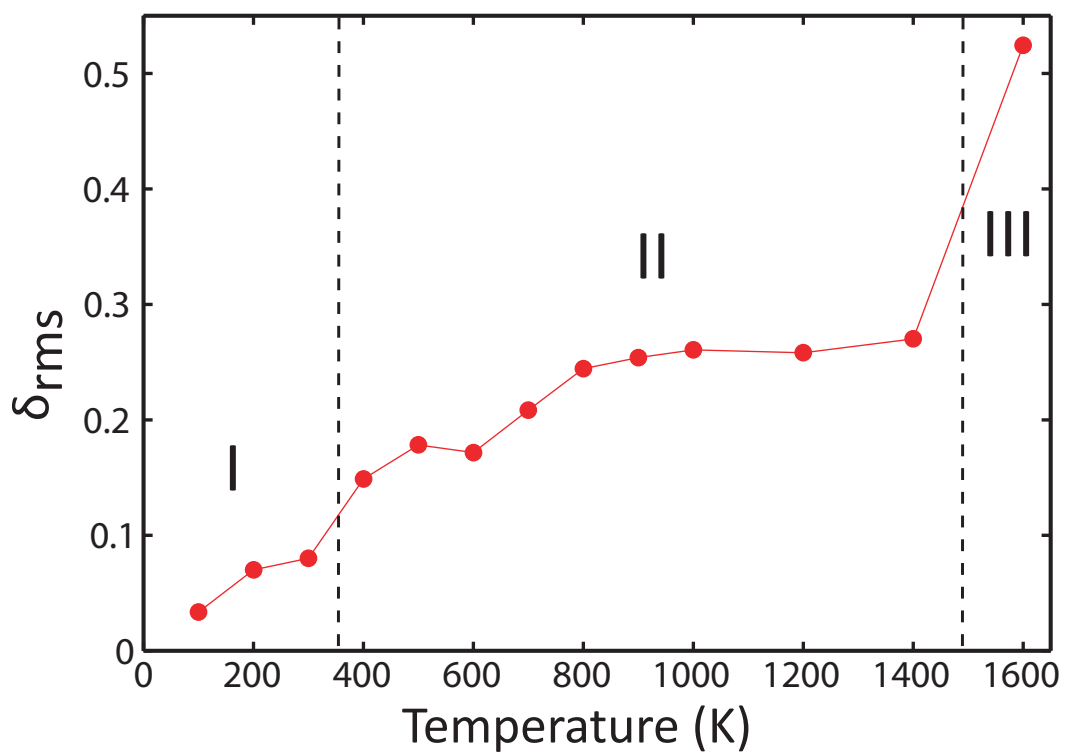


Figure 6.9: Bond length fluctuation (δ_{rms}) as a function of temperature in Al_6Ga_2 cluster

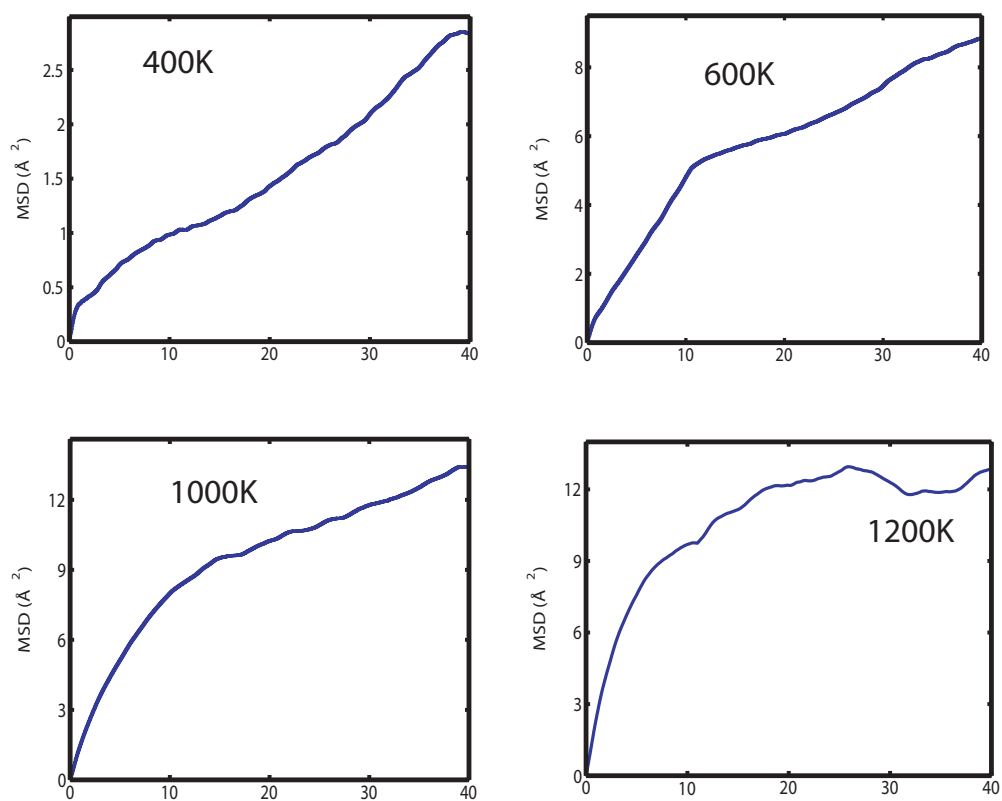


Figure 6.10: MSD of atoms in Al_6Ga_2 cluster between 200K to 1600K.

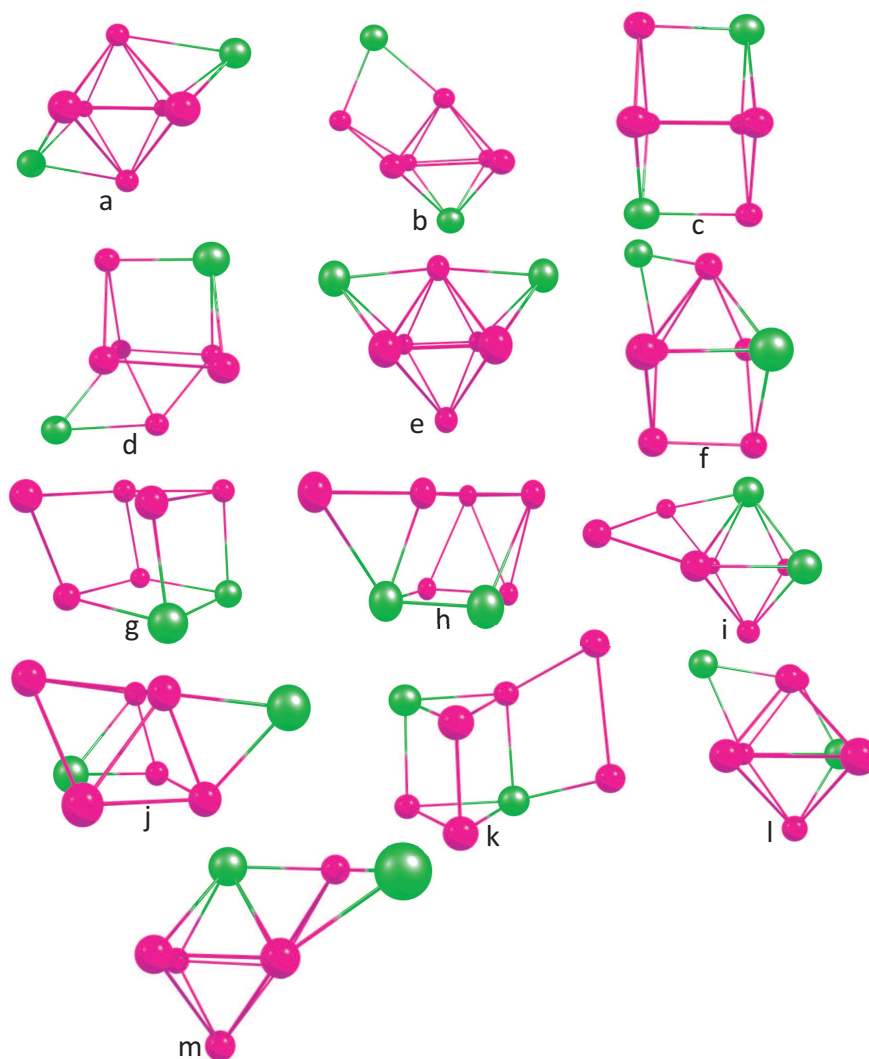


Figure 6.11: Various conformations of Al_6Ga_2 observed during an MD simulation. (a) corresponds to the ground state conformation.

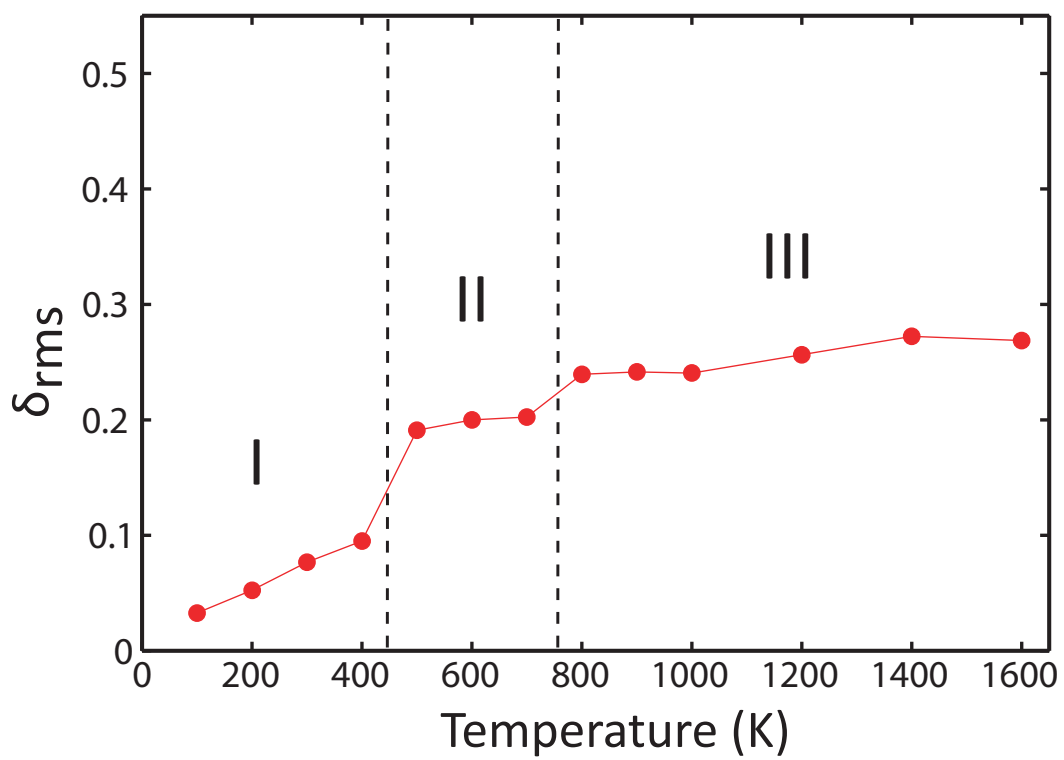


Figure 6.12: Bond length fluctuation (δ_{rms}) as a function of temperature in Al_5Ga_3 cluster

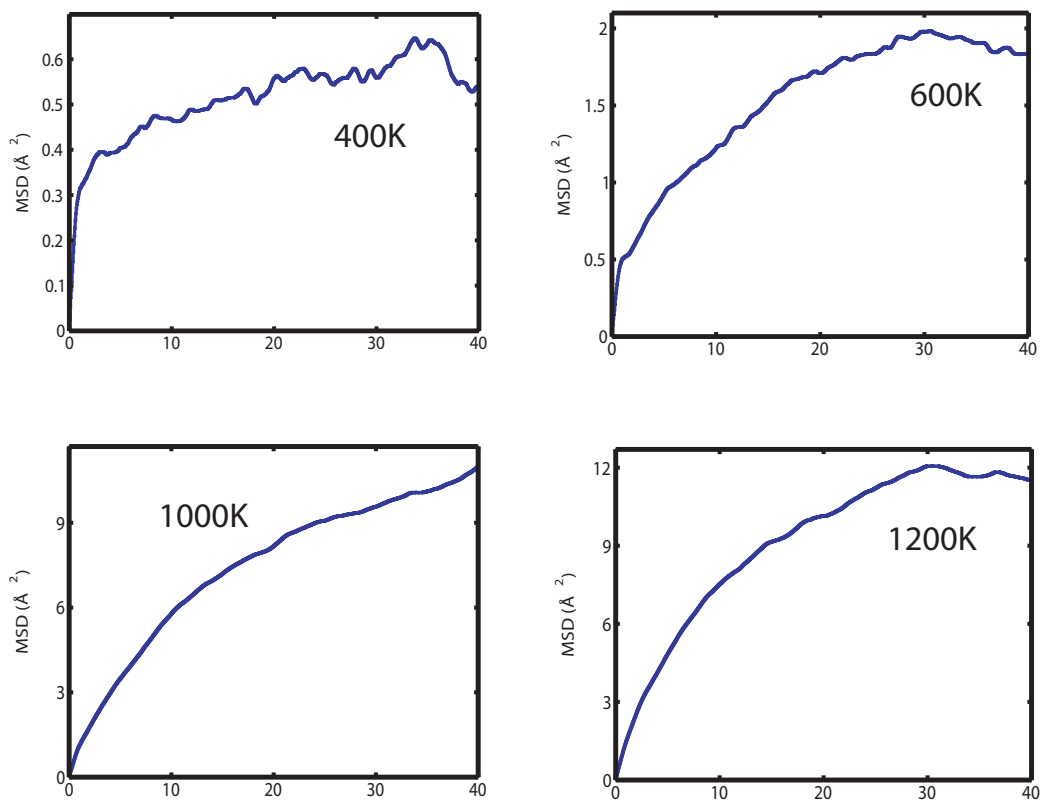


Figure 6.13: MSD of atoms in Al_5Ga_3 cluster between 200K to 1600K.

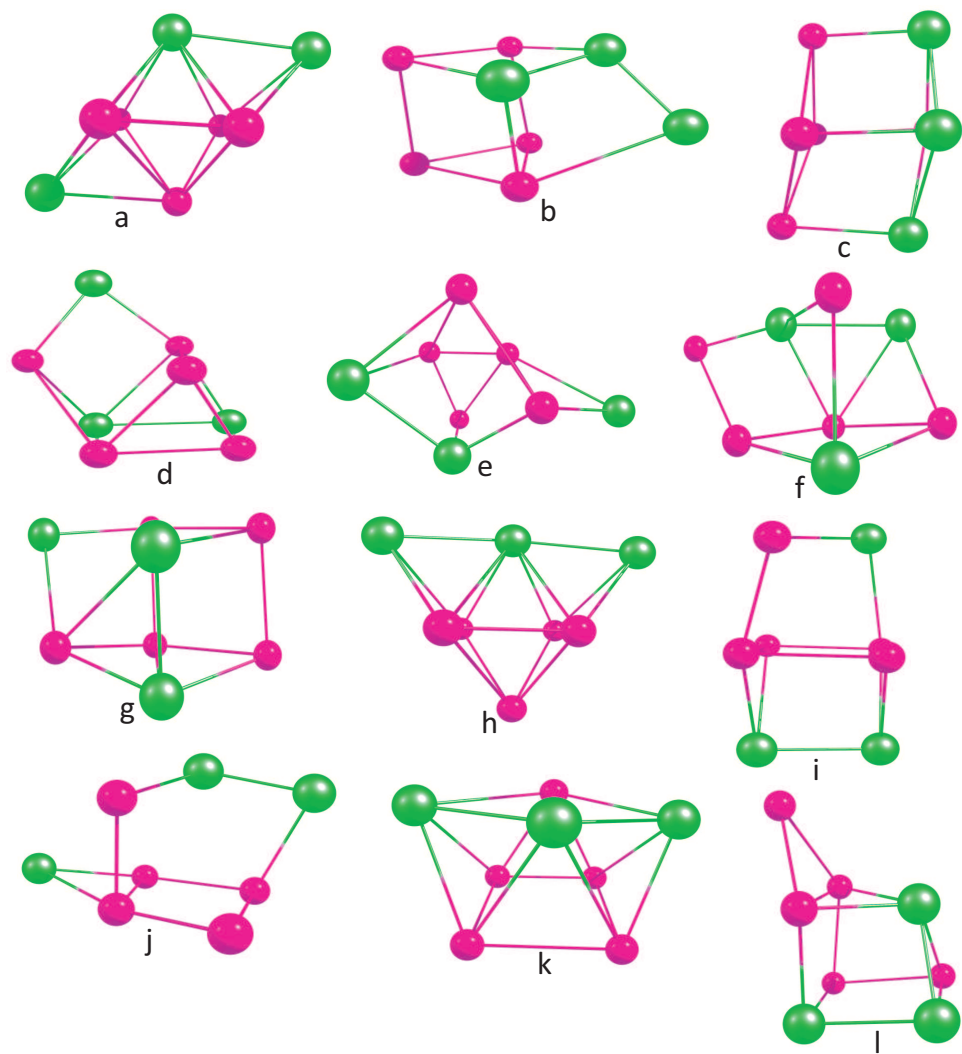


Figure 6.14: Various conformations of Al_5Ga_3 observed during an MD simulation. (a) corresponds to the ground state conformation.

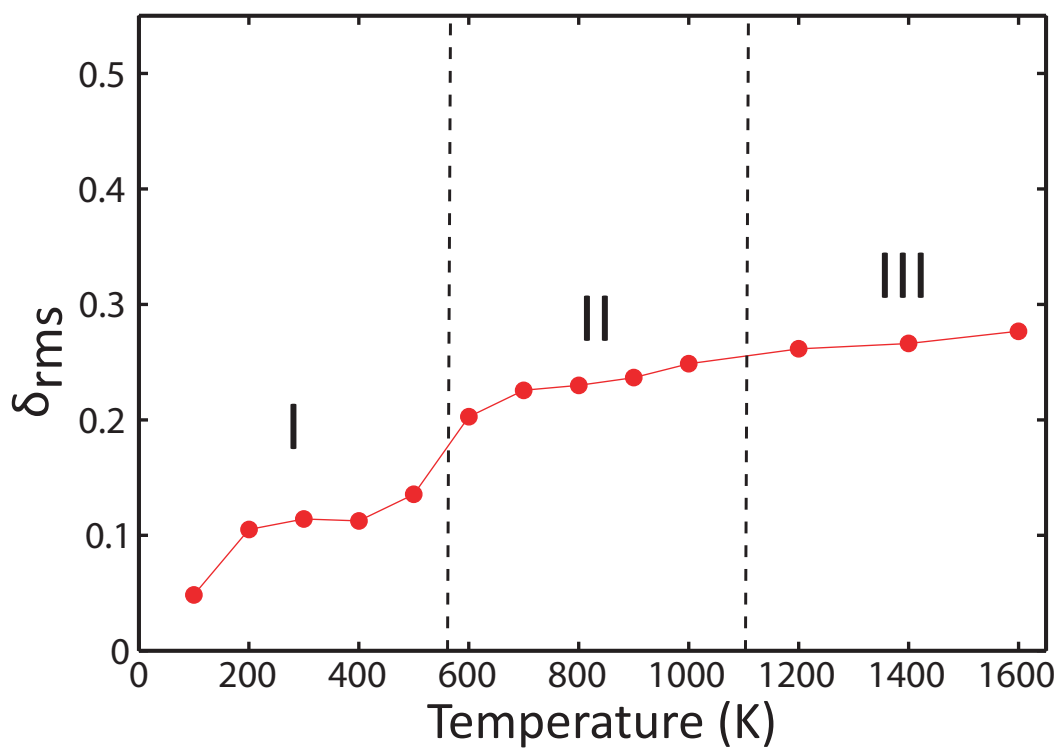


Figure 6.15: Bond length fluctuation (δ_{rms}) as a function of temperature in Al_4Ga_4 cluster

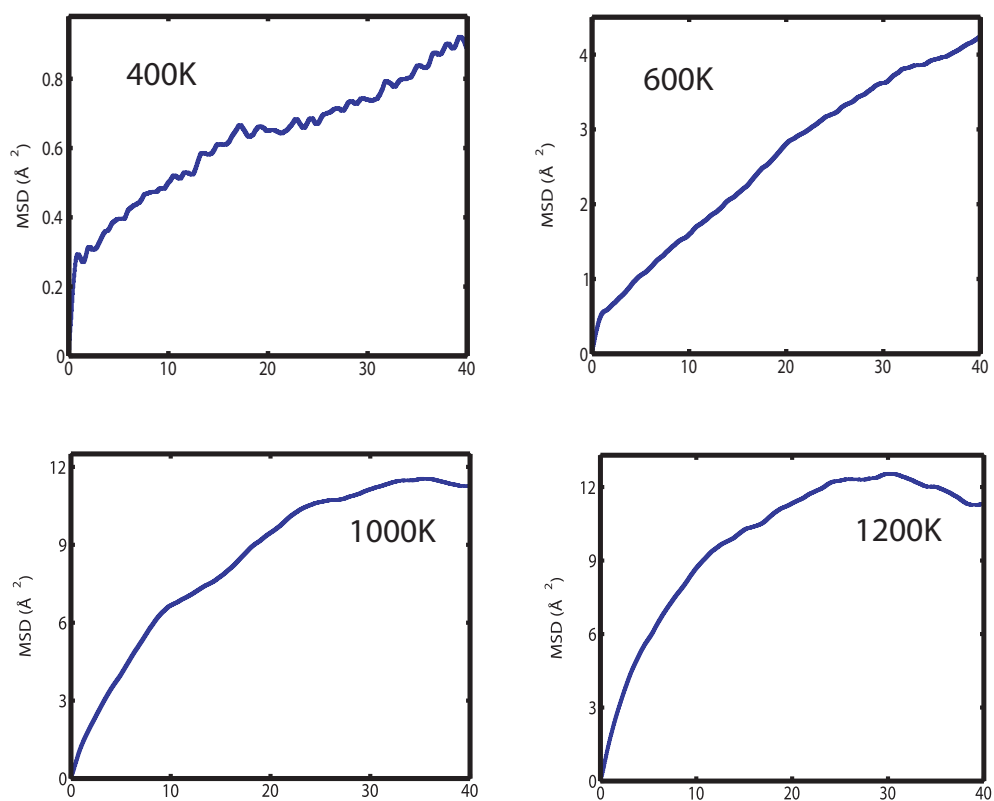


Figure 6.16: MSD of atoms in Al_4Ga_4 cluster between 200K to 1600K.

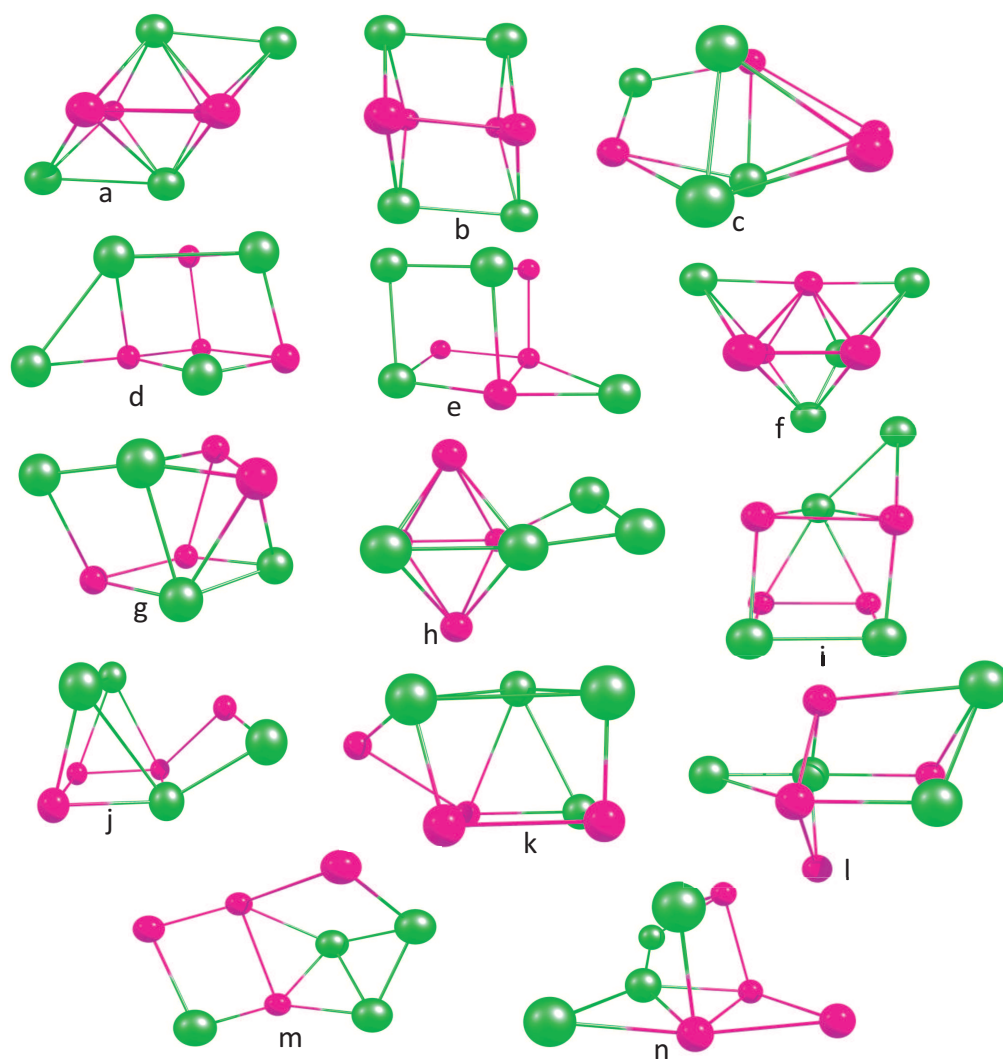


Figure 6.17: Various conformations of Al_4Ga_4 observed during an MD simulation. (a) corresponds to the ground state conformation.

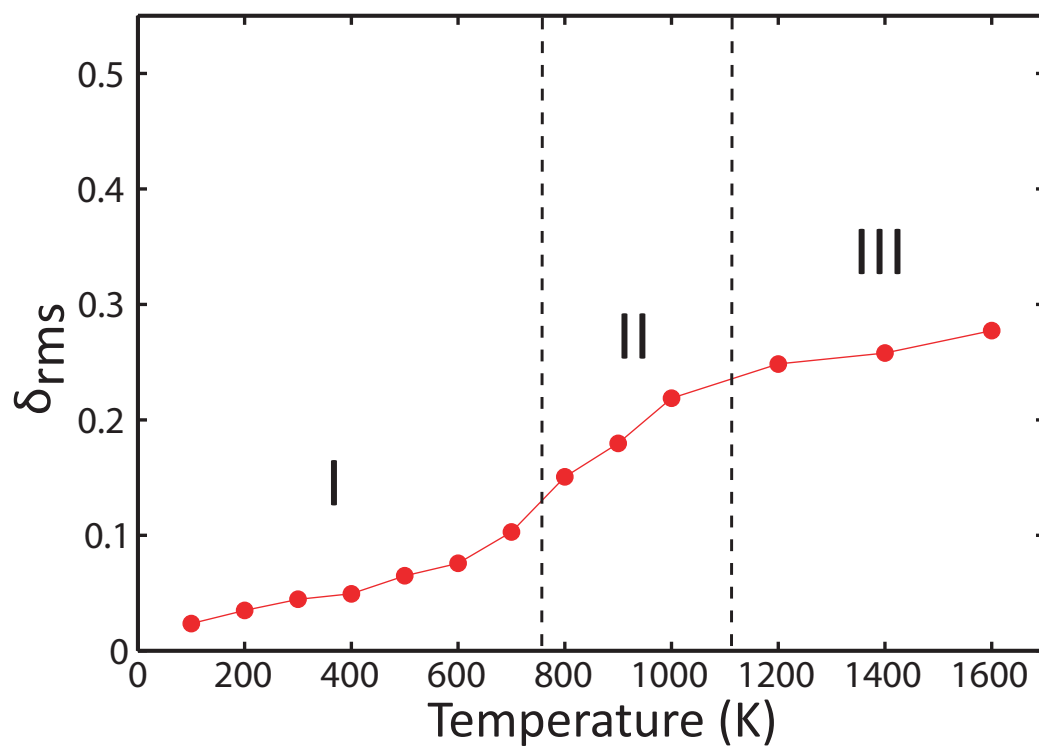


Figure 6.18: Bond length fluctuation (δ_{rms}) as a function of temperature in Ga_8 cluster

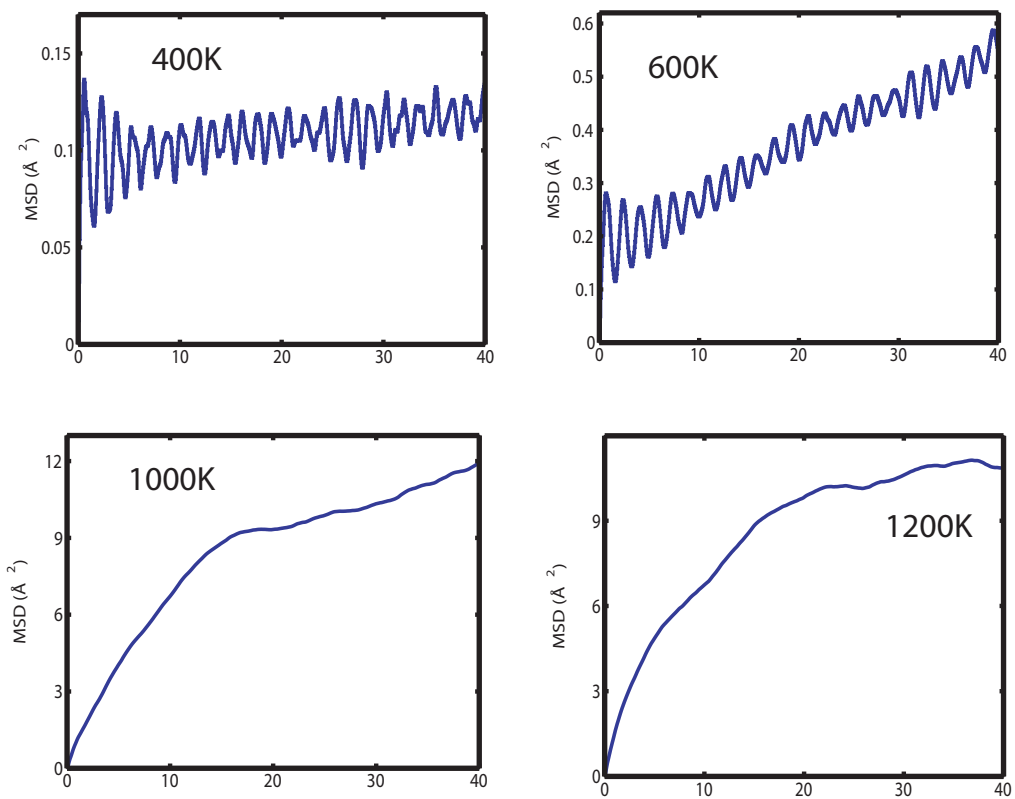


Figure 6.19: MSD of atoms in Ga_8 cluster between 200K to 1600K.

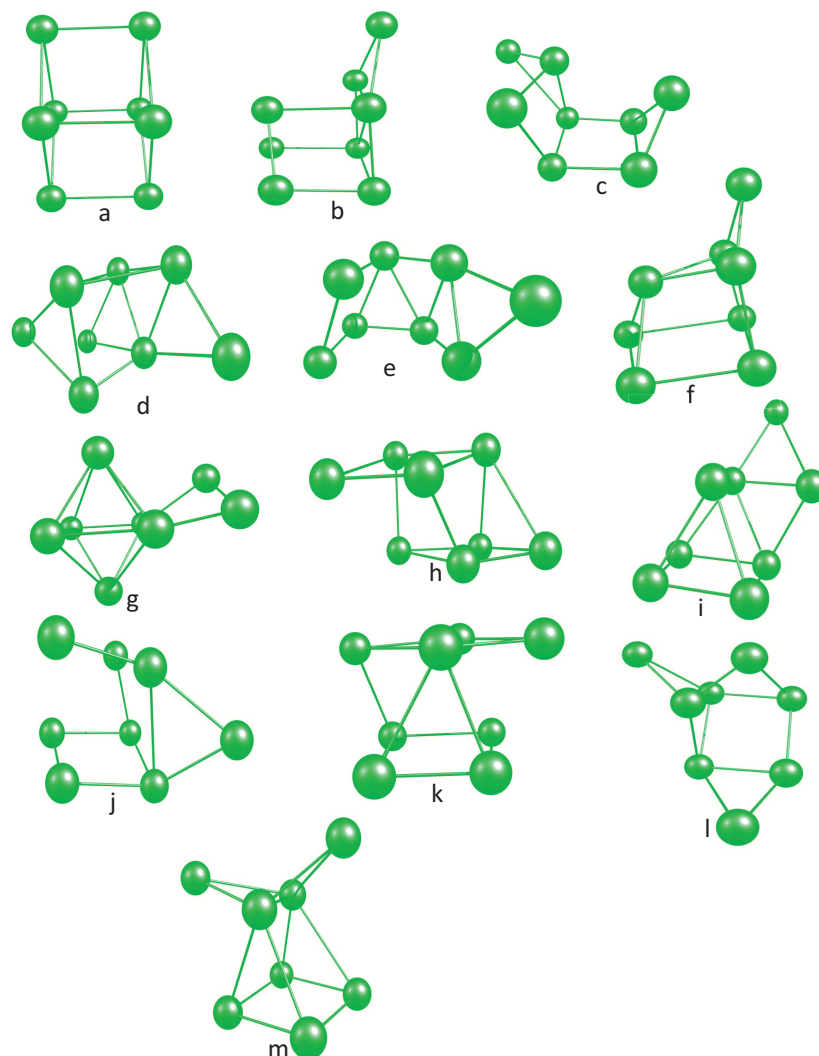


Figure 6.20: Various conformations of Ga_8 cluster observed during an MD simulation. (a) corresponds to the ground state conformation.

Bibliography

- [1] Schmidt M.; Haberland H. *C. R. Physique*, **2002**, *3*, 327.
- [2] Schmidt M.; Donges J.; Hippler T.; Haberland H. *Phys. Rev. Lett.* **2003**, *90*, 103401.
- [3] Haberland H.; Hippler T.; Donges J.; Kostko O.; Schmidt M.; Issendorff B. V. *Phys. Rev. Lett.* **2005**, *94*, 035701.
- [4] Schmidt M.; Kusche R.; Issendorff B. V.; Haberland H. *Nature (London)* **1998**, *393*, 238.
- [5] Kusche R.; Hippler T.; Schmidt M.; Issendorff B. V.; Haberland H. *Eur. Phys. J. D* **1999**, *9*, 1.
- [6] Schmidt M.; Kusche R.; Hippler T.; Donges J.; Kronmüller W.; Issendorff B. V.; Haberland H. *Phys. Rev. Lett.* **2001**, *86*, 1191.
- [7] Schmidt M.; Kusche R.; Kronmüller W.; Issendorff B. V.; Haberland H. *Phys. Rev. Lett.* **1997**, *79*, 99.
- [8] Häkkinen H.; Manninen M. *Physical review letters*, **1996**, *76*, 1599.
- [9] Martin T. P.; Bergmann T.; Göhlich H.; Lange T. *The Journal of Physical Chemistry*, **1991**, *95*, 6421.
- [10] Deshpande M.; Dhavale A.; Zope R. R.; Chacko S.; Kanhere D. G. *Phys. Rev. A.*, **2000**, *62*, 063202.
- [11] Dhavale A.; Kanhere D. G.; Majumder C.; Das G. P. *Eur. Phys. J. D.*, **1999**, *6*, 1999.
- [12] Häkkinen H.; Stephane A.; Sanchez A.; Heiz U.; Landman U.; *Angewandte Chemie International Edition*, **2003**, *42*, 1297.
- [13] Xi L.; Kiran B.; Cui L. F.; Wang L. S.; *Physical review letters*, **2005**, *95*, 253401.
- [14] Guangli C.; Lakshmi B. B.; Martin R. C.; Fisher R. E.. *Langmuir*, **1999**, *15*, 750.
- [15] Marie-Christine D.; Astruc D. *Chemical reviews*, **2004**, *104*, 293.

-
- [16] Hock C.; Strassburg S.; Haberland H.; Issendorff B. V.; Aguado A.; Schmidt M. *Phys. Rev. Lett.*, **2008**, *101*, 023401.
- [17] Cao B.; Strace A. K.; Judd O. H.; Bhattacharyya I.; Jarrold M. F.; Lopez J. M.; Aguado A. *J. Am. Chem. Soc.*, **2010**, *132*, 12906.
- [18] Cao B.; Strace A. K.; Neal C. M.; Jarrold M. F.; Noez S.; Lopez, J. M.; Aguado A. *J. Chem. Phys.*, **2008**, *129*, 124709.
- [19] Neal C. M.; Strace A. K.; Jarrold M. F. *J. Phys. Chem A.*, **2007**, *111*, 8056.
- [20] Breaux G. A.; Neal C. M.; Cao B.; Jarrold M. F. *Phys. Rev. B.*, **2005**, *71*, 073410.
- [21] Breaux G. A.; Benirschke R. C.; Sugai T.; Kinnear B. S.; Jarrold M. F. *Phys. Rev. Lett.*, **2003**, *91*, 215508.
- [22] Breaux G. A.; Cao B.; Jarrold M. F. *J. Phys. Chem.*, **2005**, *109*, 16575.
- [23] Li R.; Owen J. H. G.; Kusano S.; Miki K. *Appl. Phys. Lett.*, **2006**, *89*, 073116.
- [24] Krishnamurty S.; Chacko S.; Kanhere D. G.; Breaux G. A.; Neal C. M.; Jarrold M. F. *Phys. Rev. B.*, **2006**, *73*, 045406.
- [25] Breaux G. A.; Benirschke R. C.; Jarrold M. F. *J. Chem. Phys.*, **2004**, *121*, 6502.
- [26] Neal C. M.; Starace A. K.; Jarrold M. F. *J. Am. Soc. Mass Spectrom.*, **2007**, *18*, 74.
- [27] Zorriasatein S.; Lee M. S.; Kanhere D. G. *Phys. Rev. B.*, **2007**, *76*, 165414.
- [28] Ghazi S. M.; Lee M.S.; Kanhere D. G. *J. Chem. Phys.*, **2008**, *128*, 104701.
- [29] Chacko S.; Joshi K.; Kanhere D. G. *Phys. Rev. Lett.*, **2004**, *92*, 135506.
- [30] Neal C. M.; Starace A. K.; Jarrold M. F.; Joshi K.; Krishnamurti S.; Kanhere D. G. *J. Phys. Chem. C.*, **2007**, *111*, 17788.
- [31] Ding F.; Rosn A.; Bolton K. *Phys. Rev. B.*, **2004**, *70*, 075416.
-

-
- [32] Chuang F.; Wang C. Z.; Chelikowsky J. R.; Ho K. M. *Phys. Rev. B.*, 2004, 69, 165408.
- [33] Schebarchov D.; Hendy S. C. *Phys. Rev. Lett.*, **2005**, 95, 116101.
- [34] Aguado A.; Lopez, J. M. *Phys. Rev. B.* **2006**, 74, 115403.
- [35] Tomecka D. A.; Partoens B.; Peeters F. M. *Phys. Rev. E.* **2005**, 71, 062401.
- [36] Andriotis A. N.; Fthenakis Z. G.; Menon M. *Phys. Rev. B.*, **2007**, 75, 073413.
- [37] Luo S.; Zheng L.; Strachan A.; Swift D. C. *J. Chem. Phys.*, **2007**, 126, 034505.
- [38] Manninen K.; Rytkenen A.; Manninen M. *Eur. Phys. J. D.*, **2004**, 29, 39.
- [39] Cheng D.; Huang S.; Wang W. *Phys. Rev. B.*, **2006**, 74, 064117.
- [40] Chen F.; Curley B. C.; Rossi G.; Johnston R. L. *J. Phys. Chem. C.*, **2007**, 111, 9157.
- [41] Aguado A.; Lopez J. M. *Phys. Rev. B.*, **2005**, 71, 075415.
- [42] Aguado A.; Lopez, J. M. *Phys. Rev. B.*, **2005**, 72, 205420.
- [43] Michaelian K.; Garzon I. L. *Eur. Phys. J. D.*, **2005**, 34, 183.
- [44] Aguado A.; Lopez J. M.; Noez S. *Comput. Mater. Sci.*, 2006, 35, 174.
- [45] Joshi K.; Kanhere D. G. *J. Chem. Phys.*, **2003**, 119, 12301.
- [46] Lee M. S.; Joshi K.; Kanhere D. G. *Phys. Rev. A.*, **2005**, 72, 015201.
- [47] Lee M.S.; Gowtham S.; Haiying He; Lau K. C.; Pan L.; Kanhere D. G. *Phys. Rev. B.*, **2006**, 74, 245412.
- [48] Chandrachud P.; Joshi K.; Kanhere D. G. *Phys. Rev. B.*, **2007**, 76, 235423.
- [49] Krishnamurty S.; Joshi K.; Kanhere D. G.; Blundell S. A. *Phys. Rev. B.*, **2006**, 73, 045419.
- [50] Kumar V.; Kawazoe Y. *Phys. Rev. Lett.*, **2001**, 87, 045503.
- [51] Kawamura H.; Kumar V.; Kawazoe Y. *Phys. Rev. B.*, **2005**, 71, 075423.
-

-
- [52] Kumar V.; Kawazoe Y. *Phys. Rev. B.*, **2002**, *65*, 073404.
- [53] Kumar V.; Singh A. K.; Kawazoe Y. *Nano Lett.*, **2004**, *4*, 677.
- [54] Zorriasatein S.; Joshi K.; Kanhere D. G. *Phys. Rev. B.*, **2007**, *75*, 045117.
- [55] Mottet C.; Rossi G.; Baletto F.; Ferrando R. *Phys. Rev. Lett.*, **2005**, *95*, 035501.
- [56] Das S.; Pal S.; Krishnamurty S. *J. Phys. Chem. C.*, **2014**, *118*, 19869.
- [57] Douady J.; Calvo F.; Spiegelman F. *Eur. Phys. J. D.* **2009**, *52*, 47.
- [58] Lyalin A.; Hussein A.; Solovyou A. V.; Greiner W. *Phys. Rev. B.* **2009**, *79*, 165403.
- [59] Köster A. M.; Calaminici P.; Casida M. E.; Dominguez V. D.; Flores-Moreno R.; Geudtner G.; Goursot A.; Heine T.; Ipatov A.; Janetzko F.; del Campo J. M.; Reveles J. U.; Vela A.; Zuniga-Gutierrez B.; Salahb D. R. **deMon2k; The deMon Developers Cinvestav: Mexico City, 2006.**
- [60] Perdew J. P.; Burke K.; Ernzerhof M. *Phys. Rev. Lett.*, **1996**, *77*, 3865.
- [61] Godbout N.; Salahub D. R.; Andzelm J.; Wimmer E. *Can. J. Chem.*, **1992**, *70*, 560.
- [62] Calaminici P.; Janetzko F.; Köster A. M.; Mejia-Olvera R.; Zuniga-Gutierrez B. *J. Chem. Phys.*, **2007**, *126*, 44108.
- [63] Köster A. M.; Reveles U. J.; del Campo J. M. *J. Chem. Phys.*, **2004**, *121*, 3417.
- [64] Berendsen H. J. C.; Postma J. P. M.; van Gunsteren W. F.; DiNola A.; Haak J. R. *J. Chem. Phys.*, **1984**, *81*, 3684.

Mechanism for C–I Bond Dissociation in Iodoethane, Iodoethene and Iodobenzene for the C–C Cross Coupling Reactions over Aluminum Clusters

Energetics of the key step of cross – coupling reaction, dissociation of aliphatic and aromatic iodides using aluminium nanoclusters as catalyst are studied in the framework of density functional theory. In spite of being an unconventional catalyst for radical polymerization, cross – coupling or similar type of reactions in bulk state, Al clusters have shown significantly low activation barrier (~ 0 to ~ 30 to Kcal mol^{-1}). Further investigations reveals that the activation energies are sensitive to the shape and electronic structure of catalyst rather than the size of them, making the Al clusters attractive in the area of nanocatalysis and nanoscience. To understand the insight into the reaction mechanism, mode of binding is investigated with the Natural Bond Orbital (NBO) analysis. In short, our theoretical study highlights the efficiency of the aluminium clusters for future endeavors in the design of cost – effective and efficient catalyst for cross – coupling reaction.

7.1 Introduction and methodology

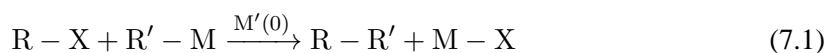
The C – C cross coupling reaction with transition metal as catalyst is the most promising tool of organic and material synthesis since the last four decades[1, 2]. Bond formation process between two carbon atom is high energy demanding and hence a slow process. Therefore C – C coupling reaction requires suitable catalyst to bring down the energy barrier and make the reaction practically viable with reasonably good chemical yield. Most extensively used catalysts are Cu, Ni and Pd complex[3, 4]. Recent development in both experimental and theoretical contexts have shown Fe and Au perform moderately well in C – C cross coupling reaction. Among all these popular methodologies, currently most versatile and efficient catalyst for cross coupling reaction is the heterogeneous Pd(0) catalyst, commonly used via the different reaction schemes developed by Kumada[5], Heck[6], Sonogashira[7], Negeshi[8], Stille[9] and Suzuki[10] in the early 70-80's. Heterogeneous Pd(0) catalyst is not only gives good chemical yield with better product quality but it's also reusable and most of the reaction schemes are less energy demanding. However, despite the fact, Pd catalyst suffers from some well known disadvantages. Heterogeneous Pd catalyst is prone to catalyst poisoning and leaching. Both Pd and Ni which are widely used catalyst for cross – coupling are highly expensive and poisonous, having low LD₅₀ values. Fine powder of Pd used as heterogeneous catalyst is pyrophoric as well.

Therefore, finding an alternatives catalyst of Ni and Pd is the prime field of research to both theoreticians and experimentalists in recent years. Among the newly developed alternative catalyst, a combined experimental and theoretical investigation propose that the most promising is Au nano cluster towards C – C cross – coupling[11, 12]. However, similar to Pd catalyst Au is a rare element and highly expensive, pulling down it's use for large scale industrial synthesis.

Al nanoclusters are well known for its catalytic activity. Specifically small sized aluminium clusters of 2 – 50 atoms are extremely reactive and their catalytic activity is comparable to that of transition metals like Au, Pd and Pt[13–15]. Al nano clusters have strong affinity to adsorb gaseous species such as H₂, D₂, O₂, N₂ and H₂O[16–20]. Further analysis based on Jellium model reveals that specific Al clusters have some unique features. For example, Al₁₃ cluster shows similarity with halogens, form stable complexes with iodine, produce ionic assemblies

with superalkali counteranions, even forms similar compounds like polyhalides[21–23]. On the other hand Al₇ shows both divalent and tetravalent valencies similar to that of carbon. All of these observations, stability and reactivity can be neatly explained by so called homogeneous electron gas (HEG) model or commonly mentioned as Jellium model first used by Knight and co-workers for similar context[24]. These potent studies on Al clusters provoke further interest to judge their catalytic properties for different chemical reactions and to observe and explain the effects of electronic structures, size and shape upon the energetics. Detail analysis can prove useful and can have promising impacts in the field of nanoscience and technologies in the upcoming days. As additional advantages it must be mentioned, Al metal is the most abundant metal in the earth crust and third most abundant element after oxygen and silicon. It is cheaper than most of the common transition metal catalysts like Pd, Au or Ni which are used for similar kind of reactions, and 100% recyclable. Al catalysts either in metal state or in form of chemical compound are mostly nontoxic and eco-friendly in nature.

All these advantages of Al nanoclusters make them an interesting choice to investigate of its catalytic behavior for cross-coupling or similar type of reactions. Figure 7.1 shows most common schematics of cross-coupling reaction using Pd as catalyst. Other catalysts e.g Ni, Fe or Au follow similar mechanistic steps. The reaction proceeds via the oxidative addition of Pd(0) complex to organo-halide to form a Pd(II) complex. Next step is the transmetalation with another organometallic reagent where the nucleophile R' is transferred from the metal to the Pd(II), which is the slowest step in the whole cycle and hence the rate determining step. The final process is the reductive elimination to give the coupled product (R-R') and regenerate the Pd(0) complex ready for next catalytic cycle. The overall catalytic reaction can be summarized as,



where M'=Pd,Ni,Au,Fe etc

In this present work we have shown small size Al nano clusters can act as a suitable catalyst for cross-coupling reaction. Accurate DFT calculation prevails that the Al nano clusters participate in C-I bond activation, effective in both aliphatic and aromatic C-I bond. Our present work signifies nanoclusters of non-transition metals can provide a source of cheaper and nontoxic alternative of transition metal catalyst used in cross-coupling reactions. With the

progress of nano science and technologies, Al nano clusters based motifs can prevail as the tool of the trade in days to come.

All the geometries are optimized at the DFT level of theory using Gaussian 09 software package with the TZVP basis set and BHandHLYP functional[25]. Only the lowest energy optimized structure in each case is chosen as one of the reactants in the C–I dissociation. Another reactants iodoethane, iodoethene and iodobenzene are also optimized using same basis and functional for C and H. However, for iodine LANL2DZ basis is used in addition with LANL2 as model potential (pseudo potential) for the core electrons. All of the optimization of reactants and transition state are performed using Berny’s eigenvalue following algorithm implemented in Gaussian 09 package. Normal modes of vibration of the optimized structures are carefully observed and it was made sure that all the energetically minimized structure (reactants) have no imaginary frequency whereas the transition states must and only have one single imaginary frequency of appropriate magnitude and which corresponds to the C–I bond itself. Intrinsic reaction coordinate (IRC) calculation are performed to confirm that all the transition structures are connected with proper reactants and products along positive and negative sides of chemical reaction coordinate. Same calculations are further repeated using Minnesota functional M06–2X in an attempt to properly bracket the activation barrier for C–I dissociation on Al clusters. Thermodynamically controlled product of the reaction for each metal cluster was determined by calculating the energies of all possible products and choosing the energetically lowest conformer. Basis set superposition error (BSSE) are corrected using Boys and Bernardi’s counterpoise correction scheme within the Gaussian 09 software. Rate constants of C–I dissociation are calculated by using the Eyring–Polanyi equation.

$$k = \frac{k_B T}{h} e^{-\frac{\Delta G^\ddagger}{RT}} \quad \text{where} \quad \Delta G^\ddagger = G_{TS}^\ddagger - G_{Reactant} \quad (7.2)$$

of transition state theory at 298 K.

NBO analysis are further used for each clusters separately to get the insight about aromatic and aliphatic C–I bond cleavage on Al nanoclusters. The second order perturbative estimation of donor – acceptor stabilization energy(E_s) within the NBO basis are computed by

$$E_s = \Delta E_{ij} = q_i \frac{F_{ij}^2}{\Delta \epsilon_{ji}} \quad (7.3)$$

where q_i is donor orbital occupancy number. F_{ij} is off – diagonal elements of Fock matrix in

NBO basis. $\Delta\epsilon_{ji} = \epsilon_j - \epsilon_i$ is the orbital energy difference between acceptor(j) and donor(i) NBO.

7.2 Results and Discussion

To investigate the catalytic property of Al atomic clusters towards C–I bond activation; we have chosen seven different atomic clusters of aluminium viz. $\text{Al}_3, \text{Al}_5, \text{Al}_6, \text{Al}_7, \text{Al}_8, \text{Al}_{13}$ and Al_{20} keeping in mind that properties of atomic cluster are size and shape sensitive. In this thesis we have only included results of Al_3 cluster. Calculations for the rest are under way and will be compiled as a full paper in the near future. As other reactants we have selected three organo-iodides which are ethyl, ethylene and benzyl iodide respectively i.e. a combination of one alkyl, one alkene and one aryl halide of choice. Although calculations are performed in three different double hybrid DFT functionals B3PW91, BHandHLYP and M06–2X, during structural and binding energy comparison and also for Natural Bond Orbital (NBO) analysis we have followed the results obtained by M06–2X functional as family of Minnesota functionals are well known for good structural prediction as well as bonding interactions. Binding energies in all cases are calculated by the conventional method $\Delta E = E(\text{Al}_n) + E(\text{R-I}) - E(\text{Al}_n \dots \text{IR})$. All the thermodynamic parameters are calculated at 298 K and in 1 atm pressure.

One of the important features of atomic clusters is that each cluster can behave drastically different from each other. The major reason lies behind is the electronic shell effect and the shape and the stability of the cluster itself. Both of these effects uniquely change the reactivity of each member of same cluster family, as a result all the parameters including thermochemistry and reaction mechanism pathway can be abruptly different for each member, even for the same reaction.

Figure 7.2 shows the reaction profile of Al_3 cluster with three organo iodide along with the changes of important structural parameters throughout the course of the reaction. The optimized structure of Al_3 is planar, triangular shaped with each bond length 2.52 Å (by M06–2X). Being very small quantum effect is pronounced in this cluster and hence Al_3 clusters are well known for its high reactivity and confirmed by previous theoretical studies (ref). Jellium model predicts a total of 9 valence electron, which is one electron higher than the magic number 8. Hence a low activation barrier for oxidative addition is expected as the cluster achieves the filled shell

magic cluster configuration upon one electron loosing. So, according to jellium model Al_3 cluster should be highly reducing. Our calculations based on DFT as shown in the tables 7.1, 7.2 and 7.3 nicely confirms our statement. For all three reactants ethyl, ethylene and benzyl iodide, Al_3 cluster indeed show low activation barrier. B3PW91 values are excessively low than other two functionals, M06-2X and BHandHLYP. In case of ethyl iodide ΔH^\ddagger value is 0.7 Kcal/mol and ΔG^\ddagger is 1.8 Kcal/mol whereas ΔH^\ddagger values are 7.3 and 6.2 and ΔG^\ddagger values are 11.2 and 7.3 Kcal/mol for BHandHLYP and M06-2X functional respectively. Similar trend continues for other two reactants. The unusual low values in B3PW91 functional is not surprising as previous theoretical benchmark investigation showed that B3PW91 has an occasional tendency to underestimate activation barrier than similar quality double-hybrid functional like BHandHLYP (ref). However, both the ΔH^\ddagger and ΔG^\ddagger values are in close agreement between the results of other two functional BHandHLYP and M06-2X, differentiating within 1-4 Kcal/mol in all three cases of Al_3 cluster. Unlike the activation barrier the exothermicity values are in better agreement within three functionals and Al_3 cluster shows high exothermicity with the reactants. Both the ΔH and ΔG values are very low (highly exothermic) within the range of -60 to -80 Kcal/mol for organo iodides. Even significantly lower than the exothermicity values of theoretically predicted gold atomic clusters for the same reaction calculated with similar functional and basis set. Highly negative ΔG values indeed indicate enhanced spontaneity of the so called reaction in accordance to thermodynamic principles. One important observation is in all the cases of our study change in Gibbs free energy of the reaction (ΔG) values are always greater than change in enthalpy of reaction (ΔH) values, hence, the reaction is entropically unfavorable, which is expected as in case of oxidative addition.

Ethyl iodides binds with Al_3 cluster from and distance of 3.4Å with a binding energy of 2.3 Kcal/mol. C-C and C-I bond length remains same as in optimized structure of isolated ethyl iodide molecule (C-C = 1.51Å and C-I = 2.18Å) calculated in same level of theory, but bond lengths of Al_3 becomes unequal (Fig 2). This asymmetry may introduce some additional angle strain (Baeyer strain) within the cluster as being a three member planer ring, the Al_3 cluster do not have any opportunity to release this stress via out of plane bending. In the transition state of ethyl iodide, C-C bond being reduced by 0.03Å, C-I bond elongated by 0.33Å and the planer ring gets more deviated. We have found that asymmetrization of bond length in reactants, transition

states and products of Al_3 cluster are indeed a common feature for all three iodides. We have also identified similar deviation of bond lengths as shown in Figure 7.2 in reactants and transition states for ethylene and benzyl iodide as well. The post-reaction complex of ethyl iodide- Al_3 reaction is shown at rightmost minima of corresponding energy profile diagram of Figure 7.2. In which C-I bond is completely dissociated and both alkyl and iodine fragment are residing at two neighboring sites of Al_3 cluster. C-Al distance in this complex is 1.97 Å, Al-I distance is 2.53 Å and C-C bond is 0.03 Å longer than isolated ethyl iodide. Other two reactants ethylene and benzyl also follow similar pathway as shown in Figure 7.2. One major noticeable difference is the mode of binding of ethyl iodide with Al than the other two iodides. In case of ethyl iodide, iodine atom interacts with Al atom via lone pair of it. Frontier molecular orbital pictures shown in Figure 7.3 clearly indicate the same.

Second order perturbation treatment of Fock matrix in the NBO basis usually provides information about most stabilizing donor-acceptor interaction between Lewis acid-base pairs. In the pre-reaction complex of ethyl iodide NBO analysis shows a high stabilization energy contribution of about 13.41 kcal/mol due to donor-acceptor interaction between nonbonding orbital (LP) of iodine to antibonding orbital (LP*) of aluminium. In case of ethylene and benzyl iodide, however the π electron cloud of carbon moiety is also taken part in the interaction with aluminium. Thus in case of ethylene iodide there are two contribution to the stability due to donor-acceptor interaction, first and major contribution is about 10.86 Kcal/mol which is due to donor-acceptor interaction between nonbonding orbital (LP) of iodine to antibonding orbital (LP*) of aluminium similar as in case for ethyl iodide. Second one is very low of 2.3 Kcal/mol due to the interaction between the π bond of C-C moiety and the antibonding orbital (LP*) of Al. However, in case of benzyl iodide although the frontier molecular orbital is showing participation of π electron cloud along with the lone pair of iodine, this interaction is not strong enough to produce any significant contribution to stabilization. Most probable reason of this as the C moiety is larger in case of benzyl group, most part of the π electron cloud is out of the overlap region of the Al_3 cluster. Hence only significant contribution is of about 7.31 Kcal/mol due to donor-acceptor interaction between LP(I)-LP*(Al) similar to ethyl and ethylene iodide. Second major difference besides the mode of binding is structure of transition states. In case of ethylene iodide, orientation of the molecule with the cluster in transition state is linear .i.e Al...I...C bond angle is nearly 180 °, where as the

orientation of ethyl and benzyl group with the Al..I bond is nearly perpendicular (106°) in their respective cases. This unusual structure in case of ethylene iodide changes the structure of Al_3 to a bilateral triangle in the transition state. The stabilizing interactions are slightly different in post-reaction complexes of $\text{Al}_3\text{-R-I}$ reaction. In case of ethyl iodide the C–Al bond is stabilized by an amount of 63.9 Kcal/mol due to the electronic interaction between nonbonding (LP) orbital of carbon and antibonding (LP^*) orbital of Al. Whereas stability of Al–I bond is similar as in case of pre-reaction complexes due to interaction between $\text{LP(I)-LP}^*(\text{Al})$, a stabilization energy of 11.3 Kcal/mol is obtained due to this interaction. Donor acceptor stability contributions in the post complexes are similar in other two cases. In case of ethylene iodide the $\text{C(LP) - Al(LP}^*)$ stabilization energy is 83.1Kcal/mol and $\text{LP(I)-LP}^*(\text{Al})$ energy is 11.4 Kcal/mol. Whereas in benzyl iodide $\text{C(LP) - Al(LP}^*)$ stabilization energy is 66.1 kcal/mol, close with the value obtained in case of ethyl iodide and contribution to $\text{LP(I) - LP}^*(\text{Al})$ interaction is 11.4 Kcal/mol which is equal with the stabilization energy values obtained in two previous cases.

7.3 Conclusion and Scope

Present study includes a theoretical investigation of dissociation of C – I bonds over Al clusters in the frame work of density functional theory. C – I bond dissociation is indeed a crucial reaction and provides key step in various important organic reactions like cross – coupling. Most commonly used catalyst are d and f block elements like Pd, Ni, Cu, Fe and Au. Our investigation shows that being a p block element, ineffective to catalyze the reaction in bulk phase, Al nano cluster is highly effective as a catalyst. Calculated activation barriers reveal that Al nano clusters are remarkably efficient catalyst towards C – I bond activation and dissociation. The catalytic efficiency is even better than the common d and f block catalyst. We have further observed that activation barriers are highly sensitive on the electronic structures and shape of the cluster rather than its size. This observation concludes that effective catalytic effect may be obtained in bigger clusters or even in solid supported clusters. Our study highlights a brief analysis including structures and thermochemistry of reacting species along with stability and mechanistic pathway of the reaction which will be highly useful for experimental implementation of the same. Al clusters

are long known for their high reactivity, as proven numerous times by both experiments and theory, our investigation also suggests in cluster state Al is significantly effective as transition metals for catalysis purpose. With the technological progress in nano cluster synthesis, separation and stabilization, Al cluster can indeed a cost-effective and eco – friendly alternative of transition metal catalysts.

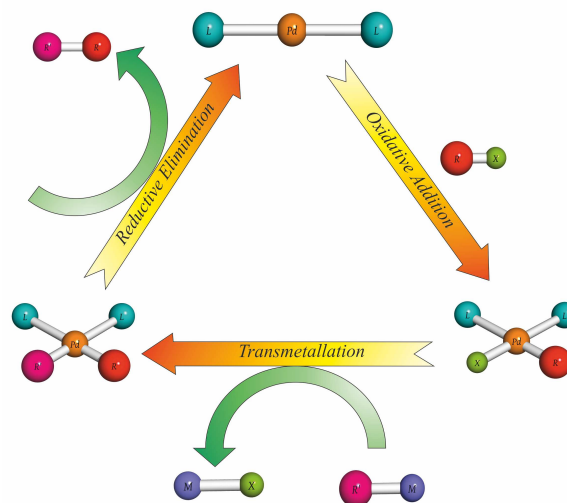


Figure 7.1: A general scheme for cross-coupling reaction cycle using Pd as catalyst.

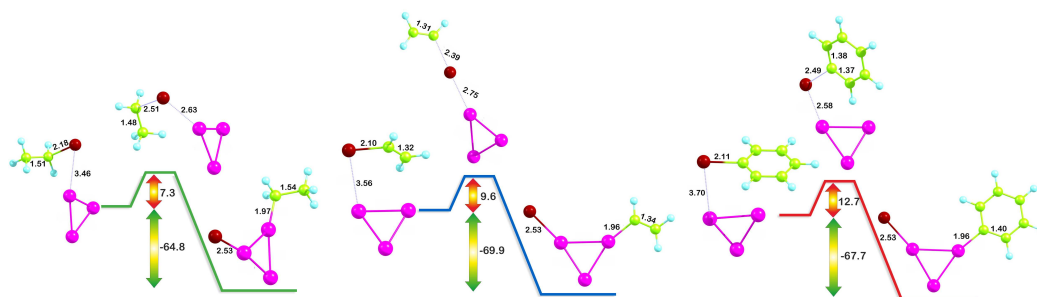


Figure 7.2: Energy profile diagrams for Al_3 clusters for all three iodides. Orange arrow highlights the activation barrier (G) and green arrow highlights corresponding exothermicity (ΔH) in M06-2X functional

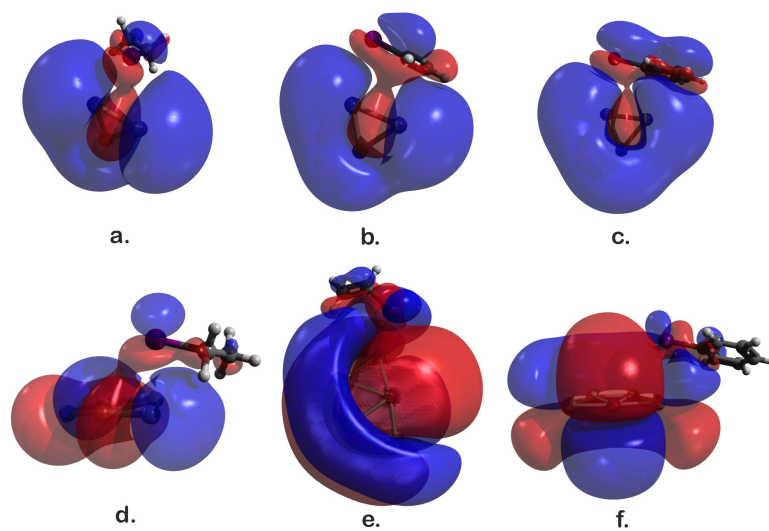


Figure 7.3: Frontier molecular orbital picture for pre-reaction complexes of Al_3 cluster

Table 7.1: Thermodynamic data of C–I bond dissociation of ethyl iodide, ethylene iodide and benzyl iodides on Al nanoclusters in B3PW91, BHandHLYP and M06–2X functionals

Al nanoclusters	R–I	Activation Barrier (Kcal/mol)					
		ΔH^\ddagger			ΔG^\ddagger		
		B3PW91	BHandHLYP	M06–2X	B3PW91	BHandHLYP	M06–2X
Al ₃	iodoethane	0.705	7.292	6.202	1.832	11.192	7.295
	iodoethene	4.006	6.826	8.791	3.863	8.654	9.586
	iodobenzene	3.481	8.143	11.948	4.950	10.796	12.721

Table 7.2: Thermodynamic data of C–I bond dissociation of ethyl iodide, ethylene iodide and benzyl iodides on Al nanoclusters in B3PW91, BHandHLYP and M06–2X functionals

Al nanoclusters	R–I	Exothermicity (Kcal/mol)					
		ΔH			ΔG		
		B3PW91	BHandHLYP	M06–2X	B3PW91	BHandHLYP	M06–2X
Al ₃	iodoethane	-68.081	-71.553	-64.846	-67.456	-68.444	-63.575
	iodoethene	-73.791	-77.766	-69.935	-72.377	-74.146	-68.929
	iodobenzene	-74.692	-78.099	-67.672	-69.841	-72.341	-67.209

Table 7.3: Thermodynamic data of C–I bond dissociation of ethyl iodide, ethylene iodide and benzyl iodide on Al nanoclusters in B3PW91, BHandHLYP and M06–2X functionals

Al nanoclusters	R–I	E.P Rate constant			Binding Energy(Kcal/mol)	
		BHandHLYP	M06–2X	B3PW91	$\Delta E(\text{M06–2X})$	$\Delta E_{BSSSE}(\text{M06–2X})$
Al ₃	iodoethene	2.815x10 ¹¹	3.845x10 ⁴	2.772x10 ⁷	5.005	4.348
	iodoethene	9.121x10 ⁹	2.792x10 ⁶	5.788x10 ⁵	4.414	3.927
	iodobenzene	1.454x10 ⁹	7.504x10 ⁴	2.910x10 ³	6.312	5.851

Bibliography

- [1] Tamao K.; Norio M. **Introduction to cross-coupling reactions**, Springer, 2002.
- [2] Norio M.; Stephen L. B. **Cross-coupling reactions: a practical guide**, Springer, 2002
- [3] François D.; Peter J. S. **Metal-catalyzed cross-coupling reactions**, John Wiley & Sons, 2008.
- [4] Irina P. B.; Andrei V. C. *Coordination chemistry reviews*, 2004, 248, 2337.
- [5] Kohei T.; Sumitani, Koji S.; Makoto K. *Journal of the American Chemical Society*, 1972, 94, 4374.
- [6] Heck R. F. **Palladium reagents in organic syntheses**, Academic Press London, vol. 6, 1985.
- [7] Sonogashira K. *Journal of organometallic chemistry*, 2002, 653, 46.
- [8] King A.; Okukado N.; Negishi E. *Journal of the Chemical Society, Chemical Communications*, 1977, 683.
- [9] Stille J. K. *Angewandte Chemie International Edition*, 1986, 25, 508.
- [10] Suzuki A. *Journal of Organometallic Chemistry*, 1999, 576, 147.
- [11] Corma A.; Juárez R.; Boronat M.; Sanchez, F.; Iglesias, M.; Garca, H. *Chemical Communications*, 2011, 47, 1446.
- [12] Nijamudheen A.; Datta A. *The Journal of Physical Chemistry C*. 2013, 117, 21433.
- [13] Khanna S.; Jena P. *Physical review letters*, 1992, 69, 1664.
- [14] Khanna S. N.; Jena P. *Physical Review B.*, 1995, 51, 13705.
- [15] Jones N.; Reveles J. U.; Khanna S.; Bergeron D.; Roach P.; Castleman Jr A. *The Journal of chemical physics*, 2006, 124, 154311.

-
- [16] Cox D.; Trevor D.; Whetten R.; Kaldor A. *The Journal of Physical Chemistry*, **1988**, *92*, 421.
- [17] Jarrold M. F.; Bower J. E. *Journal of the American Chemical Society*, **1988**, *110*, 70.
- [18] Woodward W. H.; Eyet N.; Shuman N. S.; Smith J. C.; Viggiano A. A.; Castleman Jr A. *The Journal of Physical Chemistry C*, **2011**, *115*, 9903.
- [19] Kulkarni B. S.; Krishnamurty S.; Pal S. *The Journal of Physical Chemistry C*, **2011**, *115*, 14615.
- [20] Das S.; Pal S.; Krishnamurty S. *The Journal of Physical Chemistry C*, **2014**, *118*, 19869.
- [21] Bergeron D. E.; Castleman A. W.; Morisato T.; Khanna S. N. *Science*, **2004**, *304*, 84.
- [22] Clayborne P.; Jones N. O.; Reber A. C.; Reveles J. U.; Qian M.; Khanna S. N. *Journal of Computational Methods in Science and Engineering*, **2007**, *7*, 417.
- [23] Reber A. C.; Khanna S. N.; Castleman A. W. *Journal of the American Chemical Society*, **2007**, *129*, 10189.
- [24] Knight W. D.; Clemenger K.; de Heer W. A.; Saunders W. A.; Chou M.; Cohen M. L. *Physical review letters*, **1984**, *52*, 2141.
- [25] Frisch, M. J.; Trucks, G. W.; Schlegel, H. B.; Scuseria, G. E.; Robb, M. A.; Cheeseman, J. R.; Scalmani, G.; Barone, V.; Mennucci, B.; Petersson, G. A.; Nakatsuji, H.; Caricato, M.; Li, X.; Hratchian, H. P.; Izmaylov, A. F.; Bloino, J.; Zheng, G.; Sonnenberg, J. L.; Hada, M.; Ehara, M.; Toyota, K.; Fukuda, R.; Hasegawa, J.; Ishida, M.; Nakajima, T.; Honda, Y.; Kitao, O.; Nakai, H.; Vreven, T.; Montgomery, J. J. A.; Peralta, J. E.; Ogliaro, F.; Bearpark, M.; Heyd, J. J.; Brothers, E.; Kudin, K. N.; Staroverov, V. N.; Kobayashi, R.; Normand, J.; Raghavachari, K.; Rendell, A.; Burant, J. C.; Iyengar, S. S.; Tomasi, J.; Cossi, M.; Rega, N.; Millam, J. M.; Klene, M.; Knox, J. E.; Cross, J. B.; Bakken, V.; Adamo, C.; Jaramillo, J.; Gomperts, R.; Stratmann, R. E.; Yazyev, O.; Austin, A. J.; Cammi, R.; Pomelli, C.; Ochterski, J.W.; Martin, R. L.; Morokuma, K.; Zakrzewski, V. G.; Voth, G. A.; Salvador, P;

Dannenberg, J. J.; Dapprich, S.; Daniels, A. D.; Farkas, O.; Foresman, J. B.; Ortiz, J. V.; Cioslowski, J.; Fox, D. J. **Gaussian09 Revision D.01**. *Gaussian Inc. Wallingford CT, 2009*.